CANK, KRISTOF B. Ph.D. What Do Ancient Pottery, Bees and Fungi Have in Common? The Identification, Isolation, and Structural Elucidation of Diverse Natural Products. (2022) Directed by Dr. Nicholas H. Oberlies. 165 pp.

Natural products are metabolites and/or sometimes by-products derived naturally from plants, microorganisms, or even animals. They play a significant role in therapeutic drug discovery, and they possess important agricultural and ethnobotanical relevance. As part of an interdisciplinary project to study natural products from different origins, this dissertation discusses a variety of topics involving the identification, isolation, and structure elucidation of natural products. In the first project, a novel methodology for chemical residue analysis was developed with a goal of identifying natural residues on the surface of ancient Peruvian artifacts. The identified compounds allowed us to examine the ethnobotanical relevance of these artifacts. The second project discusses the isolation and structure elucidation of novel polychlorinated secondary metabolites from a yet undescribed marine fungal species. The third project represents a distinct study to compare multiple artificial algae-based diets for honey bees. The goal of this latter project was to evaluate the key similarities and differences between the artificial and traditional pollen-based diets in honey bees, which are critical agricultural pollinators in the United States. The last study discusses the discovery of new antimalarial compounds from filamentous fungi. Throughout this study, more than 40,000 fungal strains were examined for their antimalarial activity. Several antimalarial compounds were isolated, among them a compound termed viridicatumtoxin A and a compound class termed, leucinostatin analogues, were the most potent inhibitors. Spatial mapping of the leucinostatin biosynthesizing strains and precursor directed biosynthesis of novel analogues were pursued.

WHAT DO ANCIENT POTTERY, BEES AND FUNGI HAVE IN COMMON?

THE IDENTIFICATION, ISOLATION, AND STRUCTURE ELUCIDATION OF DIVERSE

NATURAL PRODUCTS

by

Kristóf B. Cank

A Dissertation

Submitted to

the Faculty of The Graduate School at

The University of North Carolina at Greensboro

in Partial Fulfillment

of the Requirements for the Degree

Doctor of Philosophy

Greensboro

2022

Approved by

_____
Dr. Nicholas H. Oberlies
Committee Chair

This dissertation written by Kristóf B. Cank has been approved by the following committee of the Faculty of The Graduate School at The University of North Carolina at Greensboro.

Committee Chair

Committee Members

Dr. Nicholas H. Oberlies

Dr. Nadja B. Cech

Dr. Mitchell P. Croatt

Dr. Dennis E. Kyle

May 24, 2022

Date of Acceptance by Committee

May 24, 2022

Date of Final Oral Examination

ACKNOWLEDGEMENTS

This dissertation would have never been finished without the help of all the individuals who supported and challenged me every single step of the way. I will always be fortunate for everyone who has contributed to my scientific carrier and my growth as a person. The first person I would like to sincerely thank is Prof. Nicholas H. Oberlies. I am tremendously grateful to have the privilege to study in his research laboratory. His support, guidance, patience, and enthusiasm from day one made me who I am today. He did not just motivate me but gave me the passion that sparked the fire and provided me the mental and morale boost every single day to carry on in my academic carrier. I could not have imagined a better advisor and a better person to be my mentor.

I would also like to thank all my committee members, Dr. Nadja Cech, Dr. Mitchell Croatt, and Dr. Kyle for all the support, encouragement, and scientific knowledge, I have received. Without any of the committee members, I would have not acquired the precise skills, smart thinking, and attention to details, that would allow me to carry on in my future carrier.

I would sincerely thank all my fellow colleagues, not only for the ones in the laboratory but every single one of you who helped me go through this journey at UNCG. There are way too many people to thank everyone individually, but I want you all to know that I am grateful for everyone. I would like to thank Dr. Tamam El-Elimat who trained me in those few months we met and who to provided me a tremendous amount of guidance that allowed me to become a better scientist. I want to thank Mr. Tyler Graf and Dr. Huzefa Raja for always guiding me and being available to answer all my questions as a professional colleague and as a friend. Your honest feedback and never-ending help will never be forgotten. I want to give a special thank to

all the current and formal students of the Oberlies lab who helped me in many ways (Allison Wright, Zuzu Faye, Laura Bocanegra, Manuel Rangel Grimaldo, Cody Earlp, Herma Pierre, Zeinab Al Subeh, Reema Al-Qiam, Hadi Pourhadi, Soumia Amrine,). I would like to say special thanks also to my undergraduate students, Jennifer Obike and Robert Shepherd. Without them, the work of this dissertation would not have been complete. Their hard work and continuous support meant a lot to me. I would like to thank all my friends in the Department of Biochemistry, including Dr. Sonja Knowles, my formal lab member. You were always there for me, and without your friendship and knowledge, this dissertation and my journey would never be the same. I want to express my gratitude and appreciation to all the collaborators I had throughout the year. This dissertation could not have been assembled either without their contribution. I have met many great scientists through the years and gained not just expertise but many great friendships as well.

I would like to also thank my family and close friends in the United States especially Osbin Perdomo. I need to thank my mom, my dad, and my sister, to keep me going and for always pushing me to pursue my dream carrier even if they were living far away and we were separated.

Finally, I want to thank to my wife, Katharine Cank. You were always there for me behind the curtain, dealing with me after work. You always accepted my flaws and kept me going each day of our shared life. I cannot thank you enough. I could have not done it without you. Thanks for always believing in me, encouraging, and loving me for who I am.

TABLE OF CONTENTS

LIST OF TABLES

LIST OF FIGURES

xvi

CHAPTER I: INTRODUCTION

Natural products are metabolites and/or by-products derived naturally from plants, microorganisms, or even animals.[1] Their significance in the field of drug discovery is unquestionable[2], especially, in therapeutic areas against diseases such as cancer (e.g. taxol), cardiovascular (e.g. statins), and infectious diseases (e.g. penicillin).[3] For example, out of all the FDA approved drugs from 1981 to 2002, about 52% were either natural products or their derivatives, and this pattern has continued to present day.[2, 4] By the end of the 20th century, less than 10% of the world's biodiversity has been tested for biological activity, thus many more natural product leads are awaiting discovery.[5]

Throughout the evolution of life, the importance of natural compounds became unquestionable. Nature provides resources not only for human use, but also vital nutrition for plants, animals, and other organisms. By studying the occurrence, origins, and biological activities of secondary metabolites, humans can probe scientific questions that are only limited by the imagination. Thus, the study of natural products ignites scientific curiosity across many other scientific disciplines.

This dissertation includes Chapters that discuss interdisciplinary projects that involved secondary metabolite isolation, identification, and structure elucidation. Each Chapter examines distinct scientific questions in the field of natural product chemistry while being related by the knowledge base, instrumentation, and analytical techniques used.

Chapter two highlights the chemical residue analysis of ancient artifacts to identify natural residues on their surface. Analyzing ceramics from ancient cultures, many of which are degraded or damaged from hundreds or thousands of years of weathering, present some unique

challenges. Mass spectrometry coupled with separation techniques, such as liquid chromatography, provides a means to analyze residues on artifacts. However, most well-known analytical techniques usually cause at least some amount of destruction of the material during the preparation phase, leading to the loss of valuable spatial information and possibly hampering future analyses. In this study of ancient Andean sherds, we present a test case of using a non-destructive LC-MS technique, termed the droplet-liquid microjunction-surface sampling probe (i.e., droplet probe), for studying the chemistry of residues on ceramics. This method combines the benefits of mass spectrometry with the collection of chromatographic data, the combination of which affords a wealth of data. Three naturally occurring plant secondary metabolites, aurantiamide acetate, aurantiamide benzoate, and aurantiamide were identified on the surface of a vessel and a spoon sherd from the central highlands of Peru. Fragmentation patterns, mass defect filtering, and comparison to an in-house standard were used to further confirm the identification of these metabolites. The droplet probe allows for the identification of the chemistry of residues on archeological materials, and in turn, such data allow inferences regarding the potential original or final use of these artifacts.

Chapter three presents traditional isolation, purification, and structure elucidation of new and known secondary metabolites from an interesting marine derived *Periconia* sp. Studies on an organic extract of a marine fungus, *Periconia* sp. (strain G1144), led to the isolation of three halogenated cyclopentenes along with the known and recently reported rhytidhyester D; a series of spectrometric and spectroscopic techniques were used to elucidate these structures. Interestingly, two of these compounds represent tri-halogenated cyclopentene derivatives, which have been observed only rarely from Nature. The relative and absolute configurations of the compounds were established via mass spectrometry (MS), nuclear magnetic resonance (NMR)

spectroscopy, Mosher's esters method, optical rotation and GIAO NMR calculations, including correlation coefficient calculations and the use of both DP4+ and dJ DP4 analyses. Several of the isolated compounds were tested for activity in anti-parasitic, antimicrobial, quorum sensing inhibition, and cytotoxicity assays and found to be inactive.

Chapter four describes a distinct study to compare multiple artificial algae-based diets for honey bees with the goal of examining the differences and similarities to a traditional pollen-based diet. Managed honey bee colonies used for agricultural pollination are fed artificial diets to offset nutritional deficiencies related to landscape homogenization and climate change. In this study, we formulated novel microalgae diets using *Chlorella vulgaris* and *Arthrospira platensis* (spirulina) biomass and fed them to young adult honey bee workers. Diet-induced changes in bee metabolite profiles were studied relative to a natural pollen diet using LC-MS and GC-MS metabolomics approaches. The metabolomes of pollen- and microalgae-fed bees exhibited notable overlap, particularly upon subtraction of diet features that originated from the diet itself. Untargeted and targeted metabolomics identified a wide variety of metabolites that were influenced by diet, including complex lipids, essential fatty acids, and bioactive phytochemicals. The metabolomics results are useful to understand mechanisms underlying favorable growth performance as well as increased antioxidant and heat shock protein gene expression in bees fed the microalgae diets. The results showed that the tested microalgae have potential as sustainable feed additives and health-modulating natural products. Metabolomics-guided diet development could eventually help tailor feed interventions to achieve precision nutrition in honey bees and, more broadly, other livestock animals.

Chapter five presents findings from research related to antiparasitic drug discovery from filamentous fungi. *Plasmodium falciparum* is one of the protozoan parasites that causes malaria

in humans.[6-7] This disease infects nearly half of the world's population and was reported in 2021 to have roughly 241 million cases and induce more than half a million deaths.[8] Although the number of deaths caused by malaria has drastically dropped by 29% since 2010 among all groups, the number of cases per 1000 population at risk has hit a plateau in the last couple of years.[9] In addition, the emerging core drug resistance is a major concern resulting in a need for future drug development for safe and effective ways to kill the parasite.[10-11] In this Chapter, more than 40,000 fungal strains from a vast library (Mycosynthetix Inc.) were examined to evaluate their antiparasitic activity. The bests hits were processed by fermentation, dereplication, isolation, and structure elucidation, which led to a series of secondary metabolites with newly described antimalarial activities. More than 25 metabolites were evaluated (n=3) for their IC_{50} values against *P. falciparum*. Viridicatumtoxin A and class of compounds, termed leucinostatins, possessed the highest inhibition activity. To monitor the biosynthesis of leucinostatins *in situ* we used the droplet probe. We have also investigated the incorporation of $_L$-*F*-proline into the amino acid chain via precursor directed biosynthesis.

CHAPTER II: DROPLET PROBE: A NON-DESTRUCTIVE CHEMICAL RESIDUE

ANALYSIS OF WARI CERAMICS FROM THE IMPERIAL HEARTLAND

Kristóf B. Cank, Joshua M. Henkin, Anita G. Cook, and Nicholas H. Oberlies.

Introduction

The oldest known piece of pottery is from 20,000 years ago, at least 10 millennia before the emergence of agriculture [12]. Archeologists study these remains to better understand ancient culinary and subsistence practices, the role of feasting and commensal politics, and insights into local and regional lifestyles that in turn lead to inferences regarding regional economies and technologies [13-15]. Analytical techniques for organic residue analysis have been used to develop a deeper understanding of artifacts, and in the case of pottery, these methods can be used to examine the organic content preserved or absorbed on the surface, which may provide insights into their prehistoric use patterns [16-17]. During the 20th century, chemists started using spectroscopic and spectrometric tools for the investigation of archeological samples, including infrared (IR) spectroscopy, nuclear magnetic resonance (NMR) spectroscopy, and mass spectrometry (MS). A prominent example of the wealth of information attained using newer technology is the original analysis of amber and its reassessment two decades later [18-19]. NMR spectroscopy shed light on the variability of carbon functionalities within Dominican amber, thus helping researchers establish the relative chronology of the amber deposits in Dominican mining sites.

There are several analytical techniques that have been applied to archeological samples. Fourier-transform infrared spectroscopy (FT-IR) is one of the oldest and more widely used techniques to study organic residues preserved on the interior or exterior surface of a ceramic, particularly after such instruments became commercially available in the 1970s [20-21]. The IR spectrum can be used to distinguish between organic and non-organic residues or to determine the organic content in paints and pigments on ceramics [22]. It has the benefits of relatively low cost, rapid analysis, and non-destructive sample preparation. However, IR data mostly limits the identification to key functional groups, and thus, it does not give the same level of confidence that can be obtained through other analytical techniques.

A series of mass spectrometry and microscopy techniques have also been applied to archeology. Secondary ion mass spectrometry (SIMS), which provides elemental data and a cursory level of molecular information about residues, was first applied in the 1980s [23]. Some advantages are the wide elemental range and quantitative information that can be investigated. The performance of SIMS can be improved by coupling it to time-of-flight (TOF) mass analyzers; however, SIMS techniques have not been used extensively and require destruction of at least a small portion of the artifact [24]. The SIMS-TOF technique was successfully used in the past to provide information on pottery made by pre-colonial Indian tribes in Brazil [25]. Laser ablation inductively coupled plasma mass spectrometry (LA-ICP-MS) and laser induced breakdown spectroscopy (LIBS) can be considered micro-destructive [26]. Although these two methods are primarily used for analyzing elemental composition, they are highly beneficial techniques. As an example, prior to the development of LA-ICP-MS methods, archeologists struggled with finding a simple and cost-effective way to classify painted surfaces of American Southwest pottery [27]. Desorption electrospray ionization-mass spectrometry (DESI-MS) is

considered a soft-ionization technology. DESI-MS studies have facilitated the direct analysis of

proteins bounded to a surface, and this has led to a long lasting debate around preservation of

proteins on artifacts [28]. In short, there are several different types of mass spectrometry techniques

that have been used to glean information about the organic residues on archeological samples.

Such data shed light on the derivation and use of specific artifacts and allowed researchers to

provenance an even wider range of economic activities.

Currently, one of the more commonly used techniques is gas chromatography coupled to

mass spectrometry (i.e., GC-MS) [16, 29]. GC-MS is widely used for the analysis of small

molecules, such as steroids, alcohols, or fatty acids, and can be used to separate complex

mixtures, determine trace levels of organic residues, and/or perform quantitative experiments.

The adoption of GC-MS in the field of archeology dates to 1985, when it was used to identify the

pine wood origin of pitch found on King Henry VIII's shipwreck [30]. Since then, many studies

have targeted the identification of specific natural products from the residues of plant and animal

derived substances [31-33]. However, GC-MS is not without limitations, as it works best for

molecules that are easily volatilized, therefore limiting its usefulness with larger and/or polar

molecules. In most cases GC-MS requires sample preparation and is considered an invasive

method that can cause irreversible damage to the material being analyzed [34].

Other advances in chromatographic techniques can be used in a stand-alone fashion or

hyphenated to mass spectrometry for residue analysis. Direct analysis in real time mass

spectrometry (DART MS) is a fairly new technique [35], and it can perform direct analysis of

compounds that have been deposited or adsorbed on to surfaces such as plant materials, clothes

or even pesticides on vegetables [36]. While DART MS has been used for a variety of applications,

it is less commonly used for analysis of historical materials [37]. It does not require sample

preparation and only requires miniscule samples, making it a prominent technique for residue analysis [38-39]. In one of the earliest papers, DART MS was used for characterizing 16 reference papers of known manufacture in terms of pulp composition and pitch contaminants in the Library of Congress [40]. DART MS was also applied in many cases to identify dyes from various textile sources [41-44]. Another prominent example of the last decade would be when DART MS was applied for identifying the heme moiety to search for blood in an African Komo mask from the collections of the Detroit Institute of Arts [45]. That paper presents an excellent multi-analytical approach, where prior to DART MS, other spectroscopy techniques such as Raman Spectroscopy and FTIR were used.

Another technique that is wildly used in the field of residue analysis is liquid-chromatography-mass spectrometry (i.e. LC-MS). High-performance liquid chromatography coupled with mass spectrometry (HPLC-MS) can be used to characterize the lipid profile of entire archeological samples [46-47] or to identify dies from archeological textiles [48-49]. This approach has been shown to be beneficial for analyzing natural dyes from ancient Coptic textiles and historical textile fibers from the Silk Road [50-51]. Although HPLC-MS analysis also requires removal of material from the original sample, the amount needed for analysis in most cases is very small (e.g., less than 5 mm of yarn or thread used in case of textiles) [51]. Ceramics have been examined by HPLC-MS, either combined with other techniques [52-53] or in standalone manner. A notable example of the latter is the study of a well preserved Egyptian amphora, describing the red grape origin of the ancient Egyptian beverage [54]. Additional recent studies have used LC-MS to identify nicotine from a pipe that was more than a thousand years old and from miniature ceramic vessels from the Maya Area [55-56]. LC-MS was also recently used to find the first proteomic evidence of soybeans on sherds from the Middle East [57]. The value of LC-MS is quite

apparent, and for some experiments, LC-MS requires less sample preparation and less instrumentation time compared to GC-MS [55, 58].

While the aforementioned techniques possess numerous benefits for the analysis of chemical residues, the goal of this study was to examine artifacts in an innovative way that combines the benefits of chromatography and mass spectrometry but does so in a non-destructive manner that requires minimal or no sample preparation. The droplet-liquid microjunction-surface sampling probe (i.e., droplet probe) is an *in situ* LC-MS technique that analyzes a micro-extraction at the surface of an artifact (**Figure 1**). In doing so, the spatial information associated with the artifact is preserved. The technique is non-destructive, free from sample removal (i.e., no cutting or sectioning required), and thus, the materials are analyzed without sample preparation, directly under the droplet probe. [59-60]. This method has been applied to the *in situ* analysis of the chemistry of plants [61], cyanobacteria [62], and fungal cultures [59, 63-66]. Moreover, in a manner similar to ceramics, the droplet probe has been used for the chemical characterization of herbarium voucher specimens in a non-destructive manner [67]. In this study, we investigated 30 potsherds (**Table 1**) from the central highland Ayacucho valley to analyze their surfaces. Our goal was to identify any metabolites found on these ceramics, thereby providing data on their potential uses, but doing so in a non-destructive manner with a minimum of sample preparation, essentially analyzing the chemical residues directly via the droplet probe.
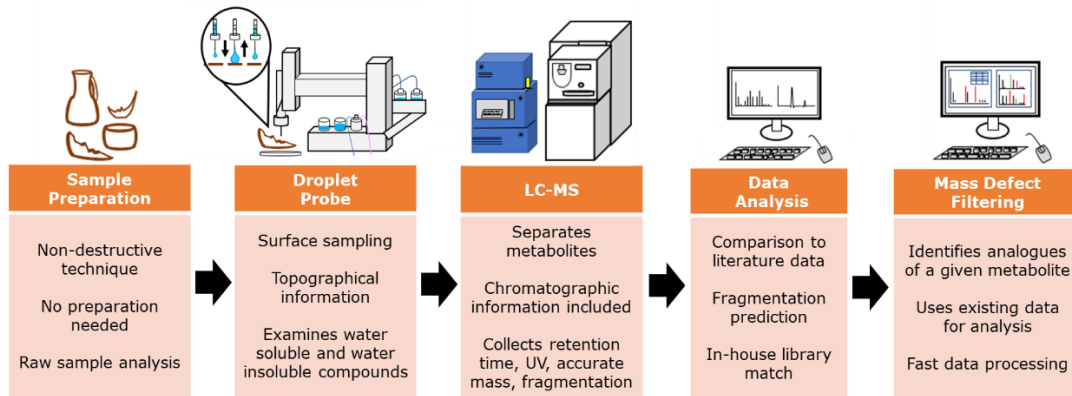
Figure 1. Schematic for the droplet probe analysis of Wari potsherds.

Experimental Section

Materials

The ceramic sherds in this analysis were from two archaeological sites in the central highland Ayacucho valley that date to the period of early empire formation in the Middle Horizon (c. 600-1000 CE). The pre-Columbian site of Huari is considered by most archaeologists as the capital of the first Andean Wari Empire. Across the valley is the second largest site of the period, namely Conchopata (**Figure 2**). A small artifact collection that was donated to the Anthropology Department at Catholic University of America represents materials from the surface of these two archaeological sites that were brought to the United States in the 1960's. The Department of Anthropology at Catholic University of America is the current custodian of these collections.

Figure 2. Excavation sites. a) Huari excavation areas photo taken in 2001, b) Conchopata excavations photo taken in 2001, c) and d) Huari excavations photos taken in 1977

The potsherds were analyzed via the droplet probe, an instrument adapted for natural product analysis in collaboration with the Organic and Biological Mass Spectrometry Group at Oak Ridge National Laboratory [59]. The system was created as detailed previously via conversion of a CTC/LEAP HTC PAL autosampler (LEAP Technologies Inc.) using in-house software [68-72]. The droplet probe analysis of the pot sherds was made using Fisher Optima LC-MS grade solvents consisting of 50:50 MeOH: H_2O. This ratio was developed to enhance the surface tension of the droplet, and variants were tested including 80:20 and 90:10 MeOH:H_2O. Consistent with other studies using this technique, we found that 50:50 MeOH:H_2O provided ample droplet retention on the syringe [59]. To analyze potsherds, no sample preparation was required. Instead, each sherd was placed on a glass surface under the instrument. The solvent mixture (5 µL) was drawn into the syringe, and approximately 4 µL of the droplet were dispensed onto the surface of the artifacts at 2 µL/s and withdrawn back into the needle. The dispense/withdrawal procedure was repeated twice at the same spot, thereby concentrating the micro extract. Repeated solvent exchange ensured longer time for surface/analyte/droplet exchange, and this was consistent with earlier studies of the droplet probe technique [59, 71]. In addition, in a few rare cases where the ceramic was too porous, we found that pre-wetting with a droplet that absorbed into the artifact, and then sampling with a second droplet on the same spot,

circumvented this problem. After analysis, the spot where the droplet probe performed the microextraction dried in a few seconds, leaving no damage to the surface that was observable by the naked eye (**Figure 3**).

Before Analysis   **During Analysis**   **After Analysis**
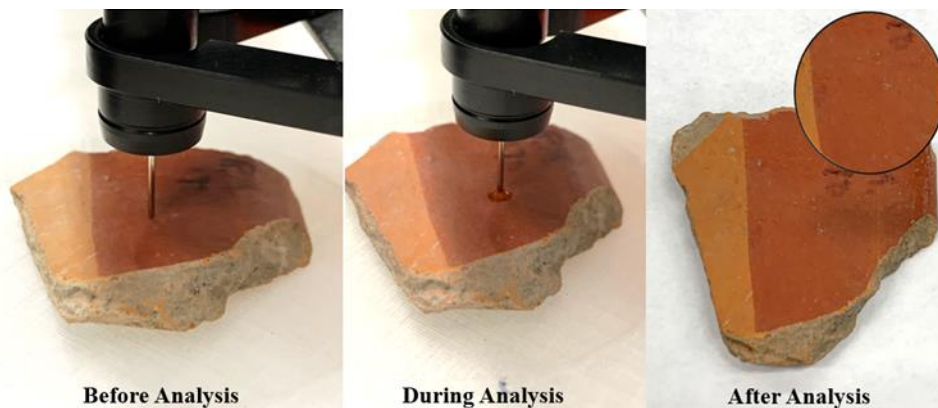
Figure 3. The sampling process via the droplet probe. To concentrate the sample, the droplet was released and retained on the same spot twice before injecting into the UPLC-MS system. The technique results in no visible sign of alteration of the surface of the examined sherds.

LC-MS-MDF Analysis

The droplet was injected into a Waters Acquity Ultraperformance Liquid Chromatography System (UPLC, Waters Corp.) coupled with a Thermo Q Exactive Plus MS (Thermo Fisher). The flow rate of the UPLC was set to 0.3 mL/min using a BEH C_{18} (2.1 x 50 mm x 1.7 µm) column equilibrated at 40 °C. The mobile phase consisted of Fisher Optima LC-MS grade CH_3CN-H_2O (with 0.1% formic acid). Over a period of 10 minutes, the analysis started at 15% CH_3CN and increased linearly to 100% CH_3CN over 8 minutes; it was then held at 100% CH_3CN over 1.5 minutes before returning to the starting conditions over 0.5 minutes. Photodiode-array (PDA) detection was used to acquire data from 200 to 500 nm with a resolution of 4 nm.

The Q Exactive Plus instrument using electrospray ionization (ESI) was used to collect high-resolution accurate mass measurements and fragmentations of the ions. The initial data

12

were collected from *m/z* 140 to 2000 at a mass resolution of 70,000 for both positive and negative mode, where the spray voltage was set to 3500 V (+) and 2500 V (-). For the fragmentation of ions, high-energy collision dissociation (HCD) was used.

The LC-MS data were analyzed in Xcalibur (Thermo Scientific, San Jose, CA, USA). Mass defect filtering was performed in Compound Discoverer software version 1.0 (Thermo Scientific, San Jose, CA, USA), and the fragments were compared to predicted data generated from ACD MS Fragmenter (Advanced Chemistry Development, Toronto, ON).

Results and Discussion

Droplet Probe Analysis of Peruvian Sherds

Potsherds were analyzed using the droplet probe, which consists of a surface sampling device coupled to an LC-MS system [59-60]. The analyzed samples include fragments of cups, bowls, a variety of spoons of different sizes, and a face-neck jar. Each piece was sampled a minimum of two times on the surface, representing both the inside and the outside of the artifacts. Using the droplet probe, a series of analytical data were collected for each sample, including retention time in a 10 minute reverse-phase UPLC chromatographic run, the full UV spectrum, the full-scan high resolution mass spectrum (i.e., HRMS), and the tandem mass spectrum (i.e., MS-MS). It total, 30 sherds were analyzed at least twice (once on the inside and once on the outside) for a minimum of 60 measurements (**Table 1**).

To start the process, we were unsure what compounds to seek out in the potsherds. Thus, an initial screening was performed, where we were simply looking for differences and similarities between the samples, and for this, base peak chromatograms were used as the starting point. From the initial sample set that consisted of 30 potsherds (**Table 1** and **3**), two artifacts, UNCG-17 and UNCG-27, displayed similar peaks in the ion chromatograms, indicating

13

compounds of potential interest (**Table 1**). To further represent the similarities between the two samples, untargeted LC-MS base peak chromatograms for both samples were individually aligned, filtered, and analyzed using MZmine 2.20 software [73]. Then, the results were compared in a graph using Altair Plotting Library (**Figure 8**). The displayed ion peaks had similar analytical data (i.e. similar retention time and accurate mass data). These data were only observed in these two samples, distinguishing them from the rest of the sample set (**Table 1**), and only on the inside of the sherds, with a trace amount on the outside of the sample.

Table 1. Ceramics from Wari collection sites analyzed with droplet probe. WA '69: sherd label refers to Wari 1969; Robles Moqo '70: refers to the Robles Moqo sector of Wari; Unknown: unlabeled sample; (?): rim is too small to determine exact shape; AP1: Airport Area 1 Conchopata. UNCG-17 and UNCG-27 are highlighted as they became the focus of these studies.

Sample ID	Sample Form	Provenience
UNCG-1	Open Bowl	WA '69
UNCG-2	Open Bowl	WA '69
UNCG-3	Cup	WA '69
UNCG-4	Small Cup	unknown
UNCG-5	Bowl (?)	Robles Moqo '70
UNCG-6	Cup	WA '69
UNCG-7	Open Bowl	Wari '69
UNCG-8	Cup	WA '69
UNCG-9	Open Bowl	WA '69
UNCG-10	Open Bowl	WA '69
UNCG-11	Face Neck Jar fragment	WA '69
UNCG-12	Small Cup bodysherd	RB '70
UNCG-13	Open Bowl fragment	WA '69

UNCG-14	Bowl fragment (?)	WA '69
UNCG-15	Possible jar fragment	WA '69
UNCG-16	Open Bowl	AP-1
UNCG-17	Open Bowl	AP-1
UNCG-18	Open Bowl	WA '69
UNCG-19	Bowl	WA '69
UNCG-20	Small cup (?)	WA '69
UNCG-21	Bodysherd	WA '69
UNCG-22	Bodysherd	WA '60
UNCG-23	Figurine Head fragment	WARI
UNCG-24	Cup base fragment	WA '69
UNCG-25	Cup base fragment	WA '69
UNCG-26	Large Spoon sherd	AP-2
UNCG-27	Medium Spoon sherd	AP-1
UNCG-28	Medium Spoon sherd	AP-1
UNCG-29	Small spoon sherd	AP-2
UNCG-30	Medium Spoon sherd	AP-2

Thus, these two samples were selected for further chemical analysis. The first sample is an interior decorated Huamanga style bowl (UNCG-17) while the other is a spoon fragment (UNCG-27) (**Figure 4**).

Figure 4. The vessel (UNCG-17) and spoon (UNCG-27) fragments were analyzed by the droplet probe (left images). The sherds were sampled multiple times with a droplet containing 50:50 MeOH:H2O. The white X's in the images on the right illustrate the spots that were sampled.

The data were analyzed in order of signal intensity of the ion peaks (**Figure 5**). The most intense signal, which had a retention time of 5.36 min, revealed HRMS data with the positively charged form of a molecule with a proton added (i.e., $[M + H]^+$) at m/z 445.2111, suggesting compound **1**. These data were used to calculate the molecular formula of **1** as $C_{27}H_{28}O_4N_2$, with a measured mass within 5 ppm of the calculated exact mass. The second most intense signal at 6.05 min was attributed to compound **2**, and its HRMS data were measured as m/z 507.2266 [M + H]$^+$, giving a molecular formula of $C_{32}H_{30}N_2O_4$, again within 5 ppm of the calculated value. At this stage, another key peak (i.e. compound **3**) was observed but was not yet identified; mass defect filtering, described in **3.2.**, was required to finalize its identification.
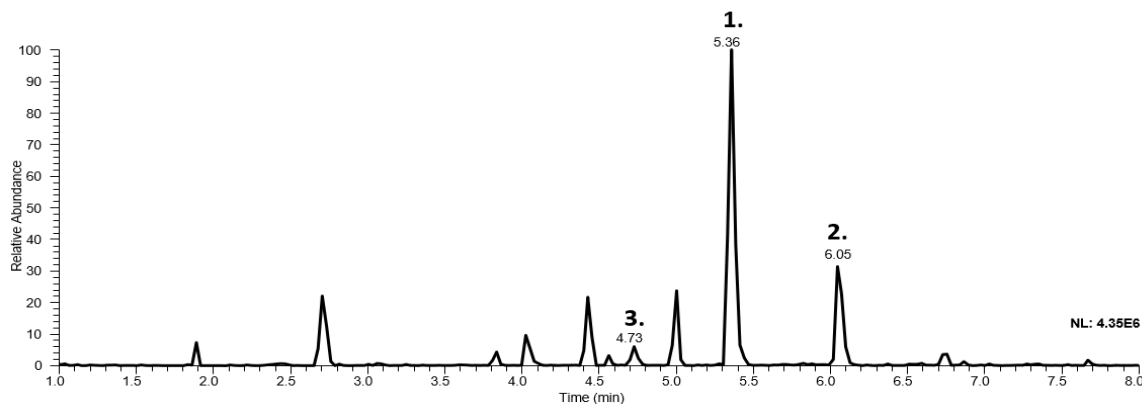
Figure 5. Droplet probe data from the analysis of the surface of the inside of an Andean spoon (UNCG-27). The figure depicts the base peak chromatographic data, with retention time on the X-axis and relative abundance, based on signal intensity in the mass spectrometer, on the Y-axis. Data were collected in (+) mode using HRESIMS. Background subtraction of the blank run was carried out on the data shown. Identified peaks are labeled according to the numbering of the compounds

As a next step, selected ion monitoring (SIM) of the molecular ion masses of **1** and **2** was conducted along with fragmentation of the compounds (**Figure 6**). Compounds with analogous structural features, and/or built from the same core, possess similarities between fragmentation patterns that are predictable [74]. To test this, the fragments were compared to a generated fragmentation pattern provided by ACD Labs Fragmenter software (**Table 4**). Based on accurate mass measurements, fragmentation, comparisons to predicted fragmentation patterns, and literature data [75-76], the compounds were identified as aurantiamide acetate (**1**) and aurantiamide benzoate (**2**) (**Figure 7**). For example, during the fragmentation of aurantiamide acetate (**1**) ($C_{27}H_{28}N_2O_4$), a key fragment that was both observed (i.e., *m/z* 194.1172) and predicted (i.e., *m/z* 194.1175) was the loss of the 2-(methylamino)-3-phenylproply acetate moiety (i.e., $C_{11}H_{16}NO_2$) (**Figure 9**). A similar match between measured (i.e., *m/z* 385.1900) and predicted (i.e., *m/z* 385.1910) fragmentation data corresponded to the loss of the acetate moiety in **1** (**Figure 9**). MS-

17

MS analysis of aurantiamide benzoate (i.e., compound **2**) also showed concordance with

measured vs predicted data (i.e., *m/z* 256.1338 and 256.1332 respectively) (**Figure 10**).
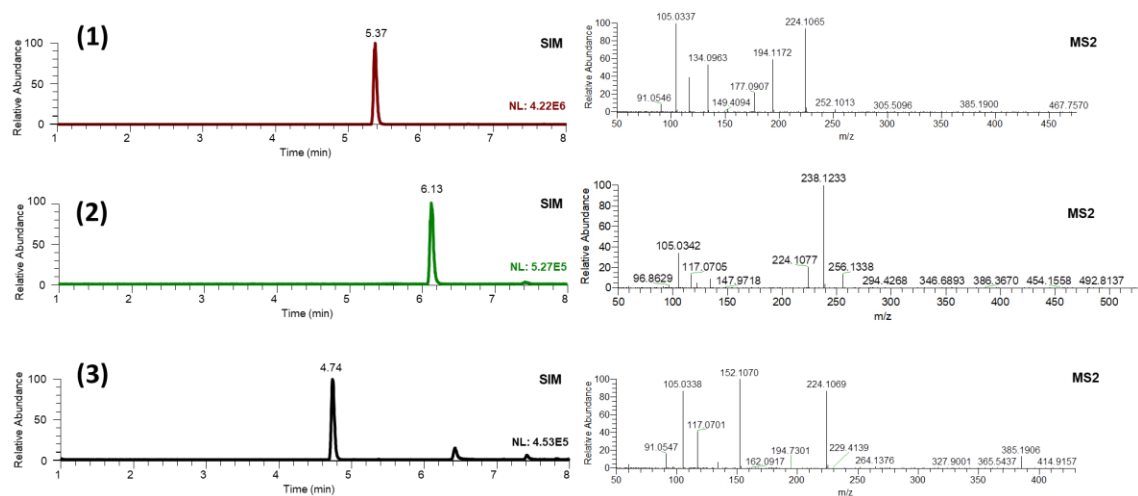
Figure 6. Selected ion chromatograms and high-resolution MS-MS data of compounds **1-3**. Since compound **3** possessed an extra alcohol functional group compared to **1** and **2**, it eluted earlier. The polarity of compounds correlates with their elution order, with **3** being the most polar and **2** being the least polar. This chromatographic data from an LC-MS system is often not reported in literature studies of chemical residue analysis; however, this use of orthogonal data further supports the identification of these compounds based on their physical properties.

Our laboratory maintains an in-house database of over 650 fungal metabolites [63, 77], and

from the LC-MS data, we have archived for each metabolite the UV-VIS spectrum,

chromatographic retention times, and both full-scan HRMS and MS-MS data in both positive

and negative electrospray ionization modes. Since aurantiamide benzoate (**2**) is known to be

produced by plant and fungal sources (see section: Ethnobotanical relevance of aurantiamide

analogues), we used our in-house standard to compare the data acquired for **2** (**Figure 11**)

Selected ion monitoring of **2** from the droplet probe analysis of the sherd and a full scan run of

the in-house standard were performed using identical experimental conditions, meaning the same

column and experimental parameters. The accurate mass and the MS-MS data matched to the in-

house standard, as well as predicted values, confirming the identification of the metabolite. Thus,

the identification of compound **2** is considered to be the first level of metabolite identification [78].

While standards for compound **1** were not available in house, it was identified as a putatively

annotated compound [78] based on the confluence of orthogonal data (i.e., accurate mass and

fragmentation pattern comparisons to predicted and literature values) [79].

Aurantiamide acetate (**1**)   Aurantiamide benzoate (**2**)   Aurantiamide (**3**)
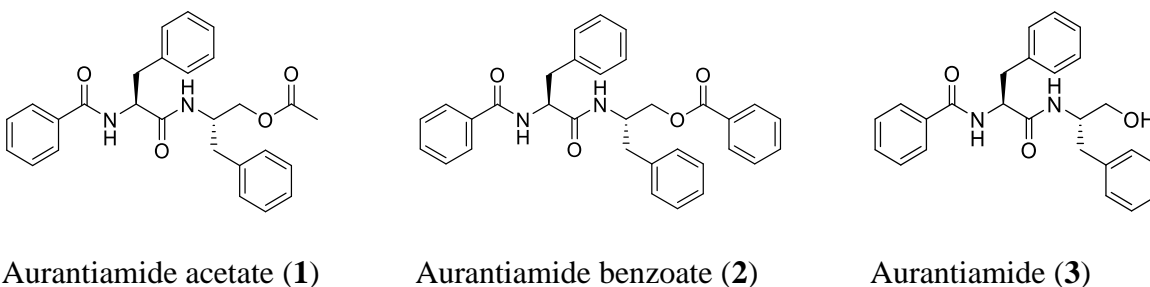
Figure 7. Structures of compounds that were identified via the droplet probe analysis of the archeological samples. Aurantiamide acetate (**1**) and aurantiamide benzoate (**2**) were present on the inside of the vessel, while all three aurantimide analogues (i.e., **1**-**3**) were identified on the inside of the spoon.

Mass Defect Filtering, as an Additional Tool for Compound Identification

While standards were available for the identification of **2**, this was not possible with

compound **3**. However, the structure of **3** was very similar to **1** and **2**. As such, mass defect

filtering was used to mine the droplet probe data as a complementary and orthogonal tool for the

identification of compound **3**. Mass defect filtering is a post-processing data mining technique

that relies upon high-resolution mass spectrometry data. The mass defect of a compound is

defined as the deviation of each atom's mass from the integer-rounded nominal mass; thus, each

element possesses a unique mass defect. That concept allows researchers to identify compounds

with high structural similarity by applying definable narrow ranges of change in the mass defect

dimension of high-resolution mass spectrometry data, regardless of the differences between the

fragmentation pattern or isotope distribution of the compounds [80-82]. The benefit of mass defect

filtering is that it helps to detect structurally related analogues [77], even if they are present at low

abundance in the sample, without further data collection or the requirement of a standard, as was the case with compound **3**. Once a potential compound has been identified, the characteristic fragmentation pattern of the analogues can be analyzed and compared to both the model structure and the literature [81-82].

Mass defect filtering was applied using aurantiamide acetate (**1**) as a model structure to seek other aurantiamide related analogues as residues on the vessel or spoon (**Figure 12**). The presence of compound **2** was confirmed in this manner. This is important, as we already had a standard of **2** in hand, and this confirmation of structure via mass defect filtering served to verify the approach. In a similar fashion, compound **3** was detected by applying a mass defect in the 150 mDa range and was identified as aurantiamide (i.e., **3**) with a $[M + H]^+$ value of *m/z* 403.2008, suggesting a molecular formula of $C_{25}H_{26}N_2O_3$ (**Figure 7**). MS-MS fragmentation of aurantiamide (**3**) showed a key fragment that was measured at *m/z* 152.1070; this matched the predicted value and was attributed to the loss of the 2-amino-3-phenylpropan-1-ol moiety, which was unique to this structure (**Figure 13**) [83]. It would have been easy to overlook this peak without the application of mass defect filtering. This fast, post-processing data mining technique can be applied easily to residue analysis after the collection of HRMS data for the discovery of additional metabolites. Moreover, the identification of three aurantiamide analogues as residues in two potsherds lends greater confidence in the relative importance of those compounds in the understanding of the use of these artifacts prehistorically.

Ethnobotanical Relevance of Aurantiamide Analogues

The three detected compounds on the surface of the spoon and vessel artifacts were aurantiamide acetate (**1**), aurantiamide benzoate (**2**) and aurantiamide (**3**) (**Figure 7**). All three compounds were predominantly found on the inside of the artifacts. Interestingly compound **2** was only found on the inside of the spoon (i.e., UNCG-27), while compounds **1** and **3** were present on the interior surface of both artifacts (i.e., UNCG-27 and UNCG-17). When looking at the exterior surfaces, the signal abundance of **1** and **3** were very low, which makes confirmation of their identification more challenging. Thus, one hypothesis could be that the presence of **1** and **3** on the outside could be due to handling of the artifacts before the analysis. The existence of these or similar chemical compounds on the surface of other examined pottery cannot be excluded simply because it is possible that the compounds are present at levels below the limit of detection. However, the identification of three related metabolites on the interior surfaces of service ware was quite surprising and unexpected, particularly because the sherds were collected from the surface of archaeological sites. We hypothesize that the spatially specific identification of metabolites from these ceramics, as compound **2** was only identified from the inside of the artifacts, while **1** and **3** were easily detected on the inside, was related to their employment for the storage and handling of some plant.

Looking at the origin of the molecules, aurantiamide and its analogues are widely spread across the Kingdom of Life and have been isolated from many different organisms, including: algae species, such as the red algae *Acanthophora spicifera*[76] or the brown algae *Cystoseira corniculata* [75] and several families of higher plants, such as Piperaceae [84], Moringaceae [85], and Euphorbiaceae [86]. Fungal species were also found to produce aurantiamides, and aurantiamide acetate was isolated from *Aspergillus* species such as *A. penicillodies* [87] and from a marine

21

Aspergillus spp. as well [88]. Since the list of natural sources for aurantiamides is extensive, we

focused on the relevant paleoethnobotanical and phytochemical literature. When limiting the

scope of the chemotaxonomic search to the genus level, the discovery of aurantiamides from

ceramic surfaces could potentially indicate the presence of *Capsicum* spp. (e.g., *Capsicum

annuum*), the sources of chili peppers and bell peppers, among others [89]; *Portulaca* spp. (e.g.,

Portulaca oleracea), the purslanes [90-91]; *Talinum* spp. (e.g., *Talinum triangulare*), the

flameflowers [92]; and *Sphagneticola* spp. (e.g., *Sphagneticola trilobata*), the creeping-oxeyes [93].

Table 2 summarizes the archaeological, biogeographical, chemotaxonomic, and

ethnobotanical/traditional use-based relevance of the plant genera reviewed as the most probable

artifactual residue source candidates, given the convincing identification of aurantiamides [83, 94-97].

Table 2. Archaeological, botanical, and phytochemical considerations for several plant genera that could account for residues from Huamanga/Late Huarpa style ceramics found as surface collections at Conchopata [a]Based on paleoethnobotanical research from the Wari site of Conchopata [98]; [b]Checks and exes represent the isolation or lack thereof demonstrated for aurantiamide and its acetate and benzoate derivatives; [c]While aurantiamides were isolated from the roots, which is not the main part used worldwide, this plant part can be employed in food/medicine.

Genus	Paleoethnobotanical presence from identified macrofossil evidence at Conchopata?[a]	Aurantiamides isolated from species native or naturalized in Peru?	Aurantiamides isolated from same plant parts with known humans use?	Aurantiamide, Aurantiamide acetate, Aurantiamide benzoate[b]
Capsicum spp.	✔	✔	✗	✔✔✔
Portulaca spp.	✔	✔	✔	✔✔✗
Talinum spp.	✗	✔	✔ [c]	✔✔✔
Sphagneticola spp.	✗	✔	✔	✔✔✗

Finally, fungal, eubacterial, or even algal sources of these aurantiamides cannot be completely discounted, as these compounds are biosynthesized broadly beyond flowering plants. However, if the presence of these compounds was due to non-specific soil contamination, it is curious that aurantiamides were not detected on the exteriors of the two ceramics for which they are present. What should not be completely discounted is the possibility that these aurantiamides are ultimately not from an angiosperm source. It is possible that the original contents of the artifacts studied were intentionally fermented or ultimately degraded by microorganisms, such as *Aspergillus* spp. or even *Streptomyces* spp., which could be responsible for the analytical results [87-88, 99-100].

Conclusion

The droplet probe, which is a microjunction-surface sampling probe coupled with a liquid chromatography system and mass spectrometry, was used for the first time to examine the chemical residues on archeological artifacts. Key aspects of this technique include the non-destructive nature of the measurements, the lack of sample preparation requirements, and the ability to generate orthogonal data with a single measurement, specifically chromatographic retention time, mass spectrometry data, and MS-MS data (i.e., fragmentation data). The use of mass defect filtering is an added benefit, allowing one to mine the LC-MS data in greater detail separate from the initial measurements. In this paper, three metabolites were identified, specifically aurantiamide acetate (**1**), aurantiamide benzoate (**2**) and aurantiamide (**3**), on the surface of Wari period sherds that are more than one thousand years old. The findings of these compounds on two separate samples that predominantly present on the 'inside' of the ceramics could provide ideas for further research into the potential use of such items.

23

Ultimately, this study demonstrated that the droplet probe can be used as a non-destructive screening tool for residue analysis of ceramics; potentially other artifact substrates could be examined. Follow-up work could be conducted with orthogonal analytical methods (e.g., optical microscopy, microCT, conventional chemical residue analysis) for the very same Huamanga/Late Huarpa spoon and bowl fragments if desired. Moreover, comparable sherds of the same style that may have better preservation and more detailed provenience data could be studied by droplet probe for comparison, with an eye towards identifying aurantiamides or other natural products of interest. Finally, droplet probe could be paired with other chromatography-mass spectrometry instruments or different ionization sources to see if varying these factors biases the surface chemistry observed.
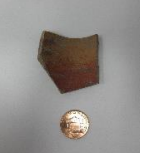
Based on previous experience examining natural products via the droplet probe, a MeOH:H_2O solvent mixture was used. Pragmatically, the H_2O was added to increase the surface tension of the droplet, providing enough droplet retention on the syringe, but it is quite possible that other solvent mixtures could be examined. Since only a small amount of solvent is injected into the system (i.e., ~4 µL), almost any solvent could be used. In this study, the isolated compounds (i.e., aurantiamides) were dipeptide derivates, which dissolved well in the solvent mixture. Depending on the type of study, solvents could be changed to acetone-water mixture (e.g., for lipids). In these cases, changing other factors might be warranted, for instance using an atmospheric pressure chemical ionization (APCI) source for lipid analysis. The parameters of such future studies depend heavily on the type of residue analysis one intends to conduct, and again, a benefit of the droplet probe is its ability to be paired with a variety of instrumentation.

The opportunity to analyze residues on ceramics, and to perform spatial mapping without destroying any part of the object, is highly beneficial. We posit that this non-destructive

approach to residue analysis could be welcomed by archaeologists interested in analyzing

samples from systematic excavations. It should be equally attractive to museum curators and

others exploring the research potential of museum collections. While this study focused on

ceramics, the droplet probe method has been applied to many different types of substrates (i.e.,

fungal cultures, plant specimens, herbarium vouchers and now ceramics), and thus, it is likely

applicable for the chemical residue analysis of different types of archeological materials.

Supplementary Data

Table 3. Analyzed potsherds from the central highland Ayacucho valley.

UNCG-1	UNCG-7	UNCG-13	UNCG-19	UNCG-25
UNCG-2	UNCG-8	UNCG-14	UNCG-20	UNCG-26
UNCG-3	UNCG-9	UNCG-15	UNCG-21	UNCG-27
UNCG-4	UNCG-10	UNCG-16	UNCG-22	UNCG-28
UNCG-5	UNCG-11	UNCG-17	UNCG-23	UNCG-29
UNCG-6	UNCG-12	UNCG-18	UNCG-24	UNCG-30
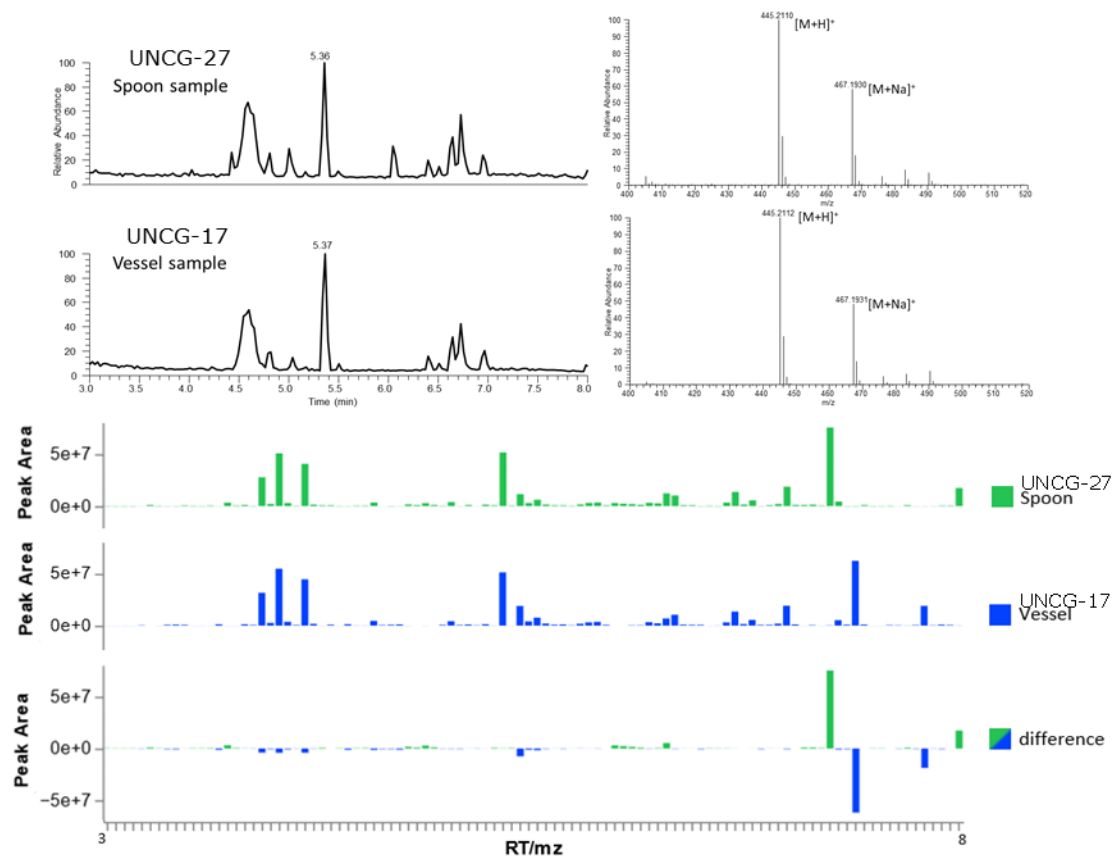
Figure 8. Similarities between the spoon (UNCG-27) and vessel (UNCG-17) samples. On the top left, the base peak chromatograms of both samples are shown without background subtraction. On the right, the mass spectra for those same two samples are shown at 5.36- and 5.37-minutes retention time; both are zoomed in the m/z 400 to 520 region, displaying ion peaks similarities, and thus compounds of potential interest. On the bottom, the similarities, and differences between peak areas using retention time over m/z values (RT/mz) of the samples are shown. This graph was generated by Altair Plotting Library after untargeted LC-MS base peak chromatograms for both samples were individually aligned, filtered, and analyzed using MZmine 2.20 software.

Table 4. Measured and predicted fragments for compounds **1-3**.

Compound 1		Compound 2		Compound 3	
$C_{27}H_{29}O_4N_2$		$C_{32}H_{31}N_2O_4$		$C_{25}H_{27}N_2O_3$	
m/z 445.2111 [M + H]$^+$		*m/z* 507.2266 [M + H]$^+$		*m/z* 403.2008 [M + H]$^+$	
(calcd for 445.2122)		(calcd for 507.2278)		(calcd for 403.2016)	
Measured **[M+H]$^+$ (*m/z*)**	**Predicted** **[M+H]$^+$ (*m/z*)**	**Measured** **[M+H]$^+$ (*m/z*)**	**Predicted** **[M+H]$^+$ (*m/z*)**	**Measured** **[M+H]$^+$ (*m/z*)**	**Predicted** **[M+H]$^+$ (*m/z*)**
91.0456	91.0542	59.7178	59.0128	91.0547	91.0542
105.0337	105.0335	105.0342	105.0335	105.0338	105.0335
117.0699	117.0699	117.0705	117.0699	117.0701	117.0699
134.0963	134.0964	122.0607	122.0362	134.0965	134.0964
152.1068	152.1070	134.0970	134.0362	152.1070	152.1070
177.0907	177.0910	224.1077	224.1070	224.1069	224.1070
194.1172	194.1176	238.1233	238.0988	225.1102	225.1149
224.1065	224.1070	239.1272	239.1179	264.1376	264.1305
385.1900	385.1911	256.1338	256.1332	385.1906	385.1911
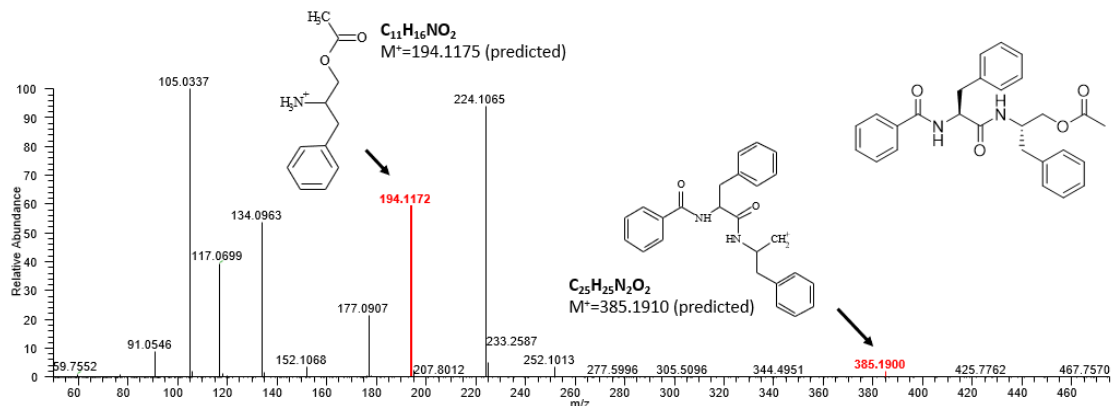
Figure 9. MS-MS data and key fragments of compound **1.**
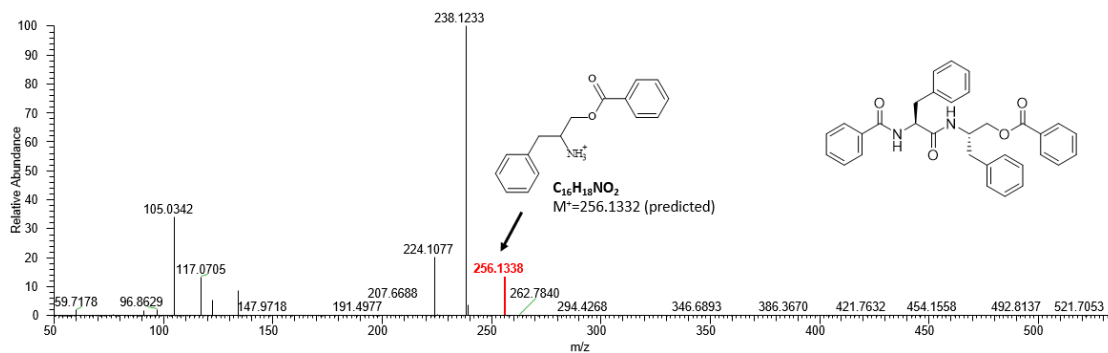
Figure 10. MS-MS data and key fragments of compound **2**.
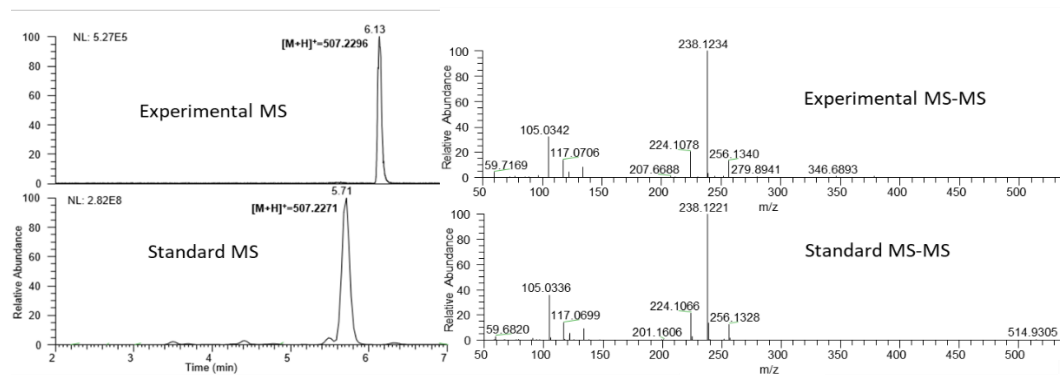
Figure 11. Comparison of compound **2** to an in-house standard. The slight retention time difference of 0.42 minutes of the standard compared to experimental is due to the more complex nature of the droplet probe instrument since it requires an extra length of pre-column tubing prior to UPLC analysis.

Formula	Predicted Compositions	Molecular Weight	RT [min]	Area (Max.)	Pattern Matches	Area
C27 H28 N2 O4	Full match	444.20349	5.352	451267.6195	C27H28O4N2	451267.6195
C32 H30 N2 O4	Full match	506.21928	6.05	188842.2755	C27H28O4N2	188842.2755
C21 H27 N O4	Full match	357.19289	6.73	186763.5864	C27H28O4N2	186763.5864
C20 H34 N2 O6	Full match	398.24243	6.63	169228.6319	C27H28O4N2	169228.6319
C24 H33 N O6	Full match	431.22978	5.501	46332.13801	C27H28O4N2	46332.13801
C16 H26 N6 O2	Full match	334.21102	6.612	36098.99005	C27H28O4N2	36098.99005
C24 H30 O6	Full match	414.20313	5.495	33404.29988	C27H28O4N2	33404.29988
C23 H26 N6 O2 S	Full match	450.18538	4.294	27630.74857	C27H28O4N2	27630.74857
C19 H22 N6 S	Full match	366.16445	3.808	25471.52926	C27H28O4N2	25471.52926
C25 H26 N2 O3	Full match	402.19318	4.721	20484.04297	C27H28O4N2	20484.04297
C25 H30 N6 O2 S	Full match	478.21681	4.972	19304.95832	C27H28O4N2	19304.95832
C26 H31 N5 S	Full match	445.23009	4.298	12967.97123	C27H28O4N2	12967.97123
C27 H39 N O4 S	Full match	473.26152	4.982	12846.07765	C27H28O4N2	12846.07765
C26 H37 N O6	Full match	459.26088	5.506	12076.56538	C27H28O4N2	12076.56538
C26 H32 N2 O S	Full match	420.22423	6.803	11780.06979	C27H28O4N2	11780.06979

Figure 12. Results of mass defect filtering. The highlighted rows are compounds **1-3**, respectively.
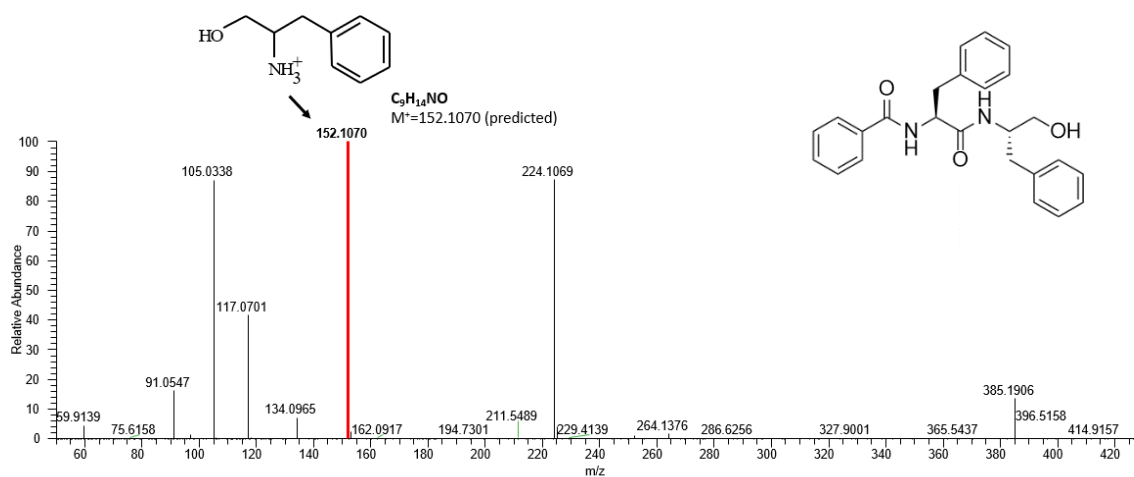
Figure 13. MS-MS data and key fragments of compound **3**.

CHAPTER III: POLYCHLORINATED CYCLOPENTENES FROM A MARINE DERIVED

PERICONIA SP. (STRAIN G1144)

Kristóf B. Cank, Robert A. Shepherd, Sonja L. Knowles, Manuel Rangel-Grimaldo, Huzefa A. Raja, Zoie L. Bunch, Nadja B. Cech, Christopher A. Rice, Dennis E. Kyle, Joseph O. Falkinham, III, Joanna E. Burdette, Nicholas H. Oberlies

Introduction

Marine and freshwater derived fungi are a rich and diverse source of specialized metabolites [101-102]. *Periconia* spp. are mitosporic (i.e., asexual) ascomycetes that occur in a variety of ecological niches. For example, they have been isolated as endophytes, pathogens [103] and saprobes [104] from both terrestrial [105] and aquatic habitats, including both marine [106] and fresh water [107]. Members of this genus are well known to biosynthesize compounds with diverse biological properties, including anti-inflammatory, antimicrobial, and anti-human immunodeficiency virus (HIV) activities [108]. In addition, a wide range of fungal metabolites have been isolated, which include sesquiterpenes and cytochalasins to diterpenoids and dihydroisocoumarins [109-113], suggesting that such fungi have rich biosynthetic capabilities [114].

Halogenated metabolites have been isolated in abundance from marine organisms, likely due to the availability of chloride (~19000 ppm) and bromide (~65 ppm) ions in seawater [115-118]. Examples of halogenated polyketide derivatives include the cyclopentones, cryptosporiopsinol and cryptosporiopsin [119], or the more recently reported cyclopericodiol [120]. Of these, cryptosporiopsinol was first described from *P. macrospinosa* over a half century ago [119];

31

however, since then, the compound has been under investigated in the literature, leading to some ambiguity in the absolute configuration of stereoisomers and/or closely related analogues [121-127].

During ongoing studies of fungal metabolites from specimens collected from aquatic habitats throughout North Carolina [64, 101, 128-130], an interesting, purple-colored marine derived mitosporic fungus was isolated from decomposing *Spartina* stems that was identified as a *Periconia* sp. (strain G1144). In addition to the typical suite of HRMS and 2D-NMR experiments used for structure elucidation of natural products, a series of orthogonal techniques, such as Mosher's esters methodology [131] and GIAO (gauge-including atomic orbitals) NMR calculations [132-139], including correlation coefficient, DP4+ [140] and dJ DP4 calculations [141], were used to ascertain the absolute configuration of these fungal metabolites.

Results and Discussion

The fungal culture (strain G1144) displayed a deep purple color when grown on agar media (**Figure 49**). This striking characteristic, and the lack of hits when this extract was analyzed via dereplication against an in-house database of over 625 fungal metabolites [63, 77], stimulated further studies. Traditional chromatographic protocols led to the isolation of four chlorine containing cyclopentenes (**1-4**). Compounds **1** and **2** represent previously undescribed tri-halogenated cyclopentene derivatives, while compounds **3** and **4** were stereoisomers of the known compound, cryptosporiopsinol [119, 122-123].
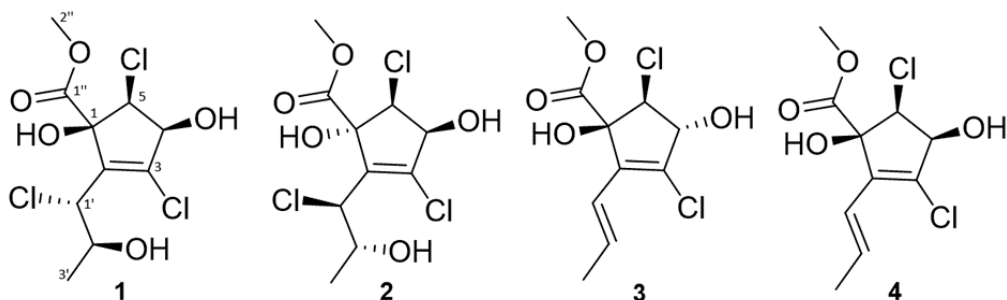
Figure 14. Structures of Compounds **1**-**4** isolated from *Periconia* sp. (strain G1144)

Compound **1** was obtained as an opaque solid material, and the molecular formula was established as $C_{10}H_{13}Cl_3O_5$ based on HRESIMS and NMR data, indicating an index of hydrogen deficiency of 3 (**Figure 18** and **19**). The molecular ion peak in the HRESIMS data showed the characteristic isotopic pattern for three chlorine atoms in the molecule (**Figure 18**). NMR data from ^1H, ^{13}C, and HSQC experiments indicated the presence of a methoxy ester (δ_H/δ_C 3.91/54.5 and a carbonyl group δ_C 171.9), plus two more signals (δ_C 137.7 and 140.4) that were indicative of a fully substituted double bond. COSY correlations between H-4 and H-5, in addition to HMBC correlations between H-5 and both C-1 and C-1″, were suggestive of a cyclopentene ring (**Figures 15**, **21**, and **22**), with the latter correlation serving to demonstrate the connection point of the methoxy ester side chain. Additionally, the chemical shifts in the ^1H and ^{13}C NMR spectra for signals attributable to the cyclopentene core were nearly identical to what was observed in cryptosporiopsinol [119, 122] and in the recently described rhytidhyester D [142], particularly for δ_{C-1} 88.2, δ_{C-2} 137.7, $\delta_{H-4}/\delta_{C-4}$ 4.47/76.0 and $\delta_{H-5}/\delta_{C-5}$ 4.43/65.0 (Table 53). The aliphatic side chain of the molecule was verified with the COSY correlations for the spin system between H-1′ to H-2′ to H-3′, and the connection of this chain to the cyclopentene core at position C-2 was supported by HMBC correlations between H-1′ to C-1 and C-3 (**Figures 15**, **24**, and **25**). The position of the hydroxy group at C-4 was noted based on COSY cross peaks between H-4 and 4-OH (**Figure**

25). The other two hydroxy groups were assigned based on the significantly different chemical shifts of 1-OH ($\delta_{\text{1-OH}}$ 4.12), which was more deshielded since it was adjacent to both the ester carbonyl and the vinyl moiety compared to 2'-OH ($\delta_{\text{2'-OH}}$ 1.95), which was on the aliphatic side chain (**Table 5**). Since $\delta_{\text{2'-OH}}$ was a broad singlet when $CDCl_3$ was used as a solvent, NMR data were also collected using DMSO-d_6 (**Figures 24-26**). ^{1}H NMR and HSQC data obtained in this aprotic solvent clearly showed the presence of three hydroxy groups with the signals for 2'-OH and 4-OH being doublets and that of 1-OH being a singlet (**Figure 24**). The 1D and 2D NMR data (**Table 5**) were used to elucidate the planar structure of **1**, and the relative configuration was suggested based on NOESY data collected in DMSO-d_6, which showed correlations between all three hydroxy protons (i.e., 1-OH, 4-OH, and 2'-OH) (**Figures 16** and **26**).

To determine the absolute configuration of **1**, both experimental and theoretical approaches were pursued. First, the configuration of the secondary hydroxy moieties (i.e., 4-OH and 2'-OH) were explored via Mosher's esters analysis. Both positions were highly reactive to Mosher's reagent, resulting in an excessively complex data set; this observation was also true for the Mosher's ester analysis of compound **3-4**. As such, we used half as much reagent (i.e. 10 µl instead of 20 µl), and for all compounds examined in this study, the reaction favored the 4-OH position. Thus, compound **1** was derivatized at the 4-OH position with both *S*- and *R*-3,3,3-trifluoro-2-methoxy-2-phenylpropanoic acid (MTPA), establishing the configuration as 4*R* (**Figure 17**). Pairing this result with the NOESY correlations between 4-OH and 2'-OH (**Figure 26**) established the 2'-position as *S*. In addition, these data were further verified using GIAO (i.e., correlation coefficient and DP4+) calculations (**Figure 53**). These calculations were in agreement with each other (**Tables 8** and **48**), suggesting that **1** was either 1*S,* 4*R,* 5*S,* 1'*R,* 2'*S* or 1*R* 4*S,* 5*R* ,1'*S,* 2'*R* (**Table 42**); the former assignments were supported by the Mosher's esters

data (**Figure 17**). In addition, optical rotation calculations were used to distinguish between these enantiomers. The calculated and specific rotation of **1** [i.e., $[\alpha]D^{20}$ +53 vs $[\alpha]D^{20}$ +158 (c 0.10, CHCl$_3$); **Table 46**] further verified the absolute configuration as 1*S,* 4*R*, 5*S,* 1'*R*, 2'*S*. Compound **1** was ascribed the trivial name cryptosporiopsinol C.

Table 5. ^{1}H and ^{13}C NMR Data of Compounds **1-4**

Pos.	1 δ$_C$, type	1 δ$_H$ (*J* in Hz)	2 δ$_C$, type	2 δ$_H$ (*J* in Hz)	3 δ$_C$, type	3 δ$_H$ (*J* in Hz)	4 δ$_C$, type	4 δ$_H$ (*J* in Hz)
1	88.2, C	-	86.6, C	-	80.4, C	-	87.3, C	-
2	137.7, C	-	137.5, C	-	134.8, C	-	133.1, C	-
3	140.4, C	-	142.1, C	-	134.0, C	-	137.0, C	-
4	76.0, CH	4.47, bs	75.8, CH	4.52, dd (12.1, 6.5)	80.5, CH	4.80, d (5.9)	75.5, CH	4.47, br s
5	65.0, CH	4.43, d (6.4)	64.9, CH	4.47, d (6.5)	67.9, CH	4.33, d (6.0)	66.0, CH	4.47, br s
1'	57.1, CH	4.51, d (7.3)	59.5, CH	4.82, d (6.7)	121.0, CH	6.18, m	120.6, CH	6.17, m
2'	69.5, CH	4.33, p (6.4)	70.0, CH	4.20, m	132.5, CH	5.93, dq (15.7, 6.6)	134.55, CH	6.17, m
3'	20.9, CH$_3$	1.34, d (6.2)	19.8, CH$_3$	1.33, d (6.4)	19.3, CH$_3$	1.81, d (7.2)	19.5, CH$_3$	1.82, d (5.1)
1"	171.9, C	-	171.9, C	-	173.0, C	-	172.1, C	-
2"	54.5, CH$_3$	3.91, s	54.6, CH$_3$	3.92, s	53.9, CH$_3$	3.82, s	54.6, CH$_3$	3.91, s
1-OH	-	4.12 s	-	5.11, s	-	-	-	-
4-OH	-	3.43, d	-	3.47, d	-	-	-	-
2'-OH	-	1.95 s	-	3.10 d	-	-	-	-

^{a} CDCl$_3$ (^{1}H NMR 400 MHz, ^{13}C NMR 100 MHz).
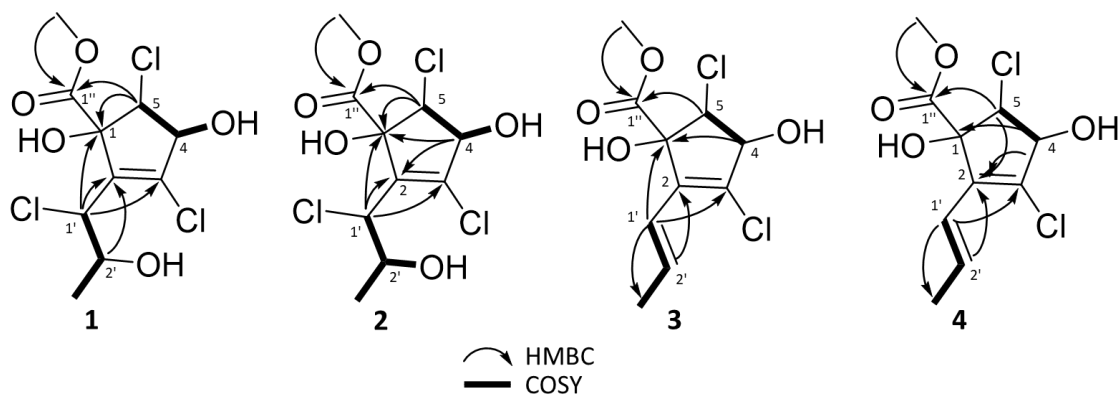
Figure 15. Key HMBC and COSY correlations for compounds **1-4**
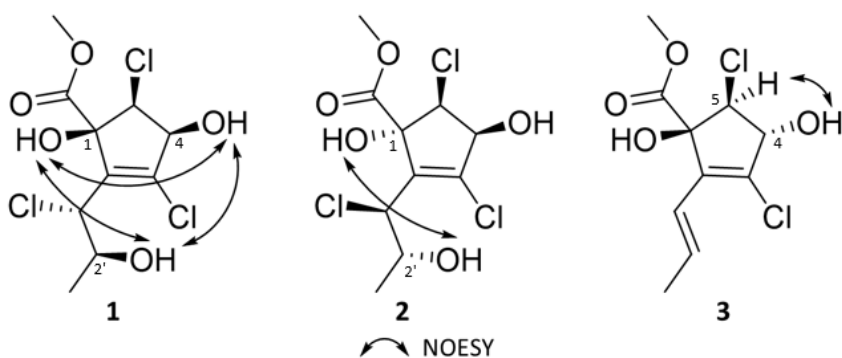
Figure 16. Key NOESY correlations for compound **1-3**
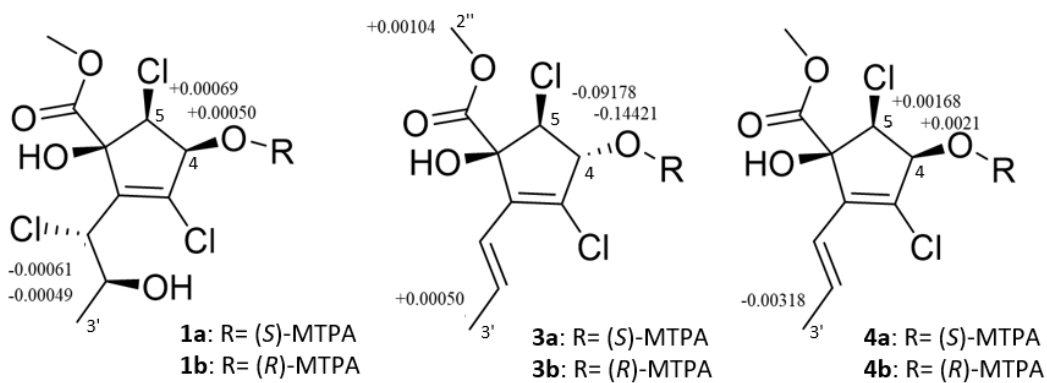
Figure 17. ΔδH values (Δδ = δS − δR) obtained for (*S*)- and (*R*)-MTPA esters of **1**, **3** and **4** in pyridine-$_{d5}$.

Compound **2** was isolated as an opaque solid material and had a molecular formula of $C_{10}H_{13}Cl_3O_5$, identical to **1**. HRESIMS data of **2** and **1** were also identical (**Figures 27** and **28**), but the slight differences in the ^{1}H and ^{13}C NMR chemical shifts (**Table 5**) indicated a stereoisomeric relationship (**Figure 29**). In fact, the HMBC correlations also showed similarities to **1**, but additional correlations were observed between H-4 to both C-1 and C-2 (**Figures 15** and **31**). COSY correlations between 2'-OH and H-2' along with 4-OH and H-4 confirmed the positions of the hydroxy groups (**Figure 15**). The relative configuration of **2** was suggested based on NOESY correlations between 1-OH and 2'-OH (**Figures 16** and **33**).

To determine the absolute configuration of **2**, Mosher's esters analysis of the compound was not possible due to paucity of sample. Thus, the knowledge base from determining the absolute configuration of **1** was leveraged by using the same approach for **2**, including the calculation of both correlation coefficient and DP4+ probabilities. For GIAO NMR calculations based on the NOESY results, 16 conformers were analyzed (**Figure 53**), where the correlation coefficient and DP4+ calculations were in agreement, indicating a configuration of either 1*S*, 4*S*, 5*R*, 1'*R*, 2'*S* or 1*R*, 4*R*, 5*S*, 1'*S*, 2'*R* (**Tables 11** and **47**). These findings were refined by examining the calculated and specific rotation of **2** [i.e., $[\alpha]D^{20}$ -10 vs $[\alpha]D^{20}$ -47 (c 0.10, CHCl$_3$); **Table 46**], thereby deducing the absolute configuration as 1*R*, 4*R*, 5*S*, 1'*S*, 2'*R*. Compound **2** was ascribed the trivial name cryptosporiopsinol D.

Compound **3**, also an opaque solid material, had an additional point of unsaturation, relative to **1** and **2**, as noted by the index of hydrogen deficiency of 4, which was derived from the formula of $C_{10}H_{12}Cl_2O_4$ based on HRESIMS and NMR data (**Figure 34** and **35**). The molecular ion peak in the HRESIMS data showed the characteristic isotopic pattern for two chlorine atoms in the molecule (**Figure 34**). The planar structure of **3** (**Table 5**) was found to be

38

similar to **1** and **2** based on ^{1}H and ^{13}C NMR data (**Figure 35**). The difference was that

compound **3** had five sp^2 carbons (δ_{C-2} 134.8, δ_{C-3} 134.0, $\delta_{C-1'}$ 121.0, $\delta_{C-2'}$ 132.5 and $\delta_{C-1''}$ 173.0) as

opposed to three observed in **1** and **2**, which was consistent with a double bond between C-1' and

C-2', possibly via the loss of a chlorine atom and hydroxy group, relative to **1** and **2**, as noted in

the molecular formula. This double bond was *trans* as noted by the *J* value of 15.7 Hz. COSY

correlations between H-1' and H-2', in combination with the HMBC correlations from H-1' to C-

2 and C-3 and from H-2' to C-2, confirmed the connection of the sidechain (**Figures 15**, **38**, and

39) to the core. Since 1-OH and 4-OH were observable in neither CDCl$_3$ nor CD$_3$OD, additional

NMR data were collected in DMSO-d_6 (**Figures 40** and **41**). Those ^{1}H NMR and COSY data

showed the presence of two hydroxy groups, with 1-OH being a singlet and 4-OH being a

doublet (**Figure 39**). The relative configuration of **3** was suggested based on NOESY data that

showed correlations between 4-OH and H-5 (**Figure 16**).

To examine the absolute configuration of **3**, Mosher's esters analysis was conducted, as

noted for **1**, establishing the configuration at position C-4 as *S* (**Figure 17**). Next, to further

examine the absolute configuration (i.e., positions C-1, C-4, and C-5), three different NMR

calculation methods were tested. First, the four possible conformers were submitted for GIAO

NMR calculations (**Figure 53**). The correlation coefficient calculations showed that the

conformer with the highest probability was 1*S*, 4*S*, 5*S* (99.75%) (**Table 14**). Then, the DP4+

method was examined, and this also yielded a likely configuration of 1*S*, 4*S*, 5*S* (**Table 47**).

Importantly, this configuration was different than that of, cryptosporiopsinol at position C-5,

which was determined by X-ray crystallography to be 1*S*, 4*S*, 5*R* [119]. In addition, a more recent

paper was published on what was termed (+)-cryptosporiopsinol, but the absolute configuration

was not established in that paper [126]. To further strengthen our findings, dJ DP4 calculations

were also conducted, which included DP4+ with direct $^3J_{HH}$ couplings, as detailed in recent literature [141]. This method has the added benefit of high performance while being more affordable in terms of computational cost [141]. The absolute configuration as determined by dJ DP4 calculations of **3** were in agreement (**Table 49**) with those noted above for the DP4+ and correlation coefficient calculations. Finally, optical rotation calculations and the results of Mosher's esters analysis (i.e., 4*S*) were used to distinguish between enantiomers. The calculated and specific rotation of **3** agreed with a configuration of 1*S,* 4*S,* 5*S* (i.e., $[\alpha]D^{20}$ +48 vs $[\alpha]D^{20}$ +166 (c 0.10, CHCl$_3$); **Table 46**). Compound **3** was ascribed the trivial name cryptosporiopsinol B.

Compound **4** was isolated as a colorless solid material and had a molecular formula of $C_{10}H_{12}Cl_2O_4$, the same as **3**. The HRESIMS data of **4** and **3** were identical (**Figures 42** and **43**), but differences between their ^1H and ^{13}C NMR data suggested a stereoisomeric relationship (**Figures 35** and **43**), although the COSY and HMBC correlations of **4** and **3** were nearly identical (**Figures 46** and **47**). Additional key HMBC correlations were observed between H-4 and C-2 and between H-5 and C-2 (**Figure 15**). To establish the presence of the hydroxy groups, additional ^1H NMR data were collected in DMSO-d_6. (**Figure 48**).

As with **1** and **3**, the absolute configuration of **4** was first examined by Mosher's esters analysis, establishing the configuration of the 4 position as *R* (**Figure 17**). Then, the absolute configuration could be probed at positions 1 and 5 (i.e., four possible conformers) using GIAO NMR calculations (**Figure 53**). The results of the correlation coefficient and DP4+ calculations were in agreement, suggesting an absolute configuration of 1*S*, 4*R*, 5*S* (or its enantiomer, 1*R*, 4*S*, 5*R*; **Tables 17** and **47**). Since δ_{H-4} and δ_{H-5} were overlapping, incorporating the $^3J_{HH}$ coupling constant into the DP4 calculations (i.e., dJ DP4) was not possible. Thus, optical rotation

40

calculations, and the results of Mosher's esters analysis, were used to distinguish between enantiomers (**Figure 17**). The specific rotation of **4** agreed with the calculated values, establishing the absolute configuration of the molecule as 1*S* 4*R* 5*S* (i.e., $[\alpha]D^{20}$ +55 vs $[\alpha]D^{20}$ +347 (c 0.10, CHCl$_3$); (**Table 46**). In conclusion, compound **4** was shown to be identical to rhytidhyester D, a stereoisomer of cryptosporiopsinol, which was described recently from an unrelated endophytic fungus (*Rhytidhysteron* sp. from *Leptospermum brachyandrum*) at the same time this study was ongoing [142].

Compounds **1**-**4** were biosynthesized from a single isolate of strain G1144, which was isolated from decomposing *Spartina* culms collected from a marine habitat. Thus, we are not entirely certain if G1144 is a true marine species in the strict sense (Overy et al., 2019; Pang et al., 2016). When the strain was cultured in peptone yeast media with 30 ppt sea salts, the fungus displayed healthy growth after three weeks. However, the strain also grew abundantly on distilled water media without sea salts (**Figure 49**). For the present study, we refer to this fungus as marine-derived, rather than a true obligate marine fungus, until additional ecological studies are carried out to determine the accurate ecology of *Periconia* sp. (strain G1144) (Overy et al., 2019; Pang et al., 2016). This conservative approach seems warranted given the fact that other *Periconia* spp. have been isolated from a variety of terrestrial and aquatic habitats.

These compounds (**1**-**4**) were isolated from a culture grown on solid rice media, where 30 ppt sea salts in distilled water were added prior to sterilizing via autoclave (see section: Fermentation, Extraction, and Isolation). An obvious question concerned whether sea salts were required to produce these chlorinated analogues. We analyzed retrospectively the extracts of this fungus grown on various media types (Amrine et al., 2018; Graf et al., 2020), so as to examine if **1**-**4** were present in growths where sea salts were not added. Interestingly, we were not able to

41

detect **1**-**4** on any other media type except when cultures were grown on rice media with 30 ppt

sea salts (**Figure 51**). Furthermore, we explored if the dechlorinated versions of **1**-**4** were present

on any media types where salts were not added (**Figure 52**), and indeed, we were able to detect

the accurate mass of the dechlorinated versions of **3** and **4** via extracted ion chromatograms

(XIC). This suggests that this fungus has the capacity to produce the dechlorinated versions of

these compounds, depending on media types. Regardless, since we were only able to detect **1**-**4**

when 30 ppt sea salts were included in the media, we hypothesize that this salt content was

needed for the organism to incorporate chlorine into the molecules, which supports similar

observations by (Henderson and Hill, 1982). Biosynthetically, those same authors proposed that

the chlorine is incorporated in cryptosporiopsinol (a stereoisomer of **3** and **4**) in one of the early

steps of the biosynthetic pathway.

Biological activity of **1**–**4** was not observed in any of the assays employed herein. They

were neither cytotoxic against a panel of cancer cell lines (IC$_{50}$ > 25 µM, **Table 50**) nor

antimicrobial against a broad series of pathogenic microorganisms (MIC > 125µg/mL, **Table

51**). The compounds were also screened against *Naegleria fowleri*, a pathogenic amoeba that is

responsible for a rapidly progressive central nervous disease called primary amebic

meningoencephalitis [143], but all were inactive (IC$_{50}$ > 25 µM) (**Table 52**). Quorum sensing

inhibition of **1** and **4** was evaluated, similar to what was described previously by Figueroa et al.

[144], and no significant inhibition of quorum sensing was observed for these compounds against a

clinical isolate of methicillin-resistant *Staphylococcus aureus* (MRSA) (**Figures 54-57**).

Conclusion

This paper explored the rich diversity of fungal metabolites obtained from *Periconia* spp. with the identification of three undescribed and one recently described compounds. The structures and absolute configurations of **1**–**4** were determined by evaluating 1D and 2D NMR data, mass spectrometry data, optical rotation calculations, Mosher's esters analysis and GIAO NMR calculations, including correlation coefficient, DP4+ and dJ DP4 calculations. Despite testing the metabolites against a suite of cytotoxicity, antimicrobial, antiparasitic, and quorum sensing inhibition assays, the potential biological activity of these structurally interesting fungal metabolites remains undetermined and is a topic that warrants further study.

Experimental

General Experimental Procedures

UV, and optical rotation data were obtained using a Varian Cary 100 Bio UV−Vis spectrophotometer (Varian Inc.), and a Rudolph Research Autopol (II) polarimeter (Rudolph Research Analytical), respectively. Flash chromatography was performed on a Teledyne ISCO CombiFlash Rf 200 using Silica Gold columns (both from Teledyne ISCO) and monitored by both UV and evaporative light-scattering detectors. Phenomenex Gemini-NX C18 analytical (5 μm; 250 × 4.6 mm), semipreparative (5 μm; 250 × 10.0 mm) and preparative (5 μm; 250 × 21.2 mm), columns (Phenomenex) were used on a Varian Prostar HPLC system equipped with ProStar 210 pumps and a Prostar 335 photodiode array detector (PDA), with data collected and analyzed using Galaxie Chromatography Workstation software (version 1.9.3.2, Varian Inc.). A Waters Acquity UPLC system (Waters Corp.) utilizing a Phenomenex Kinetex C18 column (1.3 μm; 50 × 2.1 mm) was used to evaluate the purity of the isolated compounds with data collected

and analyzed using the Thermo Fisher Scientific Xcalibur data acquisition software (Thermo Fisher Scientific). HRMS analysis utilized either a Thermo Fisher Scientific LTQ Orbitrap XL mass spectrometer or a Thermo Fisher Scientific Q Exactive Plus mass spectrometer, both equipped with an electrospray ionization source (Thermo Fisher Scientific). NMR data were collected using either a JEOL ECS-400 MHz NMR spectrometer operating at 400 MHz for ^{1}H and 100 MHz for ^{13}C, a JEOL ECA-500 MHz NMR spectrometer operating at 500 MHz for ^{1}H and 125 MHz for ^{13}C (JEOL Ltd.), or an Agilent 700 MHz NMR spectrometer (Agilent Technologies) equipped with a cryoprobe, operating at 700 MHz for ^{1}H and 175 MHz for ^{13}C. Residual solvent signals of CDCl$_3$ ($\delta_H = 7.260$ and $\delta_C = 77.160$) were utilized for referencing.

Fungal Strain Isolation and Identification

Strain G1144 was obtained from senescent brown ascospores scattered on the surface of decomposed *Spartina* culms, which were collected from Holden Beach, North Carolina, USA in July of 2020. In brief, the senescent ascospores were located with a dissecting microscope, picked with a sterile needle, and spread onto antibiotic water agar [144]. Upon germination, the ascospores were transferred aseptically onto peptone yeast glucose with 30 ppt Instant Ocean (hereafter referred to as sea salts). Examination of strain G1144 on different nutrient media from Difco, corn meal agar, Czapek-Dox agar, peptone yeast glucose with 30 ppt sea salts (30g sea salts in 1000 ml of distilled water), oatmeal agar, and potato dextrose agar with autoclaved balsa (**Figure 49**) did not reveal any sexual or asexual structures on nutrient media for phenotypic identification. Thus, the fungus was identified via molecular methods coupled with Maximum Likelihood analysis using methods outlined previously [145]. The internal transcribed spacer region (ITS 1 & 2 and 5.8S nrDNA) was PCR amplified and sequenced using primers ITS1F and ITS4 [145-147]; two sequences of the same strain were obtained for quality control. A BLAST search of

44

the ITS data in NCBI GenBank revealed ≥95% sequence similarity with members of the genus

Periconia Tode. Therefore, ITS data were downloaded from several different species of

Periconia from recent molecular studies [104, 148-153] and incorporated into a multiple sequence

alignment using MUSCLE [154] in the program Seaview version 4.5.3 [155]. The alignment was

trimmed to remove ambiguous characters using GBlocks [156]. ModelFinder [157] was used in the

program PhyloSuite v.1,2 to select the best-fit model using Akaike Information Criterion. The

best fitting substitution model was the general time reversible model with empirical base

frequencies, allowing for a proportion of invariable sites, and a discrete Gamma model with four

rate categories (GTR+F+I+G4) was selected using Akaike Information Criterion Subsequently,

the final alignment was used to infer the Maximum Likelihood of ITS sequence data using IQ-

TREE implemented in PhyloSuite [158]. Ultrafast bootstrapping was performed with 5000

replicates [159]. Nodes with UFBoot ≥90% are shown on the clades but only nodes ≥95% are

considered strongly supported. Based on these results, strain G1144 showed phylogenetic

affinities with the genus *Periconia, Periconiaceae*, *Ascomycota* (**Figure 50**), which was recently

emended so that additional modern molecular studies could be possible. [149] Based on the ITS

phylogeny, we could not place stain G1144 into any existing species, as it occurred on an

isolated clade (Fig. S33). Some of the aquatic species of *Periconia* include: *Periconia salina* [151],

P. variicolor [104] *P. aquatica, P. prolifica* [149, 160-161], and *P. submersa* [150]. Currently, the genus

Periconia is polyphyletic and needs dire taxonomic revisions, especially since the type of strain,

P. lichenoides, is unavailable for both morphological and molecular studies [148-149]. Since our

axenic culture did not produce either sexual or asexual micromorphological characters, we herein

identify strain G1144 as *Periconia* sp., *Periconiaceae, Pleosporales, Dothideomycetes*

45

Ascomycota. The ITS sequences were deposited in GenBank (accession no: ITS: MZ997836, MZ997837).

Fermentation, Extraction, and Isolation.

The cultures of fungal strain G1144 were maintained on potato dextrose agar (PDA; Difco) as well as peptone yeast glucose agar (1.25 g peptone, 1.25 g yeast extract, 5g D-glucose, 18 g agar + 30 ppt sea salts; 30 g sea salts in 1000 ml of deionized water) (**Figure 49**). Since strain G1144 showed good growth on both PDA and PYGA + salt media, the latter media was utilized for further experiments. An agar plug from the leading edge of the PYGA culture was transferred to a sterile tube with 10 ml of liquid PYG + 30 ppt sea salts, and this culture was grown for 12 days on an orbital shaker (100 rpm) at room temp. (~23 °C) and then used to inoculate solid fermentation media, such as rice. Solid-state fermentations (n=4) were carried out in 250-ml Erlenmeyer flasks. To prepare rice medium, 10 g of rice were added to each flask with 20 ml of deionized 30 ppt salt water. After autoclaving these samples at 120 °C for 20 min, the flasks were inoculated with PYG + 30 ppt cultures (described above) and incubated at room temperature for four weeks. Subsequently, each of the four solid-state fermentation cultures were chopped into small pieces using a spatula, and 60 ml of 1:1 MeOH-CHCl$_3$ were added. The cultures were then shaken overnight (~16h) at ~125 rpm at rt. The resulting slurries were filtered in vacuo and then pooled to form a combined filtrate, and the solid residue was rinsed with a small volume of 1:1 MeOH-CHCl$_3$. To the combined filtrate, 270 ml of CHCl$_3$ and 450 ml of H$_2$O were added; the solution was stirred for 20 min and transferred to a separatory funnel. The organic layer was collected and evaporated to dryness under vacuum using a rotary evaporator. The resulting organic extract was then partitioned between 100 ml of 1:1 MeOH-CH$_3$CN and 100 ml of hexanes. The MeOH-CH$_3$CN layer was collected and evaporated to dryness under

vacuum. The defatted organic extract (~228 mg) was reconstituted in $CHCl_3$ and absorbed onto celite 545. The extract was then fractionated by flash chromatography using a solvent gradient of hexane-$CHCl_3$-MeOH at a 18 ml/min flow rate and 85.0 column volumes to yield five fractions. Fraction 2 (~97 mg) was fractionated further into 11 subfractions using preparative HPLC with a solvent gradient increasing linearly from 20:80 to 75:25 CH_3CN-H_2O (acidified with 0.1% formic acid) over 20 min at a flow rate of 21.20 ml/min. Subfractions 4, 6, and 7 yielded compounds **1** (3.94 mg), **3** (5.74), and **4** (30.63 mg) which eluted at ~16 min, 18 min, and 19 min respectively. Subfraction 5 was further purified using semi-preparative HPLC with a solvent gradient of 40:60 to 50:50 CH_3CN-H_2O (acidified with 0.1% formic acid) over 30 min at a flow rate of 4.60 ml/min to yield compound **2** (0.78 mg), which eluted at 21.5 min.

Cryptosporiopsinol C (**1**): opaque solid; $[\alpha]D^{20}$=+53(c 0.10, $CHCl_3$); UV($CHCl_3$) λ_{max} (log ε) 267.5 (2.70), 241 (3.12) nm; ^1H and ^{13}C NMR, Table 1; HRESIMS m/z 318.9917 [M + H]$^+$ (calcd for $C_{10}H_{14}Cl_3O_5$, 318.9907), m/z 340.9739 [M + Na]$^+$ (calcd for $C_{10}H_{13}Cl_3O_5Na$, 340.9726)

Cryptosporiopsinol D (**2**): opaque solid; $[\alpha]D^{20}$=-10(c 0.10, $CHCl_3$); UV($CHCl_3$) λ_{max} (log ε) 241 (2.29) nm; ^1H and ^{13}C NMR, Table 1; m/z 318.9916 [M + H]$^+$ (calcd for $C_{10}H_{14}Cl_3O_5$, 318.9907), m/z 340.9738 [M + Na]$^+$ (calcd for $C_{10}H_{13}Cl_3O_5Na$, 340.9726)

Cryptosporiopsinol B (**3**): opaque solid; $[\alpha]D^{20}$=+48(c 0.10, $CHCl_3$); UV($CHCl_3$) λ_{max} (log ε) 254 (2.77), 219 (4.15) nm; ^1H and ^{13}C NMR, Table 1; HRESIMS m/z 289.0017 [M + Na]$^+$ (calcd for $C_{10}H_{12}Cl_2O_4Na$, 289.0010)

Rhytidhyester D (**4**): colorless solid; $[\alpha]D^{20}$=+55(c 0.10, $CHCl_3$); UV($CHCl_3$) λ_{max} (log ε) 257 (1.98), 216 (3.13) nm; ^1H and ^{13}C NMR, Table 1; HRESIMS m/z 289.0018 [M + Na]$^+$ (calcd for $C_{10}H_{12}Cl_2O_4Na$, 289.0010)

Cytotoxicity and Antimicrobial Assays

To evaluate the cytotoxic activity of **1**–**4** against human melanoma cancer cells (MDA-MB-435), human breast cancer cells (MDA-MB-231), and human ovarian cancer cells (OVCAR3), the assays were performed as detailed recently [162]. Taxol was used as positive control. Compounds **1-4** were analyzed in four technical replicates and three biological replicates, and all compounds were >95% pure as measured by UPLC (**Figures 18**, **27**, **34**, and **42**).

Minimal inhibitory concentrations of the compounds were measured by broth microdilution against the following bacteria: *Escherichia coli*, *Staphylococcus aureus*, methicillin-resistant *S. aureus* (MRSA), *Pseudomonas aeruginosa*, and *Bacillus anthracis*; MICs were measured by broth microdilution of fresh overnight cultures according to the Clinical and Laboratory Standards Institute (CCLI) guidelines with cation-adjusted Mueller–Hinton broth and an inoculum of 105 colony-forming units (CFUs)/ml. Stocks of the compounds were dissolved in Mueller–Hinton broth (Becton-Dickinson, Sparks, MD). The MIC (expressed as µg/ml) was defined as the lowest concentration of compound completely inhibiting the appearance of turbidity by eye and confirmed by absorbance 540 nm. All results represent the average of three independent measurements. Prior to testing, **1**-**4** were confirmed >95% pure by UPLC (**Figures 18**, **27**, **34**, and **42**).

Antiparasitic Assay

A clinical isolate of *Naegleria fowleri* obtained from a 9-year-old boy in Adelaide, Australia, that died of primary amebic meningoencephalitis (PAM) in 1969 was previously purchased from the American Type Culture Collection (ATCC 30215) [163]. Trophozoites were routinely grown axenically at 34°C in Nelson's complete medium (NCM) in non-vented 75 cm^2

tissue culture flasks (Olympus), until the cells were 80-90% confluent. For sub-culturing, cells

were placed on ice to detach the cells from the culture flasks. Detached cells were collected by

centrifugation at 4000 rpm at 4°C. Complete NCM media was produced by the addition of 10%

FBS and 125 µg of penicillin/streptomycin antibiotics. The trophocidal activity of pure

compounds were assessed using the CellTiter-Glo 2.0 luminescent viability assay (Promega,

Madison, WI), as previously described [163-166]. In brief, logarithmic trophozoites of *N. fowleri*

were seeded at 4000 cells/well into white 96-well plates (Costar 3370). All compounds were

assessed in 2-fold serial dilutions from the highest concentration of 20 µM for 72 hours. At the

72-hour time point, 25 µl of CellTiter-Glo 2.0 reagent was added to all wells of the plates. The

plates were protected from light and contents were mixed using an orbital shaker at 300 rpm at

room temperature for 2 min to induce cell lysis. After shaking, the plates were equilibrated at

room temperature for 10 min to stabilize the luminescent signal. The ATP luminescent signals

(relative light units; RLUs) were measured at 490 nm with a SpectraMax I3X plate reader

(Molecular Devices, Sunnyvale, CA). Drug inhibitory concentration (IC_{50}) curves were

generated using total ATP RLUs where controls were calculated as the average of replicates

using the Levenberg-Marquardt algorithm, using DMSO as the normalization control, as defined

in CDD Vault (Burlingame, CA, USA). Values reported are from a minimum of two biological

replicates with standard deviations. Prior to testing, **1**-**4** were confirmed >95% pure by UPLC

(**Figures 18**, **27**, **34**, and **42**).

Quorum Sensing Inhibition Assay

A 96-well plate assay was performed to evaluate the inhibition of the production of AIP-I

by MRSA, adapted from a published procedure [167]. Overnight tryptic soy broth (TSB) MRSA

cultures were diluted 1:200 with fresh TSB and shaken (200 rpm) at 37°C for 2 hours. A stock

solution (5.0 mg/ml) for each sample was prepared in DMSO, which was diluted 10-fold to yield

a solution of 0.5 mg/ml and then serially diluted with TSB to yield six concentrations (0.02

mg/ml- 0.50 mg/ml). Aliquots (50 µl) of the diluted solutions were combined in a 96-well plate

with 150 µL of TSB and 50 µL of diluted (1:200) MRSA culture. Final sample concentrations in

the wells ranged from 3.13 µg/ml to 100 µg/ml. The 96-well plate was shaken (500 rpm) for 5

hours at 37°C. Optical density readings (OD_{600}) were taken hourly at 600 nm to measure growth

of the bacteria. After incubation, cells were removed by vacuum filtration. The filtrate was

analyzed using positive mode LC-MS to determine relative quantities of AIP-I (*m/z* 961.3799)

and percent of vehicle was calculated as described previously [167]. Prior to testing, **1**, **3** and **4** were

confirmed >95% pure by UPLC (**Figures 18**, **27**, and **42**).

Computational Details

Macromodel (Version 12.6) interface Maestro (Version 12.2) program was used for all

molecular mechanics calculations. For all conformational searches, MMFF force field and

torsional sampling Monte Carlo Multiple Minimum (MCMM) method were used with extended

torsional sampling [136], The resulting conformers were filtered, checked for duplicity, and

minimized using a DFT force field at the M062X/6-31+G (d,p) level of theory. B3LYP/6-311+G

(2d,p) level of theory with the IEFPCM model were used at the GIAO method to calculate NMR

shielding constants. The obtained shielding constants were eventually converted into chemical

shifts (ppm) by referencing TMS to 0 ppm. The final ^{13}C and ^{1}H NMR shifts were calculated for

each conformer for each compound based on the total Boltzmann distribution and relative

energies. The NMR shifts for each particular species were calculated based on the work of

Willoughby et al. [136-137] To further calculate the corrected correlation coefficient (r) for the

combined ^{13}C and ^{1}H data for compounds **1-4**, the calculated ^{13}C and ^{1}H NMR data were first

empirically scaled and then the individual correlation coefficients were calculated using excel (=correl(calculated, experimental)). Then, the geometric mean of the correlation coefficients for ^{13}C and ^{1}H was taken [135, 140]. The DP4+ and dJ DP4 calculations were carried out as described by the Sarotti Group using their available spreadsheet [168]. For dJ DP4 calculations Boltzmann averaged isotropic shielding values and coupling constants (FC only) were computed using full conformational search (with no constrains) [141]. The conformers generated for the NMR calculations were taken to calculate the optical rotation values. The optical rotations were calculated at the GIAO method at the B3LYP/6-31G (d,p) level of theory in CHCl$_3$ for **1**–**4** [169-170] based on the total Boltzmann distribution and relative energies using SpecDis software [171].

Supplementary Data
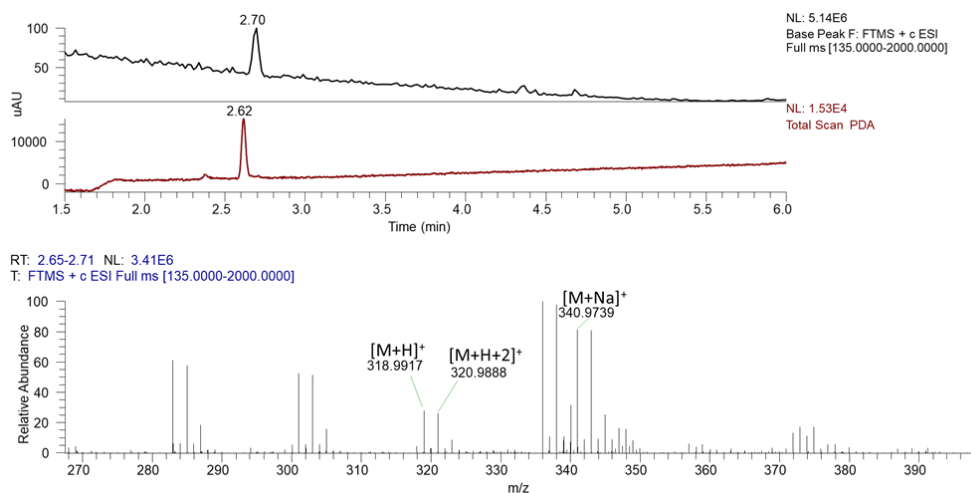
Figure 18. LC-MS chromatogram and (+)-HRESIMS spectrum of compound **1**.
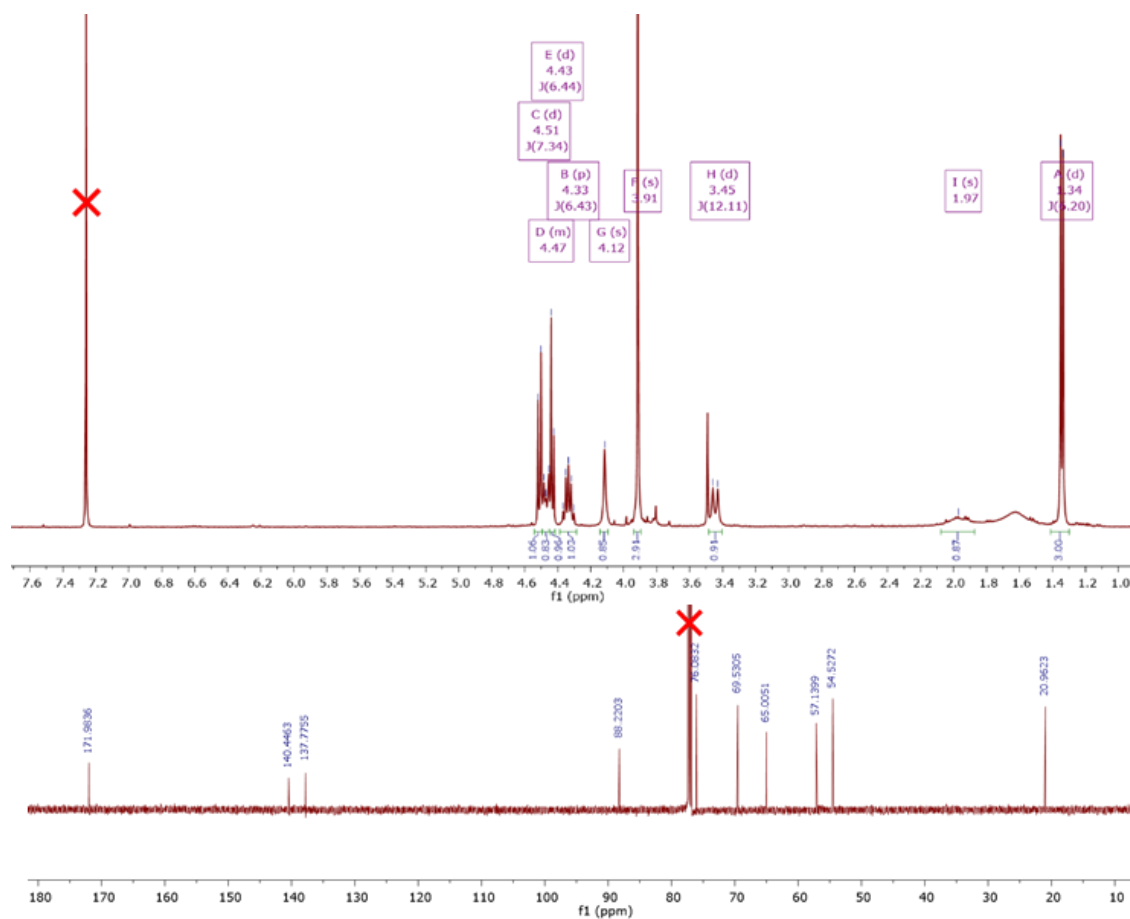
Figure 19. ^{1}H NMR spectrum (400 MHz, Top) and ^{13}C NMR spectrum (125 MHz, Bottom), both in CDCl$_3$, of compound **1**.
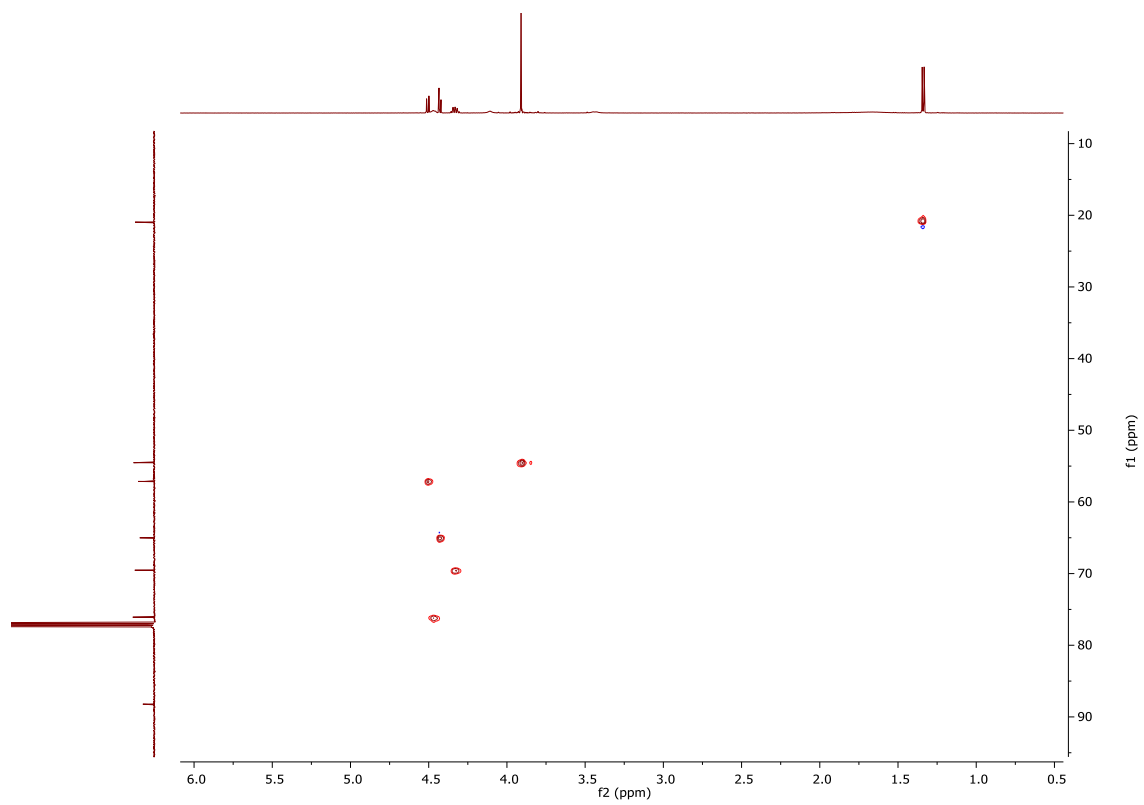
Figure 20. DEPT-edited HSQC NMR spectrum of **1** (500 MHz, CDCl₃).
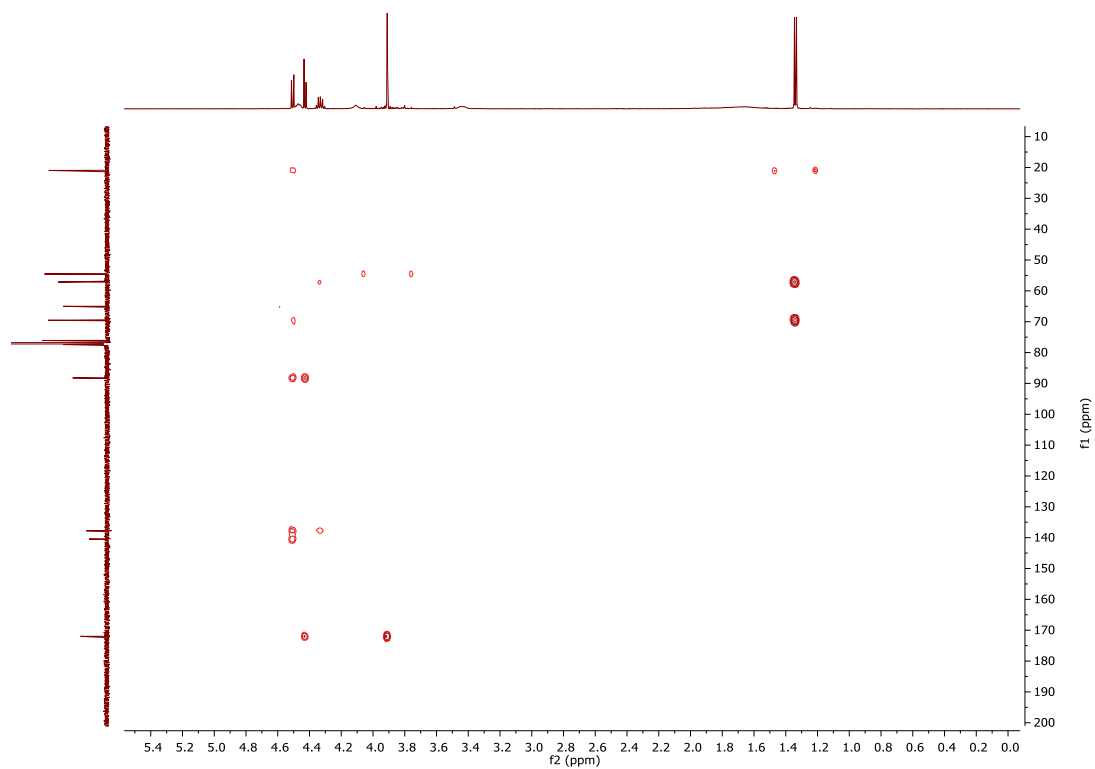
Figure 21. HMBC NMR spectrum of **1** (500 MHz, CDCl$_3$).
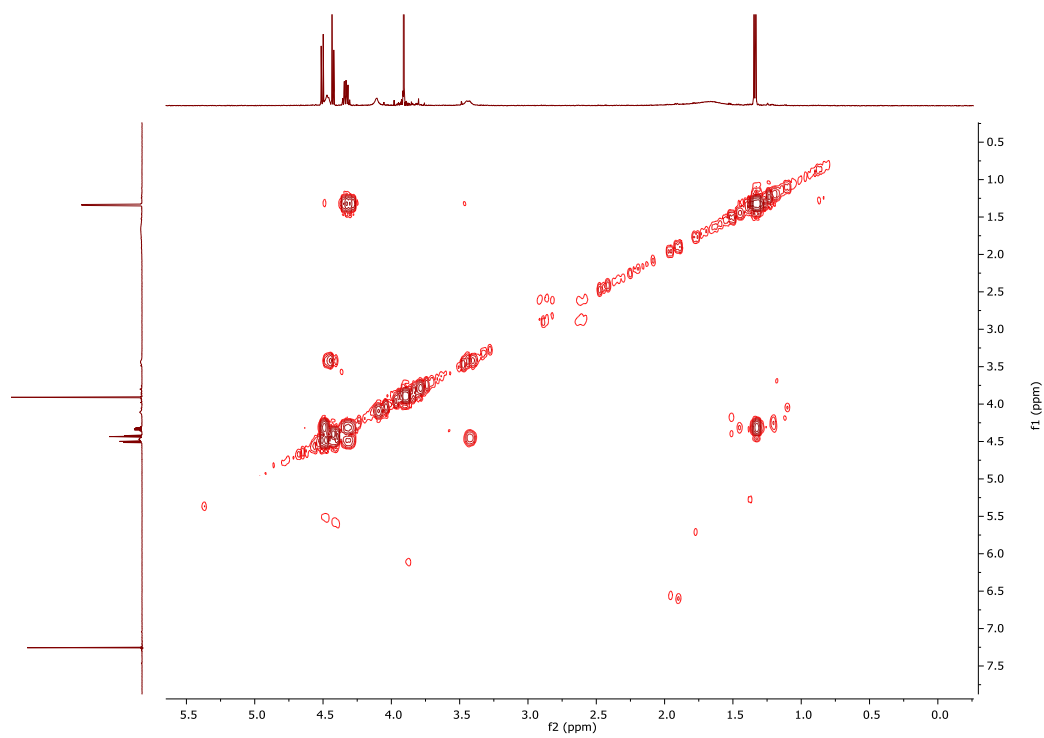
Figure 22. COSY NMR spectrum of **1** (500 MHz, CDCl$_3$).
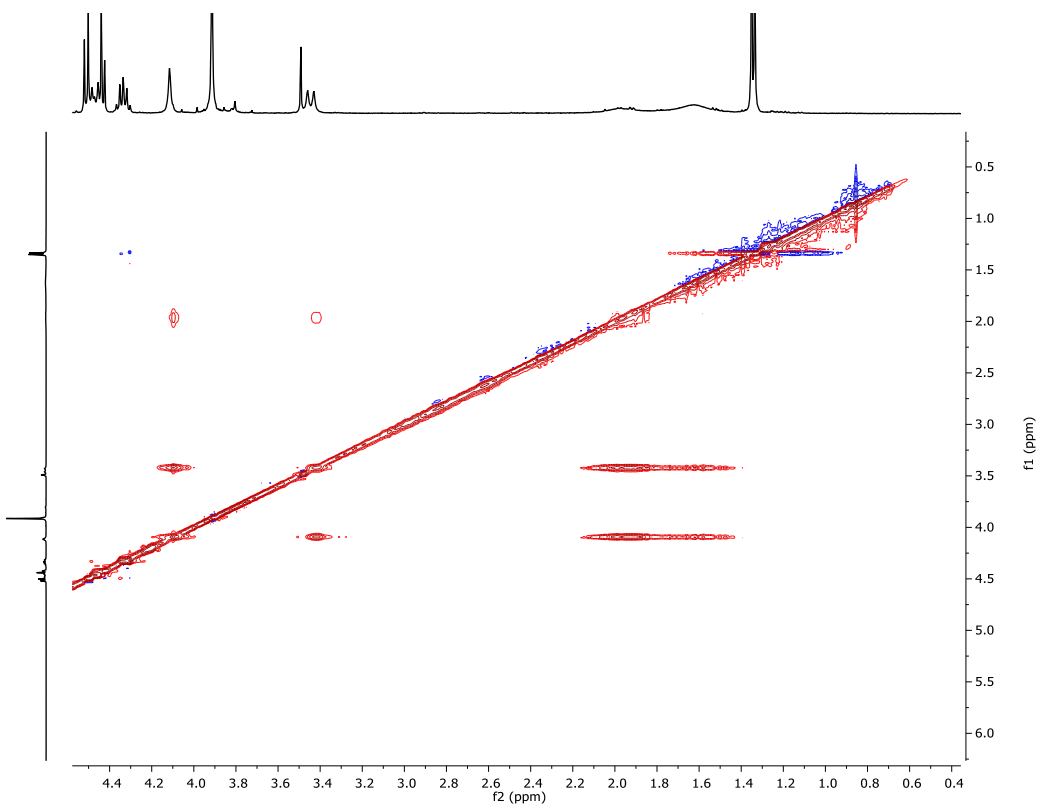
Figure 23. NOESY NMR spectrum of **1** (700 MHz, CDCl₃).
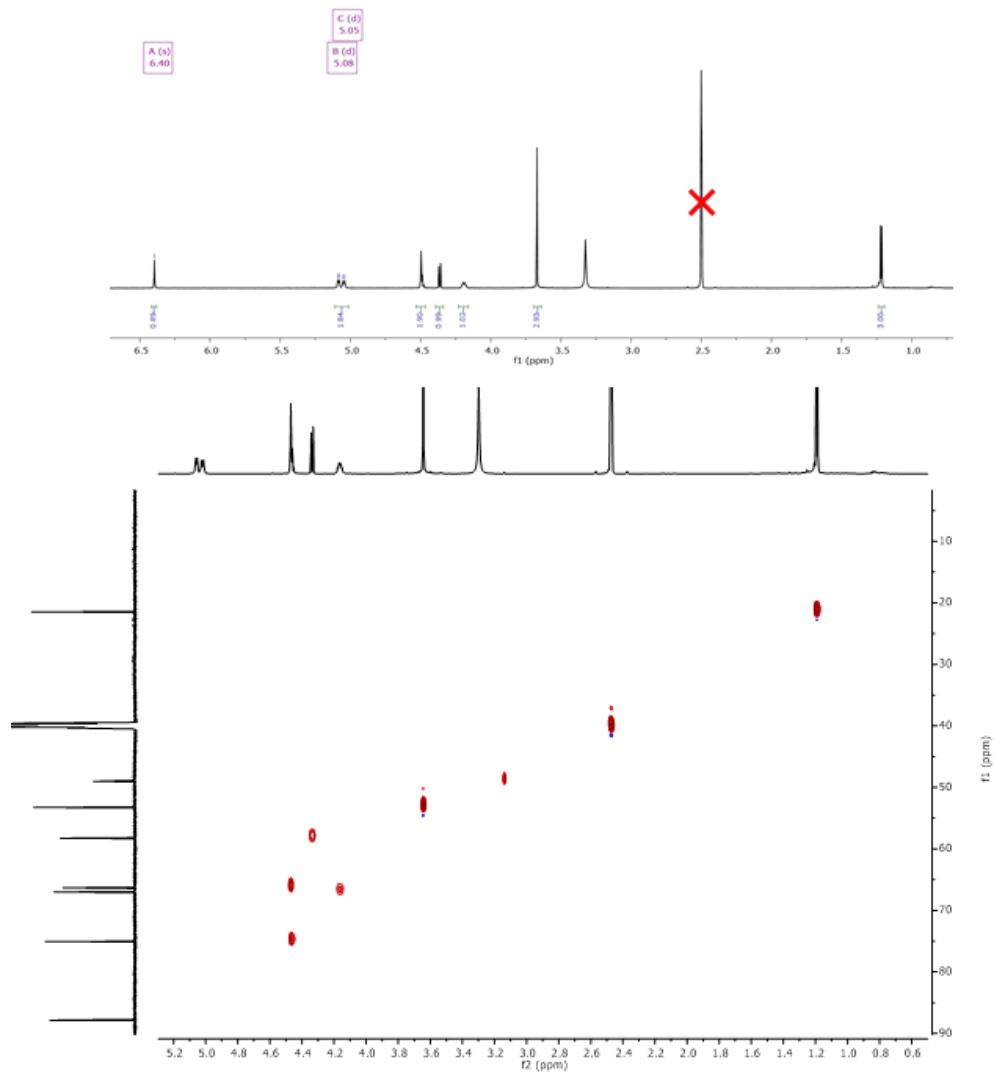
Figure 24. ¹H NMR spectrum (700 MHz, Top) and HSQC spectrum (700 MHz, Bottom), both in DMSO-$_{d6}$, of compound **1**.
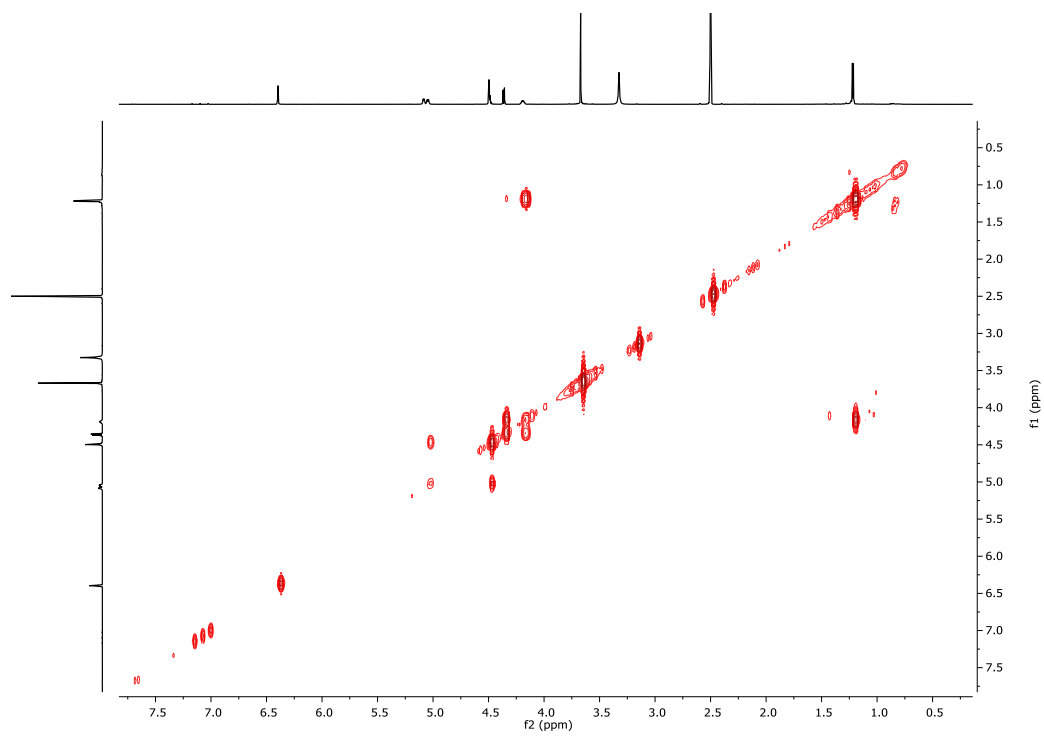
Figure 25. COSY NMR spectrum of **1** (700 MHz, DMSO-*d6*).
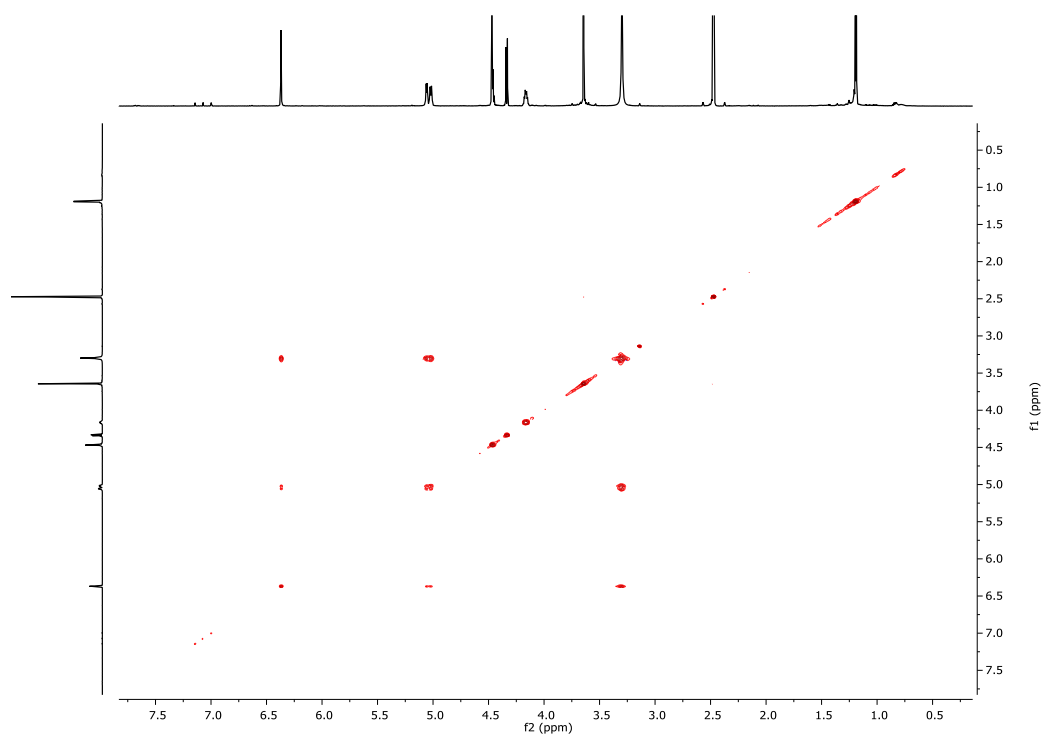
Figure 26. NOESY spectrum of **1** (700 MHz, DMSO-*d6*).
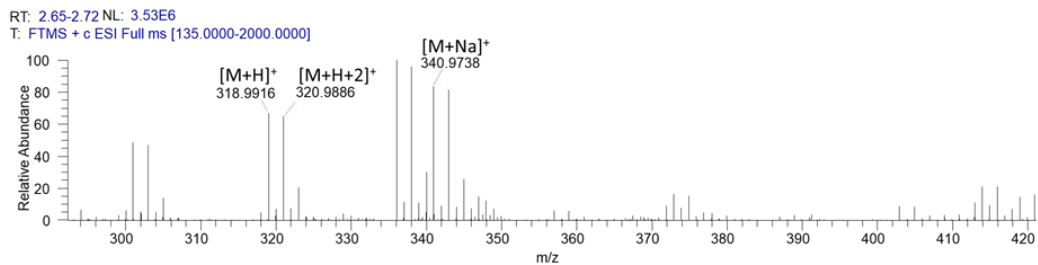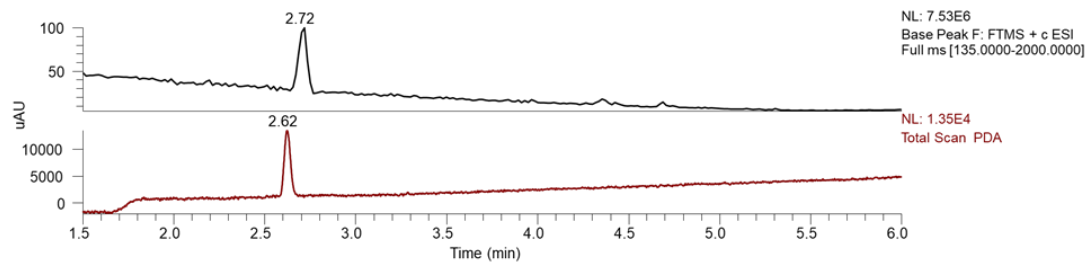
Figure 27. LC-MS chromatogram and (+)-HRESIMS spectrum of compound **2**.
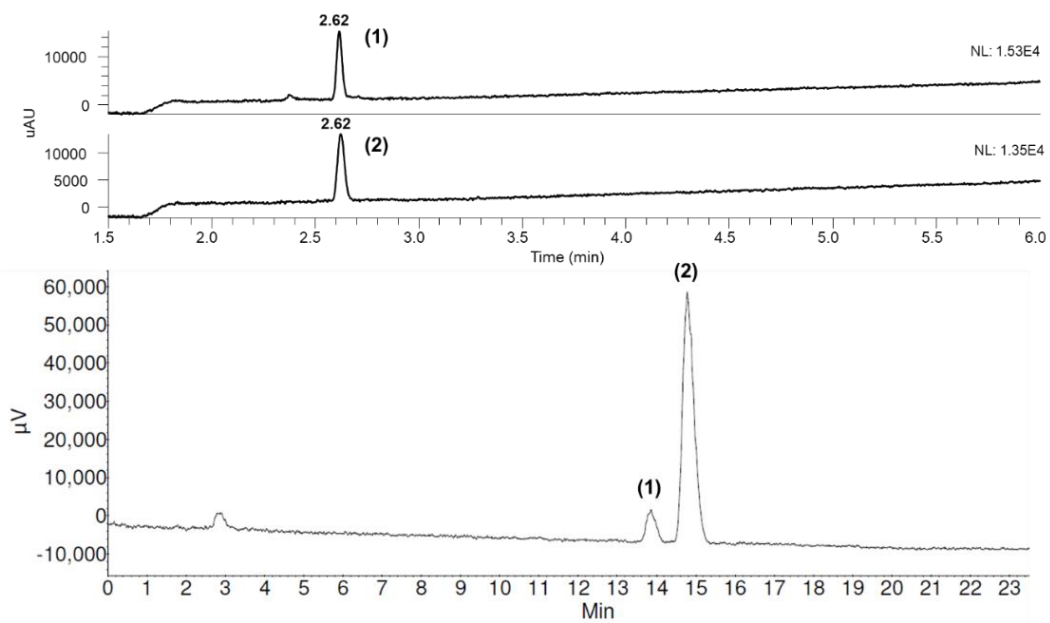
Figure 28. LC-MS chromatogram (Top) and analytical HPLC (Bottom) of **1** and **2**.
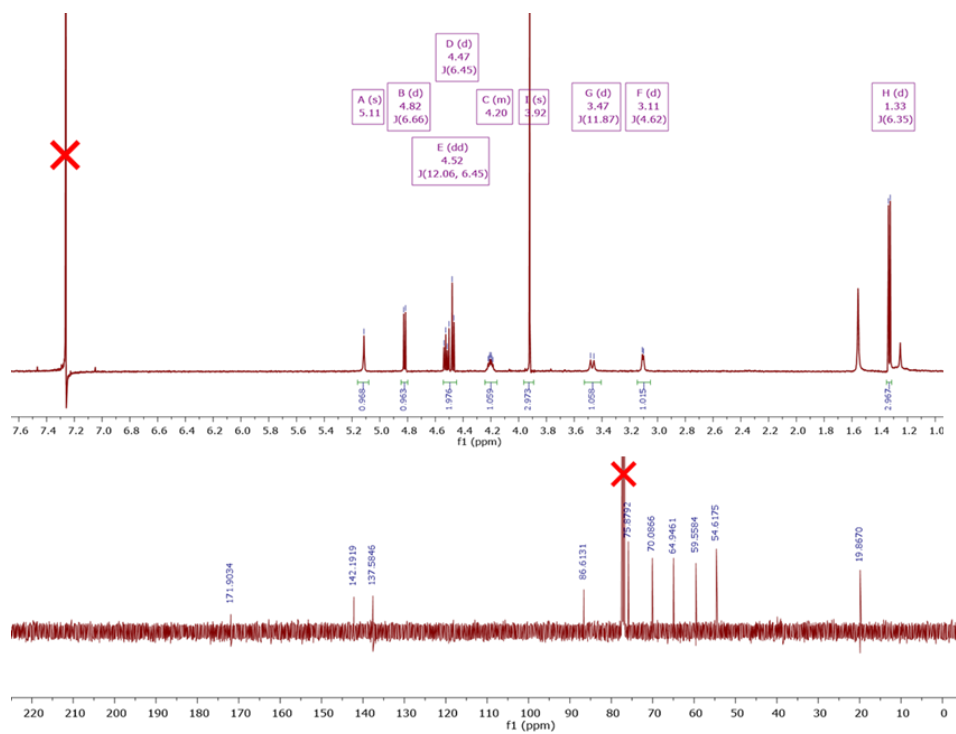
Figure 29. ^{1}H NMR spectrum (500 MHz, Top) and ^{13}C NMR spectrum (125 MHz, Bottom), both in CDCl$_3$, of compound **2**.
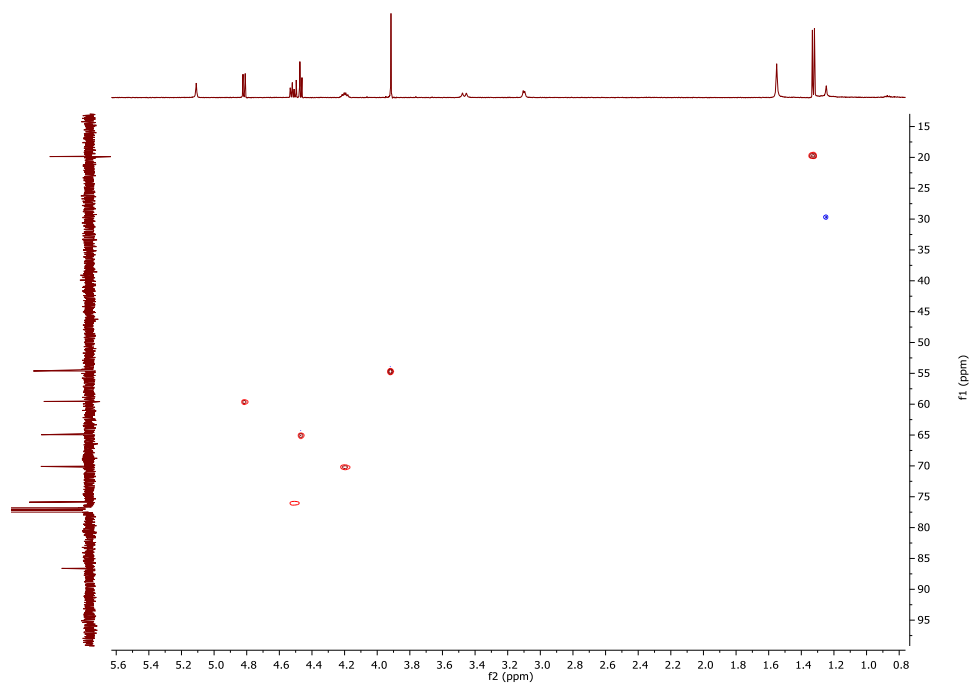
Figure 30. DEPT-edited HSQC NMR spectrum of **2** (500 MHz, CDCl$_3$).
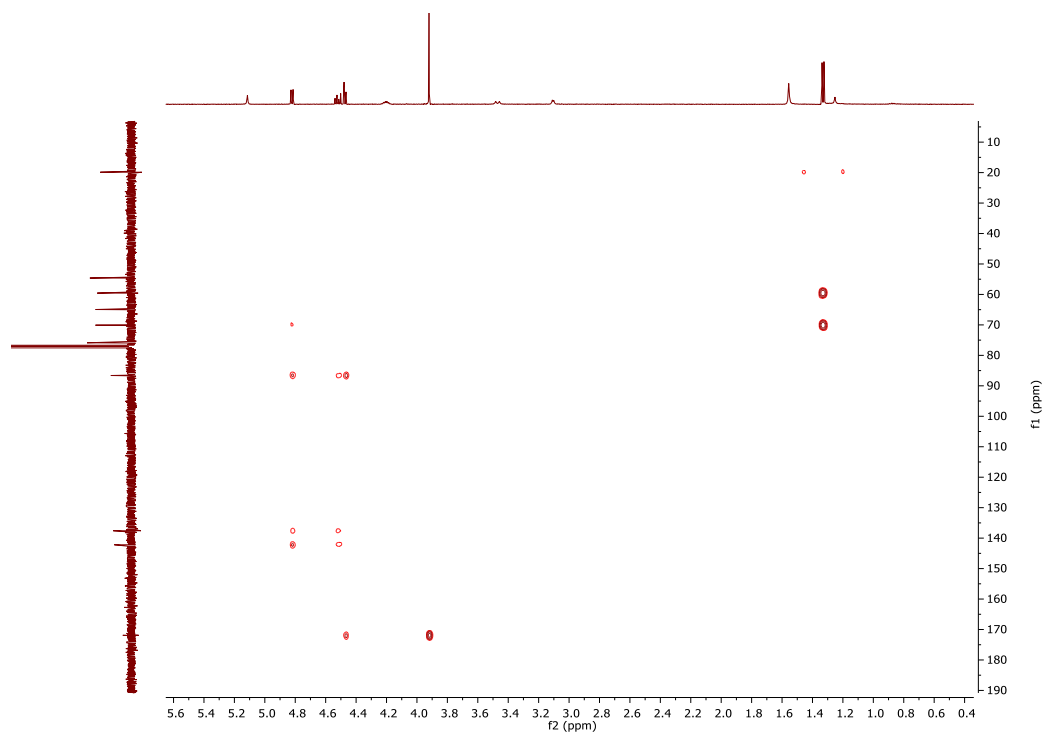
Figure 31. HMBC NMR spectrum of **2** (500 MHz, CDCl₃).
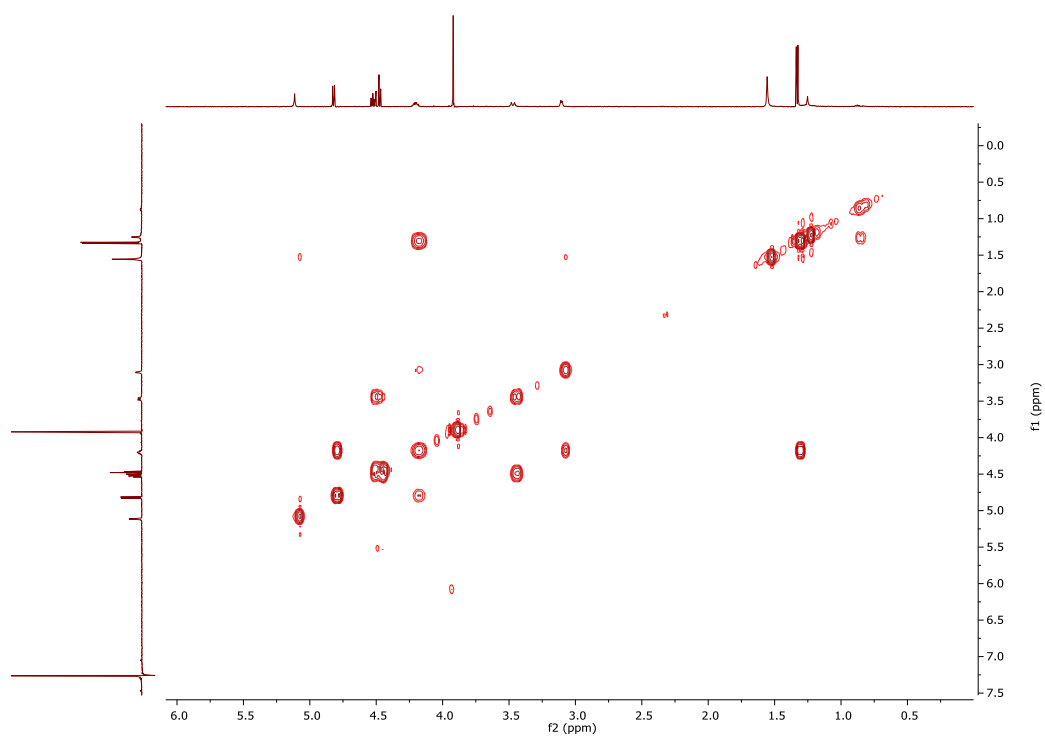
Figure 32. COSY NMR spectrum of **2** (500 MHz, CDCl₃).
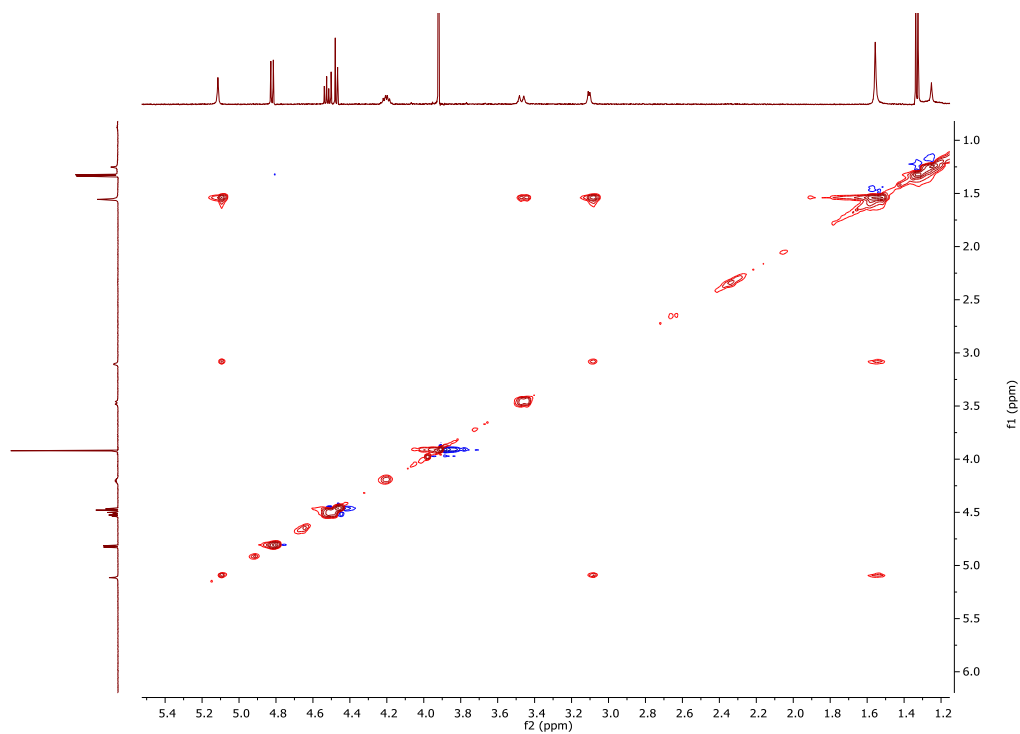
Figure 33. NOESY spectrum of **2** (400 MHz, CDCl$_3$).
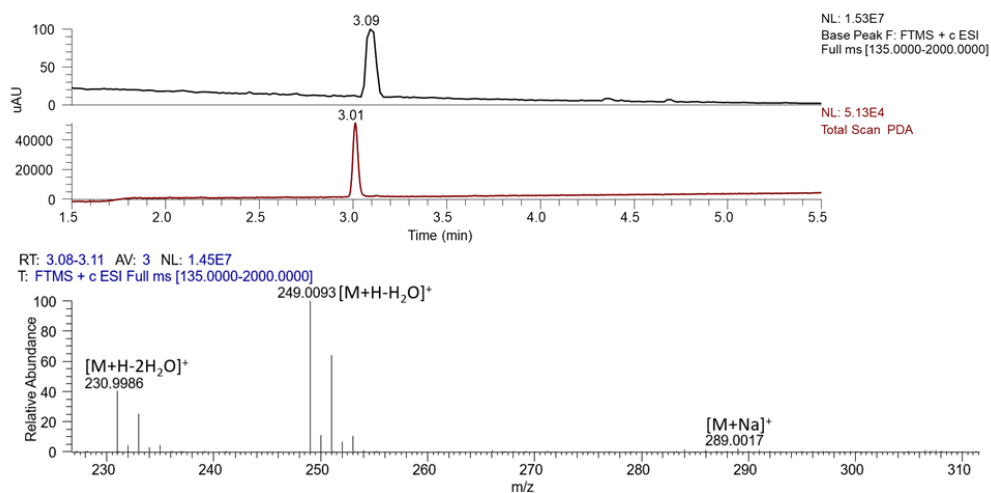
Figure 34. LC-MS chromatogram and (+)-HRESIMS spectrum of compound **3**.
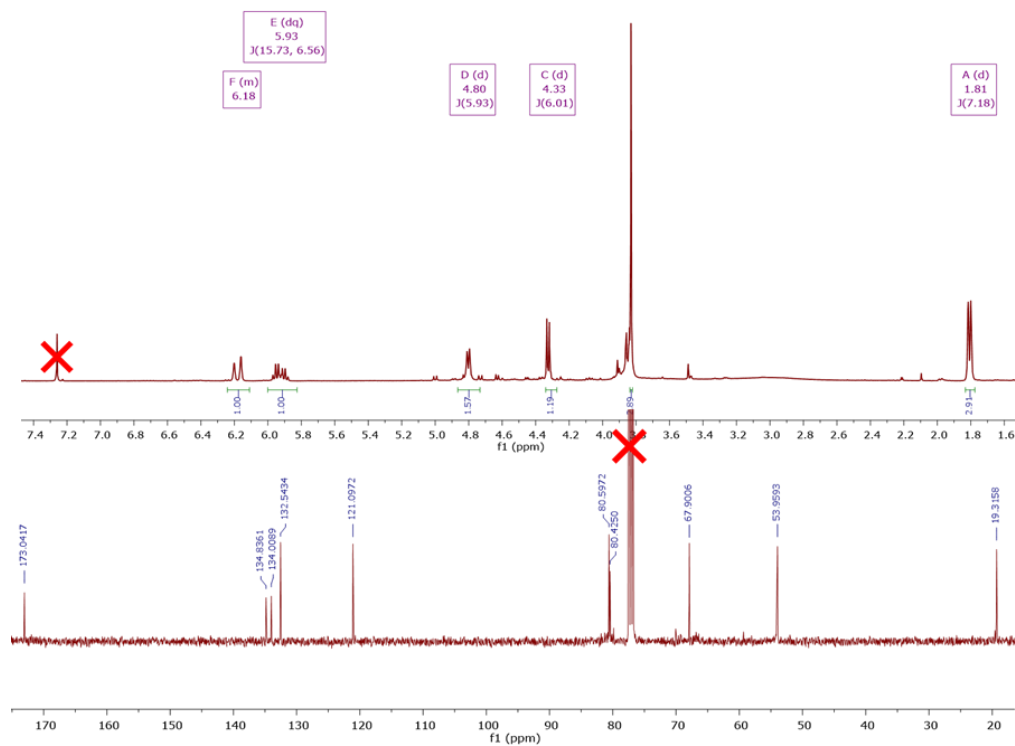
Figure 35. ^{1}H NMR spectrum (400 MHz, Top) and ^{13}C NMR spectrum (125 MHz, Bottom), both in CDCl$_3$, of compound **3**.
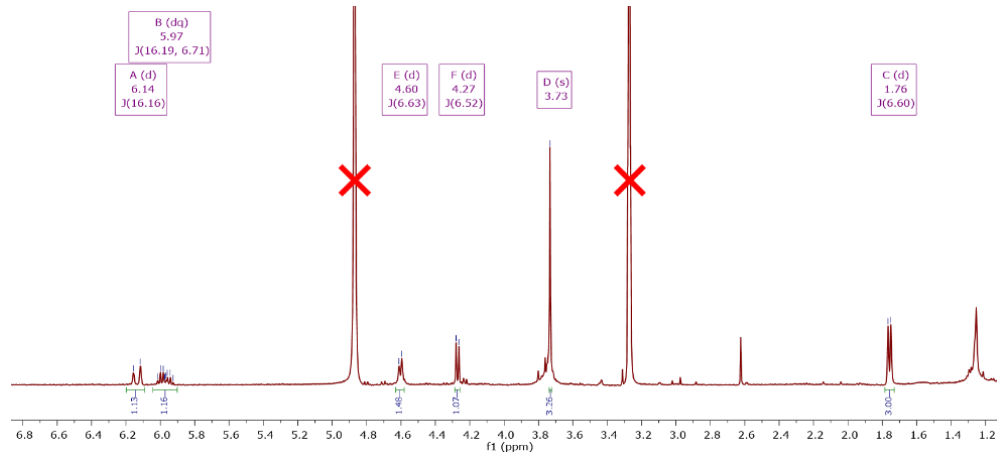
Figure 36. ^{1}H NMR spectrum (400 MHz,) of compound **3** in CD$_3$OD.
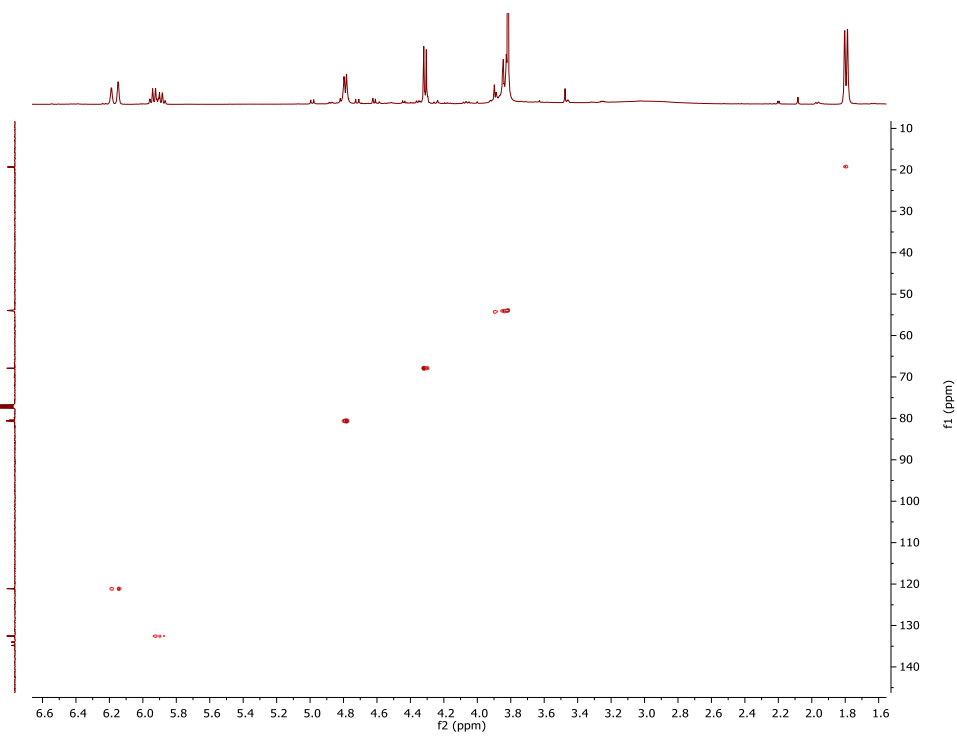
Figure 37. DEPT-edited HSQC NMR spectrum of **3** (400 MHz, CDCl3).
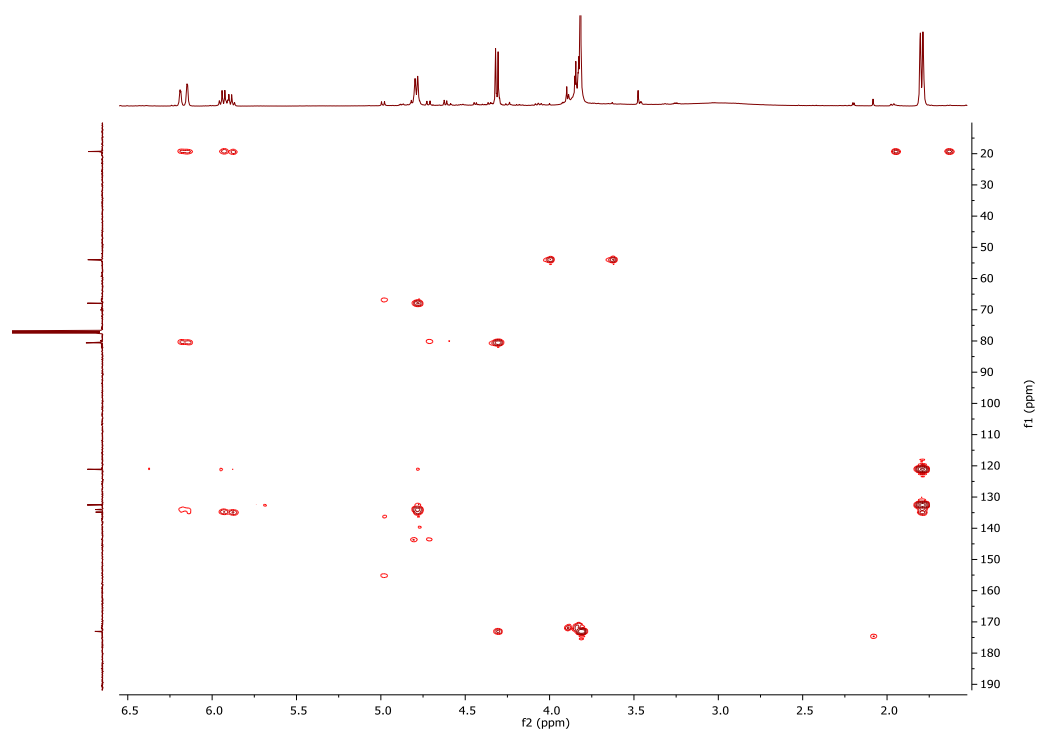
Figure 38. HMBC NMR spectrum of **3** (400 MHz, CDCl3).
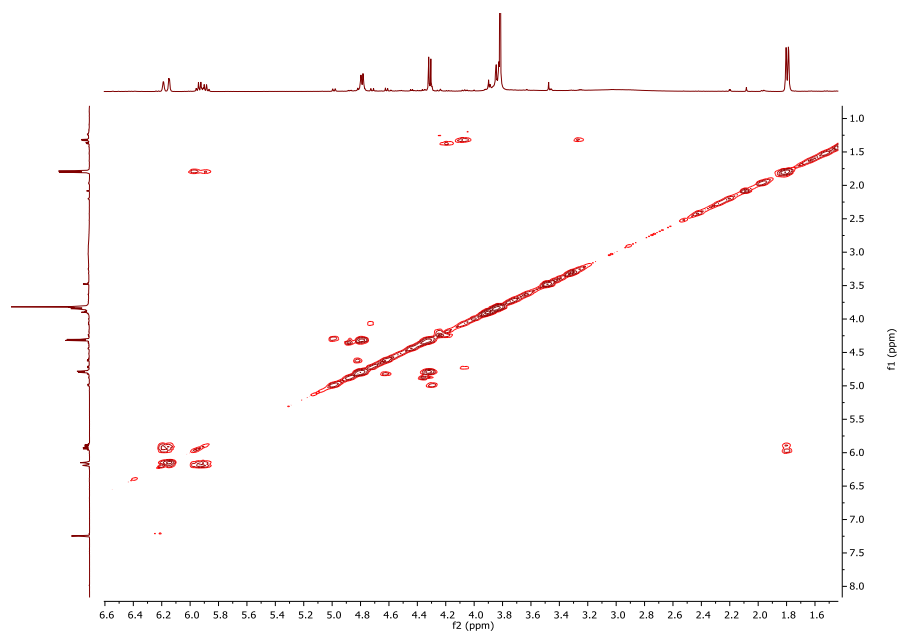
Figure 39. COSY NMR spectrum of **3** (400 MHz, CDCl₃).

Figure 40. 1H NMR spectrum (400 MHz, Top) and COSY spectrum (400 MHz, Bottom), both in DMSO-*d6*, of compound **3**.
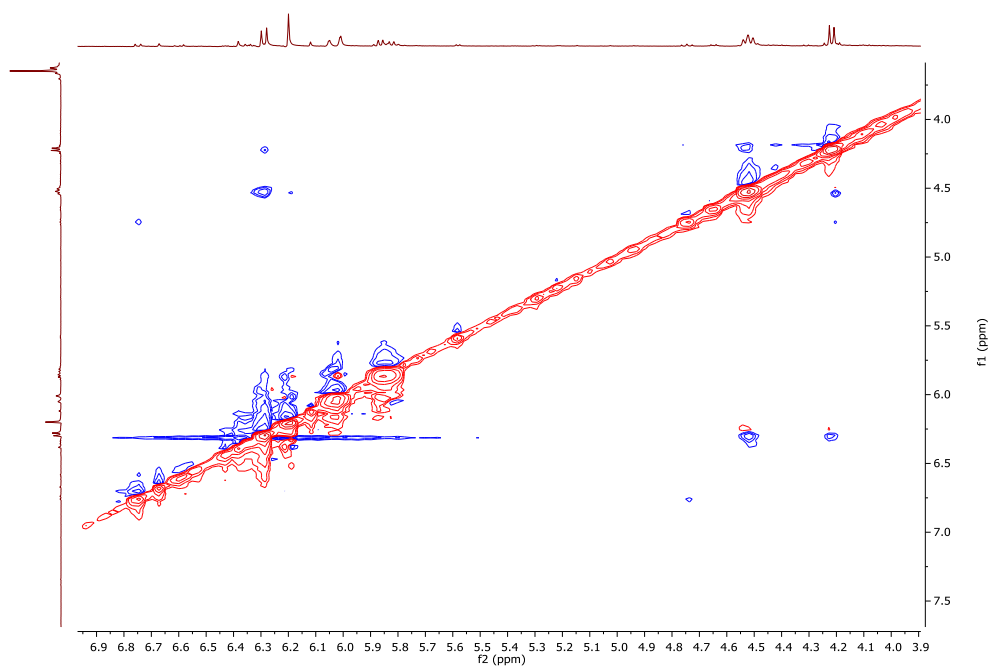
Figure 41. NOESY spectrum of **3** (400 MHz, DMSO-*d6*).
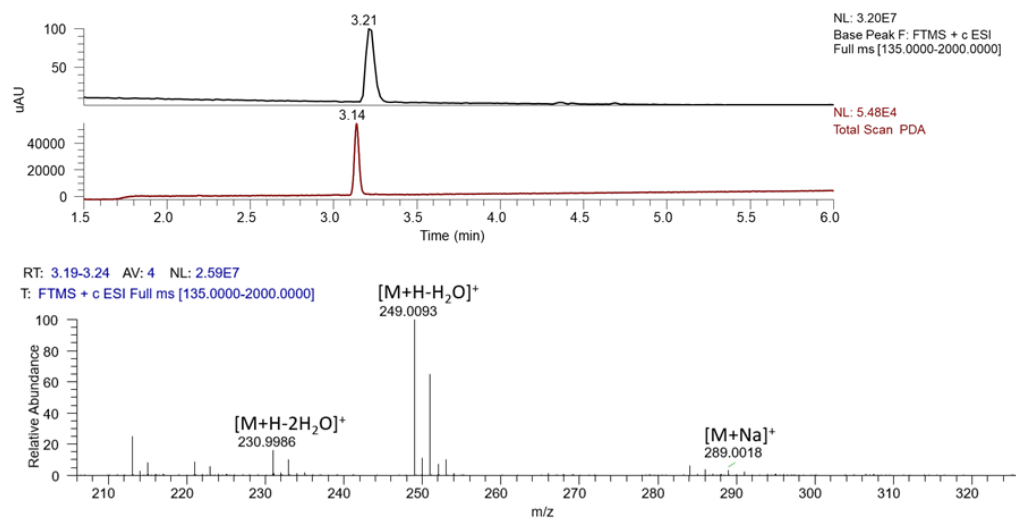
Figure 42. LC-MS chromatogram and (+)-HRESIMS spectrum of compound **4**.
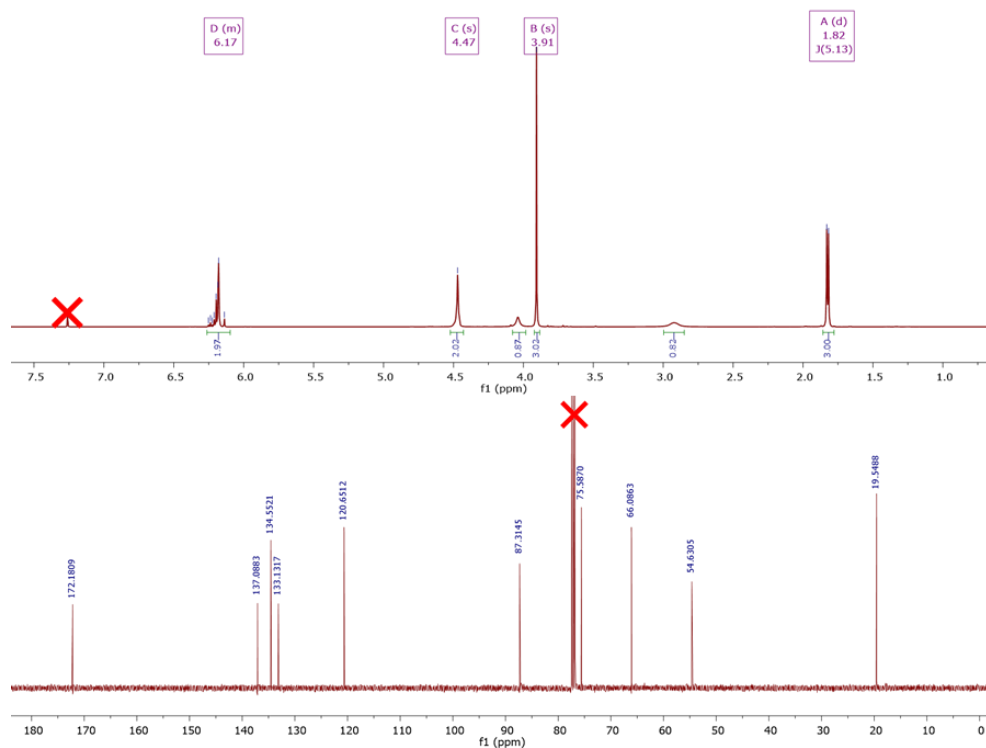
Figure 43. ^{1}H NMR spectrum (400 MHz, Top) and ^{13}C NMR spectrum (100 MHz, Bottom), both in CDCl$_3$, of compound **4**.
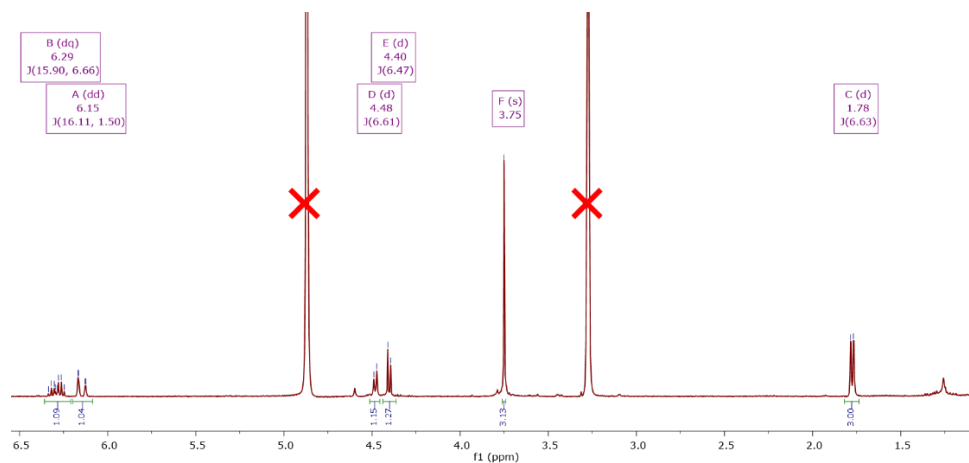
Figure 44. ^{1}H NMR spectrum (400 MHz,) of compound **4** in CD$_3$OD.
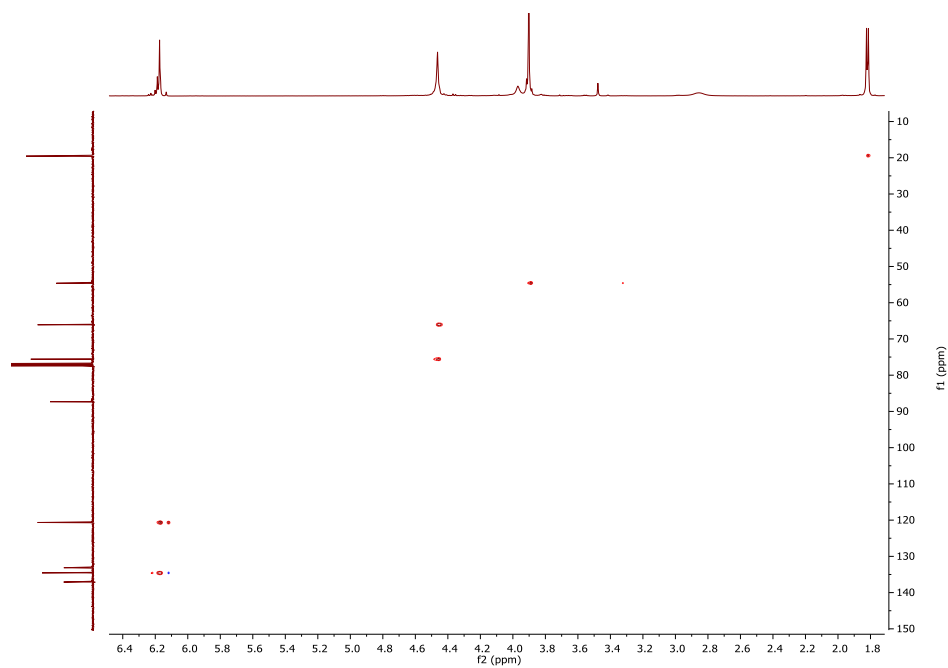
Figure 45. DEPT-edited HSQC NMR spectrum of **4** (400 MHz, CDCl₃).
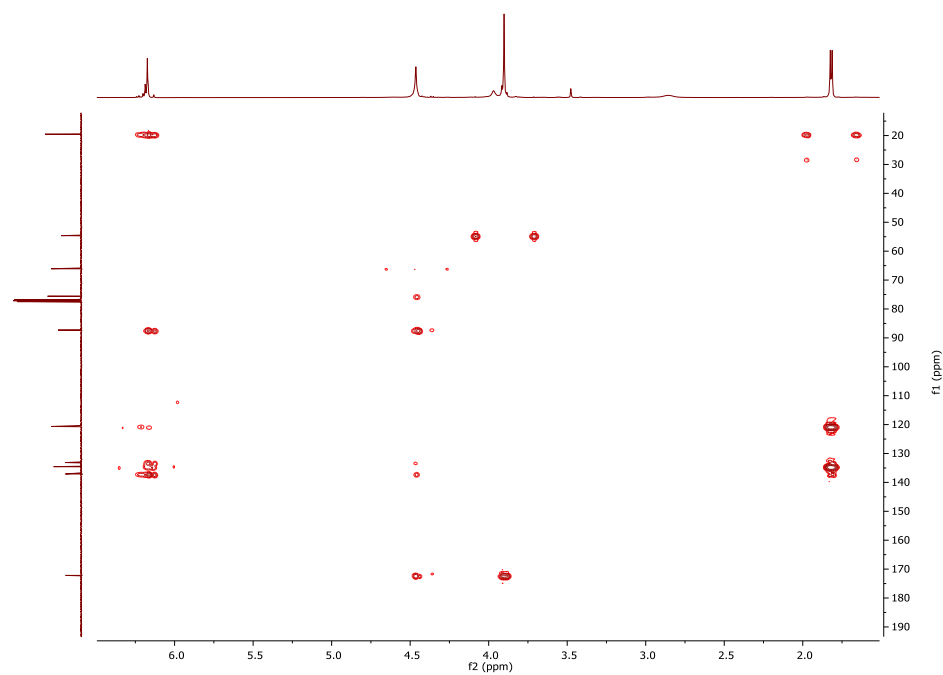
Figure 46. HMBC NMR spectrum of **4** (400 MHz, CDCl₃).
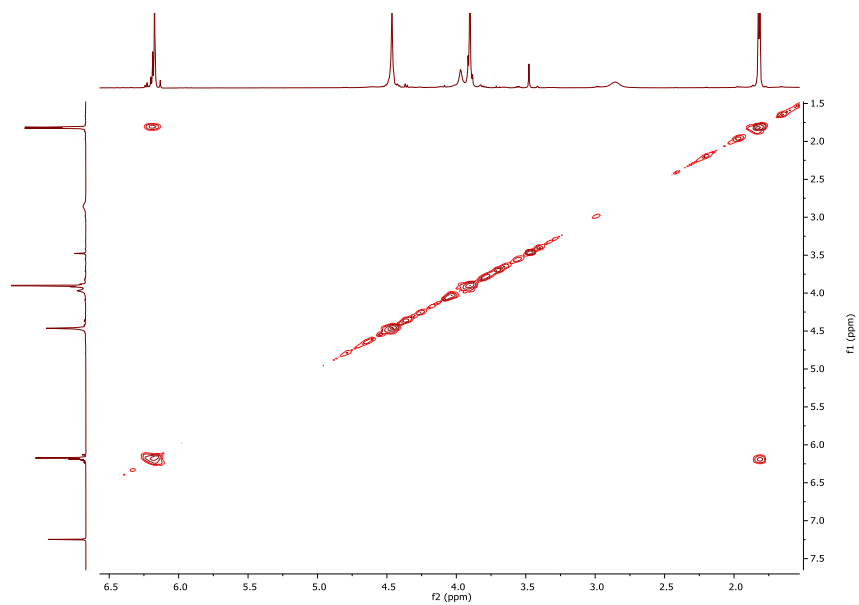
Figure 47. COSY NMR spectrum of **4** (400 MHz, CDCl₃).
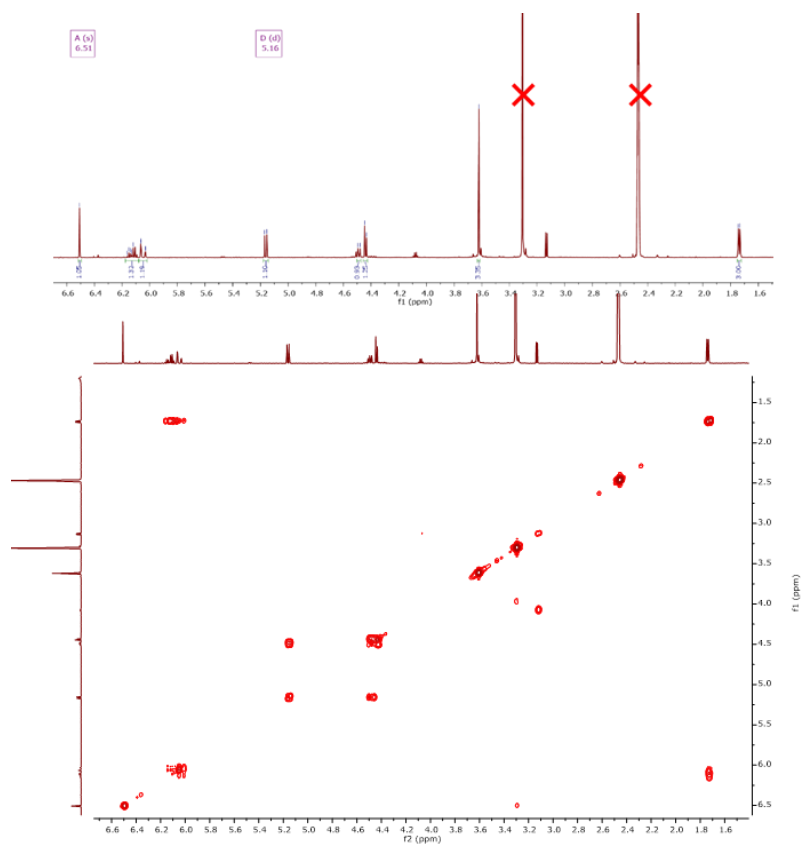
Figure 48. ¹H NMR spectrum (Top, 500 MHz) and COSY spectrum (Bottom, 400 MHz), both in DMSO-*d6*, of compound **4**.
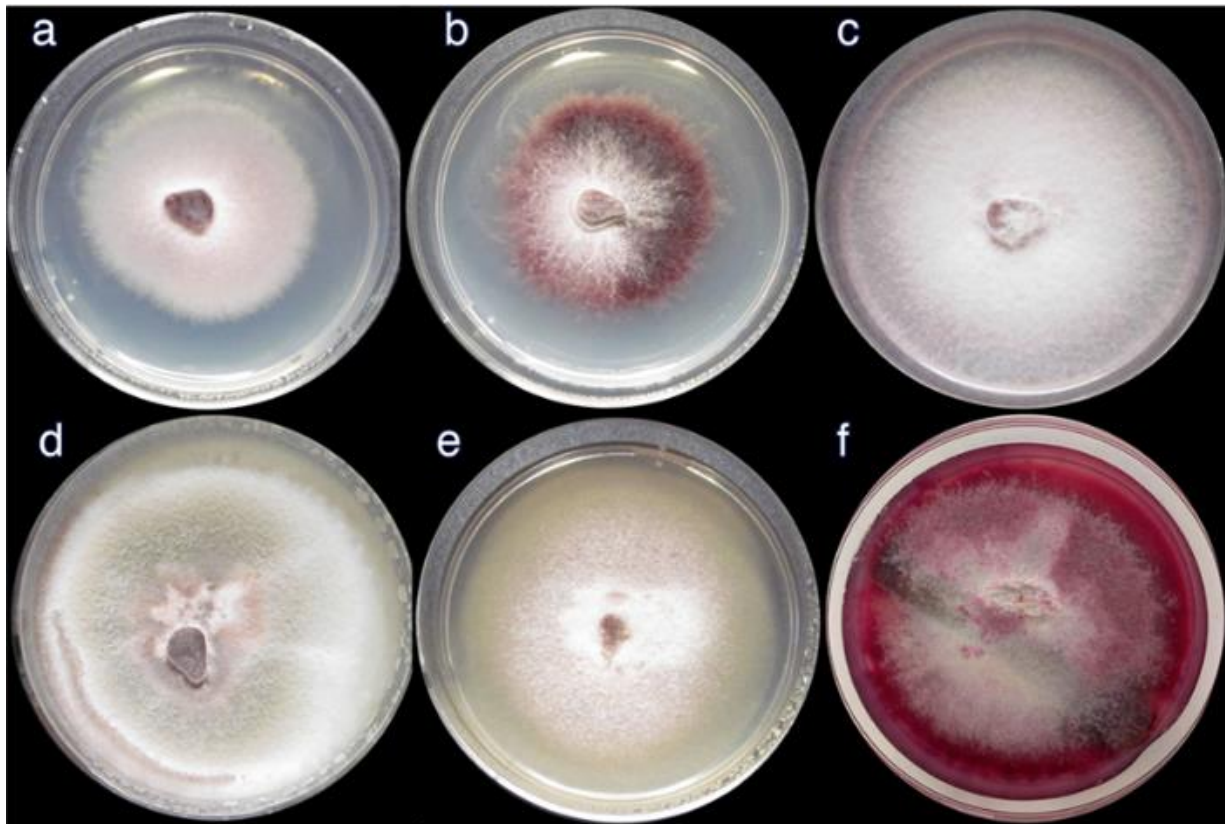
Figure 49. a-e. Three-week old cultures of strain G1144. a. Corn meal agar; b. Czapek-Dox agar; c. peptone yeast glucose agar + 30 ppt sea salts; d. oatmeal agar; e. potato dextrose agar. f. Six-week-old culture on potato dextrose agar with autoclaved balsa.
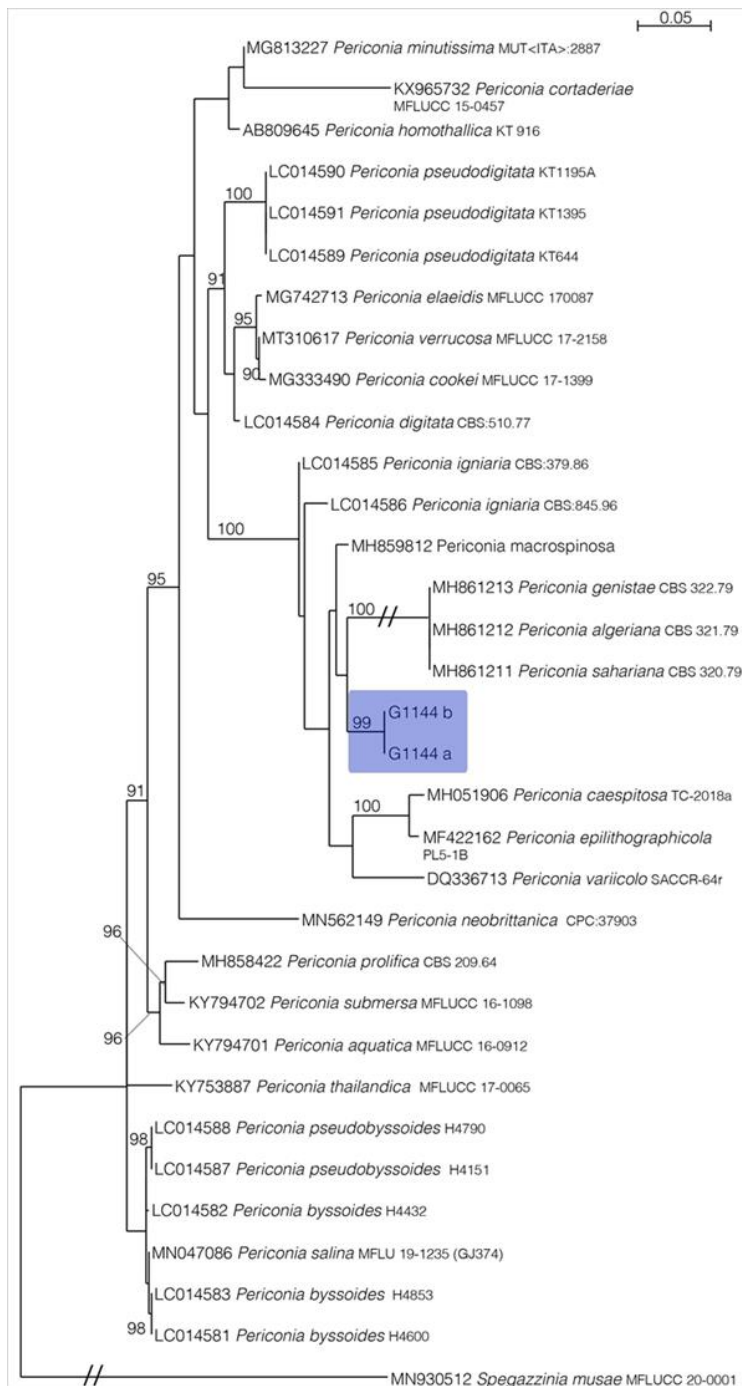
Figure 50. Molecular phylogenetic analysis of fungal ITS sequences reveal strain G1144 can be identified as *Periconia* sp., (Periconiaceae, Pleosporales. Dothideomycetes, Ascomycota). Phylogram of the most likely tree (−lnL = 2968.978) from a Maximum Likelihood analysis of 33 sequences based on the ITS region (483 bp) using IQ-TREE. Numbers refer to UFBoot support values ≥ 90% based on 5000 replicates. Nodes ≥95 are considered strongly supported. *Spegazzinia musae* MFLUCC 20-0001 was used as outgroup. Bar indicates nucleotide substitutions per site.

71
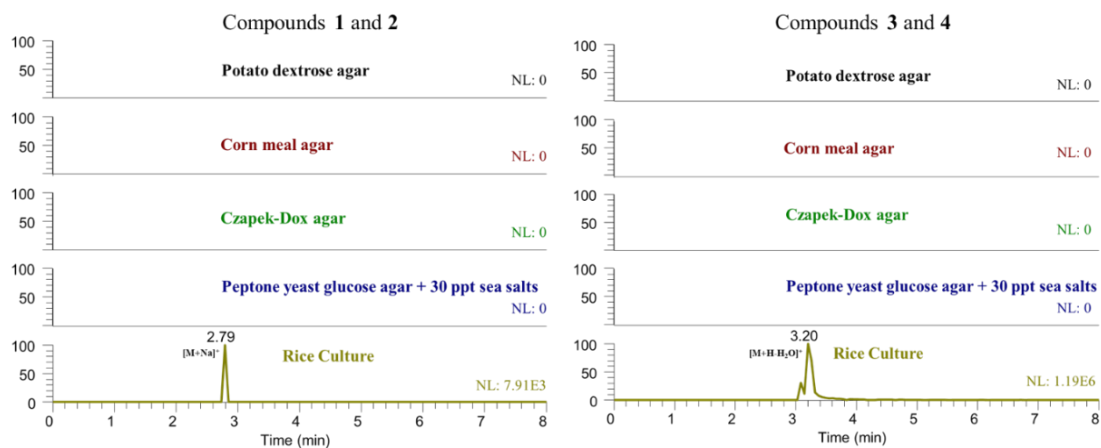
Figure 51. Extracted Ion Chromatograms (XIC) of compounds **1**-**4** grown on different media. Strain G1144 was first grown on a Petri dish culture (Corn meal agar; Czapek-Dox agar and peptone yeast glucose agar + 30 ppt sea salts). Then the PYGA + salt media was used to sale up the growth using solid fermentation media in 250-ml Erlenmeyer flasks on Rice that was autoclaved with sea salts.
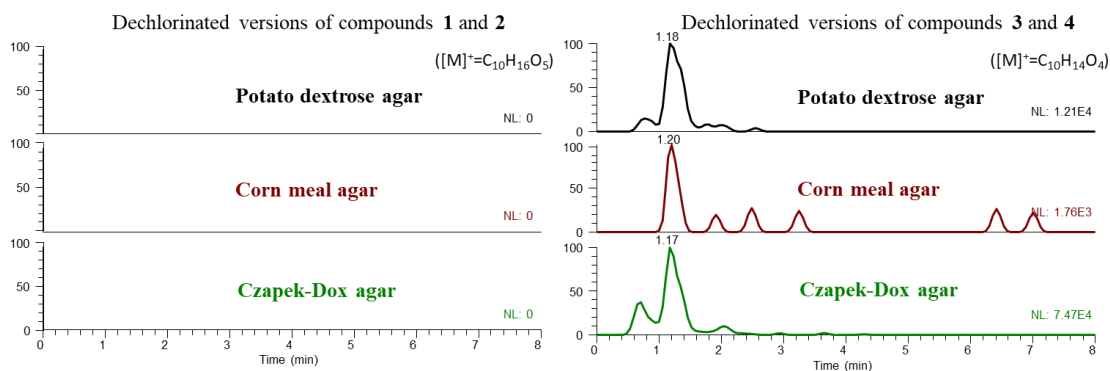
Figure 52. Extracted Ion Chromatograms (XIC) of dechlorinated versions of compounds 1-**2** ($[M]^+=C_{10}H_{16}O_5$) and 3-4 ($[M]^+=C_{10}H_{14}O_4$) in Petri dish cultures that were grown without the addition of sea salts.
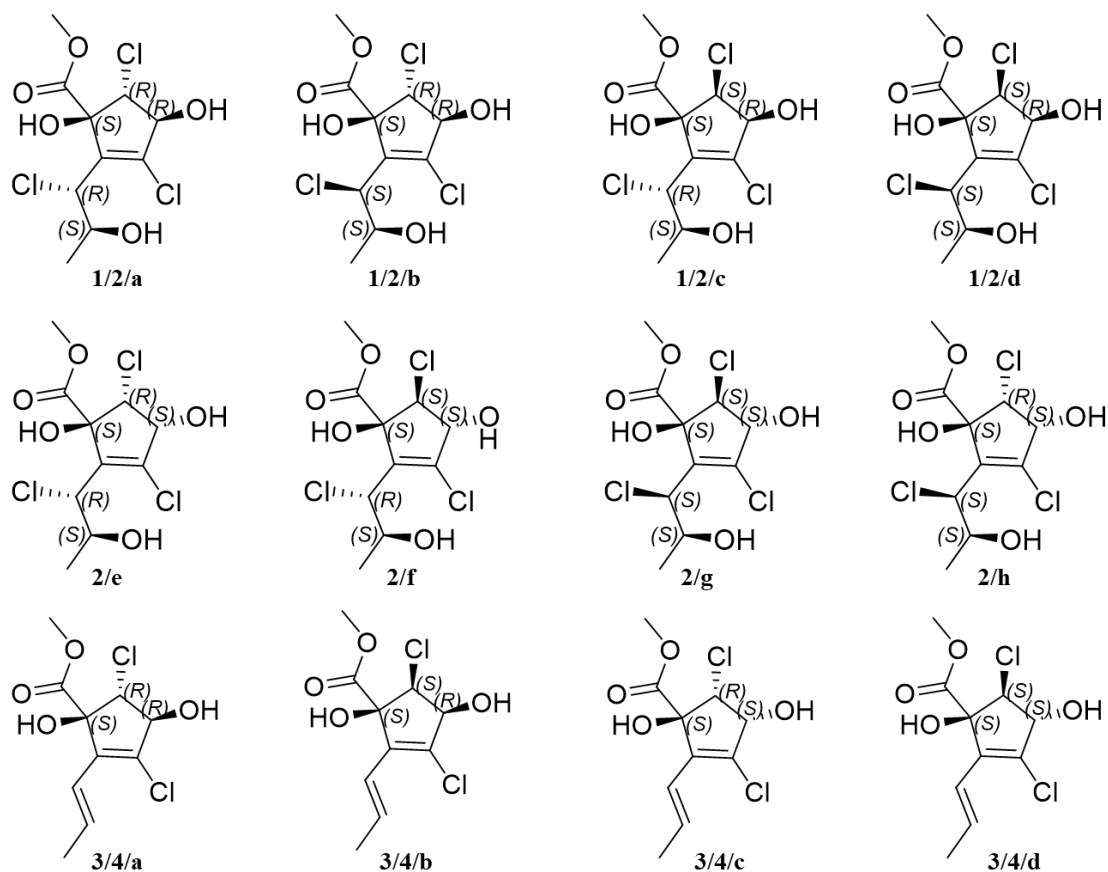
Figure 53. The structures used in GIAO NMR calculations. GIAO NMR calculations cannot distinguish between enantiomers, thus, only half of all possible stereoisomers are shown for each compound.
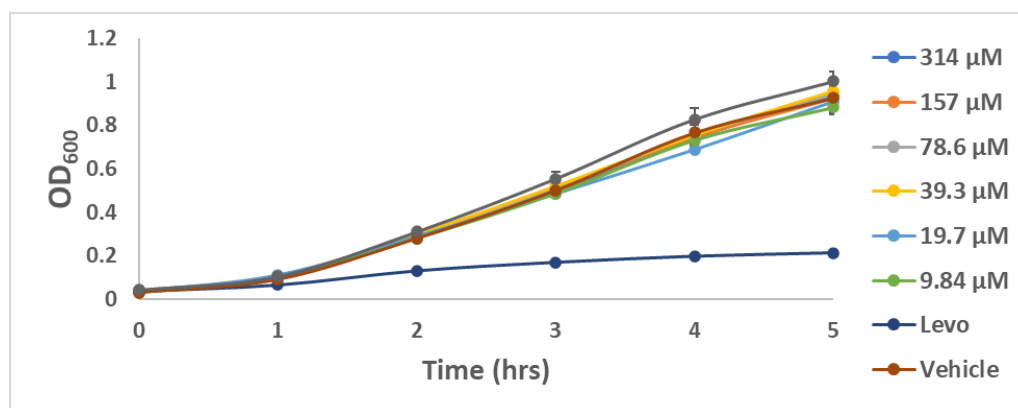
Figure 54. Growth curves for 1 incubated with methicillin resistant *Staphylococcus aureus* (MRSA) strain USA 300 (AH1263). Turbidity (measured by OD_{600}) remains consistent even in

the presence of **1**, demonstrating an absence of growth inhibition or growth delay under the assay conditions. The positive control, levofloxacin, causes significant growth inhibition, as expected.
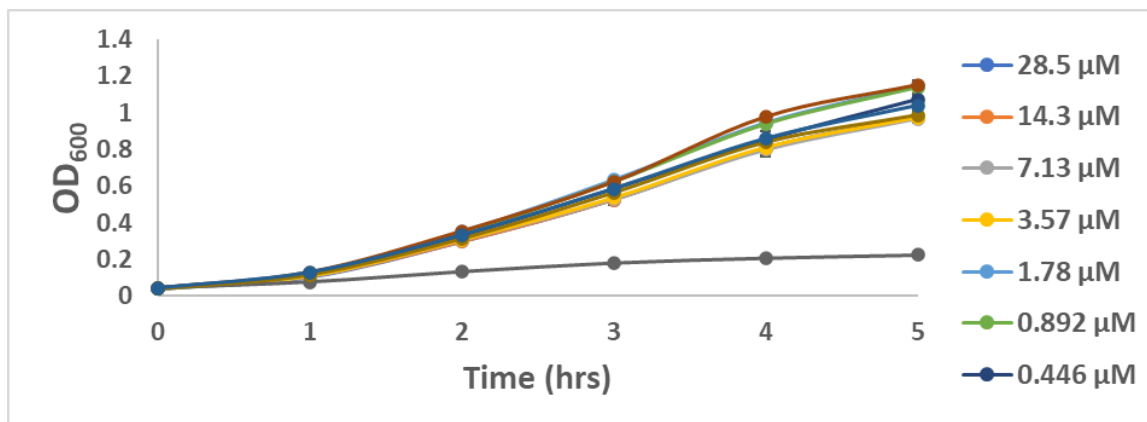
Figure 55. Growth curve for ambuic acid incubated with methicillin resistant *Staphylococcus aureus* (MRSA) strain USA 300. Ambuic acid was tested due to its known quorum sensing inhibition activity. As expected, it did not cause growth inhibition or growth delay. The known antimicrobial levofloxacin inhibited bacterial growth.
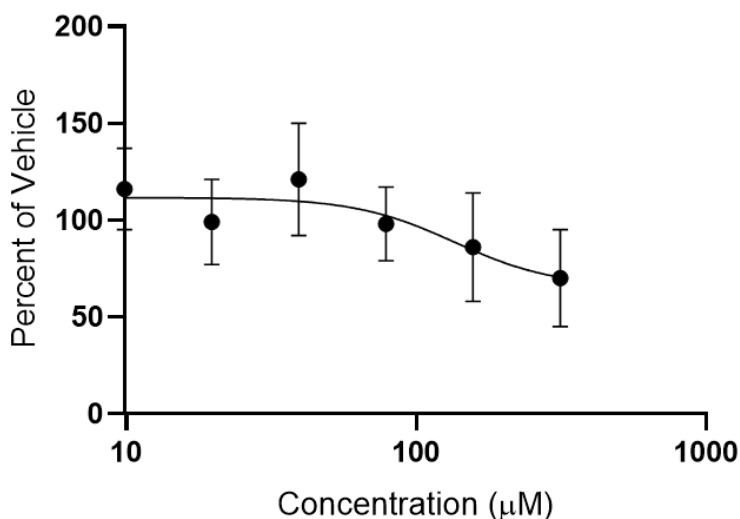
Figure 56. Evaluation of quorum sensing inhibition of 1 against methicillin resistant *Staphylococcus aureus* (MRSA) strain USA 300 (AH1263). A mass spectrometric assay is used to measure the change in peak area of the signaling molecule AIP-1, which is produced by the quorum sensing system in the absence of an inhibitor. No significant inhibition of quorum sensing was observed even at the highest concentration tested (314 µM). The positive control used in this assay was the known quorum sensing inhibitor ambuic acid, which completely inhibited production of AIP at a concentration of 10 µg/mL (28.5 µM) (data not shown).

74
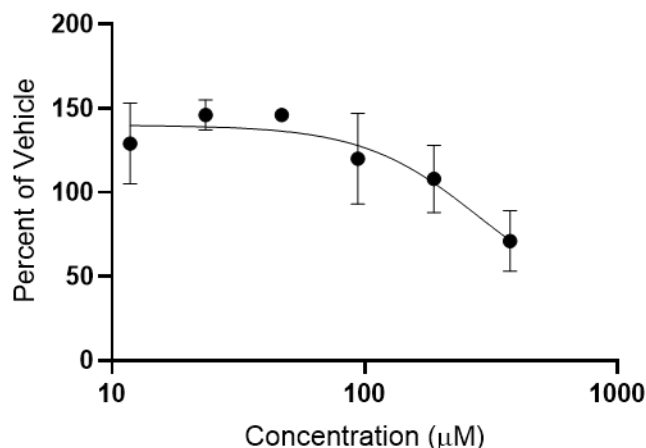
Figure 57. Evaluation of quorum sensing inhibition of 4 against methicillin resistant *Staphylococcus aureus* (MRSA) strain USA 300 (AH1263). The same assay described in Figure S38 was employed. Although a trend towards weak inhibition of quorum sensing was observed at the highest concentration tested (376 µM), slight growth inhibition was also observed for this concentration (Figure S36), thus, it is not possible to conclude any quorum sensing inhibitory activity of **4**.

Table 6. Calculated and experimental ^{13}C shifts (in ppm) for **1**.

Position	^{13}C Corrected Calculated				^{13}C Experimental
	1/a	1/b	1/c	1/d	1
1	83.27765	80.82854	81.47758	79.15492	88.22
2	135.7525	136.445	136.164	136.1466	137.77
3	145.1518	143.0541	146.2658	144.4815	140.44
4	77.38067	77.09137	75.45216	74.27148	76.08
5	73.76529	73.85792	71.96018	72.9259	65.00
1'	61.45889	68.41102	63.09973	68.57598	57.13
1''	169.1914	170.1342	169.3212	170.6907	171.98
2'	69.41832	68.93873	69.2612	69.77431	69.53
2''	49.07905	48.35699	50.69909	49.63134	54.52
3'	17.15454	14.51207	17.92909	15.97725	20.96

Table 7. Calculated and experimental ^{1}H shifts (in ppm) for **1**.

Position	^{1}H Corrected Calculated				^{1}H Experimental
	1/a	1/b	1/c	1/d	1
4	4.713598	4.649628	4.539801	4.564645	4.47
5	4.158786	4.100757	4.700688	4.535797	4.43
1'	4.684583	4.798401	4.541881	4.732902	4.51
2'	4.359176	4.346048	4.146526	4.157221	4.33
2''	3.690128	3.712688	3.673666	3.593602	3.91
3'	1.38373	1.382477	1.387438	1.405833	1.34

Table 8. Average values of the correlation coefficients for **1a-1d**. The "all" refers to ^{13}C and ^1H results combined using the geometric mean.

Compound	Correlation coefficient (all)
1/a	0.99174
1/b	0.98786
1/c	0.992656
1/d	0.98938

Table 9. Calculated and experimental ^{13}C shifts (in ppm) for **2**.

Position	^{13}C Corrected Calculated								^{13}C Experimental
	2/a	**2/b**	**2/c**	**2/d**	**2/e**	**2/f**	**2/g**	**2/h**	**2**
1	83.4253	80.97767	81.62389	79.30416	87.28655	79.85094	78.22909	84.59434	86.61
2	136.0221	136.669	136.4141	136.3576	135.8285	135.0199	135.9611	138.1912	137.58
3	145.4432	143.287	146.5351	144.7015	144.7624	147.485	146.0263	143.0825	142.19
4	77.51461	77.23547	75.58702	74.41543	74.82991	78.79241	78.26449	74.7622	75.87
5	73.89083	73.99766	72.08842	73.0684	69.55377	70.92024	70.91368	69.77974	64.94
1'	61.55583	68.54343	63.21114	68.71376	62.79037	64.92062	68.34844	68.33552	59.55
1"	169.5387	170.4036	169.6343	170.9391	169.908	169.5828	170.3196	169.6136	171.9
2'	69.53375	69.07184	69.38431	69.91339	70.67522	69.00406	68.8622	69.30477	70.09
2"	49.14722	48.4624	50.78695	49.7486	50.06028	50.74336	49.73156	49.89324	54.62
3'	17.1485	14.57191	17.95474	16.05805	17.52508	16.90063	16.56354	15.66288	19.87

Table 10. Calculated and experimental ^1H shifts (in ppm) for **2**.

Position	^{13}H Corrected Calculated								^{13}H Experimental
	2/a	**2/b**	**2/c**	**2/d**	**2/e**	**2/f**	**2/g**	**2/h**	**2**
4	4.79321	4.723439	4.613106	4.634058	4.395147	4.801949	4.668967	4.427726	4.52
5	4.216623	4.155235	4.780424	4.604249	4.459307	4.612744	4.57428	4.438642	4.47
1`	4.763056	4.877452	4.615269	4.807919	4.975743	4.686482	4.870091	4.869136	4.82
2`	4.424878	4.409165	4.204112	4.213064	4.30038	4.004369	4.088791	4.398088	4.20
2``	3.729573	3.753498	3.712351	3.630673	3.778603	3.807741	3.677844	3.798695	3.92
3`	1.33266	1.341211	1.334739	1.370037	1.35082	1.346714	1.380026	1.327713	1.33

Table 11. Average values of the correlation coefficients for **2/a-2/h**. The "all" refers to ^{13}C and ^1H results combined using the geometric mean.

Compound	Correlation coefficient (all)
2/a	0.99283
2/b	0.990822
2/c	0.993887
2/d	0.993412
2/e	0.997223
2/f	0.993243
2/g	0.993720
2/h	0.996134

Table 12. Calculated and experimental ^{13}C shifts (in ppm) for **3**.

Position	^{13}C Corrected Calculated				^{13}C Experimental
	3/a	**3/b**	**3/c**	**3/d**	**3**
1	82.40298	81.50882	85.52416	78.89527	80.42
2	134.2871	135.7755	135.4442	133.2303	134.84
3	135.6425	137.9911	135.4698	137.9726	134.01
4	78.16137	78.02165	75.07589	79.76761	80.59
5	75.49857	69.49433	72.04271	73.2208	67.90
1'	117.0761	117.6985	116.6528	118.2178	121.10
1"	170.8538	169.9947	170.2807	171.3465	173.04
2'	136.3176	135.62	137.5831	134.9608	132.54
2"	49.71809	51.48739	50.88065	50.96172	53.96
3'	17.76191	20.12814	18.76602	19.14661	19.32

Table 13. Calculated and experimental ^1H shifts (in ppm) for **3**.

Position	^1H Corrected Calculated				^1H Experimental
	3/a	**3/b**	**3/c**	**3/d**	**3**
4	4.599163	4.284394	4.312912	4.717835	4.80
5	4.124393	4.490997	4.398296	4.262317	4.33
1'	6.10401	6.269808	6.101895	6.197317	6.18
2'	6.349987	6.177793	6.387182	6.090089	5.93
2"	3.680877	3.681981	3.691649	3.661289	3.82
3'	2.01157	1.965027	1.978065	1.941153	1.81

Table 14. Average values of the correlation coefficients for **3/a-3/d**. The "all" refers to ^{13}C and ^{1}H results combined using the geometric mean.

Compound	Correlation coefficient (all)
3/a	0.99366
3/b	0.994962
3/c	0.991782
3/d	0.997549

Table 15. Calculated and experimental ^{13}C shifts (in ppm) for **4**.

Position	^{13}C Corrected Calculated				^{13}C Experimental
	4/a	4/b	4/c	4/d	4
1	82.6355	81.74797	85.80163	79.09088	87.31
2	134.7242	136.1984	135.8042	133.7003	133.13
3	136.085	138.4216	135.8298	138.4664	137.08
4	78.37717	78.24899	75.33609	79.96762	75.58
5	75.70387	69.69279	72.2979	73.38777	66.08
1'	117.4453	118.0602	116.9817	118.6119	120.65
1"	171.435	170.5335	170.6981	172.0088	172.18
2'	136.7626	136.0424	137.9465	135.4395	134.55
2"	49.82175	51.62487	51.10088	51.01631	54.63
3'	17.73958	20.15942	18.93321	19.04059	19.54

Table 16. Calculated and experimental ^{1}H shifts (in ppm) for **4**.

Position	^{1}H Corrected Calculated				^{1}H Experimental
	4/a	4/b	4/c	4/d	4
4	4.624189	4.306697	4.335755	4.746143	4.47
5	4.142768	4.514398	4.421392	4.281164	4.47
1'	6.150118	6.302658	6.13004	6.256353	6.17
2'	6.39954	6.210154	6.416171	6.146898	6.17
2"	3.693039	3.701084	3.712652	3.667652	3.91
3'	2.000346	1.975009	1.99399	1.911789	1.82

Table 17. Average values of the correlation coefficients for 4/a-4/d. The "all" refers to ^{13}C and ^{1}H results combined using the geometric mean.

Compound	Correlation coefficient (all)
4/a	0.993532
4/b	0.996964
4/c	0.996395
4/d	0.994656

Table 18. Standard orientation coordinates (Ångstroms) for the lowest-energy conformer of compound **1/2/a**.

Atom	X	Y	Z
O	-1.692195	-1.677196	1.187291
C	-2.402100	-1.156704	0.067665
C	-3.903447	-1.327345	0.241307
C	-1.973299	0.313434	0.019948
Cl	-2.726327	1.120886	-1.419723
C	-0.492269	0.516291	-0.023173
C	0.189768	1.506694	0.556040
Cl	-0.474511	2.765280	1.527186
C	1.684395	1.462752	0.314018
O	2.244248	2.695632	-0.053134
C	1.718042	0.514362	-0.883441
Cl	3.265157	-0.361988	-1.083502
C	0.474318	-0.400985	-0.764144
C	0.803524	-1.661607	0.053611
O	1.283978	-1.371817	1.250241
C	1.630413	-2.494922	2.070461
O	0.679529	-2.776375	-0.401458
O	-0.013140	-0.780295	-2.015421
H	-1.834151	-2.635665	1.229911
H	-2.065955	-1.648217	-0.855169
H	-4.449134	-0.944789	-0.623417
H	-4.142050	-2.389377	0.351097
H	-4.240081	-0.801430	1.140186
H	-2.382899	0.834361	0.890397
H	2.197619	1.028765	1.181798
H	2.520345	3.181611	0.738840
H	1.579682	1.108250	-1.790865
H	2.016342	-2.074688	2.996339
H	0.739114	-3.096004	2.261174
H	2.388288	-3.101084	1.570959
H	0.184017	-1.724165	-2.152495

Energy = -2145.069594 hartree

Table 19. Standard orientation coordinates (Ångstroms) for the lowest-energy conformer of compound **1/2/b**.

Atom	X	Y	Z
O	-4.141178	-0.526120	0.619929
C	-2.811322	-0.206252	-0.98253
C	-2.833142	1.172259	-1.621743
C	-1.928705	-0.193452	0.278225
Cl	-1.843379	-1.88436	0.956347
C	-0.542238	0.324	0.092868
C	-0.028396	1.438742	0.618629
Cl	-0.836582	2.547557	1.659842
C	1.421611	1.683897	0.257989
O	1.703722	2.996263	-0.146771
C	1.55557	0.74239	-0.937875
Cl	3.225687	0.174448	-1.231745
C	0.51981	-0.391444	-0.732725
C	1.149803	-1.568535	0.030607
O	1.55806	-1.221832	1.240979
C	2.207285	-2.256495	1.996946
O	1.282644	-2.662185	-0.466543
O	0.016069	-0.856615	-1.948019
H	-4.186101	-1.459553	-0.360861
H	-2.411863	-0.941085	-1.689686
H	-1.849967	1.430526	-2.021749
H	-3.558039	1.172728	-2.438339
H	-3.131943	1.931468	-0.891156
H	-2.444215	0.393702	1.043373
H	2.070031	1.367996	1.086327
H	1.958565	3.531943	0.620007
H	1.249739	1.285924	-1.836186
H	3.095524	-2.600103	1.463856
H	2.475064	-1.799665	2.946733
H	1.517079	-3.088771	2.145851
H	0.322619	-1.77181	-2.083784

Energy = -2145.073203 hartree

Table 20. Standard orientation coordinates (Ångstroms) for the lowest-energy conformer of compound **1/2/c**.

Atom	X	Y	Z
O	2.883065	-0.495866	-0.300066
C	2.567725	0.861440	-0.520241
C	2.218495	1.016724	-1.991083
C	1.406269	1.347626	0.366196
Cl	1.833347	1.037997	2.106129
C	0.049577	0.791196	0.062086
C	-0.969249	1.506091	-0.432435
Cl	-0.936516	3.180749	-0.846335
C	-2.276402	0.746140	-0.523204
O	-3.135975	1.056896	0.540857
C	-1.715027	-0.684627	-0.517495
Cl	-2.883428	-1.933988	-0.038284
C	-0.484003	-0.610121	0.414436
C	0.485967	-1.771643	0.177626
O	0.642976	-2.043563	-1.107516
C	1.591891	-3.075194	-1.418215
O	1.000796	-2.373025	1.092218
O	-0.916422	-0.632226	1.749205
H	3.246168	-0.604355	0.593929
H	3.430594	1.494849	-0.270342
H	1.882455	2.034660	-2.209176
H	3.098859	0.798459	-2.598969
H	1.423981	0.314730	-2.260936
H	1.357710	2.436078	0.280298
H	-2.826511	0.962997	-1.442270
H	-2.714582	0.801136	1.379389
H	-1.377936	-0.932581	-1.524229
H	1.557015	-3.185336	-2.499973
H	2.581321	-2.756046	-1.089467
H	1.303142	-4.003954	-0.923562
H	-0.237042	-1.065050	2.296040

Energy = -2145.065576 hartree

Table 21. Standard orientation coordinates (Ångstroms) for the lowest-energy conformer of compound **1/2/d**.

Atom	X	Y	Z
O	3.891758	-1.045411	-0.363768
C	2.535279	-0.906148	-0.74383
C	1.990775	-2.297231	-1.021236
C	1.751853	-0.248176	0.405461
Cl	2.324606	1.475218	0.599727
C	0.267508	-0.248919	0.26754
C	-0.607834	-0.874997	1.056719
Cl	-0.235473	-1.829267	2.439413
C	-2.055686	-0.617024	0.693022
O	-2.932308	-1.682282	0.87949
C	-1.910857	-0.080836	-0.75659
Cl	-2.024736	-1.43325	-1.925493
C	-0.470005	0.536227	-0.805873
C	-0.600416	2.031161	-0.4506
O	-1.059154	2.225977	0.776268
C	-1.19946	3.597981	1.18266
O	-0.356228	2.905571	-1.249383
O	0.162097	0.433745	-2.040073
H	4.310378	-0.170912	-0.34777
H	2.444053	-0.284094	-1.640209
H	0.977276	-2.240455	-1.426096
H	2.636991	-2.791591	-1.749664
H	1.978415	-2.896605	-0.104469
H	2.038037	-0.747947	1.334923
H	-2.436125	0.196521	1.321602
H	-2.663624	-2.433267	0.324072
H	-2.695641	0.627185	-1.030974
H	-1.591411	3.562242	2.196296
H	-0.222581	4.084298	1.159761
H	-1.888368	4.116002	0.513793
H	0.161617	1.309679	-2.467169

Energy = -2145.068111 hartree

80

Table 22. Standard orientation coordinates (Ångstroms) for the lowest-energy conformer of compound **2/e**.

Atom	X	Y	Z
O	1.240795	2.305907	0.468681
C	2.217680	1.320093	0.770553
C	2.002355	0.844370	2.198949
C	2.112325	0.150158	-0.213938
Cl	2.639568	0.712457	-1.862399
C	0.756544	-0.483823	-0.280164
C	0.495996	-1.749484	0.065763
Cl	1.629944	-2.889735	0.694326
C	-0.955843	-2.155302	-0.055606
O	-1.598231	-2.251641	1.184089
C	-1.441806	-1.029203	-0.994508
Cl	-3.191707	-0.702170	-0.893334
C	-0.550112	0.203987	-0.716553
C	-1.150665	1.017275	0.447118
O	-1.587453	2.203895	0.075133
C	-2.122395	3.021307	1.126491
O	-1.251930	0.571602	1.572734
O	-0.473319	0.945111	-1.893930
H	1.601980	2.931071	-0.178795
H	3.224814	1.743738	0.670818
H	2.739744	0.080626	2.461776
H	2.116248	1.690732	2.879774
H	0.999461	0.429174	2.324074
H	2.845865	-0.610584	0.061561
H	-1.064105	-3.132905	-0.533641
H	-1.524702	-1.394567	1.639339
H	-1.236446	-1.313231	-2.029232
H	-2.970524	2.517549	1.592865
H	-1.344171	3.208293	1.868863
H	-2.435122	3.945640	0.646216
H	-0.099091	1.819823	-1.701989

Energy = -2145.067561 hartree

Table 23. Standard orientation coordinates (Ångstroms) for the lowest-energy conformer of compound **2/f**.

Atom	X	Y	Z
O	2.815816	-0.430759	-0.659581
C	2.466968	0.935253	-0.719474
C	1.900391	1.201905	-2.103913
C	1.452606	1.331380	0.369074
Cl	2.153625	0.904925	1.992846
C	0.070623	0.771195	0.233968
C	-1.014288	1.501760	-0.049386
Cl	-1.054325	3.195610	-0.359329
C	-2.311375	0.728745	-0.023295
O	-3.151736	1.099276	-1.080940
C	-1.755238	-0.689626	-0.156872
Cl	-2.852323	-1.961778	0.439486
C	-0.390129	-0.661025	0.566105
C	0.534629	-1.780395	0.070749
O	0.479663	-1.939242	-1.241334
C	1.369472	-2.921965	-1.791488
O	1.198375	-2.448356	0.830839
O	-0.580918	-0.801081	1.946123
H	3.300341	-0.606625	0.163301
H	3.356378	1.559127	-0.551689
H	1.539633	2.231131	-2.188279
H	2.678996	1.039040	-2.852004
H	1.070883	0.518088	-2.305923
H	1.382577	2.421999	0.374440
H	-2.801288	0.874032	0.950419
H	-4.067645	0.870005	-0.861073
H	-1.599262	-0.880620	-1.219430
H	1.166669	-3.896159	-1.343570
H	1.161969	-2.935858	-2.859363
H	2.397911	-2.616647	-1.596680
H	0.182685	-1.278464	2.315141

Energy = -2145.066516 hartree

Table 24. Standard orientation coordinates (Ångstroms) for the lowest-energy conformer of compound **2/g**.

Atom	X	Y	Z
O	-3.91571	-0.13883	0.90322
C	-2.51851	-0.22864	1.09416
C	-2.26599	-1.45570	1.95576
C	-1.81131	-0.37960	-0.26621
Cl	-2.23354	1.05593	-1.31007
C	-0.32919	-0.53664	-0.17385
C	0.36636	-1.63852	-0.46976
Cl	-0.25935	-3.09879	-1.13369
C	1.83441	-1.56964	-0.09530
O	2.70995	-2.04670	-1.07901
C	1.99215	-0.05882	0.04072
Cl	3.32142	0.45141	1.11195
C	0.60990	0.45447	0.51752
C	0.40278	1.92298	0.12619
O	0.72070	2.15849	-1.13737
C	0.46866	3.49122	-1.60588
O	0.02247	2.75751	0.91534
O	0.42940	0.31048	1.89984
H	-4.12799	0.70137	0.46819
H	-2.13536	0.67138	1.59462
H	-1.20856	-1.54343	2.20905
H	-2.84465	-1.36327	2.87741
H	-2.59570	-2.35839	1.43103
H	-2.24456	-1.23597	-0.78967
H	1.99155	-2.07644	0.86747
H	2.83997	-3.00166	-0.97251
H	2.21266	0.33912	-0.95163
H	0.78283	3.49876	-2.64691
H	-0.59780	3.71053	-1.51922
H	1.04394	4.20806	-1.01802
H	0.56859	1.17035	2.33458

Energy = -2145.068897 hartree

82

Table 25. Standard orientation coordinates (Ångstroms) for the lowest-energy conformer of compound **2/h**.

Atom	X	Y	Z
O	-4.14451	0.73382	0.40241
C	2.85570	-0.38910	0.87290
C	2.98841	0.90939	1.65107
C	1.91219	-0.19759	-0.32921
Cl	1.68461	-1.80272	-1.16180
C	0.57299	0.38382	-0.01771
C	0.13078	1.59334	-0.37570
Cl	0.98643	2.74610	-1.32870
C	-1.28059	1.90609	0.07233
O	-2.19847	1.87810	-0.98565
C	-1.45169	0.81538	1.15555
Cl	-3.14189	0.31314	1.42534
C	-0.48900	-0.34789	0.79448
C	-1.20160	-1.44178	-0.01820
O	-1.63455	-1.00858	-1.19820
C	-2.32314	-1.98677	-2.00029
O	-1.37220	-2.55690	0.41064
O	0.06111	-0.92829	1.93980
H	4.12709	-1.63789	0.05199
H	2.45339	-1.17513	1.52059
H	2.04424	1.16984	2.13491
H	3.75502	0.78502	2.41859
H	3.28968	1.72757	0.98839
H	2.42673	0.43121	-1.06093
H	-1.35873	2.90470	0.51092
H	-2.15861	1.00825	-1.41172
H	-1.08762	1.20276	2.10998
H	-2.59634	-1.47167	-2.91843
H	-1.65141	-2.82134	-2.20682
H	-3.20853	-2.33920	-1.46922
H	-0.31794	-1.81839	2.05607

Energy = -2145.069909 hartree

Table 26. Standard orientation coordinates (Ångstroms) for the lowest-energy conformer of compound **3/4/a**.

Atom	X	Y	Z
C	-0.552787	2.178915	2.556917
O	0.400474	-1.191944	1.524418
C	0.081254	-1.657182	0.326080
C	0.052821	-0.551571	-0.740687
O	-0.364272	-1.097716	-1.956718
C	1.438640	0.126264	-0.876356
C	1.444141	1.327305	0.063829
O	2.222377	2.353190	-0.498573
C	-0.036707	1.614802	0.123594
Cl	-0.571915	3.110603	0.799869
C	-0.825798	0.612856	-0.291408
C	-2.279069	0.555216	-0.231165
C	-3.016129	-0.534030	-0.493518
C	-4.508060	-0.575152	-0.383133
Cl	2.824595	-0.986344	-0.650123
O	-0.136349	-2.818493	0.066299
H	1.347177	-2.875889	2.283379
H	0.815075	-1.623551	3.454319
H	-0.384646	-2.720083	2.693901
H	-0.259095	-2.064826	-1.918846
H	1.505468	0.494971	-1.902852
H	1.813561	1.049953	1.061148
H	2.458094	2.997734	0.186118
H	-2.775031	1.474111	0.080008
H	-2.524883	-1.450267	-0.817030
H	-4.958397	-0.840776	-1.345555
H	-4.822103	-1.340270	0.334919
H	-4.911898	0.388641	-0.063522

Energy = -1609.094592 hartree

Table 27. Standard orientation coordinates (Ångstroms) for the lowest-energy conformer of compound **3/4/b**.

Atom	X	Y	Z
C	-4.568031	-2.039210	1.841633
O	-1.486056	-1.237118	1.342865
C	-1.177614	-1.413652	0.064846
C	-0.007983	-0.532987	-0.374570
O	0.144595	-0.604528	-1.766379
C	1.279922	-0.938456	0.393694
C	2.162853	0.323908	0.359956
O	2.980758	0.451270	-0.774582
C	1.073128	1.369544	0.410578
Cl	1.463656	2.994513	0.839221
C	-0.132878	0.937075	0.007927
C	-1.349632	1.721025	-0.147856
C	-2.437819	1.306722	-0.812142
C	-3.680182	2.124854	-0.974962
Cl	2.049078	-2.396336	-0.279707
O	-1.716719	-2.204447	-0.675447
H	-2.326322	-3.098061	1.736267
H	-2.674351	-1.766463	2.888934
H	-3.480179	-1.812194	1.286544
H	-0.073782	-1.506582	-2.063396
H	1.024458	-1.162086	1.431398
H	2.831135	0.368263	1.224032
H	2.431355	0.381103	-1.573996
H	-1.337693	2.714966	0.298001
H	-2.435570	0.328595	-1.294880
H	-4.547330	1.597974	-0.562560
H	-3.588967	3.091088	-0.473068
H	-3.890453	2.300038	-2.035299

Energy = -1609.092228 hartree

Table 28. Standard orientation coordinates (Ångstroms) for the lowest-energy conformer of compound **3/4/c**.

Atom	X	Y	Z
C	1.081977	-1.82322	2.545992
O	0.702565	-0.93618	1.47688
C	0.429798	-1.52333	0.314449
C	0.122323	-0.51586	-0.80427
O	-0.27108	-1.21609	-1.94859
C	1.334331	0.406429	-1.10473
C	1.141818	1.704272	-0.28961
O	1.813963	1.763534	0.941869
C	-0.35885	1.676697	-0.13214
Cl	-1.16952	3.08818	0.444668
C	-0.9396	0.488919	-0.36738
C	-2.3409	0.145771	-0.17668
C	-2.84913	-1.09077	-0.28791
C	-4.28786	-1.42281	-0.04626
Cl	2.921969	-0.38018	-0.87246
O	0.444764	-2.71723	0.131807
H	1.987854	-2.36383	2.266973
H	1.259371	-1.18288	3.407146
H	0.27229	-2.52647	2.743835
H	0.084021	-2.12139	-1.90216
H	1.260825	0.639039	-2.16888
H	1.486367	2.573318	-0.85702
H	1.511649	1.026891	1.494718
H	-2.99592	0.970213	0.102298
H	-2.20054	-1.91492	-0.5807
H	-4.73608	-1.86549	-0.94221
H	-4.3841	-2.16398	0.754381
H	-4.86252	-0.53535	0.229573

Energy = -1609.09172 hartree

85

Table 29. Standard orientation coordinates (Ångstroms) for the lowest-energy conformer of compound **3/4/d**.

Atom	X	Y	Z
C	-2.226290	-1.995812	2.158044
O	-1.258839	-1.196876	1.460095
C	-1.153551	-1.423887	0.157586
C	-0.086126	-0.545332	-0.501149
O	-0.166527	-0.672161	-1.892041
C	1.312382	-0.910912	0.070575
C	2.148849	0.359181	-0.055815
O	3.109816	0.383292	0.967512
C	1.053996	1.394341	0.079143
Cl	1.476422	3.030156	0.427207
C	-0.184274	0.933949	-0.147686
C	-1.427314	1.691774	-0.169075
C	-2.584083	1.232107	-0.666569
C	-3.858451	2.016833	-0.684611
Cl	2.027846	-2.344573	-0.714187
O	-1.787016	-2.254924	-0.452927
H	-2.169690	-1.680379	3.197208
H	-3.221291	-1.810059	1.749120
H	-1.978381	-3.053746	2.057280
H	-0.419739	-1.586870	-2.110006
H	1.229566	-1.141188	1.135676
H	2.620377	0.431257	-1.046146
H	3.806055	1.021338	0.748236
H	-1.379983	2.700579	0.239720
H	-2.620755	0.237895	-1.113276
H	-4.647361	1.486251	-0.140683
H	-3.725866	3.002050	-0.231030
H	-4.215794	2.149863	-1.711198

Energy = -1609.092589 hartree

Table 30. Boltzmann Distribution of Conformers of **1/2/a**.

	Energy (kcal/mol)	Relative Energy (kcal/mol)	Boltzmann Factor	Equilibrium Mole Fraction	Number of Imaginary Frequencies
Conformer #8	-1346051.32	0.00	1.000	0.218	0
Conformer #13	-1346051.27	0.05	0.921	0.201	0
Conformer #19	-1346051.01	0.31	0.594	0.130	0
Conformer #9	-1346050.77	0.55	0.397	0.087	0
Conformer #16	-1346050.66	0.65	0.332	0.072	0
Conformer #7	-1346050.51	0.81	0.255	0.056	0
Conformer #2	-1346050.46	0.86	0.235	0.051	0
Conformer #1	-1346050.32	0.99	0.187	0.041	0
Conformer #3	-1346050.30	1.02	0.179	0.039	0
Conformer #12	-1346050.27	1.04	0.172	0.038	0
Conformer #4	-1346049.96	1.35	0.102	0.022	0
Conformer #6	-1346049.87	1.45	0.087	0.019	0
Conformer #10	-1346049.49	1.83	0.046	0.010	1
Conformer #17	-1346049.39	1.92	0.039	0.008	0
Conformer #14	-1346048.67	2.64	0.012	0.003	0
Conformer #18	-1346048.64	2.68	0.011	0.002	0
Conformer #15	-1346048.59	2.72	0.010	0.002	0
Conformer #11	-1346048.10	3.21	0.004	0.001	0
Conformer #20	-1346047.93	3.38	0.003	0.001	0

Table 31. Boltzmann Distribution of Conformers of **1/2/b**.

	Energy (kcal/mol)	Relative Energy (kcal/mol)	Boltzmann Factor	Equilibrium Mole Fraction	Number of Imaginary Frequencies
Conformer #13	-1346053.58	0.00	1.000	0.410	0
Conformer #17	-1346053.51	0.07	0.884	0.363	0
Conformer #15	-1346052.20	1.38	0.098	0.040	0
Conformer #4	-1346052.15	1.43	0.089	0.037	0
Conformer #12	-1346052.13	1.45	0.086	0.035	0
Conformer #2	-1346052.07	1.51	0.078	0.032	0
Conformer #6	-1346052.05	1.53	0.075	0.031	0
Conformer #9	-1346052.03	1.55	0.073	0.030	0
Conformer #1	-1346051.06	2.52	0.014	0.006	0
Conformer #8	-1346050.92	2.66	0.011	0.005	0
Conformer #16	-1346050.80	2.78	0.009	0.004	0
Conformer #10	-1346050.51	3.07	0.006	0.002	0
Conformer #14	-1346050.51	3.07	0.006	0.002	0
Conformer #3	-1346050.26	3.32	0.004	0.002	0
Conformer #5	-1346050.04	3.54	0.003	0.001	0
Conformer #11	-1346048.97	4.61	0.000	0.000	0
Conformer #7	-1346048.85	4.73	0.000	0.000	0

Table 32. Boltzmann Distribution of Conformers of **1/2/c**.

	Energy (kcal/mol)	Relative Energy (kcal/mol)	Boltzmann Factor	Equilibrium Mole Fraction	Number of Imaginary Frequencies
Conformer #29	-1346048.79	0	1.000	0.211	0
Conformer #64	-1346048.33	0.46	0.456	0.096	0
Conformer #20	-1346048.27	0.52	0.416	0.088	0
Conformer #16	-1346048.21	0.58	0.374	0.079	0
Conformer #46	-1346048.00	0.80	0.260	0.055	0
Conformer #69	-1346047.96	0.84	0.243	0.051	0
Conformer #56	-1346047.92	0.87	0.230	0.049	0
Conformer #30	-1346047.92	0.87	0.228	0.048	0
Conformer #27	-1346047.91	0.88	0.226	0.048	0
Conformer #19	-1346047.76	1.04	0.173	0.037	0
Conformer #59	-1346047.52	1.27	0.117	0.025	0
Conformer #26	-1346047.30	1.50	0.080	0.017	0
Conformer #8	-1346047.14	1.65	0.061	0.013	0
Conformer #72	-1346047.10	1.69	0.058	0.012	0
Conformer #23	-1346047.03	1.76	0.051	0.011	0
Conformer #5	-1346047.03	1.76	0.051	0.011	0
Conformer #1	-1346047.03	1.77	0.051	0.011	0
Conformer #61	-1346047.02	1.77	0.050	0.011	0
Conformer #2	-1346047.01	1.79	0.049	0.010	0
Conformer #58	-1346046.96	1.83	0.045	0.010	0
Conformer #73	-1346046.96	1.83	0.045	0.010	0
Conformer #67	-1346046.93	1.87	0.043	0.009	0
Conformer #9	-1346046.90	1.90	0.041	0.009	0
Conformer #28	-1346046.86	1.93	0.038	0.008	0
Conformer #10	-1346046.71	2.08	0.030	0.006	0
Conformer #15	-1346046.69	2.11	0.028	0.006	0
Conformer #63	-1346046.60	2.19	0.025	0.005	0
Conformer #48	-1346046.40	2.39	0.018	0.004	0
Conformer #37	-1346046.37	2.43	0.017	0.003	0
Conformer #41	-1346046.34	2.45	0.016	0.003	0
Conformer #13	-1346046.32	2.48	0.015	0.003	0
Conformer #44	-1346046.22	2.58	0.013	0.003	0
Conformer #52	-1346046.20	2.59	0.013	0.003	0
Conformer #66	-1346046.14	2.65	0.011	0.002	0
Conformer #74	-1346046.14	2.65	0.011	0.002	0
Conformer #42	-1346046.10	2.69	0.011	0.002	0
Conformer #65	-1346046.09	2.70	0.010	0.002	0
Conformer #33	-1346046.07	2.73	0.010	0.002	0
Conformer #49	-1346046.01	2.78	0.009	0.002	0
Conformer #55	-1346046.01	2.78	0.009	0.002	0
Conformer #7	-1346045.74	3.05	0.006	0.001	0
Conformer #68	-1346045.70	3.09	0.005	0.001	1
Conformer #3	-1346045.67	3.12	0.005	0.001	0
Conformer #6	-1346045.67	3.12	0.005	0.001	0
Conformer #21	-1346045.63	3.16	0.005	0.001	0
Conformer #4	-1346045.54	3.26	0.004	0.001	0
Conformer #57	-1346045.42	3.37	0.003	0.001	0
Conformer #43	-1346045.38	3.41	0.003	0.001	0
Conformer #24	-1346045.34	3.45	0.003	0.001	0
Conformer #35	-1346045.30	3.50	0.003	0.001	0
Conformer #60	-1346045.28	3.51	0.003	0.001	0
Conformer #18	-1346045.26	3.54	0.003	0.001	0
Conformer #40	-1346045.24	3.55	0.002	0.001	0
Conformer #34	-1346045.11	3.69	0.002	0.000	0
Conformer #38	-1346045.07	3.72	0.002	0.000	0
Conformer #12	-1346045.07	3.72	0.002	0.000	0
Conformer #62	-1346045.06	3.73	0.002	0.000	0
Conformer #11	-1346045.01	3.78	0.002	0.000	0
Conformer #54	-1346044.93	3.86	0.001	0.000	0
Conformer #36	-1346044.83	3.96	0.001	0.000	0
Conformer #70	-1346044.69	4.11	0.001	0.000	0
Conformer #14	-1346044.52	4.28	0.001	0.000	1
Conformer #53	-1346044.48	4.31	0.001	0.000	0
Conformer #51	-1346044.46	4.34	0.001	0.000	0
Conformer #31	-1346044.30	4.49	0.001	0.000	0
Conformer #50	-1346043.98	4.81	0.000	0.000	0
Conformer #47	-1346043.78	5.01	0.000	0.000	0
Conformer #25	-1346043.65	5.14	0.000	0.000	0
Conformer #32	-1346043.53	5.27	0.000	0.000	0
Conformer #22	-1346043.37	5.42	0.000	0.000	0
Conformer #39	-1346043.11	5.69	0.000	0.000	1
Conformer #45	-1346042.90	5.90	0.000	0.000	0
Conformer #71	-1346042.86	5.93	0.000	0.000	0

Table 33. Boltzmann Distribution of Conformers of **1/2/d**.

	Energy (kcal/mol)	Relative Energy (kcal/mol)	Boltzmann Factor	Equilibrium Mole Fraction	Number of Imaginary Frequencies
Conformer #26	-1346050.38	0	1.000	0.617	0
Conformer #2	-1346049.67	0.71	0.300	0.185	0
Conformer #10	-1346048.74	1.65	0.062	0.038	0
Conformer #16	-1346048.70	1.68	0.058	0.036	0
Conformer #4	-1346048.50	1.88	0.042	0.026	0
Conformer #8	-1346048.42	1.96	0.036	0.022	0
Conformer #31	-1346048.39	1.99	0.035	0.021	0
Conformer #25	-1346047.89	2.50	0.015	0.009	0
Conformer #15	-1346047.49	2.89	0.008	0.005	0
Conformer #13	-1346047.45	2.93	0.007	0.004	0
Conformer #19	-1346047.45	2.93	0.007	0.004	0
Conformer #1	-1346047.42	2.97	0.007	0.004	0
Conformer #23	-1346047.37	3.02	0.006	0.004	0
Conformer #28	-1346047.18	3.20	0.004	0.003	0
Conformer #3	-1346047.16	3.22	0.004	0.003	0
Conformer #29	-1346047.16	3.23	0.004	0.003	0
Conformer #9	-1346047.11	3.28	0.004	0.002	0
Conformer #18	-1346047.05	3.33	0.004	0.002	0
Conformer #5	-1346046.85	3.54	0.003	0.002	0
Conformer #32	-1346046.83	3.56	0.002	0.002	0
Conformer #24	-1346046.79	3.59	0.002	0.001	0
Conformer #27	-1346046.64	3.74	0.002	0.001	0
Conformer #17	-1346046.64	3.74	0.002	0.001	0
Conformer #14	-1346046.60	3.79	0.002	0.001	0
Conformer #22	-1346046.42	3.96	0.001	0.001	0
Conformer #12	-1346046.30	4.09	0.001	0.001	0
Conformer #7	-1346046.14	4.25	0.001	0.000	0
Conformer #21	-1346046.13	4.26	0.001	0.000	0
Conformer #30	-1346046.06	4.32	0.001	0.000	0
Conformer #6	-1346045.85	4.53	0.000	0.000	0
Conformer #11	-1346045.82	4.56	0.000	0.000	0
Conformer #20	-1346044.93	5.45	0.000	0.000	0

Table 34. Boltzmann Distribution of Conformers of **2/e**.

	Energy (kcal/mol)	Relative Energy (kcal/mol)	Boltzmann Factor	Equilibrium Mole Fraction	Number of Imaginary Frequencies
Conformer #3	-1346050.04	0.0	1.000	0.275	0
Conformer #2	-1346049.63	0.4	0.500	0.138	0
Conformer #1	-1346049.61	0.4	0.486	0.134	0
Conformer #25	-1346049.39	0.6	0.336	0.092	0
Conformer #49	-1346049.38	0.7	0.330	0.091	0
Conformer #13	-1346049.32	0.7	0.298	0.082	0
Conformer #39	-1346048.69	1.3	0.103	0.028	0
Conformer #35	-1346048.64	1.4	0.094	0.026	0
Conformer #28	-1346048.48	1.6	0.072	0.020	0
Conformer #7	-1346048.40	1.6	0.062	0.017	0
Conformer #29	-1346048.35	1.7	0.057	0.016	0
Conformer #17	-1346048.18	1.9	0.043	0.012	0
Conformer #40	-1346048.06	2.0	0.035	0.010	0
Conformer #34	-1346047.89	2.2	0.026	0.007	0
Conformer #47	-1346047.88	2.2	0.026	0.007	0
Conformer #27	-1346047.78	2.3	0.022	0.006	0
Conformer #31	-1346047.77	2.3	0.022	0.006	0
Conformer #44	-1346047.63	2.4	0.017	0.005	0
Conformer #33	-1346047.55	2.5	0.015	0.004	0
Conformer #8	-1346047.49	2.5	0.014	0.004	0
Conformer #24	-1346047.38	2.7	0.011	0.003	0
Conformer #12	-1346047.37	2.7	0.011	0.003	0
Conformer #32	-1346047.32	2.7	0.010	0.003	0
Conformer #4	-1346047.09	3.0	0.007	0.002	0
Conformer #30	-1346046.95	3.1	0.005	0.001	0
Conformer #21	-1346046.88	3.2	0.005	0.001	0
Conformer #5	-1346046.74	3.3	0.004	0.001	0
Conformer #26	-1346046.71	3.3	0.004	0.001	0
Conformer #18	-1346046.63	3.4	0.003	0.001	0
Conformer #48	-1346046.51	3.5	0.003	0.001	0
Conformer #43	-1346046.40	3.6	0.002	0.001	0
Conformer #42	-1346046.40	3.6	0.002	0.001	0
Conformer #10	-1346046.30	3.7	0.002	0.000	0
Conformer #20	-1346046.24	3.8	0.002	0.000	0
Conformer #23	-1346046.23	3.8	0.002	0.000	0
Conformer #11	-1346046.18	3.9	0.001	0.000	0
Conformer #6	-1346046.05	4.0	0.001	0.000	0
Conformer #16	-1346046.01	4.0	0.001	0.000	0
Conformer #46	-1346045.96	4.1	0.001	0.000	0
Conformer #14	-1346045.72	4.3	0.001	0.000	0
Conformer #9	-1346045.30	4.7	0.000	0.000	0
Conformer #38	-1346044.71	5.3	0.000	0.000	0
Conformer #37	-1346044.27	5.8	0.000	0.000	0
Conformer #22	-1346044.26	5.8	0.000	0.000	0
Conformer #41	-1346044.24	5.8	0.000	0.000	0
Conformer #45	-1346043.64	6.4	0.000	0.000	0
Conformer #19	-1346043.32	6.7	0.000	0.000	0

Table 35. Boltzmann Distribution of Conformers of **2/f**.

	Energy (kcal/mol)	Relative Energy (kcal/mol)	Boltzmann Factor	Equilibrium Mole Fraction	Number of Imaginary Frequencies
Conformer #39	-1346049.38	0.0	1.000	0.160	0
Conformer #24	-1346049.31	0.1	0.888	0.142	0
Conformer #68	-1346049.31	0.1	0.887	0.142	0
Conformer #46	-1346049.02	0.4	0.537	0.086	0
Conformer #59	-1346048.96	0.4	0.491	0.078	0
Conformer #78	-1346048.94	0.4	0.476	0.076	0
Conformer #2	-1346048.87	0.5	0.418	0.067	0
Conformer #67	-1346048.78	0.6	0.361	0.058	0
Conformer #15	-1346048.73	0.7	0.333	0.053	0
Conformer #58	-1346047.91	1.5	0.083	0.013	0
Conformer #25	-1346047.77	1.6	0.066	0.011	1
Conformer #75	-1346047.62	1.8	0.051	0.008	0
Conformer #26	-1346047.57	1.8	0.047	0.008	0
Conformer #1	-1346047.56	1.8	0.046	0.007	0
Conformer #60	-1346047.50	1.9	0.041	0.007	1
Conformer #12	-1346047.38	2.0	0.034	0.005	0
Conformer #11	-1346047.38	2.0	0.034	0.005	0
Conformer #65	-1346047.35	2.0	0.032	0.005	0
Conformer #17	-1346047.32	2.1	0.030	0.005	0
Conformer #74	-1346047.26	2.1	0.028	0.004	0
Conformer #21	-1346047.24	2.1	0.027	0.004	0
Conformer #41	-1346047.23	2.1	0.026	0.004	0
Conformer #42	-1346047.19	2.2	0.024	0.004	0
Conformer #54	-1346047.18	2.2	0.024	0.004	0
Conformer #3	-1346047.13	2.2	0.022	0.004	0
Conformer #49	-1346047.12	2.3	0.022	0.004	0
Conformer #6	-1346047.12	2.3	0.022	0.003	0
Conformer #71	-1346047.10	2.3	0.021	0.003	0
Conformer #51	-1346047.09	2.3	0.021	0.003	0
Conformer #32	-1346047.09	2.3	0.021	0.003	0
Conformer #34	-1346047.01	2.4	0.018	0.003	0
Conformer #38	-1346047.00	2.4	0.018	0.003	0
Conformer #53	-1346046.83	2.6	0.013	0.002	0
Conformer #16	-1346046.48	2.9	0.007	0.001	0
Conformer #64	-1346046.45	2.9	0.007	0.001	0
Conformer #50	-1346046.41	3.0	0.007	0.001	0
Conformer #19	-1346046.41	3.0	0.007	0.001	0
Conformer #47	-1346046.40	3.0	0.006	0.001	0
Conformer #23	-1346046.35	3.0	0.006	0.001	0
Conformer #35	-1346046.30	3.1	0.005	0.001	0
Conformer #77	-1346046.25	3.1	0.005	0.001	0
Conformer #44	-1346046.21	3.2	0.005	0.001	0
Conformer #27	-1346046.21	3.2	0.005	0.001	0
Conformer #52	-1346046.21	3.2	0.005	0.001	0
Conformer #56	-1346046.18	3.2	0.004	0.001	0
Conformer #40	-1346046.16	3.2	0.004	0.001	0
Conformer #29	-1346046.13	3.3	0.004	0.001	0
Conformer #28	-1346046.04	3.3	0.004	0.001	0
Conformer #30	-1346046.03	3.4	0.003	0.001	0
Conformer #13	-1346045.72	3.7	0.002	0.000	0
Conformer #83	-1346045.63	3.8	0.002	0.000	0
Conformer #80	-1346045.48	3.9	0.001	0.000	0
Conformer #36	-1346045.48	3.9	0.001	0.000	0
Conformer #37	-1346045.37	4.0	0.001	0.000	0
Conformer #10	-1346045.36	4.0	0.001	0.000	0
Conformer #62	-1346045.34	4.0	0.001	0.000	0
Conformer #45	-1346045.29	4.1	0.001	0.000	0
Conformer #72	-1346045.25	4.1	0.001	0.000	0
Conformer #43	-1346045.17	4.2	0.001	0.000	0
Conformer #31	-1346045.10	4.3	0.001	0.000	0
Conformer #20	-1346045.08	4.3	0.001	0.000	0
Conformer #33	-1346044.93	4.5	0.001	0.000	0
Conformer #63	-1346044.83	4.5	0.000	0.000	0
Conformer #57	-1346044.76	4.6	0.000	0.000	0
Conformer #14	-1346044.75	4.6	0.000	0.000	0
Conformer #4	-1346044.41	5.0	0.000	0.000	0
Conformer #7	-1346044.39	5.0	0.000	0.000	0
Conformer #22	-1346044.26	5.1	0.000	0.000	0
Conformer #5	-1346044.15	5.2	0.000	0.000	0
Conformer #18	-1346044.12	5.3	0.000	0.000	0
Conformer #82	-1346043.93	5.5	0.000	0.000	0
Conformer #8	-1346043.93	5.5	0.000	0.000	0
Conformer #84	-1346043.88	5.5	0.000	0.000	0
Conformer #70	-1346043.76	5.6	0.000	0.000	0
Conformer #73	-1346043.64	5.7	0.000	0.000	0
Conformer #55	-1346043.54	5.8	0.000	0.000	0
Conformer #9	-1346043.31	6.1	0.000	0.000	0
Conformer #66	-1346043.09	6.3	0.000	0.000	0
Conformer #79	-1346042.78	6.6	0.000	0.000	0
Conformer #48	-1346042.75	6.6	0.000	0.000	0
Conformer #61	-1346042.60	6.8	0.000	0.000	0
Conformer #81	-1346042.21	7.2	0.000	0.000	0
Conformer #69	-1346041.51	7.9	0.000	0.000	0

Table 36. Boltzmann Distribution of Conformers of **2/g**.

	Energy (kcal/mol)	Relative Energy (kcal/mol)	Boltzmann Factor	Equilibrium Mole Fraction	Number of Imaginary Frequencies
Conformer #27	-1346050.88	0.0	1.000	0.323	0
Conformer #41	-1346050.61	0.3	0.638	0.206	0
Conformer #4	-1346050.20	0.7	0.317	0.103	0
Conformer #1	-1346050.11	0.8	0.272	0.088	0
Conformer #5	-1346049.36	1.5	0.076	0.025	0
Conformer #20	-1346049.29	1.6	0.069	0.022	0
Conformer #22	-1346049.26	1.6	0.065	0.021	0
Conformer #13	-1346049.17	1.7	0.056	0.018	0
Conformer #51	-1346049.15	1.7	0.054	0.017	0
Conformer #38	-1346049.12	1.8	0.051	0.017	0
Conformer #32	-1346049.07	1.8	0.047	0.015	0
Conformer #28	-1346049.02	1.9	0.043	0.014	0
Conformer #49	-1346048.97	1.9	0.040	0.013	0
Conformer #42	-1346048.84	2.0	0.032	0.010	0
Conformer #24	-1346048.82	2.1	0.031	0.010	0
Conformer #10	-1346048.78	2.1	0.029	0.009	0
Conformer #50	-1346048.77	2.1	0.028	0.009	0
Conformer #26	-1346048.72	2.2	0.026	0.008	0
Conformer #2	-1346048.71	2.2	0.026	0.008	0
Conformer #6	-1346048.54	2.3	0.019	0.006	0
Conformer #11	-1346048.54	2.3	0.019	0.006	0
Conformer #21	-1346048.50	2.4	0.018	0.006	0
Conformer #17	-1346048.43	2.4	0.016	0.005	0
Conformer #7	-1346048.43	2.4	0.016	0.005	0
Conformer #25	-1346048.42	2.5	0.016	0.005	0
Conformer #47	-1346048.30	2.6	0.013	0.004	0
Conformer #29	-1346048.28	2.6	0.012	0.004	0
Conformer #19	-1346048.04	2.8	0.008	0.003	0
Conformer #12	-1346048.01	2.9	0.008	0.003	0
Conformer #9	-1346047.94	2.9	0.007	0.002	0
Conformer #39	-1346047.81	3.1	0.006	0.002	0
Conformer #16	-1346047.79	3.1	0.005	0.002	0
Conformer #48	-1346047.76	3.1	0.005	0.002	0
Conformer #58	-1346047.75	3.1	0.005	0.002	0
Conformer #30	-1346047.64	3.2	0.004	0.001	0
Conformer #8	-1346047.63	3.2	0.004	0.001	0
Conformer #23	-1346047.34	3.5	0.003	0.001	0
Conformer #3	-1346047.30	3.6	0.002	0.001	0
Conformer #18	-1346047.28	3.6	0.002	0.001	0
Conformer #55	-1346046.94	3.9	0.001	0.000	0
Conformer #53	-1346046.45	4.4	0.001	0.000	0
Conformer #15	-1346046.45	4.4	0.001	0.000	0
Conformer #40	-1346046.17	4.7	0.000	0.000	1
Conformer #33	-1346046.13	4.8	0.000	0.000	0
Conformer #43	-1346045.65	5.2	0.000	0.000	0
Conformer #46	-1346045.37	5.5	0.000	0.000	0
Conformer #54	-1346045.32	5.6	0.000	0.000	0
Conformer #57	-1346044.99	5.9	0.000	0.000	1
Conformer #44	-1346044.79	6.1	0.000	0.000	0
Conformer #52	-1346044.59	6.3	0.000	0.000	0
Conformer #34	-1346043.99	6.9	0.000	0.000	0
Conformer #56	-1346042.86	8.0	0.000	0.000	0
Conformer #45	-1346042.66	8.2	0.000	0.000	0
Conformer #37	-1346042.18	8.7	0.000	0.000	0

Table 37. Boltzmann Distribution of Conformers of **2/h**.

	Energy (kcal/mol)	Relative Energy (kcal/mol)	Boltzmann Factor	Equilibrium Mole Fraction	Number of Imaginary Frequencies
Conformer #23	-1346051.51	0.00	1.000	0.514	0
Conformer #6	-1346051.07	0.45	0.470	0.242	0
Conformer #5	-1346050.10	1.41	0.092	0.047	0
Conformer #14	-1346050.10	1.42	0.092	0.047	0
Conformer #1	-1346049.88	1.64	0.063	0.032	0
Conformer #2	-1346049.74	1.77	0.050	0.026	0
Conformer #17	-1346049.72	1.79	0.048	0.025	0
Conformer #13	-1346049.36	2.15	0.026	0.014	0
Conformer #26	-1346049.11	2.40	0.017	0.009	0
Conformer #33	-1346049.00	2.51	0.014	0.007	0
Conformer #30	-1346048.94	2.57	0.013	0.007	0
Conformer #7	-1346048.84	2.68	0.011	0.006	0
Conformer #10	-1346048.83	2.68	0.011	0.006	0
Conformer #22	-1346048.75	2.76	0.009	0.005	0
Conformer #9	-1346048.45	3.07	0.006	0.003	0
Conformer #4	-1346048.44	3.07	0.006	0.003	0
Conformer #31	-1346048.33	3.19	0.005	0.002	0
Conformer #3	-1346048.24	3.27	0.004	0.002	0
Conformer #15	-1346048.06	3.46	0.003	0.001	0
Conformer #24	-1346047.63	3.88	0.001	0.001	0
Conformer #21	-1346047.57	3.94	0.001	0.001	0
Conformer #20	-1346046.97	4.54	0.000	0.000	0
Conformer #8	-1346046.48	5.03	0.000	0.000	0
Conformer #19	-1346046.28	5.23	0.000	0.000	0
Conformer #12	-1346046.28	5.24	0.000	0.000	0
Conformer #11	-1346046.22	5.29	0.000	0.000	0
Conformer #34	-1346046.15	5.37	0.000	0.000	0
Conformer #28	-1346045.47	6.05	0.000	0.000	0
Conformer #26	-1346045.39	6.12	0.000	0.000	0
Conformer #25	-1346045.39	6.13	0.000	0.000	0
Conformer #27	-1346045.22	6.30	0.000	0.000	0
Conformer #32	-1346043.83	7.68	0.000	0.000	0
Conformer #29	-1346043.24	8.27	0.000	0.000	0

Table 38. Boltzmann Distribution of Conformers of **3/4/a**.

	Energy (kcal/mol)	Relative Energy (kcal/mol)	Boltzmann Factor	Equilibrium Mole Fraction	Number of Imaginary Frequencies
Conformer #2	-1009721.97	0.0	1.000	0.451	0
Conformer #4	-1009721.95	0.0	0.973	0.439	0
Conformer #1	-1009720.41	1.6	0.072	0.033	0
Conformer #3	-1009720.24	1.7	0.054	0.024	0
Conformer #11	-1009720.18	1.8	0.049	0.022	0
Conformer #6	-1009720.14	1.8	0.046	0.021	0
Conformer #9	-1009718.84	3.1	0.005	0.002	0
Conformer #5	-1009718.71	3.3	0.004	0.002	0
Conformer #12	-1009718.71	3.3	0.004	0.002	0
Conformer #14	-1009718.54	3.4	0.003	0.001	0
Conformer #7	-1009718.40	3.6	0.002	0.001	0
Conformer #10	-1009718.403	3.6	0.002	0.001	0

Table 39. Boltzmann Distribution of Conformers of **3/4/b**.

	Energy (kcal/mol)	Relative Energy (kcal/mol)	Boltzmann Factor	Equilibrium Mole Fraction	Number of Imaginary Frequencies
Conformer #2	-1009720.48	0.0	1.000	0.785	0
Conformer #1	-1009718.90	1.6	0.069	0.054	0
Conformer #5	-1009718.89	1.6	0.067	0.053	0
Conformer #10	-1009718.26	2.2	0.023	0.018	0
Conformer #15	-1009718.12	2.4	0.019	0.015	0
Conformer #34	-1009718.10	2.4	0.018	0.014	0
Conformer #8	-1009718.07	2.4	0.017	0.013	0
Conformer #4	-1009717.77	2.7	0.010	0.008	0
Conformer #11	-1009717.77	2.7	0.010	0.008	0
Conformer #41	-1009717.64	2.8	0.008	0.006	0
Conformer #3	-1009717.34	3.1	0.005	0.004	0
Conformer #7	-1009717.32	3.2	0.005	0.004	0
Conformer #14	-1009717.07	3.4	0.003	0.002	0
Conformer #6	-1009717.05	3.4	0.003	0.002	0
Conformer #21	-1009716.87	3.6	0.002	0.002	0
Conformer #40	-1009716.86	3.6	0.002	0.002	0
Conformer #25	-1009716.80	3.7	0.002	0.002	0
Conformer #18	-1009716.65	3.8	0.002	0.001	0
Conformer #22	-1009716.65	3.8	0.002	0.001	0
Conformer #28	-1009716.65	3.8	0.002	0.001	0
Conformer #42	-1009716.54	3.9	0.001	0.001	0
Conformer #16	-1009716.49	4.0	0.001	0.001	0
Conformer #27	-1009716.24	4.2	0.001	0.001	0
Conformer #45	-1009715.99	4.5	0.001	0.000	0
Conformer #29	-1009715.87	4.6	0.000	0.000	0
Conformer #17	-1009715.72	4.8	0.000	0.000	0
Conformer #30	-1009715.57	4.9	0.000	0.000	0
Conformer #9	-1009715.54	4.9	0.000	0.000	0
Conformer #38	-1009715.27	5.2	0.000	0.000	0
Conformer #32	-1009715.02	5.5	0.000	0.000	0
Conformer #31	-1009715.02	5.5	0.000	0.000	0
Conformer #23	-1009715.00	5.5	0.000	0.000	0
Conformer #19	-1009714.88	5.6	0.000	0.000	0
Conformer #12	-1009714.86	5.6	0.000	0.000	0
Conformer #37	-1009714.82	5.7	0.000	0.000	0
Conformer #26	-1009714.53	6.0	0.000	0.000	1
Conformer #13	-1009714.14	6.3	0.000	0.000	1
Conformer #20	-1009713.88	6.6	0.000	0.000	0
Conformer #33	-1009713.51	7.0	0.000	0.000	0
Conformer #24	-1009713.26	7.2	0.000	0.000	0
Conformer #36	-1009712.45	8.0	0.000	0.000	1

Table 40. Boltzmann Distribution of Conformers of **3/4/c**.

	Energy (kcal/mol)	Relative Energy (kcal/mol)	Boltzmann Factor	Equilibrium Mole Fraction	Number of Imaginary Frequencies
Conformer #6	-1009720.17	0.0	1.000	0.544	0
Conformer #1	-1009719.53	0.6	0.340	0.185	0
Conformer #2	-1009719.13	1.0	0.175	0.095	0
Conformer #14	-1009718.63	1.5	0.075	0.041	0
Conformer #19	-1009718.63	1.5	0.075	0.041	0
Conformer #3	-1009718.50	1.7	0.060	0.033	0
Conformer #4	-1009718.04	2.1	0.027	0.015	0
Conformer #9	-1009718.03	2.1	0.027	0.015	0
Conformer #11	-1009717.78	2.4	0.018	0.010	0
Conformer #10	-1009717.54	2.6	0.012	0.006	0
Conformer #15	-1009717.52	2.6	0.011	0.006	0
Conformer #8	-1009717.52	2.6	0.011	0.006	0
Conformer #7	-1009716.83	3.3	0.004	0.002	0
Conformer #5	-1009716.27	3.9	0.001	0.001	0
Conformer #13	-1009715.08	5.1	0.000	0.000	0
Conformer #18	-1009714.74	5.4	0.000	0.000	0
Conformer #12	-1009714.31	5.9	0.000	0.000	0
Conformer #16	-1009714.27	5.9	0.000	0.000	0

Table 41. Boltzmann Distribution of Conformers of **3/4/d**.

	Energy (kcal/mol)	Relative Energy (kcal/mol)	Boltzmann Factor	Equilibrium Mole Fraction	Number of Imaginary Frequencies
Conformer #1	-1009720.71	0.0	1.000	0.294	0
Conformer #8	-1009720.71	0.0	0.995	0.293	0
Conformer #3	-1009720.70	0.0	0.977	0.287	0
Conformer #2	-1009719.44	1.3	0.116	0.034	0
Conformer #4	-1009719.34	1.4	0.098	0.029	0
Conformer #6	-1009718.74	2.0	0.036	0.011	0
Conformer #14	-1009718.74	2.0	0.036	0.011	0
Conformer #18	-1009718.74	2.0	0.036	0.011	0
Conformer #22	-1009718.73	2.0	0.035	0.010	0
Conformer #11	-1009718.60	2.1	0.028	0.008	0
Conformer #15	-1009718.47	2.2	0.023	0.007	0
Conformer #5	-1009717.66	3.0	0.006	0.002	0
Conformer #10	-1009717.41	3.3	0.004	0.001	0
Conformer #13	-1009717.40	3.3	0.004	0.001	0
Conformer #9	-1009717.28	3.4	0.003	0.001	0
Conformer #21	-1009717.12	3.6	0.002	0.001	0
Conformer #19	-1009716.35	4.4	0.001	0.000	0
Conformer #16	-1009715.92	4.8	0.000	0.000	0
Conformer #23	-1009715.92	4.8	0.000	0.000	0
Conformer #7	-1009715.90	4.8	0.000	0.000	0
Conformer #20	-1009715.54	5.2	0.000	0.000	0
Conformer #12	-1009714.00	6.7	0.000	0.000	0
Conformer #17	-1009713.82	6.9	0.000	0.000	0

Table 42. $[\alpha]\lambda$ [deg dm-1 (g/mL)-1] values for **1/c**.

Conformer	B3LYP 589.3 nm
Conformer #1	207.99
Conformer #2	204.98
Conformer #3	-85.75
Conformer #4	228.09
Conformer #5	211.23
Conformer #6	-18.33
Conformer #7	217.48
Conformer #8	-46.25
Conformer #9	271.19
Conformer #10	38.71
Conformer #11	27.08
Conformer #12	156.57
Conformer #13	-42.92
Conformer #15	-31.71
Conformer #16	307.13
Conformer #17	43.06
Conformer #18	31.63
Conformer #19	-6.61
Conformer #20	195.35
Conformer #21	254.34
Conformer #22	46.99
Conformer #23	83.68
Conformer #24	71.72
Conformer #25	165.04

Conformer #26	42.59
Conformer #27	102.42
Conformer #28	242.16
Conformer #29	177.29
Conformer #30	3.74
Conformer #31	-124.63
Conformer #32	-65.26
Conformer #33	35.11
Conformer #34	-82.38
Conformer #35	56.03
Conformer #36	-93.96
Conformer #37	279.73
Conformer #38	283.92
Conformer #39	276.56
Conformer #40	106.17
Conformer #41	106.17
Conformer #42	331.95
Conformer #43	-59.43
Conformer #44	-26.10
Conformer #45	-102.26
Conformer #46	270.38
Conformer #47	78.28
Conformer #48	208.15
Conformer #49	134.70
Conformer #50	-39.32
Conformer #51	20.06
Conformer #52	51.93
Conformer #53	-27.52
Conformer #54	-0.48
Conformer #55	-55.06
Conformer #56	41.26
Conformer #57	265.59
Conformer #58	34.91
Conformer #59	172.63
Conformer #60	96.77
Conformer #61	-17.94
Conformer #62	-60.57
Conformer #63	106.89
Conformer #64	143.00
Conformer #65	-41.52
Conformer #66	66.20
Conformer #67	98.09
Conformer #68	190.39
Conformer #69	102.97
Conformer #70	-8.24
Conformer #71	-60.95
Conformer #72	-10.33
Conformer #73	73.74
Conformer #74	127.71

Table 43. [α]λ [deg dm-1 (g/mL)-1] values for **2/e**.

Conformer	B3LYP 589.3 nm
Conformer #1	67.090
Conformer #2	17.230
Conformer #3	-1.250
Conformer #4	52.220
Conformer #5	9.060
Conformer #6	0.740
Conformer #7	115.640
Conformer #8	-4.480
Conformer #9	-3.110
Conformer #10	29.450
Conformer #11	18.280
Conformer #12	93.560
Conformer #13	113.590
Conformer #14	47.620
Conformer #15	-11.770
Conformer #16	-41.720
Conformer #17	-80.430
Conformer #18	-46.850
Conformer #19	-91.220
Conformer #20	-2.390
Conformer #21	-7.390
Conformer #22	-98.890
Conformer #23	-20.750
Conformer #24	93.690
Conformer #25	180.750
Conformer #26	27.870
Conformer #27	181.990
Conformer #28	122.450
Conformer #29	47.350
Conformer #30	60.930
Conformer #31	181.940
Conformer #32	62.870
Conformer #33	-49.950
Conformer #34	50.440
Conformer #35	42.530
Conformer #36	-7.990
Conformer #37	-46.520
Conformer #38	-55.430
Conformer #39	36.930
Conformer #40	44.760
Conformer #41	-32.200
Conformer #42	-18.030
Conformer #43	-0.360
Conformer #44	193.980
Conformer #45	-38.730
Conformer #46	0.920
Conformer #47	19.110
Conformer #48	46.360
Conformer #49	45.040

Table 44. [α]λ [deg dm-1 (g/mL)-1] values for **3/d**.

Conformer	B3LYP 589.3 nm
Conformer #1	135.50
Conformer #2	140.15
Conformer #3	177.24
Conformer #4	187.62
Conformer #5	178.36
Conformer #6	176.78
Conformer #7	-40.50
Conformer #8	140.54
Conformer #9	107.04
Conformer #10	-313.73
Conformer #11	243.39
Conformer #12	309.55
Conformer #14	208.80
Conformer #15	-256.24
Conformer #16	464.93
Conformer #17	-187.61
Conformer #18	208.31
Conformer #19	-354.23
Conformer #20	-119.89
Conformer #22	208.72
Conformer #23	464.97

Table 45. [α]λ [deg dm-1 (g/mL)-1] values for **4/b**.

Conformer	B3LYP 589.3 nm
Conformer #1	317.15
Conformer #2	304.46
Conformer #3	256.10
Conformer #4	283.74
Conformer #5	264.35
Conformer #6	388.56
Conformer #7	256.68
Conformer #8	280.14
Conformer #9	271.57
Conformer #10	380.16
Conformer #11	284.38
Conformer #12	385.48
Conformer #13	444.59
Conformer #14	219.22
Conformer #15	247.17
Conformer #16	309.20
Conformer #17	248.28
Conformer #18	473.90
Conformer #19	-143.13
Conformer #20	491.26
Conformer #21	252.65
Conformer #22	565.47
Conformer #23	325.39
Conformer #24	419.00
Conformer #25	-297.79

Conformer #26	82.01
Conformer #27	336.91
Conformer #28	565.66
Conformer #29	-338.28
Conformer #30	-264.43
Conformer #31	600.32
Conformer #32	521.29
Conformer #33	-60.27
Conformer #34	241.81
Conformer #35	-410.25
Conformer #36	126.73
Conformer #37	-251.51
Conformer #38	-188.26
Conformer #39	344.04
Conformer #40	203.27
Conformer #41	255.10
Conformer #42	-245.24
Conformer #44	167.79
Conformer #45	-94.58

Table 46. Calculated $[\alpha]_D$ for **1/c**, **2/e**, **3/d**, **4/b**.

Compound	$[\alpha]_D$ (Calculated) CHCl$_3$	$[\alpha]_D$ (Experimental) CHCl$_3$
1/c	+158	+53
2/e	-47	-10
3/d	+166	+48
4/b	+347	+55

Table 47. DP4+ Analysis of **1-4**.

	1			
	1/a (SRRRS)	**1/b (SRRSS)**	**1/c (SRSRS)**	**1/d (SRSSS)**
DP4+ (H)	13.89%	6.99%	62.04%	17.08%
DP4+ (C)	44.51%	0.02%	55.44%	0.03%
DP4+ (All Data)	15.23%	0.00%	84.75%	0.01%

	2							
	2/a (SRRRS)	**2/b (SRRSS)**	**2/c (SRSRS)**	**2/d (SRSSS)**	**2/e (SSRRS)**	**2/f (SSSRS)**	**2/g (SSSSS)**	**2/h (SSRSS)**
DP4+ (H)	0.26%	0.41%	1.51%	15.49%	27.09%	0.99%	6.36%	47.88%
DP4+ (C)	0.18%	0.00%	0.38%	0.00%	99.12%	0.00%	0.00%	0.32%
DP4+ (All Data)	0.00%	0.00%	0.02%	0.00%	99.41%	0.00%	0.00%	0.57%

	3			
	3/a (SRR)	**3/b (SRS)**	**3/c (SSR)**	**3/d (SSS)**
DP4+ (H)	0.20%	0.15%	0.08%	99.57%
DP4+ (C)	0.27%	65.89%	0.03%	33.82%
DP4+ (All Data)	0.00%	0.29%	0.00%	99.71%

	4			
	4/a (SRR)	**4/b (SRS)**	**4/c (SSR)**	**4/d (SSS)**
DP4+ (H)	0.076%	83.04%	9.39%	6.81%
DP4+ (C)	0.17%	43.33%	55.71%	0.79%
DP4+ (All Data)	0.00%	87.19%	12.67%	0.13%

Table 48. Boltzmann averaged isotropic shielding values and coupling constants of isomers **3/a-3/d**.

Atom	Experimental	Calculated shielding tensors			
		3/a (SRR)	**3/b (SRS)**	**3/c (SSR)**	**3/d (SSS)**
1	80.42	93.22688	95.16144	90.0816	97.78001
2	134.84	38.69259	36.65783	36.992	39.84777
3	134.01	37.26795	34.26914	36.96479	34.7916
4	80.59	97.68515	98.92087	101.1933	96.84992
5	67.9	100.484	108.114	104.419	103.8301
1'	121.1	56.78278	56.14621	56.97655	55.85422
1"	173.04	0.258177	-0.2331	-0.05629	-0.79179
2'	132.54	36.55844	36.82547	34.71735	38.00274
2"	53.96	127.5813	127.5268	126.9247	127.5629
3'	19.32	161.1697	161.3345	161.0784	161.4842
4	4.8	26.96194	27.37004	27.26855	26.86186
5	4.33	27.5104	27.14114	27.17113	27.36928
1'	6.18	25.22351	25.17037	25.22736	25.2138
2'	5.93	24.93936	25.27231	24.90186	25.33324
2"	3.82	28.02276	28.03747	27.97739	28.03879
3'	1.81	29.95117	29.93971	29.93254	29.95493
J4-5	5.97	5.821669	5.113242	6.096246	5.812667
J1'-2'	15.73	14.19895	14.25269	14.19092	14.23564

Table 49. Results of dJ-DP4 calculations of **3**.

	Compound 3			
	3/a (SRR)	3/b (SRS)	3/c (SSR)	3/d (SSS)
DP4 (H)	0.87%	0.40%	0.14%	98.58%
DP4 (C)	0.47%	64.52%	0.07%	34.94%
DP4 (H+C)	0.01%	0.75%	0.00%	99.24%
DP4 J	26.82%	24.84%	20.22%	28.12%
DP4 (All Data)	0.01%	0.66%	0.00	99.32%

Table 50. Cytotoxic activities of compounds **1-4** against three cancer cell line

Compound	Cancer cell lines (IC$_{50}$ in µM)		
	MDA-MB-231	OVCAR3	MDA-MB-435
1	>20	>25	>25
2	>20	>25	>25
3	>20	>25	>25
4	>20	>25	>25
Taxol[*]	63	36	14

[*] IC$_{50}$ values are reported in nM.

Table 51. Minimal Inhibitory Concentrations (MICs) in µg/mL for compounds **1-4** against a series of pathogenic microorganisms

Compound	E. coli	S. aureus	MRSA	P. aeruginosa	M. smegmatis	B. subtilis	B. anthracis	S. cerevisiae	C. albicans	A. niger
1	> 138	> 125	> 125	> 125	> 125	> 125	> 125	> 125	> 125	> 125
2	> 125	> 125	> 125	> 125	> 125	> 125	> 125	> 125	> 125	> 125
3	> 125	> 125	> 125	> 125	> 125	> 125	> 125	> 125	> 125	> 125
4	> 125	> 125	> 125	> 125	> 125	> 125	> 125	> 125	> 125	> 125

Minimal Inhibitory Concentrations (MIC) values are in µg/mL

Table 52. Antiparasitic activities of **1**-**4** against *Naegleria fowleri*.

Compound	*N. fowleri* inhibition (IC$_{50}$ in µM)
1	>20
2	>20
3	>20
4	>20
Azithromycin	0.318

Table 53. Spectral similarities of the cyclopentene ring in **1** and its literature analogues (rhytidhyester D and cryptosporiopsinol)

Position	**1**[a]		rhytidhyester D[b]		cryptosporiopsinol[c]	
	δ_C	δ_H (*J* in Hz)	δ_C	δ_H (*J* in Hz)	δ_C	δ_H (*J* in Hz)
1	88.2		87.3		-	-
2	137.7		137.9		136.9	-
3	140.4		132.1		133.0	-
4	76.0	4.47 bs	74.3	4.53 m	75.5	-
5	65.0	4.43 d (6.44)	67.9	4.48 d (6.5)	66.0	-

[a]Data collected in CDCl$_3$, 400 (^{1}H) and 100 (^{13}C) MHz, [b]Data collected in DMSO-d_6, at 500 (^{1}H) and 125 (^{13}C) MHz; [c]Data collection was not specified

[b]Zhang, S., Wang, W., Tan, J., Kang, F., Chen, D., Xu, K., Zou, Z., 2021. Rhytidhyesters A–D, 4 New Chlorinated Cyclopentene Derivatives from the Endophytic Fungus *Rhytidhysteron* sp. BZM-9. Planta Med. 87, 489-497.
[c]Giles, D., Turner, W. B., 1969. Chlorine-containing metabolites of *Periconia macrospinosa*. J. Chem. Soc. C Org., 2187-2189.
Holker, J. S. E., Young, K., 1975. Biosynthesis of metabolites of *Periconia macrospinosa* from [1-13C]-, [2-13C]-, and [1,2-13C]-acetate. J. Chem. Soc., Chem. Commun., 525-526.

CHAPTER IV: METABOLOMICS-GUIDED COMPARISON OF POLLEN AND NOVEL

MICROALGAE-BASED ARTIFICIAL DIETS IN HONEY BEES

Vincent A. Ricigliano[⊥], Kristof B. Cank[⊥], Daniel A. Todd, Sonja L. Knowles, Nicholas H.

Oberlies

[⊥]Authors contributed equally to this study

Introduction

The honey bee (*Apis mellifera*) is the world's premier managed pollinator. In the United

States alone, honey bee pollination services contribute ~$20 billion per year to the value of crop

production. Nevertheless, commercial beekeepers are experiencing annual colony losses that are

on average twice as high as historical records, jeopardizing pollination services and human food

security.[172] Honey bee colony losses are attributed to multiple stressors, notably parasites and

pathogens. However, many lines of evidence indicate that malnutrition is a major interactive

factor underlying colony mortality.[173-175] Abundant floral resources are required for honey bee

colony growth, immune function, and stress responses.[176-180] Nectar provides energy in the form

of carbohydrates, while pollen is the main source of proteins, lipids, and micronutrients.[177] Under

ideal conditions, varied flower sources are necessary to meet bee nutritional requirements, since

the composition of pollen varies by plant species.[181-182] Unfortunately, modern intensive

agriculture is associated with reduced flower diversity and, hence, lower nutritional value.[183-185]

Plant responses to climate change, such as altered flower, nectar, and pollen production, as well

as the timing of when flowers bloom, will likely alter the landscape of floral resource availability, all of which may further exacerbate the challenges of honey bee nutrition, and hence their health, especially within a managed setting.[186-188]

Managed bee colonies used for agricultural pollination are routinely fed artificial "pollen substitute" diets to compensate for a lack of pollen forage in the environment and to prevent nutritional deficiencies. Various diet formulations have been used as a substitute for natural pollen, and these often incorporate protein-rich ingredients, such as soy, corn gluten, yeast, casein, and egg, as a source of essential amino acids.[177] However, comparisons of diet efficacies suggest the existence of potentially overlooked nutritional factors or other pollen components that might improve artificial diet effectiveness (i.e. providing components that might stimulate bee immunity or improve stress resistance).[189-191] In addition to protein content, pollen contains a variety of necessary lipids, essential fatty acids,[192-194] and a broad diversity of bee health-modulating bioactive compounds, such vitamins and phenolic acids.[195-196] Thus, there are opportunities to enhance alternative feeds to more closely mimic the chemical composition of pollen, especially to serve the growing demands of 87% of US beekeepers, who feed supplemental nutrition to their colonies (Bee Informed Partnership, National Management Survey, https://bip2.beeinformed.org/survey/). Importantly, given the challenges of feeding the world's human population, sustainable ingredients that do not compete with human food production are good candidates to address this crucial need of modern beekeeping.

Microalgae are nutritious and sustainable feed ingredients that have been used in a variety of livestock,[197] including recent applications in managed honey bees.[198] Notably, eukaryotic microalgae in the genus *Chlorella* and prokaryotic cyanobacteria (blue-green microalgae) in the genus *Arthrospira* (commonly called spirulina) are excellent sources of

protein, fatty acids, sterols, and other bioactive compounds with nutraceutical potential. These microalgae are bioavailable in honey bees and appear to reproduce many physiological effects of a natural pollen diet;[199-200] however, little is known about the metabolic mechanisms underlying their impact on bee health.

Mass spectrometry-based metabolomics enables comprehensive and systematic analyses of metabolites in an organism,[201] and it has emerged as a powerful tool in nutrition and food sciences.[202] Metabolomics-guided diet development could enable precision nutrition and an improved understanding of the mechanisms underlying the effects of feed.[203] The objective of this study was to investigate diet-induced changes in honey bees using mass spectrometry-based metabolomics to better understand the nutritional and metabolic effects of microalgae relative to the bee's natural pollen diet (**Figure 58**).

<p align="center">**Materials and Methods**</p>

Honey Bee (*Apis mellifera* L.) Experimental Design

Experiments were conducted in the summer of 2021 at the USDA-ARS Honey Bee Breeding Genetics and Physiology Laboratory in Baton Rouge, Louisiana, USA. Newly emerged worker bees were produced by incubating sealed brood frames obtained from healthy colonies at 35 °C and 50% relative humidity overnight. Bees (< 24 h old) were collected into a container then randomly assigned to diet treatment groups (50 bees/cage). Four cages were established for each diet (16 cages total). Thus, each diet had four biological replicates. After 8 days of ad libtum feeding, bees were separately collected from each cage, frozen on dry ice, then stored at - 80 °C.

Diet Preparation and Consumption Measures

The different diet groups consisted of sugar, bee-collected pollen, Chlorella (*Chlorella vulgaris*) and spirulina (*Arthrospira platensis*). All diets were mixed into a paste with 1:1 (v/v) sucrose syrup:honey and loaded into modified microcentrifuge tubes (see experimental design schematic **Figure 66**), then stored at -20 °C before use. There were four cage replicates per diet treatment (i.e., biological replicates). For the pollen diet, mixed corbicular pollen pellets were collected using entrance-mounted pollen traps during late fall of 2020 (thus, predominantly *Solidago spp.* in floral composition) from a USDA-ARS apiary in Baton Rouge, Louisiana and frozen at -80 °C until needed. The Chlorella diet consisted of organic, powdered, cracked cell wall *Chlorella vulgaris* biomass (Micro Ingredients, California, USA). The spirulina diet consisted of organic, powdered *Arthrospira platensis* biomass (Micro Ingredients, California, USA). Approximately 1.25 g of formulated diet paste was provided to each cage. The amount of diet consumed by each cage was recorded on day 4, then the diet was refreshed with approximately 1.25 g of new diet paste and consumption was measured again at day 8. As a control, diet samples were placed in cages without bees and weight loss was measured to determine the evaporation rate for each diet type. Diet consumption in each cage was adjusted for daily moisture loss and recalculated to give the total diet consumed over the 8-day period

Honey Bee Dissection

Frozen bees were dissected on dry ice into three parts: head, thorax (excluding legs and wings), and abdomens with guts intact. Then, dissected parts from each cage were collected into pools of 8 parts. Two separate pools of 8 abdomens were made for each cage. One abdomen pool was used for RNA extraction and gene expression, while the other abdomen pool was used for metabolite extraction and metabolomic analyses.

Honey Bee Physiological Measures and Gene Expression Analyses

Average head and thorax weights per bee per cage were determined by drying pools of 8

heads or thoraces to a constant weight (60 °C for 48 h) and recording to the nearest 0.1 mg. For

gene expression analyses, pools of 8 frozen bee abdomens per cage were subjected to RNA

extraction with a Monarch total RNA miniprep kit (New England BioLabs) according to the

manufacturers protocol. cDNA synthesis was carried out using 1 μg of DNAase-treated RNA

and a LunaScript RT SuperMix Kit (New England BioLabs) according to the manufactures

protocol. Quantitative PCR (qPCR) was performed in triplicate to quantify expression levels of

vitellogenin (vg), *superoxide dismutase* (*CuZn SOD*), *catalase*, *heat shock protein 70* (*hsp70*),

and *heat shock protein 90* (*hsp90*). All qPCR reactions were performed as follows: initial

denaturation at 95 °C for 5 min; 40 cycles with denaturation at 95 °C for 15 s; and a primer-pair-

specific annealing and extension temperature (**Table 55**) for 30 s. The reactions were carried out

using SsoAdvanced Universal SYBR® Green Supermix (Biorad) in triplicate on a CFX96 Real-

Time PCR Detection System (Biorad). To confirm the absence of contaminating genomic DNA

and primer dimers, amplification and melting curves were tested in negative control reactions

containing only DNase-treated total RNA. Relative transcript levels were determined based on

standardized Ct values (Δ Ct) using β-actin for normalization.

Extraction of Honey Bee Metabolites

Each bee sample represented one biological replicate that contained 8 honey bee

abdomens fed on a specific diet (i.e., sugar, pollen, *Chlorella vulgaris* or *Arthrospira platensis*).

First, the abdomens were ground with a mortal and pestles using liquid nitrogen (**Figure 67**).

Then, the crushed abdomens were transferred to a scintillation vial and submerged with 5 mL

acetone and were shaken for 16 h. The solvent was transferred to an Eppendorf's tube and

centrifuged. The supernatant (i.e., acetone layer) was retained. The residual solids were resuspended in 1:1 MeOH:CHCl$_3$ (5 mL) and sonicated for 30 min. The solvent layer was transferred to an Eppendorf tube and centrifuged, where the supernatant (i.e., MeOH:CHCl$_3$ layer) was saved and combined with the acetone layer described above. The combined layers were dried under nitrogen to produce a bee extract fed on a diet, and each of these consisted of four biological replicates. Standards of pollen, Chlorella (*Chlorella vulgaris*) and spirulina (*Arthrospira platensis*) were treated and extracted in a manner identical to the above.
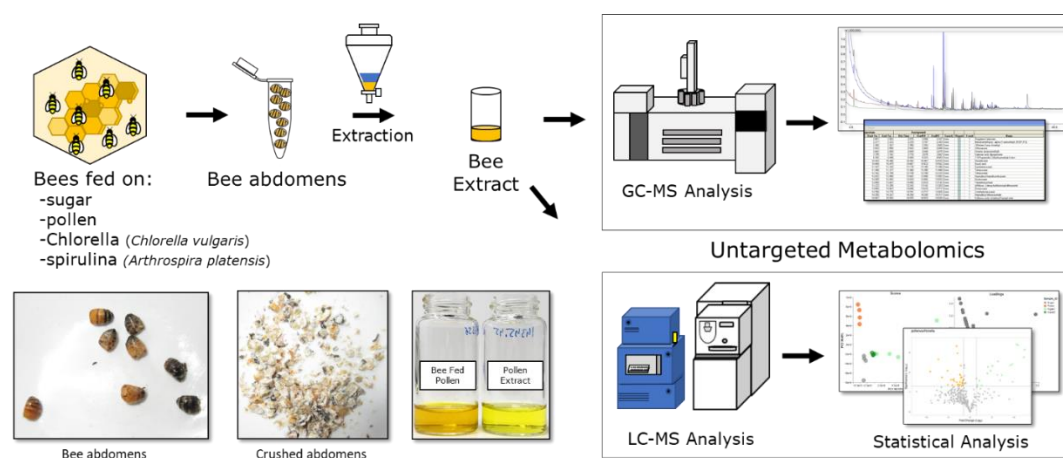
Figure 58. Schematic overview of metabolite extraction and analyses. Bees were fed on four different diets, namely sugar, pollen, *Chlorella* (*Chlorella vulgaris)* and spirulina (*Arthrospira platensis*). The bee abdomens were harvested, extracted, and examined through untargeted LC-MS and GC-MS analysis to analyze their metabolomic composition.

Mass Spectrometry Analysis

LC-MS Analysis

The extracts were examined at a 0.2 mg/mL dissolved in MeOH. An Acquity ultra performance liquid chromatography system (UPLC, Waters Corp.) coupled with a Thermo Q Exactive Plus MS (Thermo Fisher) was used for the analysis. The flow rate of the UPLC was set to 0.3 mL/min using a BEH C18 (2.1 × 50 mm x 1.7 μm) column equilibrated at 40 °C. The mobile phase consisted of Fisher Optima LC-MS grade CH$_3$CN–H$_2$O (with 0.1% formic acid

added). The analysis started at 15% CH$_3$CN and increased linearly to 100% CH$_3$CN over 8 min; it was then held at 100% CH$_3$CN over 1.5 min before returning to the starting conditions over 0.5 min, making the total run time 10 min. Photodiode-array (PDA) detection was used to acquire data from 200 to 500 nm with a resolution of 4 nm. The Q Exactive Plus with electrospray ionization (ESI) was used to collect high-resolution accurate mass measurements and fragmentations of the detected ions. The initial data were collected from *m/z* 135 to 2000 at a resolving power of 70,000 for both positive and negative mode, where the spray voltage was set to either 3000 V (+) or 3000 V (−). Sheath gas was 47.50, aux gas was set to 11.25, spare gas 2.25, the heater temperature was 350.0 °C capillary temperature was 256.25 °C and s-lens was 50.0. The acquired LC-MS data were analyzed using Xcalibur (Thermo Scientific).

GC-MS Analysis

The extracts were analyzed with a GCMS-QP2010S (Shimadzu). The samples were prepared at 1 mg/mL dissolved in CHCl$_3$. An AOC-20i/s auto sampler was used for injection of the samples, with the injection temperature at 270 °C and split mode used (10.0 ratio), all via an Agilent DB-1HT (30 mm x 0.10 µm x 0.25 mm) column. The analysis started at 50 °C, where it was held for 5 min, then increased to 350 °C at a rate of 15 degrees °C per min, where it was held for 20 min. GCMS solution Version 4.20 (Shimadzu) was used to process the results and to apply the similarity search to a NIST library (2011).

Statistical Analysis

Data generated by LC-MS and GC-MS were processed through MZmine 2.53.[204] To filter and clean the LC-MS data for PCA and Volcano plots, a 1×10^4 blank cutoff was used, and the mass spectrometry data were filtered between *m/z* 135 and *m/z* 2000 with a retention time window of 0 to 10 min. Four technical injections per each biological replicate were used and

averaged with an 0.4 RSD cutoff.[205] To filter the GC-MS data, the blank cutoff was 1×10^2, and the mass spectrometry data were filtered between m/z 19 to m/z 350 with a retention time window of 10 to 22.75 min with a 0.4 RSD cutoff. For generation of the PCA plots, Jupyter lab (Python) was used. Volcano plots were made by VolcaNoseR.[206] Venn diagrams were made by using an available webtool (https://bioinformatics.psb.ugent.be/webtools/Venn/). To generate the PCA and volcano plots that display only the unique and/or upregulated features, the data acquired from MZmine were further filtered.[204] The features (peak areas and appropriate m/z over retention time values) from bees fed sugar, as well as features from the specific diet samples (i.e., pollen, *Chlorella*, or spirulina), were all subtracted from the feature list acquired from bees fed on the respective diets. Thus, the generated filtered feature list only contained the unique and or upregulated metabolites when the bees were fed on the pollen, *Chlorella*, or spirulina diets (**Figure 68**).

Results and Discussion

Diet Consumption and Growth Performance

Diet consumption and body weights were measured in caged honey bees fed sugar, pollen, *Chlorella*, and spirulina diets following 8 days of ad libitum feeding. Consumption is an important metric in feed comparison studies, since the amount of diet consumed dictates the pool of available nutrients. Of the protein-containing diets, consumption was highest for the pollen diet and lowest for the *Chlorella* diet (P < 0.0001). Overall diet consumption was as follows: sugar > pollen > spirulina > *Chlorella* (**Figure 59**). These results are consistent with our previous observations that bees consume less spirulina than pollen in similar experimental designs.[200, 207-208] Bees fed sugar had the lowest head weights, but there were no head weight differences between bees fed pollen and either *Chlorella* or spirulina (P = 0.0013). Similarly, the sugar diet

produced the lowest thorax weights ($P < 0.0001$), but there were no significant differences

between pollen- and either *Chlorella-* or spirulina-fed bees (**Figure 59**). Increases in head and

thorax weights respectively reflect increased head gland development and flight muscle mass,

attributes that are central to honey bee colony fitness and productivity.[178, 209-210] Despite reduced

consumption, the high bioavailability of microalgae may have led to body weights that were the

same as pollen-fed bees. Since honey bees do not appear to consume pollen based on its

nutritional quality,[211] it can be postulated that non-nutrient components might underlie pollen's

attractiveness. Indeed, pollen phagostimulants are solvent-extractable in sufficient quantities to

increase the consumption of artificial diets by honey bees, although the specific compounds

involved are largely unknown.[212]
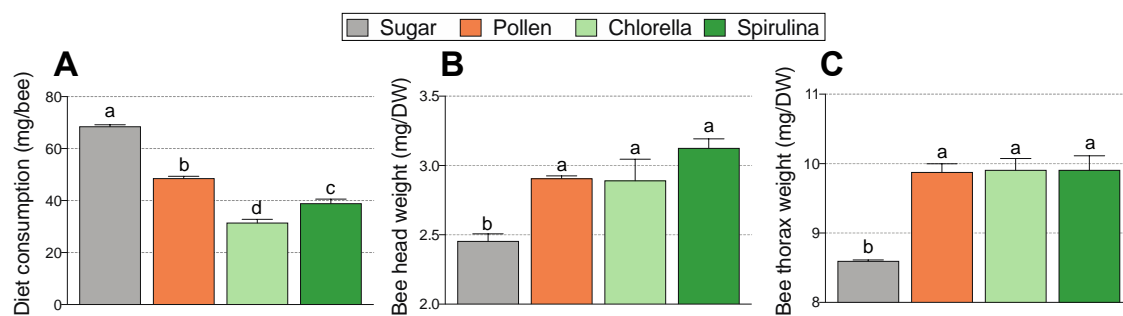
Figure 59. Effects of feeding treatments on honey bee diet consumption and growth performance after 8 days. (A) Diet consumption. (B) Average head weight. (C) Average thorax weight. Error bars represent standard error (SE). Columns with different letters are significantly different at α = 0.05.

Nutritionally Regulated Gene Expression

Nutrigenomics examines how nutrients affect gene expression and can measure an

organism's response to changes in feed composition as well as provide information on diet

limitations.[213] Nutritionally-regulated gene expression was measured in bees fed the various

diets. In honey bees Vitellogenin (Vg) is a central storage and regulatory protein that has been

used as a biomarker of nutritional status since *Vg* levels are linked to diet quality.[180, 214-215] *Vg* mRNA expression was highest in pollen- and *Chlorella*-fed bees and lowest in sugar-fed bees (P = 0.0010). Overall *vg* expression was as follows: pollen = *Chlorella* > spirulina > sugar, with *Chlorella*-fed bees trending towards higher *vg* levels than pollen-fed bees (**Figure 60**). Antioxidant enzyme gene expression is associated with longevity in honey bees[216] and is nutritionally regulated.[217] Bees fed spirulina had significantly higher transcript levels of the antioxidant genes *catalase* (P < 0.0001) and *superoxide dismutase* (P < 0.0001). Heat shock proteins are highly conserved and have important roles in protecting cells from thermal-induced (including cold) and oxidative stresses,[218] as well as innate immune functions.[219] Bees fed sugar and spirulina had higher levels of *heat shock protein 70* (*hsp70*) (P = 0.0073). Spirulina-fed bees had the highest levels of *heat shock protein 90* (*hsp90*) (P < 0.0001) (**Figure 60**).
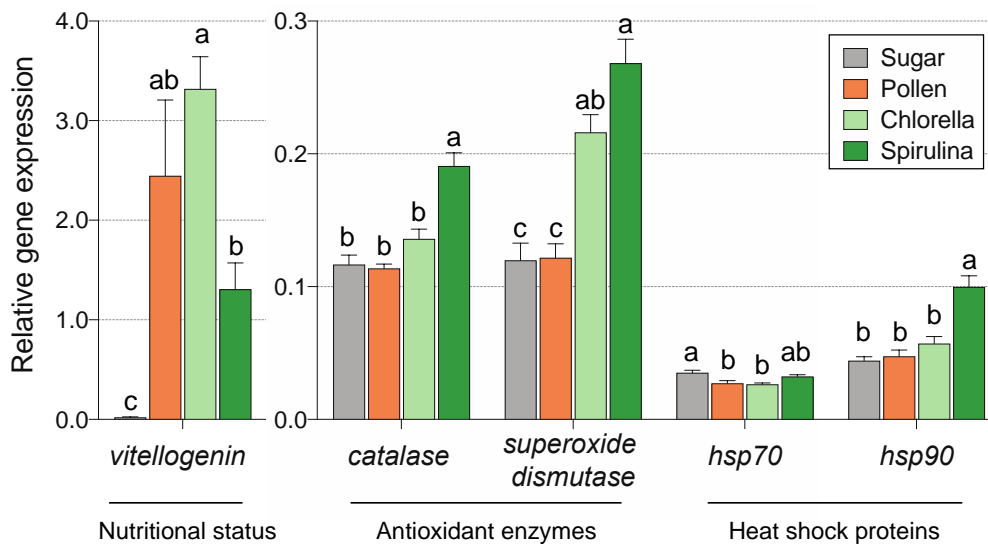
Figure 60. Gene expression profiles of honey bees fed pollen and microalgae diets. Overall nutritional status was assessed by quantifying transcript levels of the nutritional storage protein *vitellogenin* (*vg*). Stress response potential was measured by quantifying transcript levels of the antioxidant proteins *catalase* and *superoxide dismutase* as well as *heat shock proteins 70* (*hsp70*) and *90* (*hsp90*). For each gene, columns with different letters are significantly different at α = 0.05.

110

Untargeted Metabolomics through LC-MS and GC-MS

Untargeted metabolomics has proven applicable to identify bee metabolites,[220] and thus, a combination of both LC-MS and GC-MS were used to study the effects of these diets on the bee metabolomes. These techniques generate mass to-charge ratio (*m/z*) and retention time (RT) pairs, hereafter referred to as features.[221] The generated feature lists acquired by LC-MS and GC-MS were compared using a suite of computational tools and plotting techniques to analyze honey bee metabolome compositions.

LC-MS analyses revealed 248 features that were shared among bees fed the various diets, whereas GC-MS analyses revealed 87 shared features (**Figure 61**); in the case of GC-MS data, a threshold of 500 for the peak area for each feature was applied.
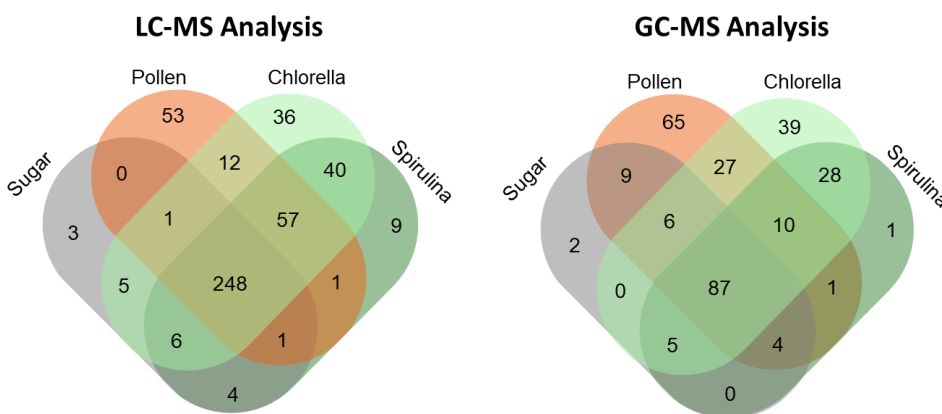
Figure 61. Venn diagrams showing feature distributions of bee metabolites from LC-MS and GC-MS analyses. These diagrams represent the number of features belonging to bees fed the various diets. Each feature is defined as a *m/z* value and retention time pair. These orthogonal approaches revealed a high number of shared features across bees fed the four various diets (i.e., 248 and 87 respectively).

To explore metabolomes among diet treatment groups, principal component analyses (PCA) were performed. We also used a subtractive approach to represent unique and/or upregulated features of bee metabolomes that responded to the pollen, *Chlorella* or spirulina

111

diets. To accomplish this, features of sugar-fed control bees and features from the respective diet

extracts were subtracted from the total feature list (**Figure 68**). For example, unique and/or

upregulated features of pollen-fed bees were determined by subtracting sugar-fed bee features

and features that were specific to the pollen extract itself (**Figure 68**). As displayed in the PCA

plots (**Figures 62** and **63**), metabolomes of bees fed pollen and either *Chlorella* or spirulina had

distinct separation regardless of using an LC-MS or GC-MS approach. Interestingly, bees fed

Chlorella and spirulina exhibited some overlap despite taxonomic divergence of the source

biomass used for these diets. Pollen grains are the male gametophytes of flowering plants,

whereas *Chlorella* is a eukaryotic microalga and spirulina is derived from *Arthrospira,* a genus

of prokaryotic cyanobacteria. Consistent with our PCA results, a large-scale analysis of mass

spectrometry data from divergent algae samples revealed similar clustering patterns among

marine and freshwater algae groups when compared to groups of actinobacteria (both marine and

terrestrial) and lichens.[222]
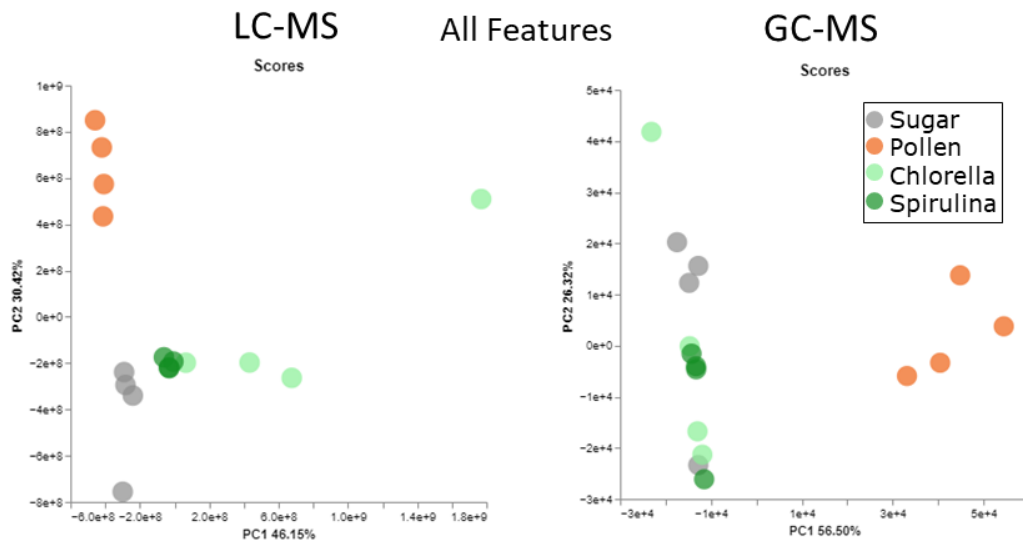
Figure 62. Principal component analysis (PCA) plots of untargeted honey bee metabolites
acquired through LC-MS and GC-MS. Four bee diets were explored, and each data point
represents a biological replicate (i.e., eight bees pooled from an independent cage, and each of

these injected for four technical replicates). Bees fed pollen, *Chlorella*, or spirulina had distinct separation that was supported by both the LC-MS and GC-MS approaches. *Chlorella-* and spirulina-fed bees exhibited overlapping metabolome profiles and were more similar to each other than to the metabolome of bees fed pollen.
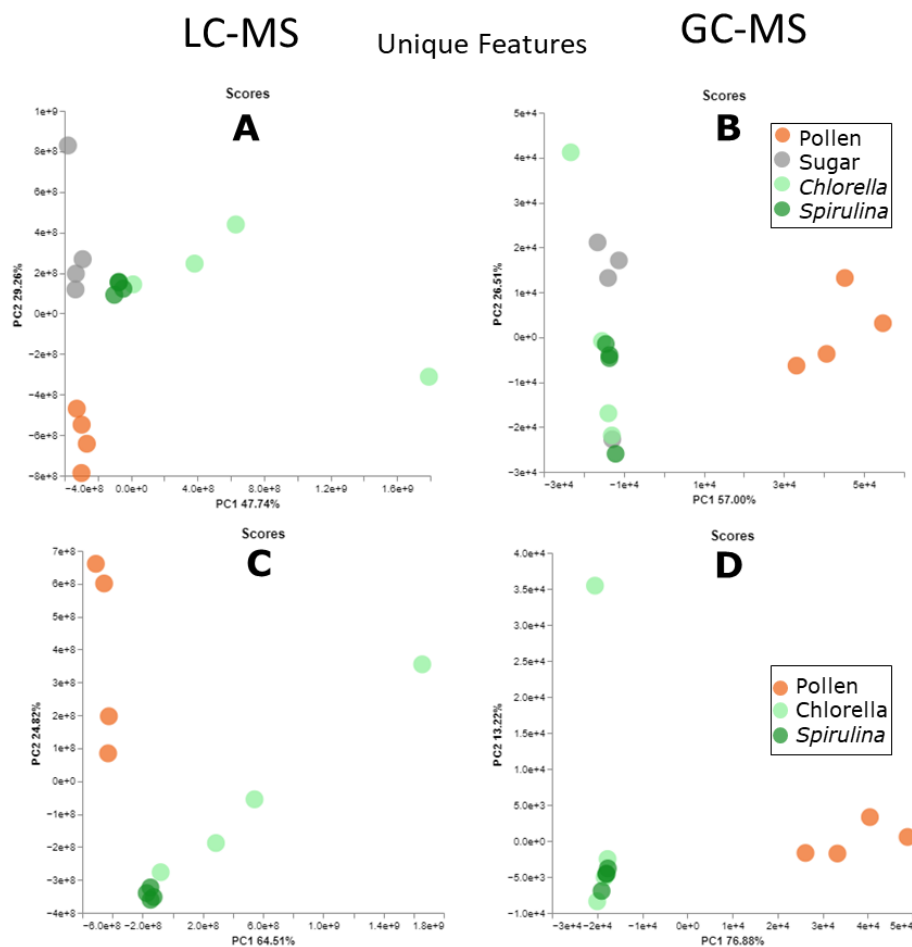
Figure 63. Principal component analysis (PCA) plots of untargeted honey bee metabolites acquired through LC-MS (scores plots **A** and **C**) and GC-MS (scores plots **B** and **D**) after applying a subtractive metabolomics approach. To better evaluate diet uniqueness, the features originating from the extracts of pollen, *Chlorella,* or spirulina were subtracted from the respective feature lists of the bees fed those diets (scores plots **A** and **B**). Further, features of sugar-fed bees were separately subtracted (scores plots **C** and **D**). Bees fed *Chlorella* and spirulina diets exhibited similarities to pollen-fed bees, but their metabolome profiles were more similar to each other than to pollen fed bees.

Volcano plots were generated based on LC-MS and GC-MS data (Figures 7 and S4, respectively). Each dot on the plots represents a feature (i.e., RT/*m/z* value). All features that exhibited >1.5 fold change were considered statistically significant (P < 0.05). Subtractive analyses (**Figure 68**) removed features associated with diet extracts and indicated bee metabolites that were differentially expressed upon consumption of the various diets (**Figure 64 an**d **69**, Unique Features panel). In general, LC-MS and GC-MS volcano plots revealed high similarities among the metabolomes of bees that were fed pollen, *Chlorella*, and spirulina. Using the LC-MS data, we identified selected features that might contribute to diet effects on bee physiology (**Figure 64** and **Table 56**). Identification was based on accurate mass searches in the *Dictionary of Natural Products*[223] and aimed to highlight the potential of volcano plot data for addressing diet deficiencies. For example, the feature 8.27/463.378 (RT/*m/z*) was putatively identified as tricosanedioic acid, a fatty acid which was upregulated in bees fed pollen but not in bees fed *Chlorella* when all features were examined (**Figure 64**, Pollen vs *Chlorella,* All features plot). Upon subtraction of diet extract features, the feature remained, suggesting a potentially important role in the nutritional value of the pollen diet (**Figure 64**, Pollen vs *Chlorella,* Unique features plot). Similarly, the feature 5.52/335.221(RT/*m/z*) was putatively identified as 10,11-dihydroxy-8,12-octadecadienoic acid, a fatty acid which was upregulated in bees fed pollen but not in bees fed spirulina after subtractive analyses (**Figure 64**, Pollen vs *Chlorella,* Unique features plot). These results highlight the potential of untargeted metabolomics for artificial diet development in honey bees. By comparison to pollen, the bee's natural source of macro- and micronutrients, feed could ultimately be tailored to reproduce the metabolomes of pollen-fed bees. This approach could further be applied to optimize feed ingredients that support seasonal

and regional nutritional requirements of honey bees, which vary based on interactions between

available pollen forage and seasonal colony demography.[224]

Figure 64. Volcano plots of honey bees fed on four different diets using untargeted metabolomics through LC-MS analysis. "All features" plots represent all RT/*m/z* values processed without applying our subtractive approach. The "Unique features" plots only shows uniquely expressed and/or upregulated features produced by the bees. On these plots, our subtractive approach was used, thus the features that came from the bees fed on sugar diet and the features found in the pollen and algae extracts were subtracted out. We have putatively identified a handful of the RT/*m/z* pairs (highlighted dots) that might contribute to diet effects on

115

bee physiology. These features are further discussed in Table S2. LC-MS volcano plots showed high similarities among the metabolomes of bees that were fed pollen, *Chlorella*, and spirulina.Z

Unique features of *Chlorella*- and/or spirulina-fed bee metabolomes warrant further investigation to better understand the effects of specific algal metabolites on bee physiology, particularly since such compounds are not naturally encountered. Some metabolites derived from these microorganisms appear to have ecological roles as allelochemicals, including compounds that may inhibit competing microorganisms. These allelochemicals may also serve as protection against aquatic invertebrates and their larvae.[225] Commercially grown *Chlorella* and spirulina are generally recognized as safe for human and animal consumption. However, strains can coexist in the same habitats as potentially toxic algae, and if so, such biomass can become contaminated with toxins produced by other microorganisms.[226] Therefore future work could incorporate screening for known algal toxins and their metabolites in bees, especially when testing novel strains and wild-harvested biomass. On the other hand, microalgae are a rich source of natural products with unique structures that also have potential as therapeutic drugs.[222] Notably, a sulphated polysaccharide derived from the red alga, *Porphyridium* spp., led to decreased parasite loads and decreased honey bee mortality due to infection by the gut parasite *Nosema cerane*.[227] In our study, microalgae diets led to increased levels of antioxidant enzymes and heat shock protein gene expression. These genes apparently respond to diet quality in honey bees and may be differentially regulated by certain algal metabolites. Consistent with our results, dietary spirulina supplementation led to increased antioxidant gene expression and total antioxidant capacity in rainbow trout.[228] It remains to be determined if prolonged upregulation of antioxidant gene pathways are beneficial to bees, or if it presents a metabolic cost. Nevertheless, further

studies could lead to the identification of potentially health-modulating metabolites for therapeutic development in honey bees.

Honey bee Metabolites Identified by LC-MS and GC-MS

Prominent bee metabolites were identified by LC-MS and GC-MS. Specifically, LC-MS data were used to identify metabolites through comparisons to available standard materials. Extracted ion chromatograms (XIC) of each compound were examined (**Figure 70-76**). Each the metabolites were examined across all the diet, using all the four biological and four technical replicates per biological samples. The identified metabolites were consistently present in all the replicates. The relative abundances of the compounds were calculated based on the average peak area of the compounds (**Table 57**). Accurate mass measurements, retention time and UV absorptions were used to confirm identification[229] of the following compounds: linoleic acid, α-linolenic acid, zeaxanthin, lutein, quinic acid, α-tocopherol, β-carotene (**Figure 70-77**). Linoleic acid and α-linolenic acid are two polyunsaturated fatty acids that are considered essential for honey bees. [192-194] The *Chlorella* diet led to the highest levels of linoleic acid, and the levels of α-linolenic acid was comprable to pollen-fed bees (**Figure 65**). Spirulina-fed bees accumulated the lowest levels of both essential fatty acids (**Figure 65**). The abundance of pollen-derived polyunsaturated fatty acids is positively correlated with abdominal Vitellogenin expression. [192-194] Consistent with linoleic and α-linolenic acid levels, bees fed pollen and *Chlorella* had significantly higher abdominal *vitellogenin* mRNA levels than spirulina-fed bees (**Figure 60**). Lipid accumulation in green algae, such as *Chlorella*, is well known to exceed that of cyanobacteria such as spirulina, which are renowned for their protein content. [197] Based on fatty acid composition and *vitellogenin* expression, our results suggest that *Chlorella* and related green algae are promising lipid sources for bee diet development. Nevertheless, spirulina is a natural

117

source of many bioactive phytochemicals that occur in pollen, including carotenoids, which are potent antioxidants and vitamin A precursors that modulate gene activity in a variety of animals.[230] For instance, diets containing the carotenoid β-carotene extracted from spirulina led to increased expression of *superoxide dismutase* and *catalase* as well as increased total antioxidant capacity in Nile tilapia.[231] In our study, spirulina-fed bees accumulated significantly higher levels of β-carotene (**Figure 65**), which may explain the observed increases in *catalase*, *superoxide dismutase,* and *heat shock protein 90* (**Figure 60**). Other bioactive carotenoids, lutein and zeaxanthin, were only identified in microalgae-fed bees (**Figure 65**). Lutein and astaxanthin from *Chlorella* are in regular use as feed ingredients for fish and poultry.[230] Similarly, our results indicated that microalgae are promising natural sources of carotenoids for incorporation into bee feed.
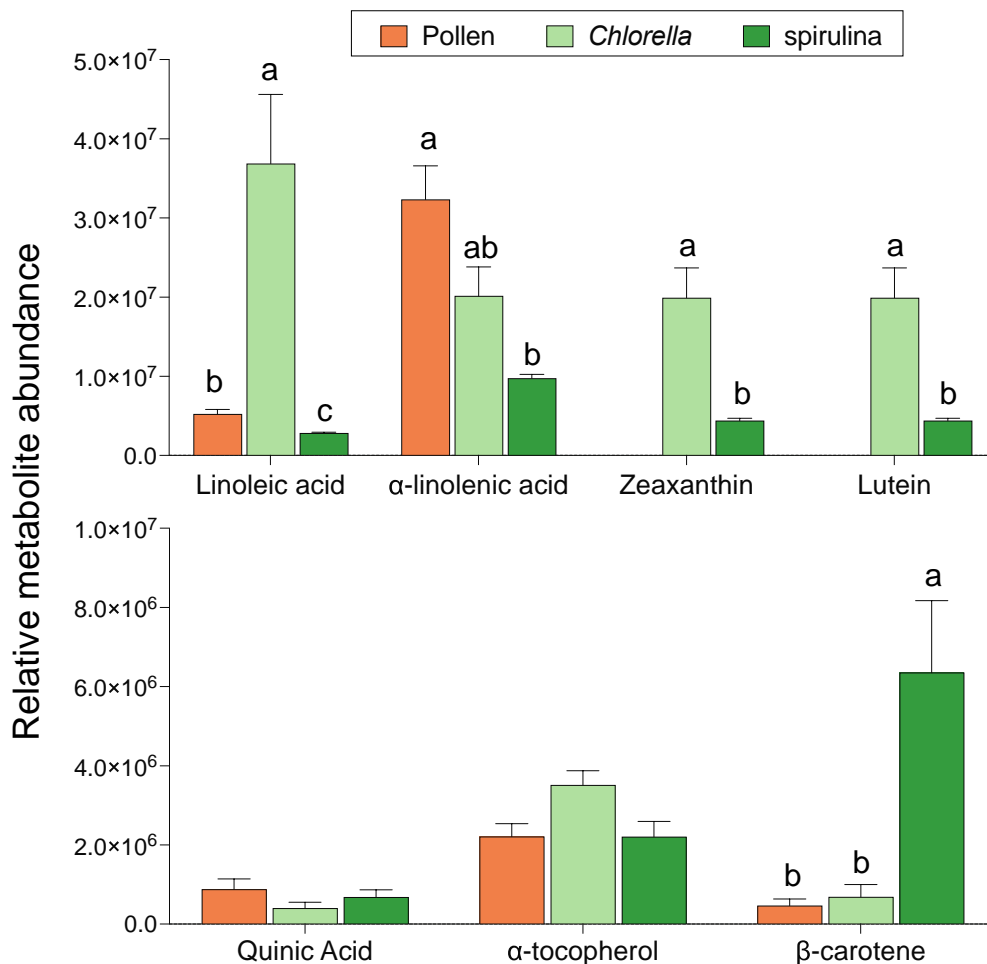
Figure 65. LC-MS targeted metabolite analyses of bees fed pollen and microalgae diets. For each compound, columns with different letters are significantly different at $\alpha = 0.05$.

For metabolite identification through GC-MS, total ion chromatograms (TIC) were used, and the peaks were compared to a NIST 2011 library for similarity match based on their ion fragmentation. The putatively identified metabolites all possessed higher than 90% similarity scores (**Table 54**). The prominent compounds identified by this technique were mainly fatty alcohols and hydrocarbons (**Figure 77**). Insects rely on blends of waxy cuticular hydrocarbons as pheromones for mating and nestmate recognition.[232] Insect cuticular hydrocarbons are influenced by nutrition, as experimentally demonstrated using different host plants and artificial diets.[233] In

honey bees, currently unknown factors in the colony environment may contribute directly or indirectly to molecular processes regulating pheromone synthesis.[234] Thus, it is plausible that local nutrition could contribute to the development of similar pheromone profiles among individuals. To test this hypothesis within the context of our study, relative metabolite abundances were calculated based on average peak areas of the compounds detected by GC-MS (**Table 58**). The abundances of 1-heneicosanol, *n*-nonadecanol-1, *n*-tetracosanol, and docosane were significantly impacted by diet. These results suggest that nutrition can influence honey bee cuticular hydrocarbon profiles, which may have future utility as dietary or health biomarkers. Two fatty acids, *n*-hexadecanoic (i.e., palmitic) acid and erucic acid, were also significantly impacted by diet.

Table 54. Putatively identified metabolites from GC-MS analysis of bees fed pollen and microalgae diets. Comparison to NIST 2011 compound library was used for metabolite identifications.
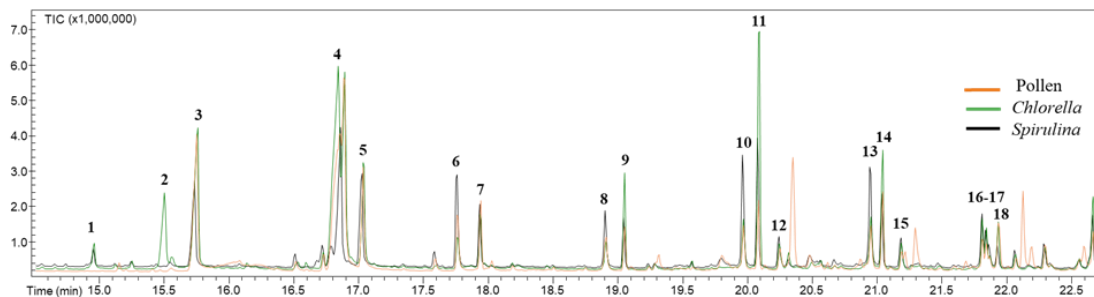
Compound No.	Compound Name	Retention Time (min)	Compound No.	Compound Name	Retention Time (min)
1	phytol acetate	14.94	10	n-tetracosanol	19.95
2	1,11,13-octadecatriene	15.49	11	hexacosane	20.07
3	n-hexadecanoic acid	15.75	12	tetratetracontane	20.25
4	erucic acid	16.88	13	octacosanol	20.95
5	octadecanoic acid	17.02	14	pentacosane	21.03
6	1-heneicosanol	17.75	15	2-methyloctaconsane	21.17
7	heneicosane	17.93	16	1-heptacosnaol	21.81
8	n-nonadecanol-1	18.90	17	9-Tricosene	21.85
9	octacosane	19.04	18	docosane	21.90

Conclusion

Malnutrition is a serious threat to managed honey bees that is exacerbated by landscape agricultural intensification and climate change. As beekeeper reliance on artificial diets increases, there is a growing need for efficacious and sustainable feed formulations that can support bee nutritional requirements across diverse management conditions. Current methods for honey bee diet development involve measuring a few pre-selected biochemical and/or physiological parameters to test the effects of diet formulations on growth performance.

121

However, orthogonal methods that can directly target diet deficiencies are necessary. Here, we applied mass spectrometry-based metabolomics to better understand the nutritional and metabolic impacts of microalgae-based artificial diets relative to a natural pollen diet. The use of both LC-MS and GC-MS methods provided coverage across a broad range of metabolite groups and overcame the individual limitations associated with these approaches. Pollen and microalgae diets had similar nutritional and metabolomic impacts in bees, especially after subtraction of unique diet features in data analysis. *Chlorella* provided more essential fatty acids than spirulina, which likely contributed to its enhanced nutritional value. Nevertheless, spirulina is a promising food source of bioactive compounds, notably carotenoids, that may augment stress response pathways in bees. We conclude that the tested microalgae have potential as sustainable bee feed additives and health-modulating natural products. Finally, this study showed that metabolomics approaches have significant potential to help tailor feed interventions to achieve nutritional monitoring in honey bees as well as identify beneficial diet attributes in natural and artificial diets.

Brood frames removed from healthy honey bee colony

Worker brood frame incubated overnight to obtain newly emerged worker bees

Newly emerged worker bees randomly assigned to diet treatments

Diet treatments:

50 bees   50 bees   50 bees   50 bees

Sugar   Pollen   Chlorella   spirulina

x 4 cage replicates per diet
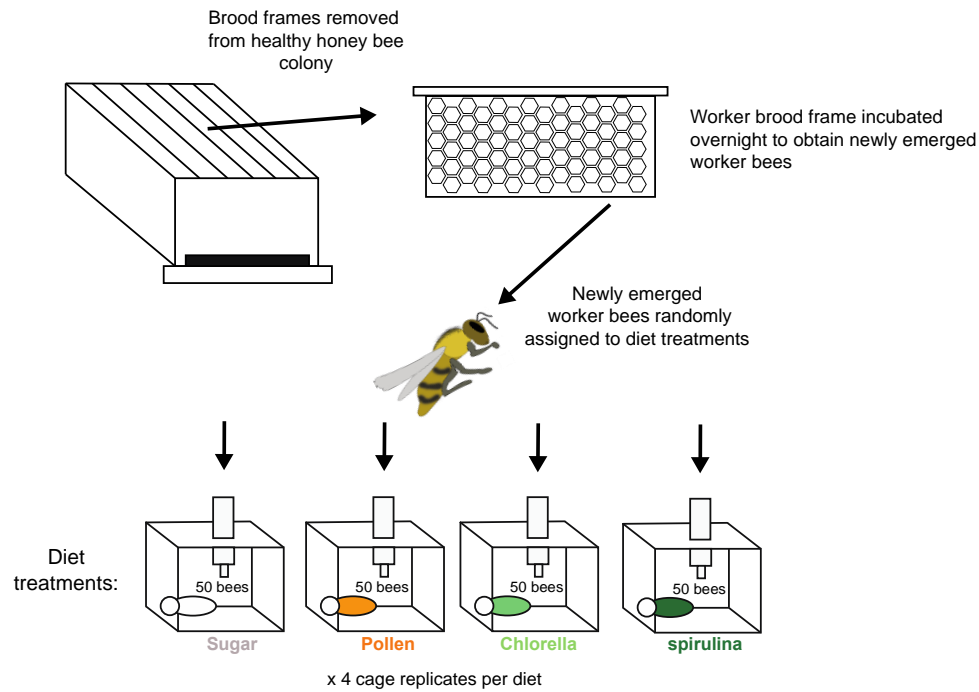
Figure 66. Schematic overview of the honey bee feeding experiment. Worker brood frames were sourced from a healthy bee colony and incubated overnight to obtain newly emerged bees. Individuals were randomly assigned to feeding groups consisting of sugar, pollen, *Chlorella*, or spirulina diets.

Extraction Step 1
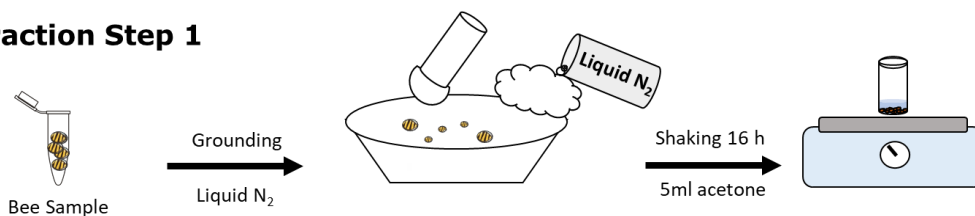
Extraction Step 2
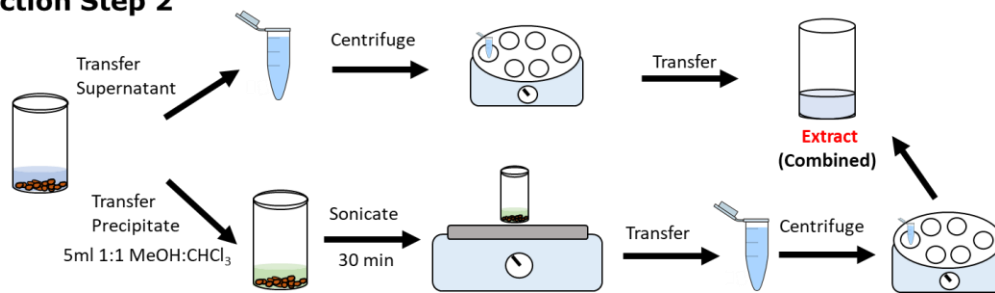
Figure 67. Metabolite extraction of bee abdomens. The samples were ground with mortar and pestles under liquid nitrogen. Then they were transferred to a scintillation vial and then submerged in acetone (5 mL). Samples were shaken for approximately 16 hrs. The acetone layer was transferred to an Eppendorf and centrifuged. Then the acetone layer was removed and saved. The original samples were resuspended in 1:1 MeOH:CHCl$_3$ (5 mL) and sonicated for 30 min. The solvent was transferred to an Eppendorf and centrifuged. The supernatants from this step and the saved acetone layer was combined and dried under nitrogen to yield the bees fed on diet extract. This extraction procedure was used for the algae and pollen extracts as well.
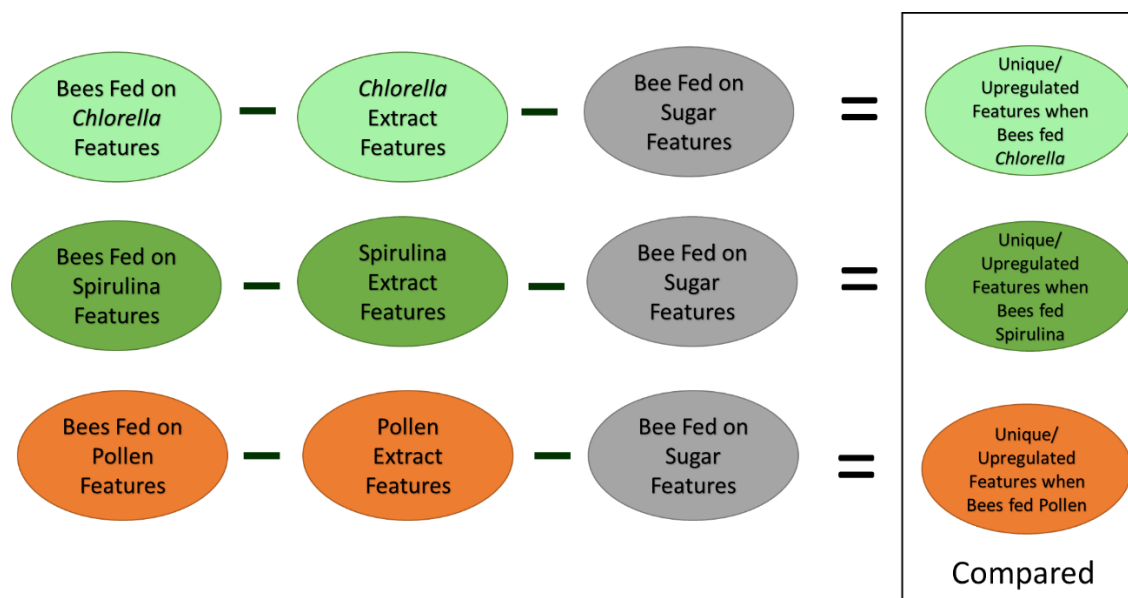
Figure 68. Process of feature filtering of raw data from LC-MS and GC MS analysis. The peak area of each RT/m/z was used for subtraction. Each biological replicate consisted of 8 bee abdomens harvested from one cage. Four biological replicates were used per diet and each biological replicate was replicated 4 times (technical replicates).

Figure 69. Volcano plots of honey bees fed on four different diets using untargeted metabolomics through GC-MS analysis.
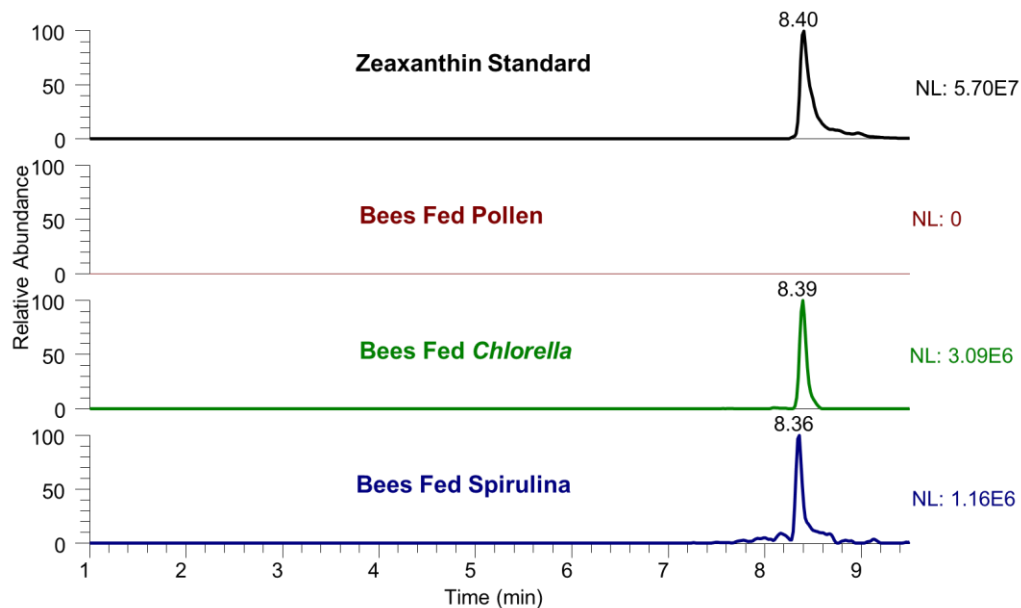
Figure 70. Extracted ion chromatograms (XIC) of zeaxanthin in the standard and in the bees fed various diets.
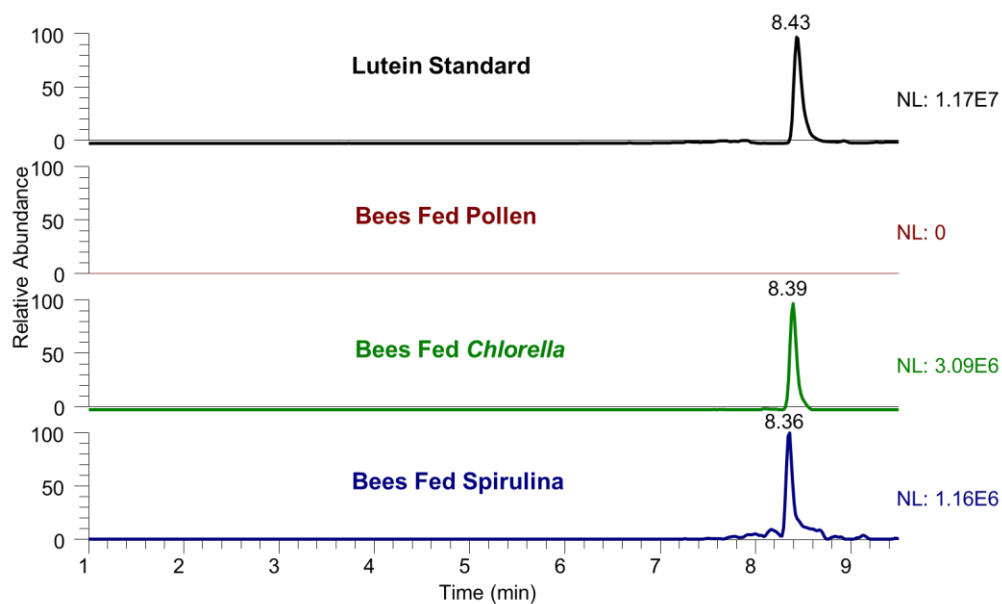
Figure 71. Extracted ion chromatograms (XIC) of lutein in the standard and in the bees fed various diets.

127
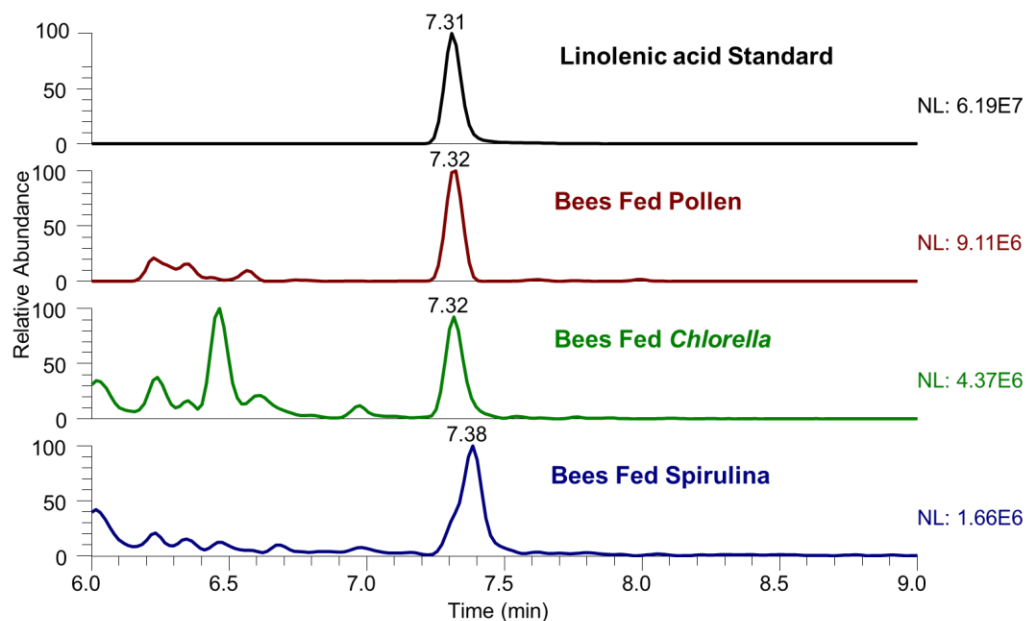
Figure 72. Extracted ion chromatograms (XIC) of linolenic in the standard and in the bees fed various diets.
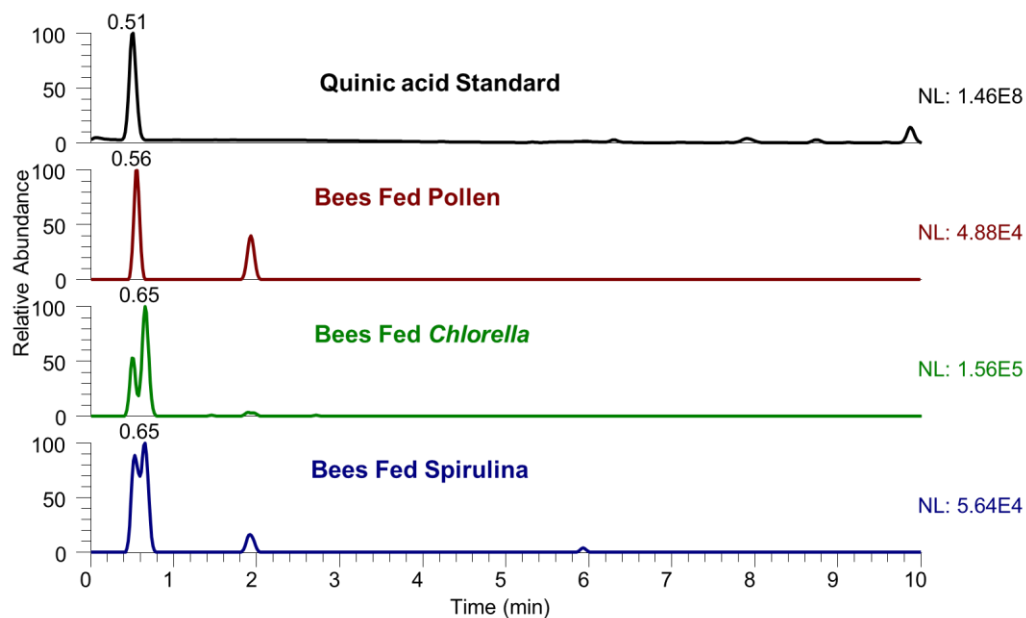
Figure 73. Extracted ion chromatograms (XIC) of quinic acid in the standard and in the bees fed various diets.

128
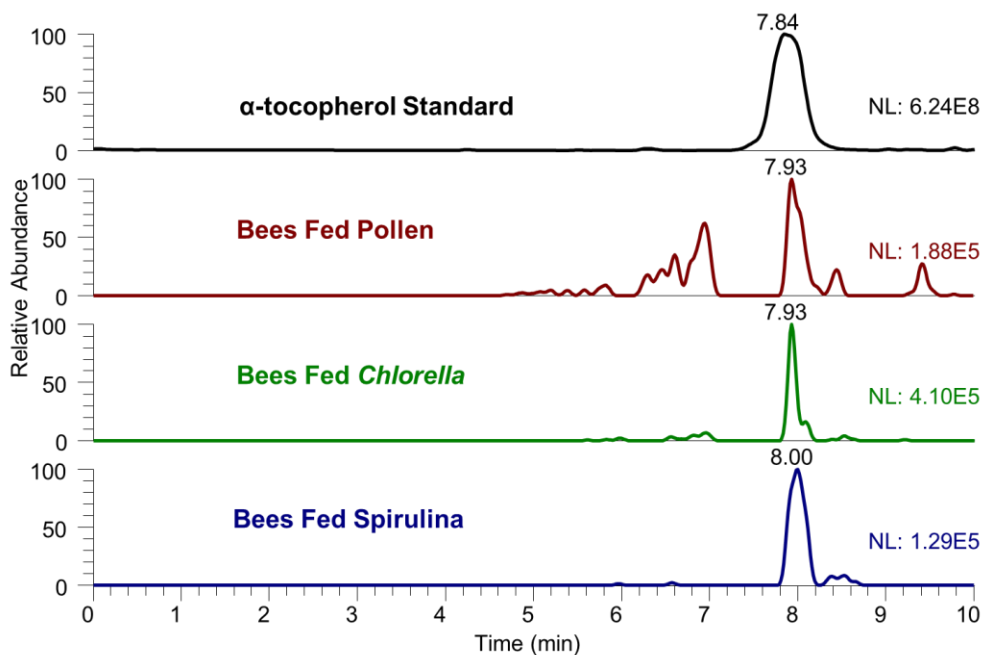
Figure 74. Extracted ion chromatograms (XIC) of α-tocopherol in the standard and in the bees fed various diets.
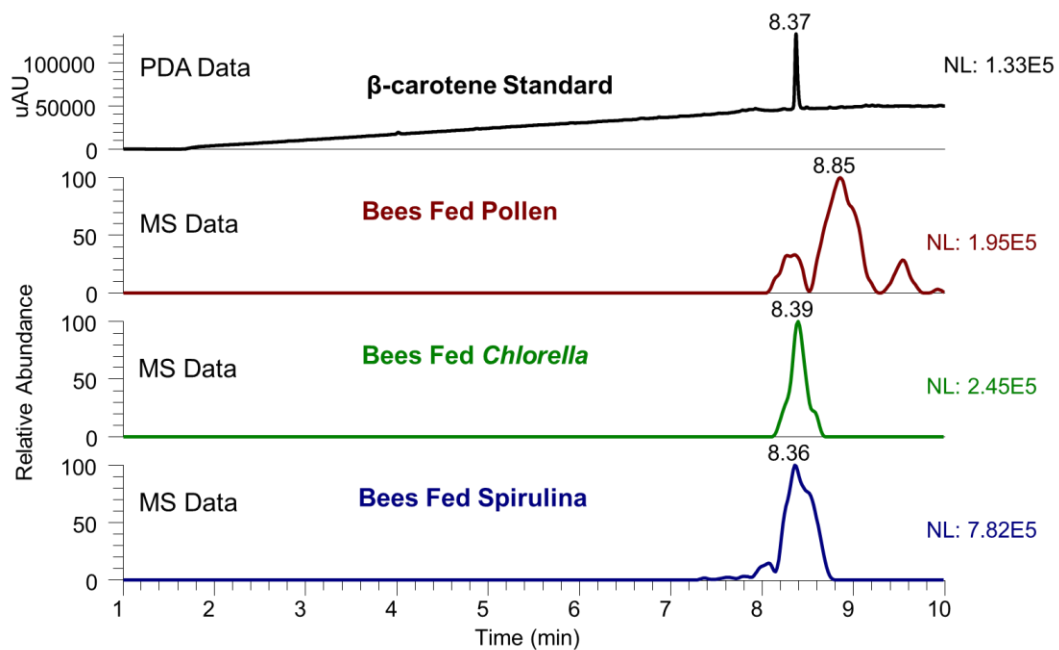
Figure 75. Extracted ion chromatograms (XIC) of β-carotene in the standard and in the bees fed various diets.
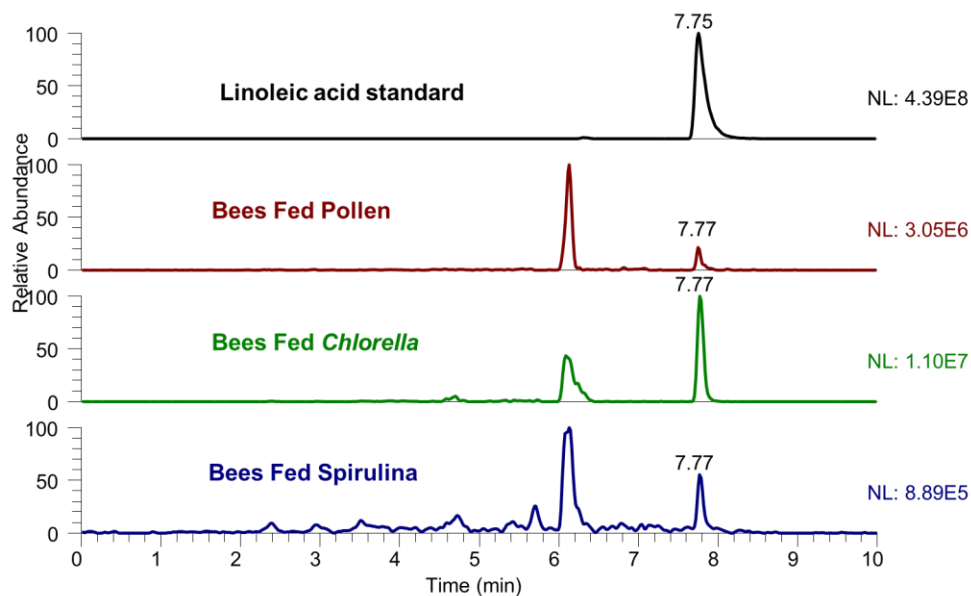
Figure 76. Extracted ion chromatograms (XIC) of linoleic acid in the standard and in the bees fed various diets
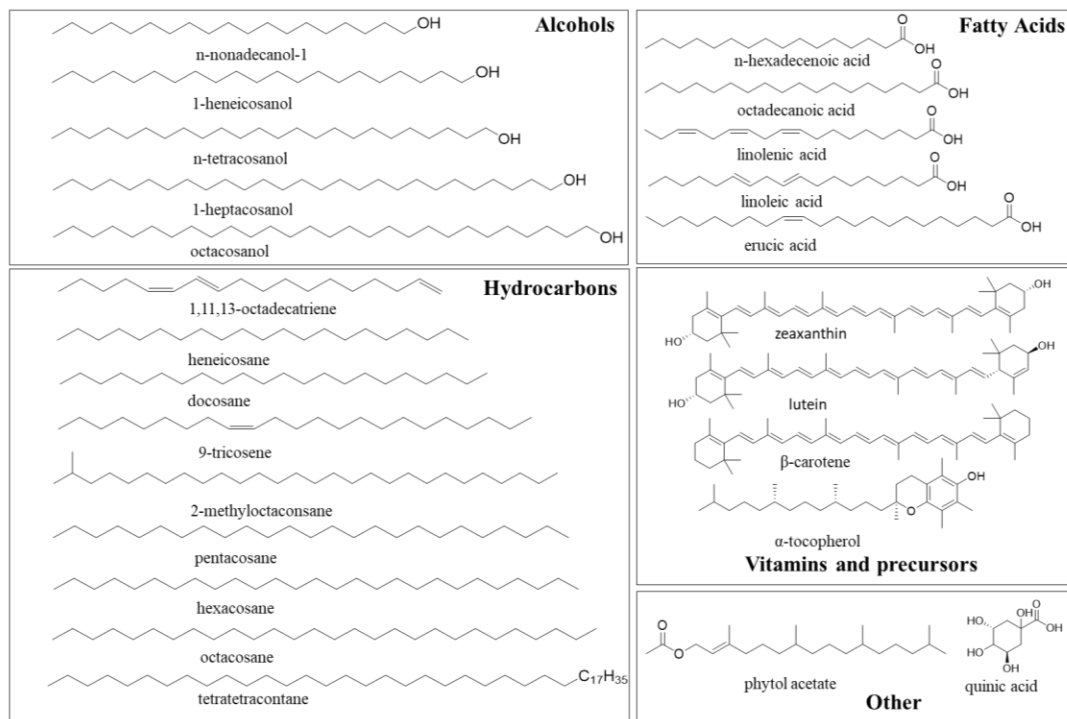
Figure 77. Structures of all compounds identified through untargeted GC-MS and targeted LC-MS analysis.

130

Table 55. Primers used in this study

Gene (accession number)	Forward 5'-3'	Reverse 5'-3'	Annealing temperature (°C)	Study
actin (XM_623378)	TGCCAACACTGT CCTTTCTG	AGAATTGACCC ACCAATCCA	55.0	Alaux et al., 2011
vitellogenin (vg) (AJ517411)	GTTGGAGAGCA ACATGCAGA	TCGATCCATTC CTTGATGGT	57.5	Salmela et al., 2016
catalase (NM_001178069)	TTCTACTGTGGG TGGCGAAAG	GTGTGTTGTTA CCGACCAAATC C	60.0	Li et al., 2014
CuZn Sod (NM_001178027)	TCAACTTCAAGG ACCACATAGTG	ATAACACCACA AGCAAGACGAG	60.0	Li et al., 2014
HSP70 (GB19503)	GACGCGGGAGC GATAGCAGG	AAGCCATAAGC AATCGCCGCC	60.0	Ramirez et al., 2017
HSP90 (GB14758)	ATGCCGGAGGA CGTCACCAT	TTGTGCAATTTC AGCTTGGAAAG CG	56.0	Ramirez et al., 2017

Table 56. Identified features from LC-MS volcano plot analysis.

RT/*m/z* value	Identified ion	Accurate mass [M+H]$^+$	Molecular Formula	Example of possible compound Using Dictionary of Natural Products
5.69/255.23	[M+H-H2O]+	273.2433	$C_{16}H_{32}O_3$	2-Hydroxyhexadecanoic acid
5.15/274.275	[M+H]+	274.2752	$C_{16}H_{35}NO_2$	2-Amino-1,3-hexadecanediol
7.76/263.238	[M+H-H2O]+	281.2490	$C_{18}H_{32}O_2$	4,6-Dimethyl-2,4-hexadecadienoic acid
5.03/287.223	[M+H]+	287.2226	$C_{16}H_{30}O_4$	2,16-Dihydroxy-6-hexadecenoic acid
5.52/335.221	[M+Na]+	313.2386	$C_{18}H_{32}O_4$	10,11-Dihydroxy-8,12-octadecadienoic acid
4.02/314.270	[M+H]+	314.2702	$C_{18}H_{35}NO_3$	2-Amino-4,9-octadecadiene-1,3,8-triol
7.99/371.102	[M+H]+	371.1025	$C_{22}H_{14}N_2O_4$	Caulerpinic acid
8.03/386.364	[M+H]+	386.3646	$C_{23}H_{47}NO_3$	2-Amino-11-tricosene-1,3,4-triol
8.27/463.378	[M+Na]+	441.3958	$C_{27}H_{52}O_4$	Tricosanedioic acid; Di-Et ester

Table 57. Relative abundance and average peak areas of compounds identified through LC-MS analysis. The closer the p value to 0, the more significantly different the given metabolite in a pairwise comparison between diets.

Compound Name	Avrg T Pollen 1	Avrg T Pollen 2	Avrg T Pollen 3	Avrg T Pollen 4	Avrg T Chlor 1	Avrg T Chlor 2	Avrg T Chlor 3	Avrg T Chlor 4	Avrg T Spir 1	Avrg T Spir 2	Avrg T Spir 3	Avrg T Spir 4	Pollen vs *Chlorella* p value	Pollen vs Spirulina p value	*Chlorella* vs Spirulina p value
Zeaxanthin	0.00E+00	0.00E+00	0.00E+00	0.00E+00	1.66E+07	3.13E+07	1.56E+07	1.61E+07	3.71E+06	4.29E+06	5.13E+06	4.49E+06	0.01	0.00	0.03
Lutein	0.00E+00	0.00E+00	0.00E+00	0.00E+00	1.66E+07	3.13E+07	1.56E+07	1.61E+07	3.71E+06	4.29E+06	5.13E+06	4.49E+06	0.01	0.00	0.03
Linolenic acid	3.12E+07	3.35E+07	2.19E+07	4.27E+07	1.54E+07	3.04E+07	1.43E+07	2.05E+07	9.67E+06	9.80E+06	8.51E+06	1.10E+07	0.07	0.01	0.06
Linoleic acid	1.60E+07	1.96E+07	1.95E+07	2.71E+07	2.50E+07	4.56E+07	1.55E+07	2.84E+07	9.31E+06	8.04E+06	8.69E+06	9.57E+06	0.30	0.01	0.05
Quinic Acid	8.90E+05	2.74E+05	1.55E+06	7.98E+05	8.35E+05	2.28E+05	1.92E+05	3.60E+05	7.02E+05	1.18E+06	3.15E+05	5.36E+05	0.18	0.57	0.28
α-tocopherol	3.11E+06	2.17E+06	1.57E+06	2.01E+06	3.29E+06	4.41E+06	2.69E+06	3.67E+06	2.74E+06	2.63E+06	1.07E+06	2.40E+06	0.04	0.99	0.05
β-carotene	2.13E+05	9.28E+05	5.07E+05	2.18E+05	6.02E+04	6.21E+05	1.56E+06	5.20E+05	1.21E+06	6.37E+06	8.76E+06	9.08E+06	0.56	0.05	0.05

Table 58. Relative abundance comparison of metabolites identified through GC-MS library match.

Number	Compound Name	Retention Time (min)	Bees Fed Pollen Av. Peak Area	STD	Bees Fed *Chlorella* Av. Peak Area	STD	Bees Fed *Spirulina* Av. Peak Area	STD	P value Pollen vs *Chlorella*	P value Pollen vs *Spirulina*	P value *Chlorella* vs *Spirulina*
1	phytol acetate	14.94	0	0	175853	257268	426433	305071	0.016	0.000	0.197
2	1,11,13-octadecatriene	15.49	0	0	1314769	1779794	0	598626	0.084	-	0.084
3	n-hexadecanoic acid	15.75	9333143	2263486	2329692	3153895	4340992	3307856	0.707	0.015	0.030
4	erucic acid	16.88	21902384	8384166	1711860	2473759	7197180	9569427	0.040	0.033	0.675
5	octadecanoic acid	17.02	5629793	1487609	1793998	2509197	4223074	2464495	0.610	0.156	0.177
6	1-heneicosanol	17.75	2871594	470090	307831	460642	3455166	936533	0.004	0.309	0.011
7	heneicosane	17.93	2338711	266333	499212	582511	1569180	671090	0.117	0.058	0.738
8	n-nonadecanol-1	18.90	1915827	305636	244236	355805	1986565	435208	0.035	0.757	0.024
9	octacosane	19.04	1534084	237002	636673	915781	1219038	419638	0.690	0.170	0.348
10	n-tetracosanol	19.95	2162397	175568	275813	362398	3267355	401246	0.096	0.096	0.039
11	hexacosane	20.07	2772426	774512	2424181	3368633	3538234	856917	0.380	0.358	0.617
12	tetratetracontane	20.25	927306	31987	250747	296997	837254	244406	0.879	0.507	0.744
13	octacosanol	20.95	1548033	400058	412719	564245	2849318	300887	0.423	0.063	0.129
14	pentacosane	21.03	3234855	969954	985985	1299905	2042859	1496701	0.332	0.093	0.670
15	2-methyloctaconsane	21.17	922473	424013	195850	237436	843081	201821	0.973	0.771	0.661
16	1-heptacosnaol	21.81	1861544	494334	554963	675891	2520581	708811	0.137	0.507	0.209
17	(Z)-9-Tricosene	21.85	1317965	592440	457363	652279	2458617	679084	0.528	0.305	0.216
18	docosane	21.90	2993371	727064	353063	500972	770969	1281773	0.008	0.007	0.212

132

CHAPTER V: DISCOVERY OF NOVEL ANTIMALARIAL COMPOUNDS FROM

FILAMENTOUS FUNGI

Introduction

Malaria is an endemic disease in more than a hundred countries. In 2015, it resulted in approximately 215 million infectious cases and around 438,000 deaths worldwide.[9, 235] Although the death toll of malaria has significantly decreased since the start of the 21th century, resistance to the current treatment strategies remains a serious problem, and this may be even more important now, since the gains of controlling malaria have slowly plateaued.[11, 236] Thus, there is an unmet need for the development of drug leads that can be used to treat malaria.

Natural products have already played a huge role in human's constant fight against malaria, providing the most significant drugs such as artemisinin and quinine.[237] As just one metric, the first Nobel Prize for malaria in Physiology or Medicine was awarded in 1902 to Ronald Ross for laying down the foundation for antimalarial research.[238] In a more recent year, another Nobel Prize for Physiology or Medicine was awarded to Youyou Tu in 2015, for discovering artemisinin.[239]

Microorganisms have been recognized as an exceptional source of new pharmaceutical leads,[240] and thus, their investigation for antimalarial drug discovery is highly relevant. To demonstrate, there are likely more than 1.5 million fungal species in the world[241] and only around 130,000 have been studied so far. By the year 2016, roughly 33,500 bioactive microbial metabolites have been described and about 47% (15,600) were from fungal origins,[242-245] and very few of these were antimalarial leads.[246] That leaves a vast and untapped biodiversity open for antimalarial drug discovery.

There are certain challenges that commonly arise when researchers deal with secondary metabolites isolated from Nature. For instance, given the excess number of undescribed fungal species, the decision where to start the investigation can be challenging. In addition, significant time and effort must be invested into the isolation and purification of the metabolites. This can be sometimes tedious due to the re-isolation of unwanted metabolites, especially if the amounts present are insufficient for structure elucidation. These issues collectively contribute to hamper natural products research. We aimed to overcome these common challenges by addressing them head-on.

We have evaluated 40,000 fungal strains based on their antimalarial capacities using a preliminary screening for bioactivity. As a result, 71 antimalarial fungal strains were targeted and examined in this project. These have been selected carefully after confirming their activity in multiple concentrations at the extract level. They have been re-fermented on larger scales and tested multiple times, expressing replicated dose-dependent activity against the parasite (**Figure 78**).
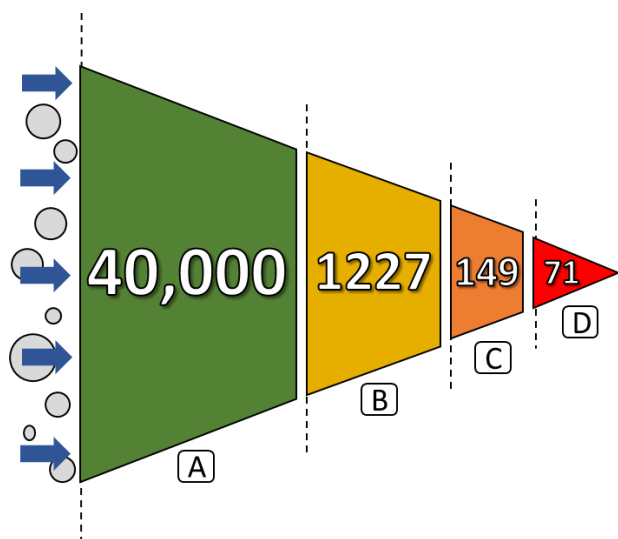
Figure 78. Overview of the active strains prioritized in the study. **A)** 40,000 fungal cultures were examined against *Plasmodium falciparum*. **B)** From those, just over 1200 were active, inhibiting

the parasite's growth by at least 33% when tested at a concentration of 50 µg/mL. **C)** Moreover, nearly 150 of those hits were extremely potent, inhibiting the same assay by over 67% when tested at 50 µg/mL. **D)** After evaluation of the preliminary antimalarial and cytotoxicity results combined with in-house dereplication data, 71 fungal strains were selected for this study.

To overcome the challenge of re-isolation metabolites of non-interest, we have applied our in-house ultra-performance liquid chromatography–photodiode array–high-resolution tandem mass spectrometric (UPLCPDA-HRMS-MS/MS) dereplication method.[63, 77] Extraction, early fractionation and follow up biological evaluation resulted in more than 100 highly active fungal fractions from the 71 fungal strains that were the focus of this study. Bioactivity guided isolation and structure elucidation, combined with our in-house dereplication protocol (**Figure 79**), led to the isolation of a series of newly described antimalarial fungal metabolites.
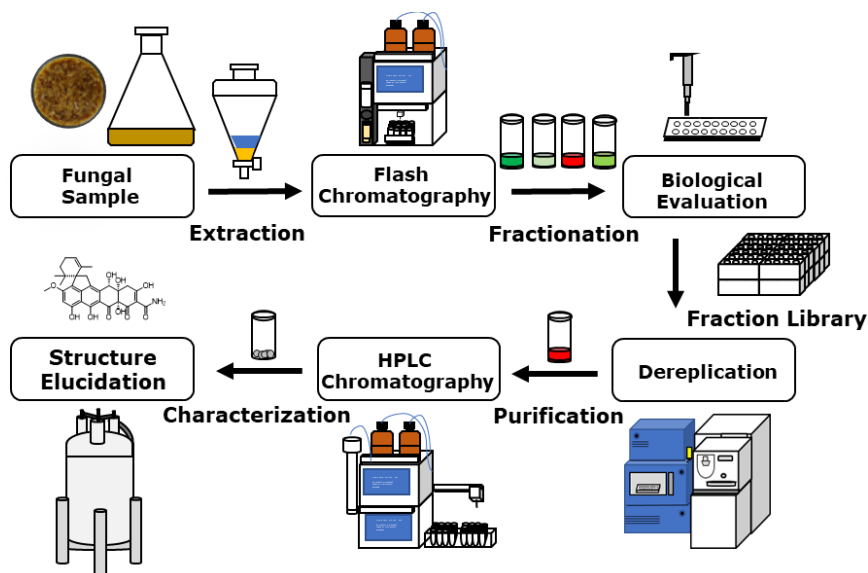
Figure 79. Illustrated workflow of the antimalarial drug discovery project.

Results and Discussion

Preliminary Screening of Active Fractions of 71 MSX (Fungal Strains)

The major antimalarial hits of this study have been selected after confirming their activity multiple times at a concentration of 50 µg/mL. The 71 fungal strains provided by Mycosynthetix Inc., (i.e. MSX) were scaled up and extracted with our extraction protocol.[247] The generated daughter and the original parent fractions (i.e. 184 and 71 respectively) were re-screened at a single-dose concentration of 10 µg/mL against *Plasmodium falciparum* parasite (n=3). The cumulative inhibitions of the fractions were evaluated. (**Figure 90**). Samples that exhibited above 289% cumulative inhibition (n=3) were prioritized first in this study. This resulted in 107 highly active daughter fractions (not counting the original extracts). These fractions originated from 45 of the MSX fungal strains. This hit rate was expected due to the strains being evaluated previously as highly potent and selected for this study.

Dereplication Results of Active Fractions

On the path to the discovery of new active antimalarial molecules, a challenge is the re-isolation of known metabolites. Moreover, metabolites that express higher cytotoxicity but less selectivity toward inhibiting *Plasmodium falciparum* can overshadow molecules with high antimalarial selectivity. To address this problem, we have applied our dereplication protocol by recording HRMS and MS/MS spectra of the extracts and active antimalarial fractions (**Figure 80**).
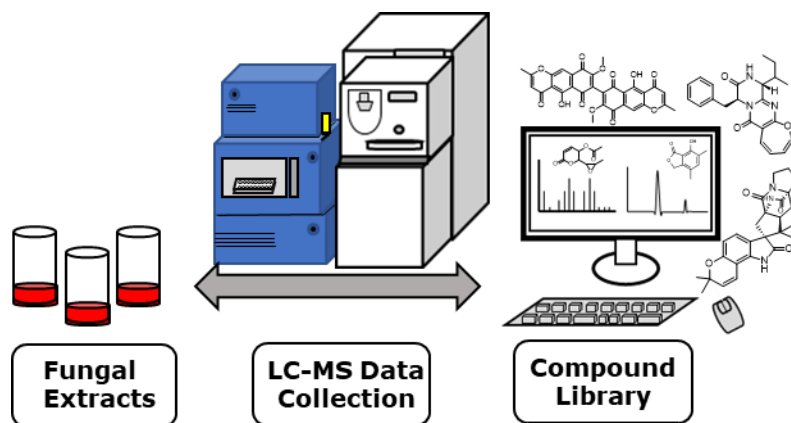
Figure 80. Cartoon of our in-house dereplication protocol.

Our in-house metabolite library contains over 700 secondary metabolites. By comparison of the experimental data (i.e., accurate mass, retention time, UV and MS/MS data), the 107 active fractions were examined for known cytotoxic and/or antimalarial compounds. Fractions were further prioritized based on their dereplication results. If a fraction was found to contain a series of mycotoxins (e.g., analogues of sterigmatocystin or cytochalasins[248-250]), the sample was put into a lower priority group, as it is well know such compounds have general cytotoxicity.[248] On the other hand, if a sample contained unknown peaks of interest that were not in our dereplication database, it was further prioritized. Furthermore, this process allowed us to identify known antimalarial fungal metabolites that were found in the examined fractions, such as apicidin, verrucarin A, roridin E, or pycnidion.[246] These result served to validate our approach. A notable example of our dereplication protocol is shown on **Figure 81**. Structures of the most abundant compounds found through dereplication are displayed on **Figure 82**. In conclusion, our automated dereplication procedure greatly reduced our time and efforts and led us to focus valuable human resources on promising leads.
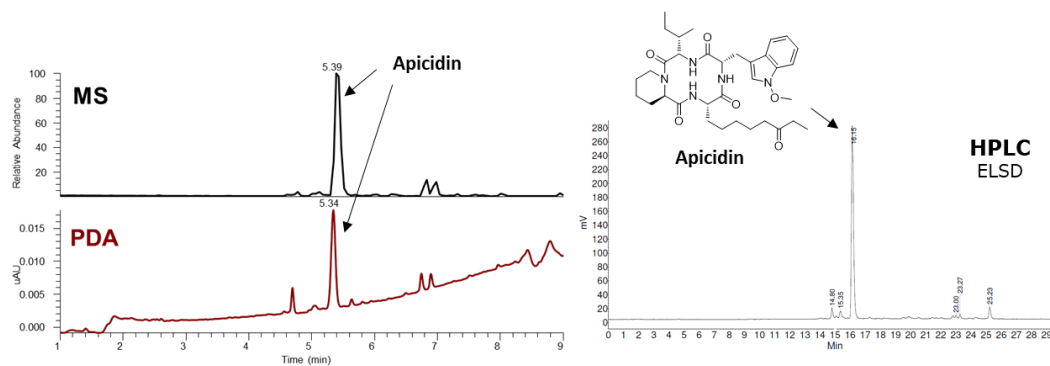
Origin	Accurate Mass [M+H]$^+$	Retention Time (min)	MS/MS Fragments (m/z)									
Extract	624.3735	5.39	596	595	593	592	511	467	464	464	295	294
Standard	624.3737	5.44	596	594	593	592	511	481	467	464	420	294

Figure 81. Example of a dereplication hit. Apicidin is a known antimalarial metabolite isolated from fungi.[251] By comparison of accurate mass, retention time, and MS/MS fragments of the compound observed in the extract vs. the compound in our library, we were able to confidently identify the metabolite. High Performance Liquid Chromatography (HPLC) data of the fraction using as evaporative light scattering detector (ELSD) revealed that the compound was present in high concentrations in the sample. Thus, this fraction resulted in a lower prioritization, as the antimalarial activity could be ascribed to a known compound with reported antimalarial activity.
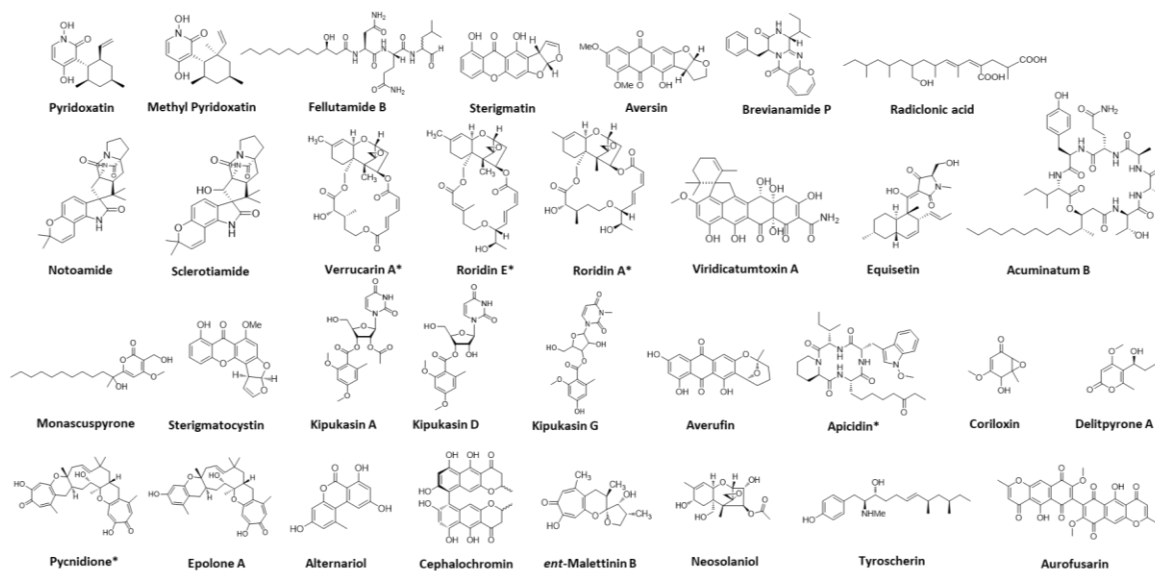
Figure 82. Compounds found in high abundance across the dereplicated active fractions. Compounds marked with an "*" are known in the literature to express antimalarial activities.[246]

138

Antimalarial Capabilities of Viridicatumtoxin A

Investigation of the dereplication results of the high priority active fractions (107) has led to several known secondary metabolites with antimalarial activity (**Figure 82**). Out of the known dereplicated hits, one molecule, viridicatumtoxin A was found to be highly active against *Plasmodium falciparum* (**Figure 83**). The dereplication data of active fractions showed that this compound was biosynthesized by numerous strains with antimalarial activity. Strain MSX29065.2 produced almost solely viridicatumtoxin A in high concentration across its generated daughter fractions (**Figure 83**), and as such the compound was re-isolated from this strain for biological evaluation (**Figure 91**). Viridicatumtoxins belong to a rare class of fungal tetracycline-like molecules that contains a common tetracyclic carboxamide core with a tetracycline intermediate anhydrotetracycline.[252-253] Viridicatumtoxin A was first isolated from *Penicillium viridicatum*, [254] but it has been reported since to be biosynthesized by several species of *Penicillium*.[252] The compound has been previously reported to express nephrotoxicity[254] and modest antitumor activity.[255] Although it was reported as a "mycotoxin" when first isolated, oral dosage of the compound has been shown to be non-toxic to mice (up to 350 mg/kg) and rats (up to 150 mg/kg).[256] Some members of the tetracycline class are known to be active against malaria and has been used prophylactically for the prevention of mefloquine-resistant *Plasmodium falciparum*.[257-259] Due to structural complexity of the molecule, and the prominent history that tetracyclic compounds have in drug discovery[260], it can be considered as a prominent candidate for structural modifications for tunning its selectivity toward *Plasmodium falciparum*.[252]
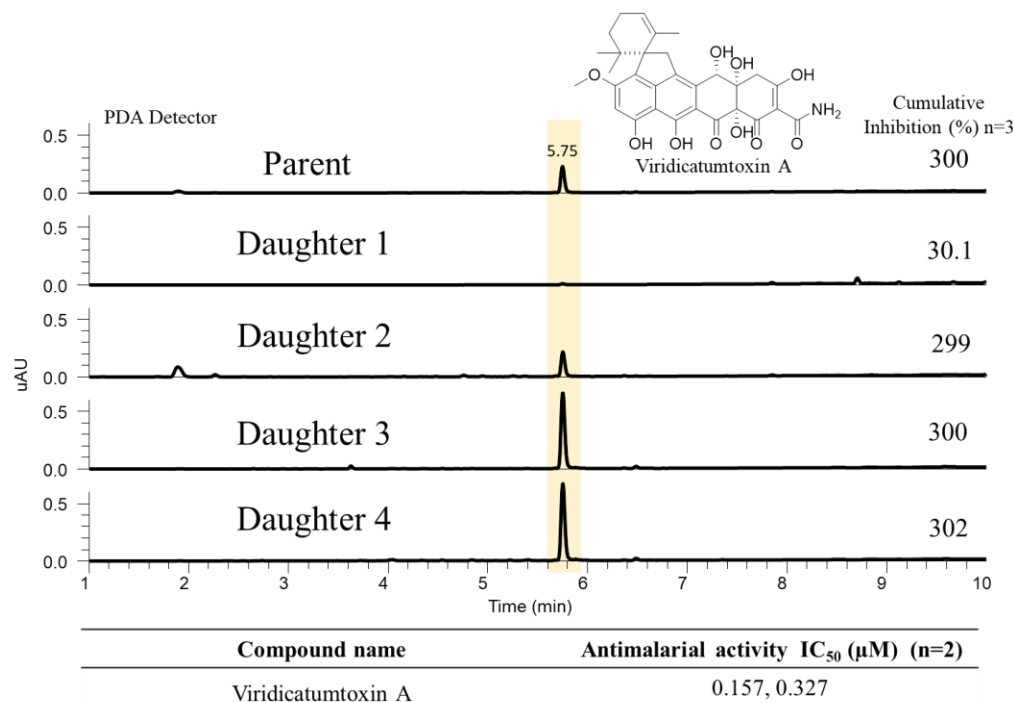
Figure 83. Presence of viridicatumtoxin A in MSX29065.2 across the parent extract and the daughter fractions generated by flash chromatography. The cumulative inhibition of the fractions is shown. Viridicatumtoxin A was further isolated, and its antimalarial activity (i.e., IC$_{50}$ value) was evaluated. Current studies are ongoing to examine the selectivity of the compound.

Leucinostatins and Their Antimalarial Capacities

During our ongoing study of the most potent fractions, we have identified and isolated several leucinostatin analogues from two fungal strains (i.e., MSX23383 and MSX22677). Leucinostatins are antimicrobial peptides, which were isolated from *Purpureocillium lilacinum*.[261] They are among the most potent antiprotozoal agents ever described, yet little is known about their antiprotozoal structure activity relationship.[262] The name "leucinostatin" originates from the presence of multiple leucines in these molecules, which were isolated originally as a mixture of several similar compounds. With the emergence of mass spectrometry techniques, more than 20 leucinostatin analogues have been described in literature,[263-264] yet, to the best of our knowledge, only leucinostatin A was shown to express antimalarial activity[265]

which was described by the Nobel prize winner, Satoshi Omura and his research group. Thus, further evaluating the isolated leucinostatins against *Plasmodium falciparum* seemed worthwhile.

As noted above, two fungal strains, MSX23383 and MSX22677, were found to biosynthesize leucinostatins. Based on the morphology of the strain MSX22677, it can be putatively identified as *Purpureocillium lilacinum*. The molecular identification of the fungus (i.e., DNA barcoding) is currently ungoing.[145] Strain MSX23383 has been identified as a low producer of the compounds, while strain MSX22677 mainly produced leucinostatins. (Figures **84** and **85**).
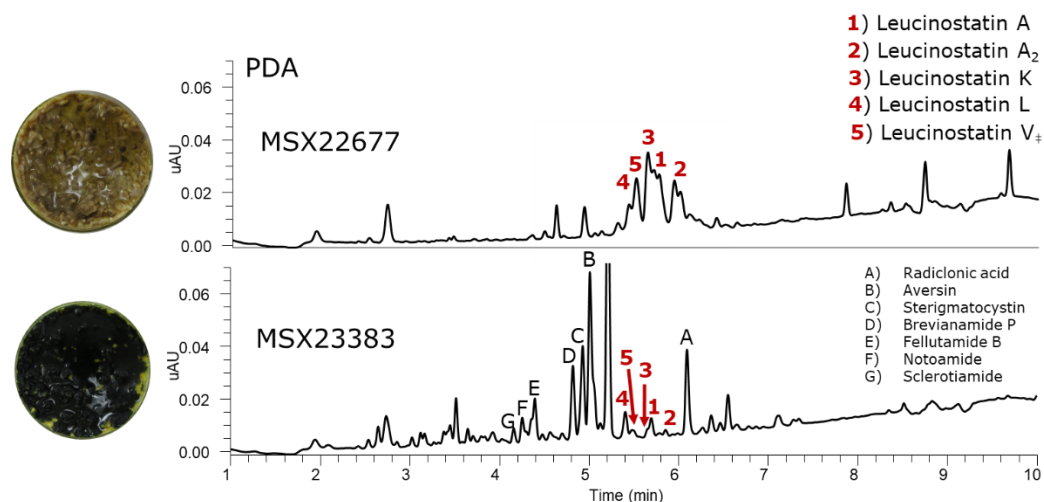
Figure 84. Photodiode-Array (PDA) detector data of the two leucinostatin producer strains MSX22677 and MSX23383. When the relative abundance of the compounds was compared (at 0.2 mg/mL concentration), the latter strain (MSX23383) produced smaller quantities of the leucinostatins (1-5) and more nuisance compounds (A-G). Meanwhile, MSX22677 mainly produced leucinostatins.
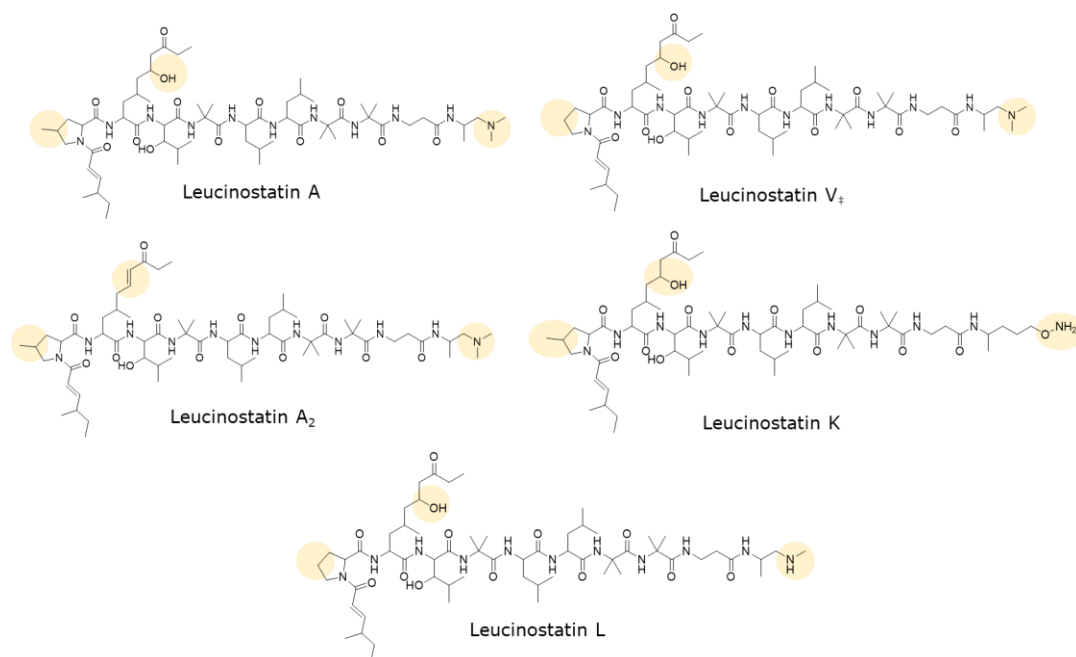
Figure 85. Structures of identified and/or isolated leucinostatins. The structural differences between the molecules are highlighted.

Leucinostatin A, A_2 and $V_{\ddagger}$ were isolated from cultures of strain MSX22677 (**Figure 92**) The identity and purity of the isolated compound were confirmed by MS/MS and HRMS data, elucidating upon the distinct fragmentation patterns of these compounds (**Figures 93** and **94**). As an orthogonal method to confirm the structures of the isolated compounds, Marfey's analysis of leucinostatin A[266] was carried out (**Figure 95**).

The antimalarial activity of leucinostatin A, A_2 and $V_{\ddagger}$ were evaluated against *Plasmodium falciparum*. (**Figure 86**). These compounds found to be more selective toward inhibiting the parasite cells than expressing cytotoxic activity. The Selectivity Index (SI) of the compounds were calculated (**Figure 86**). Leucinostatin A_2 and $V_{\ddagger}$ exhibited greater selectivity toward *Plasmodium* parasites than leucinostatin A. Since there is a lack of information in the literature related to the antiprotozoal activity and mode of actions of leucinostatins,[262] structure-

activity relationship of the leucinostatins relative to their antimalarial activity warrant further study.

Compound Name	Antimalarial activity IC_{50} (nM) n=2	Cytotoxicity (nM)	Selectivity Index
Leucinostatin A	19.1, 12.7	163	10.5
Leucinostatin A$_2$	26.7, 4.26	216	20.3
Leucinostatin V$_‡$	39.0, 12.4	502	22.8

Figure 86. Anti-Plasmodium activity of Leucinostatin A, A$_2$ and V$_‡$. The Selectivity Index (SI) is defined as the ratio of the toxic concentration of a sample against its effective antimalarial concentration. Thus, a higher number SI represents more selective antimalarial activity. (SI= cytotoxicity/ geometric mean of antimalarial activity).

Mapping the Production of Leucinostatin by Strain MSX22677

Since fungal strain MSX22677 produced mainly leucinostatins, we investigated the spatial distribution of the compounds. Using the droplet–liquid microjunction–surface sampling probe (i.e., the droplet probe) to examine the surface the fungal culture grown on potato dextrose agar plates. This technique was described in detail in Chapter Two, where it was used to carry out chemical residue analysis of ancient potteries. To demonstrate the diverse use of the droplet probe, this technique was used to map the relative intensities of selected molecular ion peaks of the leucinostatins across the plate (**Figure 87**). The culture was sampled across the entire plate, and it was observed that the fungus only produced the leucinostatins at the outer ring of the plate (Figures **88** and **96**). This part of the fungus was visually different (i.e., white), meaning this is the youngest, growing part of the fungus. We hypothesize that leucinostatins are produced by strain MSX22677 to defend itself from environmental challenges, thus spatially localized at the outside, growing part of the fungus.
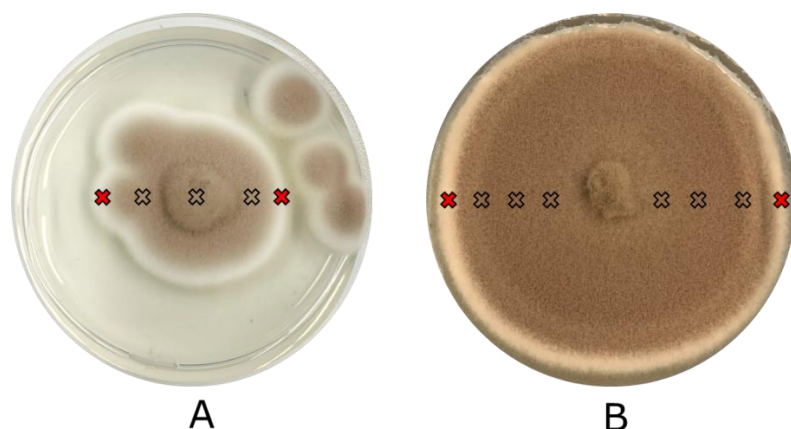
Figure 87. Spatial analysis of strain MSX22677 via droplet probe. A) One week old culture of this strain on potato dextrose agar. B) Three weeks old culture of this strain on potato dextrose agar. X marks indicate the spots where the culture was sampled by the droplet probe. Red X marks indicate the locations where biosynthesis of leucinostatins was observed.
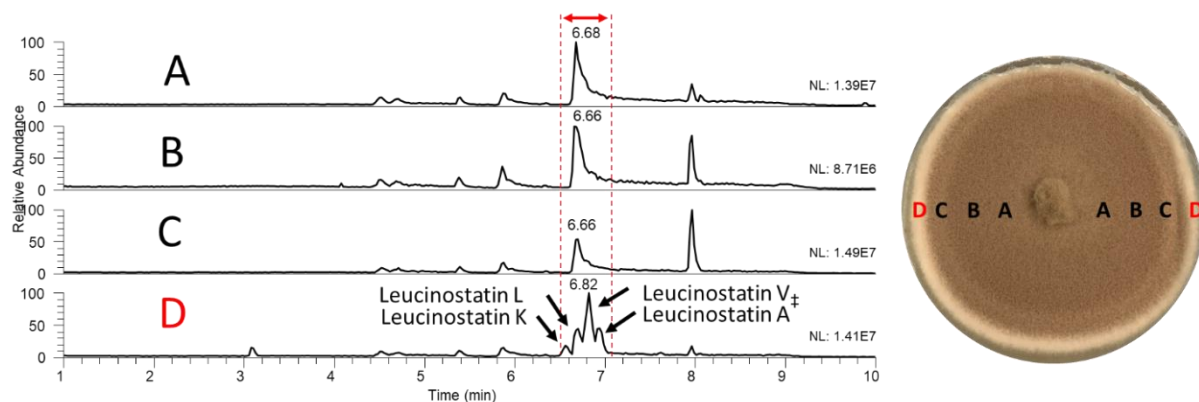
Figure 88. Base peak chromatogram of the droplet probe data of strain MSX22677. The fungus was sampled at A, B, C, D locations, and leucinostatins were observed only at location D.

Precursor-Directed Biosynthesis of Leucinostatins.

More than 30% of the drugs available on the market contain at least one fluorine atom in their structure.[267] Given the potential benefits of fluorine atoms in drug development such as high electronegativity, small atomic radius, and low polarizability of the C–F bond [268-269] -that can alter physicochemical profiles by modulating acid/base properties or lipophilicity of the compound- we have pursued the precursor-directed biosynthesis of leucinostatins with a goal of

144

incorporating fluorinated proline into the amino acid sequence. Strain MSX22677 was grown on potato dextrose agar with $_L$-*F*-proline [purchased as (2*S*,4*S*)-4-fluoropyrrolidine-2-carboxylic acid hydrochloride] (Advanced ChemBlocks Inc.) added to the media in three different concentrations, 100, 250 and 500 ppm respectively, similar to our previously described methodologies.[270-271] Then the cultures were analyzed *in situ* via a droplet probe coupled to a UPLC-PDA-HRESIMS-MS/MS system. As a results, we were able to detect trace amounts (only a few scans with low abundance) of the accurate mass of fluorinated leucinostatin L on the plate where 500 ppm $_L$-*F*-proline was added. After the analysis, the plates were chopped, extracted with acetone, dried under N_2 gas, and re-analyzed via LC-MS to confirm the presence of fluorinated leucinostatins. The results were more conclusive once the plate was extracted and re-analyzed through traditional LC-MS method (**Figure 89**). A peak for the fluorinated leucinostatin L appeared and was detected when 500 ppm concertation of $_L$-*F*-Proline was used (**Figure 89**). Apart from producing the non-fluorinated versions of the leucinostatin analogues the fungus has biosynthesized fluorinated leucinostatin L when $_L$-*F*-proline was induced in the media.
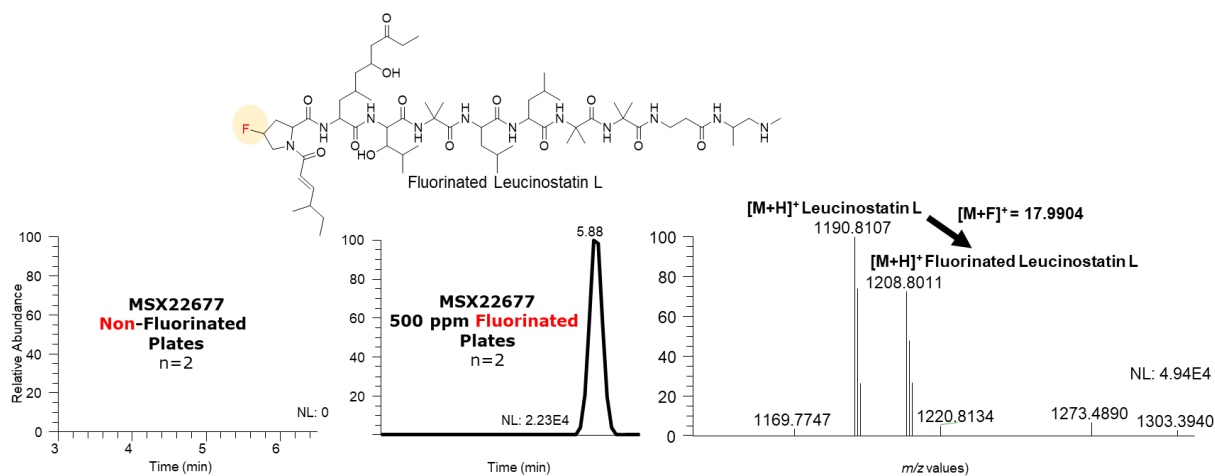
Figure 89. Detection of fluorinated leucinostatin L by LC-MS. The XIC search of the compound shown of the left two base peak chromatograms meanwhile the ion spectrum of the detected peaks is shown on the right. Leucinostatin was detected only on the plate where 500 ppm L-*F*-Proline was added.

Future Directions

During ongoing studies to discover novel antimalarial compounds from the 71 chosen fungal strains, a series of compounds were isolated and found to express antimalarial activity (**Figure 97**). As a future goal, we will be investigating further highly active strains and focus on the isolation of known and novel compounds with newly described antimalarial activities. Since the highest activities were shown, so far, by leucinostatin analogues, one of our primary future aims will be the isolation of more leucinostatins. The LC-MS analysis of extracts of strain MSX22677 revealed a series of leucinostatin analogues, and thus, a scale up of the fungal strain is a prominent goal for future bioactivity studies. Besides the isolation of leucinostatin analogues, we also aim to scale up the precursor directed biosynthesis of fluorinated leucinostatin L to produce material for structure elucidation and biological evaluation. Further studies are ongoing to investigate the underlaying structure activity relationships of

146

viridicatumtoxin A- and leucinostatins, and their selectivity toward killing the *Plasmodium* parasite.

Conclusion

In conclusion, 40,000 fungal strains were evaluated to find the most potent antimalarial producers. Our search toward antimalarial compounds has led us to 71 MSX strains that expressed repeatable dose dependent activity against *Plasmodium falciparum*. The best hits completely killed the parasite, as opposed to only inhibiting its growth. From the 71 examined MSX strains, we have narrowed our focus down to 45 fungal strains that produced 106 fractions with the highest inhibition of the parasite. Our dereplication methodology resulted in the identification of five known antimalarial compounds, (i.e., apicidin, verrucarin A, roridin E and pycnidion). We have also isolated a dozen compounds with antimalarial activities, among which viridicatumtoxin A and class of compounds termed leucinostatins possessed the highest inhibition activity. Leucinostatin producer strains MSX23383 and MSX22677 were evaluated for biosynthesis of these compounds. To monitor the biosynthesis of leucinostatins *in situ* we used the droplet-liquid microjunction-surface sampling probe (i.e., droplet probe). As a results leucinostatins were shown to be produced at the outer ring (the youngest part) of the fungus. We have attempted the incorporation of fluorinated proline into the peptide chain by feeding strain MSX22677 with L-*F*-proline and the results showed the presence of fluorinated leucinostatin L. Further studies are ongoing to examine the structure activity relationship behind the antiplasmodials effects of leucinostatins and viridicatumtoxin A.

Experimental

General Experimental Procedures

Flash chromatography was performed on a Teledyne ISCO CombiFlash Rf 200 using Silica Gold columns (from Teledyne ISCO) and monitored by both UV and evaporative light-scattering detectors. Phenomenex Gemini-NX C18 analytical (5 μm; 250 × 4.6 mm), and preparative (5 μm; 250 × 21.2 mm), columns (Phenomenex) were used on a Varian Prostar HPLC system equipped with ProStar 210 pumps and a Prostar 335 photodiode array detector (PDA), with data collected and analyzed using Galaxie Chromatography Workstation software (version 1.9.3.2, Varian Inc.). A Waters Acquity UPLC system (Waters Corp.) utilizing a Phenomenex Kinetex C18 column (1.3 μm; 50 × 2.1 mm) was used to evaluate the purity of the isolated compounds with data collected and analyzed using the Thermo Fisher Scientific Xcalibur data acquisition software (Thermo Fisher Scientific). HRMS analysis utilized either a Thermo Fisher Scientific LTQ Orbitrap XL mass spectrometer or a Thermo Fisher Scientific Q Exactive Plus mass spectrometer, both equipped with an electrospray ionization source (Thermo Fisher Scientific).

Fermentation, Extraction, and Isolation

The 71 solid fermentation cultures were stored on a malt extract slant and were transferred periodically. A fresh culture was grown on a similar slant, and a piece was transferred to a medium containing 2% soy peptone, 2% dextrose, and 1% yeast extract (YESD media). Following incubation (7 d) at 22 °C with agitation, the culture was used to inoculate 50 mL of a rice medium, prepared using rice to which was added a vitamin solution and twice the volume of rice with H_2O in a 250 mL Erlenmeyer flask. This was incubated at 22 °C until the culture showed good growth (approximately 14 d) (250 mL Erlenmeyer flask containing 10 g of rice and

50 mL of H_2O, which was inoculated using seed cultures grown in the YESD media and incubated at 22 °C for 14 days). To each of the solid fermentation cultures grown in 250 mL Erlenmeyer flask (2 flask per strain) 60 ml of 1:1 MeOH-CHCl$_3$ was added, and the culture was chopped into small pieces using a spatula. The cultures were then shaken overnight (~16 h) at ~125 rpm at rt. The resulting slurries were filtered in vacuo and then pooled to form the two combined filtrate, and the solid residue was rinsed with a small volume of 1:1 MeOH-CHCl$_3$. To the combined filtrate, 270 mL of CHCl$_3$ and 450 mL of H_2O were added; the solution was stirred for 20 min and transferred to a separatory funnel. The organic layer was collected and evaporated to dryness under vacuum using a rotary evaporator. The resulting organic extract was then partitioned between 100 mL of 1:1 MeOH-CH$_3$CN and 100 mL of hexanes. The MeOH-CH$_3$CN layer was collected and evaporated to dryness under vacuum. The defatted organic extracts (approx. 150 mg/ strain) was reconstituted in CHCl$_3$ and absorbed onto celite 545. The extracts were then fractionated by flash chromatography using a solvent gradient of hexane-CHCl$_3$-MeOH at a 18 mL/min flow rate and 85.0 column volumes to yield four fractions per strain. MSX 29065.2 fraction 3 (74.6 mg) was purified by HPLC with a solvent gradient increasing linearly from 45:55 to 100:00 CH$_3$CN-H$_2$O (acidified with 0.1% formic acid) over 20 min at a flow rate of 21.20 mL/min to result pure viridicatumtoxin A (17.19 mg). Leucinostatins were purified from MSX22677 flash chromatography fraction 4 (256.6 mg) through HPLC with a solvent gradient increasing linearly from 35:65 to 45:55 CH$_3$CN-H$_2$O (acidified with 0.1% formic acid) over 20 min at a flow rate of 21.20 mL/min to result leucinostatin V$_\ddagger$ (fraction 1, 6.59 mg), leucinostatin A$_2$ (fraction 2, 16.17 mg) and leucinostatin A (fraction 3 22.67 mg).

Dereplication

The extracts were compared to a fungal library containing more than 700 fungal metabolites. All extracts and standards were analyzed on the same instrument, column and method described below. The raw data files were filtered through MZmine 2.2 Dereplication via an in-house developed python script (Python, JupyterLab). The accurate mass (in 5 ppm range), retention time (in 0.25-minute window), UV and fragmentation patterns of the metabolites were matched to the compounds in the database. HRESIMS was performed on a Thermo LTQ Orbitrap XL mass spectrometer (ThermoFisher, San Jose, CA, USA) equipped with an electrospray ionization source. Source conditions in the positive ionization mode were set at 275 °C for the capillary temperature, 4.5 kV for the source voltage, 20 V for capillary voltage, and 95 V for the tube lens. Nitrogen was utilized for the sheath gas and set to 25 and 20 arb for the positive mode. Scan events were carried out, full-scan (100–2000) and ion-trap MS/MS of the most intense ion from the parent mass list utilizing CID with a normalized collision energy of 30. Thermo Scientific Xcalibur 2.1 software was used for instrument control and data analysis. UPLC was carried out on a Waters Acquity system [using a BEH C18 (2.1 × 50 mm, 1.7 μm) column (Waters Corp., Milford, MA, USA) equilibrated at 40 °C]. A mobile phase consisting of CH_3CN–H_2O (acidified with 0.1% formic acid) was used, starting with 15:85 then increasing linearly to 100% CH_3CN within 8 min, holding for 1.5 min, and then returning to the starting conditions within 0.5 min. An Acquity UPLC photodiode array detector was used to acquire PDA data, which were collected from 200 to 500 nm with 4 nm resolution. Samples were dissolved in methanol (Optima) and made to a 0.25 mg/mL concentration for the analysis.

The Droplet Probe

The experimental procedure of the droplet probe was described above in Chapter two, experimental section.

Antimalarial and Cytotoxicity Assays

Plasmodium Falciparum Cultivation

P. falciparum strain W2[272] was continuously cultured in RPMI media (Gibco) supplemented with 10% inactivated human plasma (Interstate Blood Bank) and 5% hematocrit (Interstate Blood Bank) based on methods previously described.[273] Forty-eight hours before assay initiation, parasites were synchronized using filter-sterilized 5% D-sorbitol (Millipore-Sigma) in water such that assays were started with >90% rings as previously described in detail.[274]

Extract and Fractions Antimalarial Screening

The initial single-concentration screen of separated fungal extracts was performed by plating 5 μL of 360 extracts at 10 mg/mL (1000× final concentration) into a 384-well plate (Greiner Bio-one). For normalization, 5 μL dehydrated, sterile DMSO (Tocris) was plated into 8 negative control wells and 5 μL 1 mM atovaquone (Sigma-Aldrich) was plated in 16 positive controls wells. Plates were sealed using foil sealing tape (VWR) and kept in a desiccator until used to inoculate *P. falciparum* assay plates. Assay plates were prepared by plating 20 μL of culture media to prewet all wells in a separate 384-well plate (Greiner Bio-one), followed by addition of a compound using a 40-nL pin tool (V&P Scientific) as previously described.[275] Plates were then inoculated with 20 μL of *P. falciparum* culture at 2% parasitemia and 0.75% hematocrit, leading to dilution of all test compounds to 1× and DMSO to 0.1% in complete media. Assay plates were maintained in bioassay dishes with water cups to prevent the edge

effect due to evaporation for 72 h as previously described.[276] The single-concentration screen was performed in three independent experiments.

Pure Compounds Antimalarial Assay

For pure compounds, a small aliquot of the dried material was diluted to 10 mM in dehydrated, sterile DMSO (Tocris) and a duplicate-well, 12-point, 3-fold semilog dilution series was prepared at 1000× final concentration in 384-well plates (Greiner Bio-one) in DMSO using a Biomek 4000 (Beckman Coulter). DMSO was plated as the negative control and dihydroartemisin was diluted from 1 μM as the positive control. Plates were sealed using foil sealing tape (VWR) and kept in a desiccator until used to inoculate *P. falciparum* assay plates. Dose-response assays were initiated as described below.

Antimalarial Imaging and Data Analysis

After 72 h of incubation, assay plates (either single-concentration or dose-response) were simultaneously fixed and stained by adding to each well 40 μL of Hoechst 33342 (Thermo Fisher Scientific) and 0.1% glutaraldehyde (Electron Microscopy Resources), similar to that previously described.[277] Plates were maintained for 24 h in 4 °C and imaged the following day using the Lionheart FX high content imager (Biotek). Using a 4× objective, a single field of view was captured for each well using the DAPI filter and a background flattening algorithm to reduce Hoechst 33342 autofluorescence to identify Hoeschst 33342-stained parasite DNA. The net DNA-area data was then exported to CDD Vault (Collaborative Drug Discovery), and inhibition values were normalized using the DMSO negative control and either atovaquone (for singe-concentration) or dihydroartemsinin (for dose-response) positive control wells whereby

$$\% \text{ Inhibition} = 100 \ x \ \frac{(Raw\ Data - Average\ Negative\ Control)}{(Average\ Positive\ Control - Average\ Negative\ Control)}$$

For single-concentration assays, a Z' factor was determined for the controls and found between 0.19-.85 for the three replicate plates.[278] For dose-response assays, compound potency was determined by constructing a dose-response curve fit using the Levenberg-Marquardt algorithm[279-280] to calculate pEC_{50}'s. Outliers, if any, were identified by comparing inhibition values across replicate wells and were manually removed using CDD Vault's user interface. Each grouping of compounds was tested in 2 independent experiments, and the presented data is the average and standard deviation from all independent experiments.

Cytotoxicity measurements

The HepG2 human hepatocyte line from hepatocellular carcinoma (ATCC HC-8065) was cultured in rat collagen I-coated (5 μg/cm^2) flasks (Corning) at 20−90% confluence in EMEM (Lonza) supplemented with 1 mM sodium pyruvate (Lonza), 2 mM L-glutamine (Gibco), and 10% fetal bovine serum (Hyclone) in a cell culture incubator at 37 °C and 5% CO_2. Cells were passed by treating with Trypsin LE (Gibco) for 7 min at 37 °C. Toxicity assays were started by harvested cells from a flask, counting viability by trypan blue, and seeding 2000 live cells in 40 μL per well into rat-tail collagen I- coated 384-well plates (Greiner Bio-one) using a Biomek NX (Beckman Coulture). Compounds were then added using the 40 nL pin tool as above, using the same source plate used for the *P. falciparum* assay as above. After 72 h, media was removed, and cells were fixed with 4% paraformaldehyde (Thermo Fisher Scientific) in PBS and then stained with 10 μg/mL Hoechst 33342 for 1 h. The entire culture area of each well of assay plates was imaged with a Lionheart FX with a 4× objective, and net hepatic nuclei per well were quantified. Data were loaded into CDD Vault for normalization, curve fitting, and pCC50 calculation as described above but using puromycin as the positive control.

Supplementary Data

ID	Pr	Dau 1	Dau 2	Dau 3	Dau 4	ID	Pr	Dau 1	Dau 2	Dau 3	Dau 4
118-1	144	56.2	50.2	105	31.2	118-9	256	235	145	229	262
118-2	300	262	-10.3	222	301	118-10	260	55.5	269	268	236
118-3	181	252	222	251	241	118-11	258	-31.2	217	228	232
118-4	301	244	99.4	300	266	118-12	243	99.7	249	246	250
118-5	63.6	118	257	234	82.7	118-13	203	46.8	16.3	172	128
118-6	243	105	206	272	251	118-14	241	50.2	20.1	267	243
118-7	279	76	-9.2	258	207	118-15	168	47.8	15.2	252	93.4
118-8	301	254	158	195	302	118-16	220	65.1	-1.92	190	149

ID	Pr	Dau 1	Dau 2	Dau 3	Dau 4	ID	Pr	Dau 1	Dau 2	Dau 3	Dau 4
118-33	301	301	302	269	264	118-41	182	124	223	203	138
118-34	267	246	233	265	300	118-42	300	302	301	299	302
118-35	300	300	300	301	301	118-43	301	300	299	302	196
118-36	274	262	302	284	302	118-44	302	303	302	302	302
118-37	282	231	278	274	277	118-45	301	302	301	302	284
118-38	300	30.1	299	300	302	118-46	43.7	20.1	301	246	222
118-39	243	142	144	256	159	118-47	58.7	3.27	296	242	250
118-40	265	267	300	256	227	118-48	245	225	245	229	245

ID	Pr	Dau 1	Dau 2	Dau 3	Dau 4	ID	Pr	Dau 1	Dau 2	Dau 3	Dau 4
118-17	193	52.1	-9.34	258	192	118-25	303	230	244	255	299
118-18	253	92.2	0.412	275	225	118-26	299	260	301	279	284
118-19	302	164	17.5	302	301	118-27	301	301	302	252	240
118-20	280	289	261	225	216	118-28	302	301	301	257	250
118-21	96.8	252	289	228	299	118-29	302	301	302	300	298
118-22	247	277	261	286	260	118-30	302	114	299	106	268
118-23	300	260	272	294	294	118-31	302	302	302	302	273
118-24	295	288	267	295	270	118-32	302	299	301	299	301

ID	Pr	Dau 1	Dau 2	Dau 3	Dau 4	ID	Pr	Dau 1	Dau 2	Dau 3	Dau 4
118-49	55.4	297	301	263	201	118-57	301	301	300	301	300
118-50	253	256	302	257	260	118-58	294	71.7	291	292	297
118-51	208	298	301	295	296	118-59	297	77.7	284	285	289
118-52	88.4	129	150	209	132	118-60	298	299	294	302	299
118-53	302	280	297	302	302	118-61	299	230	300	302	300
118-54	303	297	302	302	301	118-62	300	302	301	302	301
118-55	256	247	301	299	300	118-63	301	301	300	302	301
118-56	300	296	301	276	273	118-64	295	301	274	299	296

ID	Pr	Dau 1	Dau 2	Dau 3	Dau 4
118-65	226	234	294	235	287
118-66	190	-0.74	243	248	252
118-67	221	11.8	236	242	241
118-68	26.4	-10.4	261	237	223
118-69	9.91	3.68	228	168	-7.36
118-70	301	302	-24.3	301	48.8
118-71	302	297	302	301	302

Figure 90. Cumulative antimalarial inhibition of the fractions extracted from 71 MSX. The dark red colors represent the highest activity. The higher the activity the higher the number is (n=3), where 300% indicates 100% inhibition thrice.

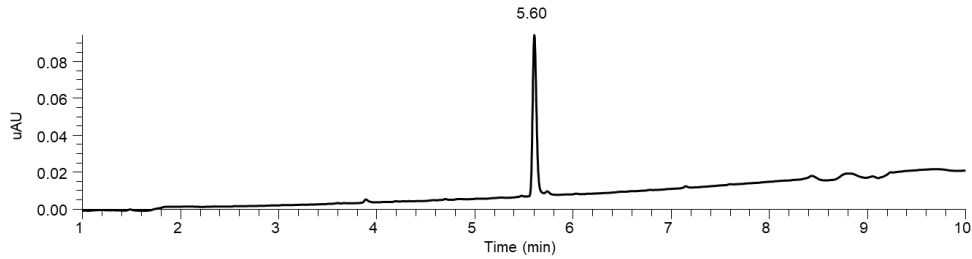**Figure 91**. Photodiode-Array (PDA) detector data of viridicatumtoxin A
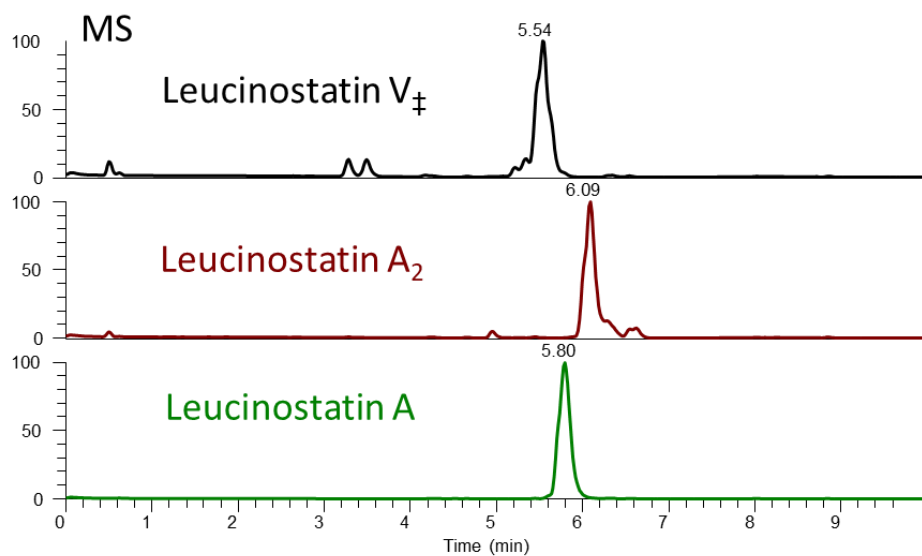
Figure 92. HRMS data (base peak chromatogram) of the isolated leucinostatins.
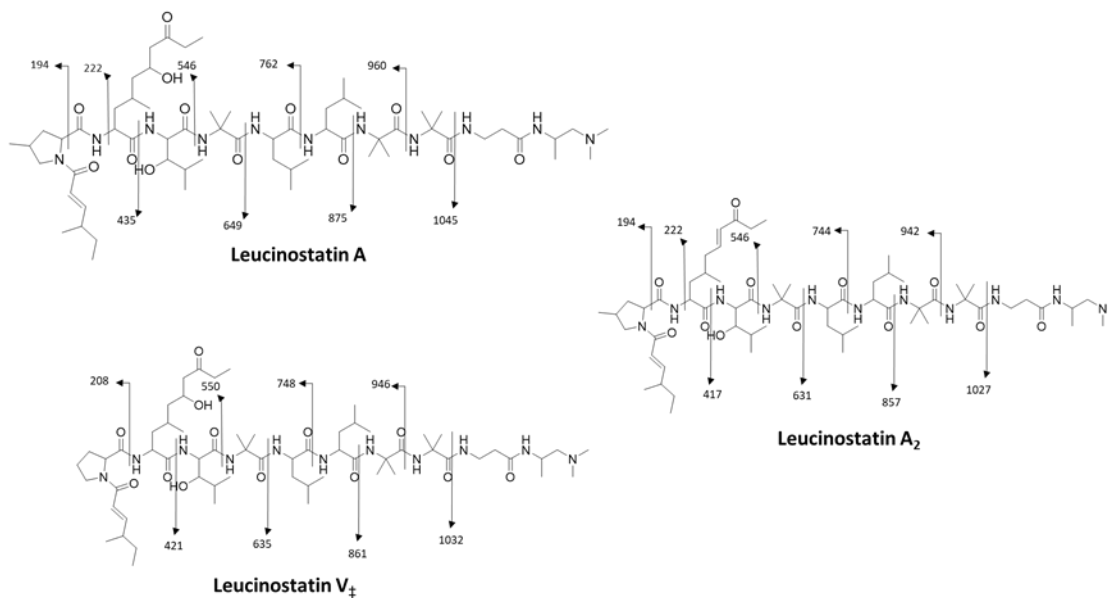
Figure 93. Key MS/MS fragmentation differences (*m/z* values) between leucinostatins. [263-264, 281]
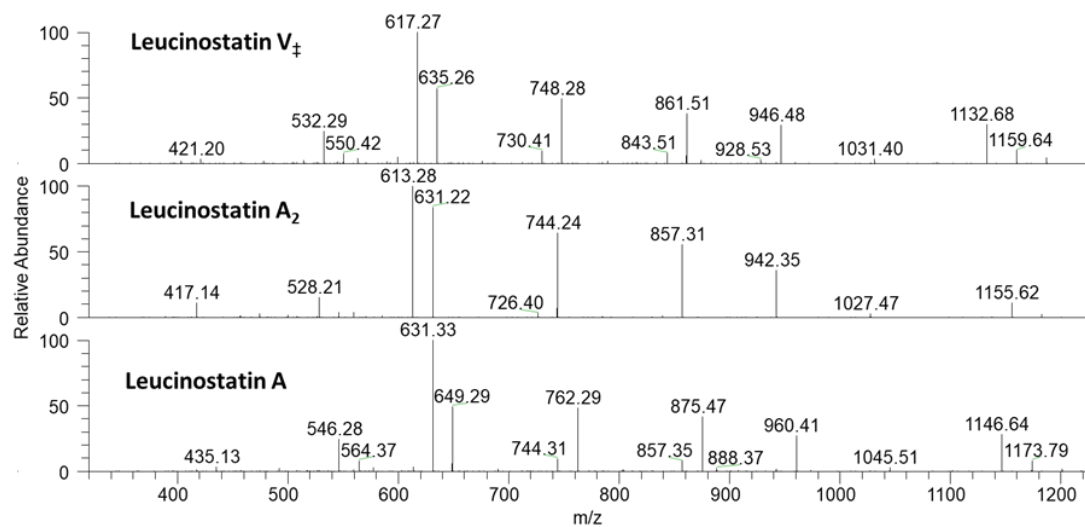
Figure 94. MS/MS fragmentation data of the isolated leucinostatins.
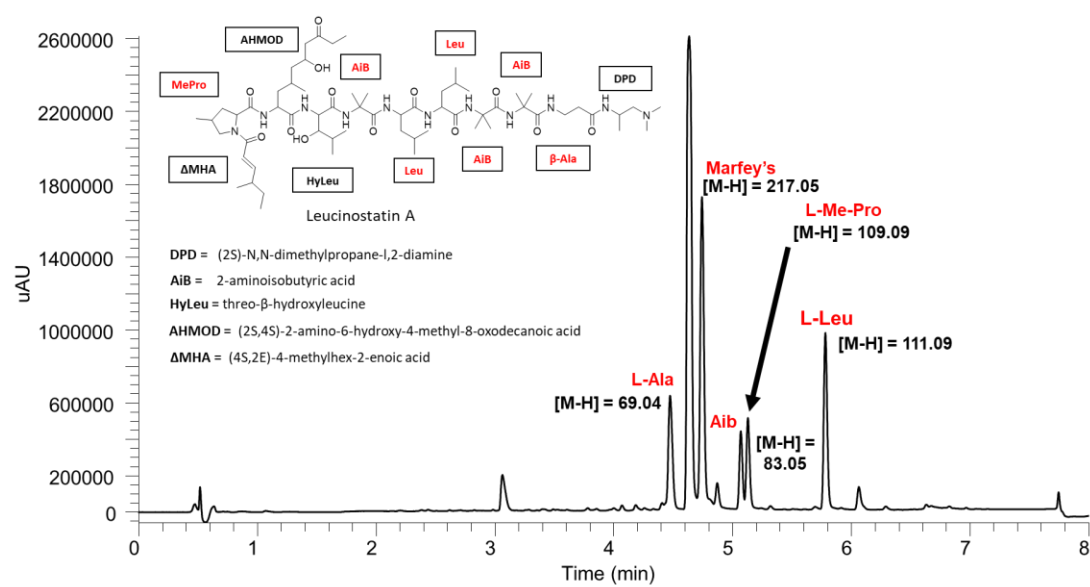
Figure 95. Marfey's analysis of leucinostatin A.

156
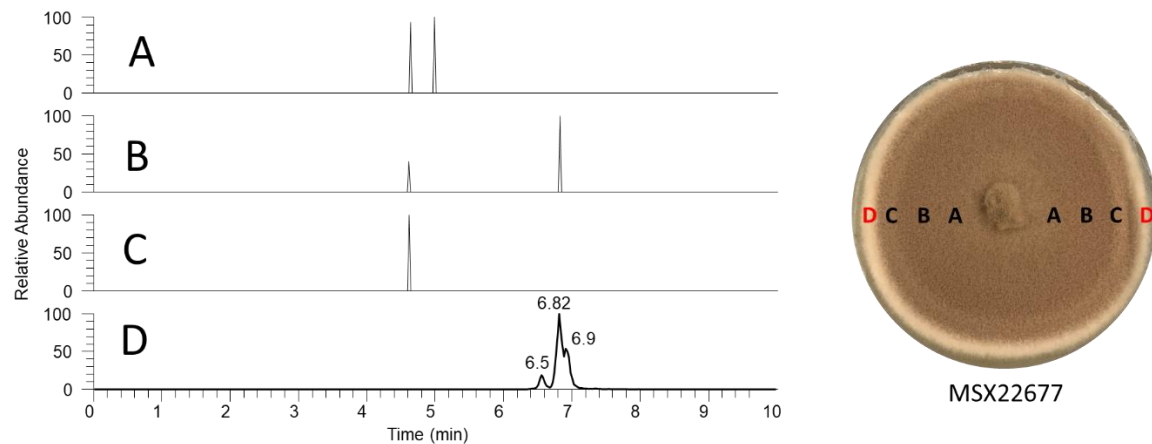
Figure 96. Extracted Ion Chromatogram (XIC) of Leucionsatin L, K, A and V$_{\ddagger}$. across the fungal plate. The sharp peaks at A,B,C represents unrelated single ion scans, while the peaks in D between 6-7 minutes retention time show the presence of leucinostatins.
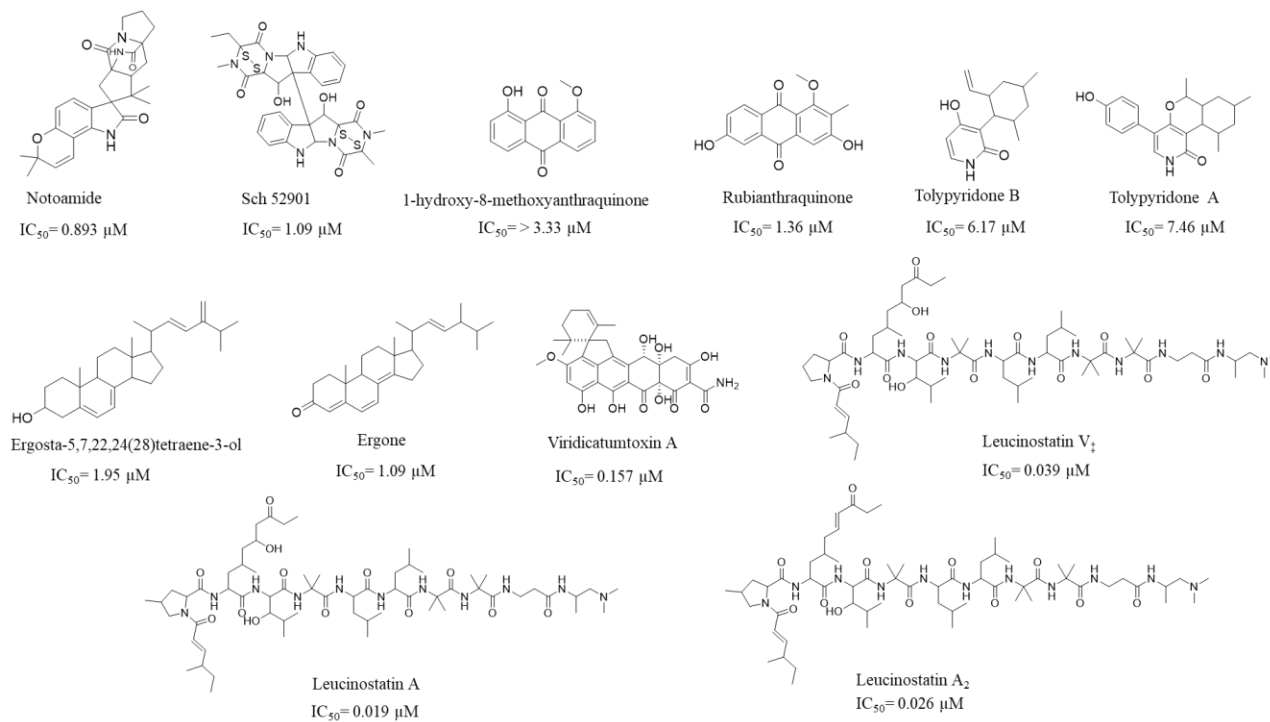
Figure 97. Structures of isolated compounds with antimalarial activity.

REFERENCES

1. Strobel, G.; Daisy, B.; Castillo, U., et al., *J. Nat. Prod.* **2004,** *67* (2), 257-68.

2. Chin, Y.-W.; Balunas, M. J.; Chai, H. B., et al., *AAPS J.* **2006,** *8* (2), E239-E253.

3. Atanasov, A. G.; Zotchev, S. B.; Dirsch, V. M., et al., *Nat. Rev. Drug Discov.* **2021,** *20* (3), 200-216.

4. Newman, D. J.; Cragg, G. M., *J. Nat. Prod.* **2020,** *83* (3), 770-803.

5. Harvey, A., *Drug Discov. Today* **2000,** *5* (7), 294-300.

6. Trampuz, A.; Jereb, M.; Muzlovic, I., et al., *Crit. Care* **2003,** *7* (4), 315-23.

7. Bousema, T.; Drakeley, C., *Clin. Microbiol. Rev.* **2011,** *24* (2), 377-410.

8. World Health, O., *World Malaria Report 2021*. World Health Organization: Geneva, 2021.

9. World Health, O., *World Malaria Report 2019*. World Health Organization: Geneva, 2019.

10. Wells, T. N. C.; van Huijsduijnen, R. H.; Van Voorhis, W. C., *Nat. Rev. Drug Discov.* **2015,** *14* (6), 424-442.

11. Ashley, E. A.; Dhorda, M.; Fairhurst, R. M., et al., *N. Engl. J. Med.* **2014,** *371* (5), 411-423.

12. Wu, X.; Zhang, C.; Goldberg, P., et al., *Science* **2012,** *336* (6089), 1696-700.

13. Shepard, A. O., *Ceramics for the archaeologist*. Carnegie Institution of Washington: Washington DC, 1954; Vol. Publication 609.

14. Bronitsky, G., 4 - The Use of Materials Science Techniques in the Study of Pottery Construction and Use. In *Advances in Archaeological Method and Theory*, Schiffer, M. B., Ed. Academic Press: San Diego, 1986; pp 209-276.

15. Rice, P. M., *Pottery analysis : a source book*. first ed ed.; University of Chicago Press: Chicago, 1987.

16. Evershed, R. P., *Archaeometry* **2008,** *50* (6), 895-924.

17. Shillito, L. M.; Almond, M. J.; Wicks, K., et al., *Spectrochim. Acta A. Mol. Biomol. Spectrosc.* **2009,** *72* (1), 120-125.

18. Beck, C.; Wilbur, E.; Meret, S., et al., *Archaeometry* **1965,** *8* (1), 96-109.

19. Lambert, J. B.; Frye, J. S.; Poinar Jr, G. O., *Archaeometry* **1985,** *27* (1), 43-51.

20. Oudemans, T. F. M.; Boon, J. J.; Botto, R. E., *Archaeometry* **2007,** *49* (3), 571-294.

21. Shoval, S., Fourier transform infrared spectroscopy (FT-IR) in archaeological ceramic analysis. In *The Oxford handbook of archaeological ceramic analysis*, Hunt, A., Ed. Oxford University Press: Oxford, 2016; pp pp. 508-530.

22. Maniatis, Y.; Tsirtsoni, Z., *Archaeometry* **2002,** *44* (2), 229-239.

23. Spoto, G., *Thermochim. Acta* **2000,** *365* (1), 157-166.

24. Vickerman, J. C., *Surf. Interface Anal.* **1987,** *10* (8), 435-435.

25. Felicissimo, M. P.; Peixoto, J. L.; Bittencourt, C., et al., *J. Archaeol. Sci.* **2010,** *37* (9), 2179-2187.

26. Ruan, F.; Zhang, T.; Li, H., *Appl. Spectrosc. Rev.* **2019,** *54* (7), 573-601.

27. Speakman, R. J.; Neff, H., *Am. Antiq.* **2002,** *67* (1), 137-144.

28. Heaton, K.; Solazzo, C.; Collins, M. J., et al., *J. Archaeol. Sci.* **2009,** *36* (10), 2145-2154.

29. Bonaduce, I.; Ribechini, E.; Modugno, F., et al., *Topics. Curr. Chem.* **2016,** *374* (1), 6.

30. Evershed, R. P.; Jerman, K.; Eglinton, G., *Nature* **1985,** *314* (6011), 528-530.

31. Olsson, M.; Isaksson, S., *J. Archaeol. Sci.* **2008,** *35* (3), 773-780.

32. Reber, E. A.; Kerr, M. T., *J. Archaeol. Sci.* **2012,** *39* (7), 2312-2319.

33. Zagorevski, D. V.; Loughmiller-Newman, J. A., *Rapid Commun. Mass Spectrom.* **2012,** *26* (4), 403-411.

34. Kałużna-Czaplińska, J.; Rosiak, A.; Kwapińska, M., et al., *Crit. Rev. Anal. Chem.* **2016,** *46* (1), 67-81.

35. Gross, J. H., *Anal. Bioanal. Chem.* **2014,** *406* (1), 63-80.

36. Calvano, C. D.; van der Werf, I. D.; Palmisano, F., et al., *Anal. Bioanal. Chem.* **2016,** *408* (25), 6957-6981.

37. Cleland, T. P.; Newsome, G. A.; Hollinger, R. E., *Analyst* **2019,** *144* (24), 7437-7446.

38. Armitage, R. A.; Arrazcaeta, R.; Torres, S., et al., *Archaeometry* **2020**.

39. Manfredi, M.; Robotti, E.; Bearman, G., et al., *J. Anal. Methods. Chem.* **2016,** *2016*, 6853591.

40. Adams, J., *Int. J. Mass Spectrom.* **2011,** *301* (1), 109-126.

41. Selvius DeRoo, C.; Armitage, R. A., *Anal. Chem.* **2011,** *83* (18), 6924-6928.

42. Geiger, J.; Armitage, R. A.; DeRoo, C. S., Identification of Organic Dyes by Direct Analysis in Real Time-Time of Flight Mass Spectrometry. In *Collaborative Endeavors in the Chemical Analysis of Art and Cultural Heritage Materials*, American Chemical Society: 2012; Vol. 1103, pp 123-129.

43. Day, C. J.; DeRoo, C. S.; Armitage, R. A., Developing Direct Analysis in Real Time Time-of-Flight Mass Spectrometric Methods for Identification of Organic Dyes in Historic Wool Textiles. In *Archaeological Chemistry VIII*, American Chemical Society: 2013; Vol. 1147, pp 69-85.

44. Armitage, R. A.; Jakes, K.; Day, C., *Sci. Technol. Archaeol. Res.* **2015,** *1* (2), 60-69.

45. Fraser, D.; DeRoo, C. S.; Cody, R. B., et al., *Analyst* **2013,** *138* (16), 4470-4474.

46. Regert, M., *Mass Spectrom. Rev.* **2011,** *30* (2), 177-220.

47. Saliu, F.; Modugno, F.; Orlandi, M., et al., *Anal. Bioanal. Chem.* **2011,** *401* (6), 1785-1800.

48. Zhang, X.; Boytner, R.; Cabrera, J. L., et al., *Anal. Chem.* **2007,** *79* (4), 1575-1582.

49. Mantzouris, D.; Karapanagiotis, I.; Valianou, L., et al., *Anal. Bioanal. Chem.* **2011,** *399* (9), 3065-3079.

50. Szostek, B.; Orska-Gawrys, J.; Surowiec, I., et al., *J. Chromatogr. A* **2003,** *1012* (2), 179-192.

51. Liu, J.; Mouri, C.; Laursen, R., et al., *J. Archaeol. Sci.* **2013,** *40* (12), 4444-4449.

52. Stern, B.; Heron, C.; Tellefsen, T., et al., *J. Archaeol. Sci.* **2008,** *35* (8), 2188-2203.

53. Evershed, R. P.; Dudd, S. N.; Copley, M. S., et al., *Acc. Chem. Res.* **2002,** *35* (8), 660-668.

54. Guasch-Jané, M. R.; Andrés-Lacueva, C.; Jáuregui, O., et al., *J. Archaeol. Sci.* **2006,** *33* (1), 98-101.

55. Brownstein, K. J.; Tushingham, S.; Damitio, W. J., et al., *Front. Mol. Biosci.* **2020,** *7* (133).

56. Zimmermann, M.; Brownstein, K. J.; Pantoja Díaz, L., et al., *Sci. Rep.* **2021,** *11* (1), 1590.

57. Chowdhury, M. P.; Campbell, S.; Buckley, M., *J. Archaeol. Sci.* **2021,** *132*, 105414.

58. Perez, E. R.; Knapp, J. A.; Horn, C. K., et al., *J. Anal. Toxicol.* **2016,** *40* (3), 201-207.

59. Sica, V. P.; Raja, H. A.; El-Elimat, T., et al., *J. Nat. Prod.* **2015,** *78* (8), 1926-1936.

60. Oberlies, N. H.; Knowles, Sonja L.; Amrine, C. S. M., et al., *Nat. Prod. Rep.* **2019,** *36* (7), 944-959.

61. Sica, V. P.; El-Elimat, T.; Oberlies, N. H., *Anal. Methods.* **2016a,** *8* (32), 6143-6149.

62. Crnkovic, C. M.; Krunic, A.; May, D. S., et al., *J. Nat. Prod.* **2018,** *81* (9), 2083-2090.

63. El-Elimat, T.; Figueroa, M.; Ehrmann, B. M., et al., *J. Nat. Prod.* **2013,** *76* (9), 1709-1716.

64. Paguigan, N. D.; Raja, H. A.; Day, C. S., et al., *Phytochemistry* **2016,** *126*, 59-65.

65. Sica, V. P.; Figueroa, M.; Raja, H. A., et al., *J. Ind. Microbiol. Biotechnol.* **2016b,** *43* (8), 1149-1157.

66. Sica, V. P.; Rees, E. R.; Raja, H. A., et al., *Phytochemistry* **2017,** *143*, 45-53.

67. Kao, D.; Henkin, J. M.; Soejarto, D. D., et al., *Phytochem. Lett.* **2018,** *28*, 124-129.

68. Ovchinnikova, O. S.; Kertesz, V.; Van Berkel, G. J., *Anal. Chem.* **2011,** *83* (2), 598-603.

69. Kertesz, V.; Berkel, G. J. V., *Bioanalysis* **2013,** *5* (7), 819-826.

70. Kertesz, V.; Paranthaman, N.; Moench, P., et al., *Bioanalysis* **2014a,** *6* (19), 2599-2606.

71. Kertesz, V.; Van Berkel, G. J., *Rapid Commun. Mass Spectrom.* **2014b,** *28* (13), 1553-1560.

72. Kertesz, V.; Weiskittel, T. M.; Van Berkel, G. J., *Anal. Bioanal. Chem.* **2015,** *407* (8), 2117-2125.

73. Pluskal, T.; Castillo, S.; Villar-Briones, A., et al., *BMC Bioinform.* **2010,** *11* (1), 395.

74. Xie, T.; Liang, Y.; Hao, H., et al., *J. Chromatogr. A* **2012,** *1227*, 234-244.

75. Maiti, B. C.; Thomson, R. H., *Experientia* **1976,** *32* (9), 1106-1107.

76. Wahidulla, S.; D'Souza, L.; Kamat, S. Y., *Phytochemistry* **1991,** *30* (10), 3323-3325.

77. Paguigan, N. D.; El-Elimat, T.; Kao, D., et al., *J. Antibiot. (Tokyo)* **2017,** *70* (5), 553-561.

78. Sumner, L. W.; Amberg, A.; Barrett, D., et al., *J. Metabolomics* **2007,** *3* (3), 211-221.

79. Songue, J. L.; Kouam; Dongo, E., et al., *Molecules* **2012,** *17* (11), 13673-13686.

80. Zhang, H.; Zhang, D.; Ray, K., et al., *J. Mass Spectrom.* **2009,** *44* (7), 999-1016.

81. Sleno, L., *J. Mass Spectrom.* **2012,** *47* (2), 226-236.

82. Ekanayaka, E. A. P.; Celiz, M. D.; Jones, A. D., *Plant Physiol.* **2015,** *167* (4), 1221-1232.

83. Chen, L.; Liu, Y.; Jia, D., et al., *J. Agric. Food. Chem.* **2016,** *64* (17), 3445-3455.

84. Banerji, A., *Indian J. Chem.* **1975,** *13*, 1234–1236.

85. Sashidhara, K. V.; Rosaiah, J. N.; Tyagi, E., et al., *Eur. J. Med. Chem.* **2009,** *44* (1), 432-436.

86. Catalán, C. A. N.; de Heluani, C. S.; Kotowicz, C., et al., *Phytochemistry* **2003,** *64* (2), 625-629.

87. Isshiki, K.; Asai, Y.; Tanaka, S., et al., *Biosci. Biotechnol. Biochem.* **2001,** *65* (5), 1195-1197.

88. Yoon, C. S.; Kim, D. C.; Lee, D. S., et al., *Int. Immunopharmacol.* **2014,** *23* (2), 568-74.

89. Wu, C.; Kao, C.; Li, H., et al., *Chem. Nat. Compd.* **2019,** *55* (1), 175-177.

90. Tian, J.-L.; Liang, X.; Gao, P.-Y., et al., *Chem. Nat. Compd.* **2015,** *51* (4), 760-761.

91. Jiang, M.; Zhang, W.; Yang, X., et al., *Nat. Prod. Res.* **2018,** *32* (20), 2431-2436.

92. Umeokoli, B. O.; Muharini, R.; Okoye, F. B., et al., *Fitoterapia* **2016,** *109*, 169-73.

93. Hui, Y.; Zhou, X.-Q.; Chen, G.-Y., et al., *Chem. Nat. Compd.* **2019,** *55* (1), 160-163.

94. De, A. K. E., *Capsicum: the genus Capsicum*. first ed. ed.; CRC Press: Boca Raton, 2003; p 269.

95. Aja, P. M.; Okaka, A. N. C.; Onu, P. N., et al., *Pak. J. Nutr.* **2010,** *9* (6), 527-530.

96. Youssef, K. M.; Mokhtar, S. M., *J. Nutr. Food Sci.* **2014,** *4* (6).

97. Balekar, N.; Nakpheng, T.; Srichana, T., *Chiang Mai J. Sci.* **2014,** *41*, 590-605.

98. Sayre, M.; Whitehead, W., Ritual and Plant Use at Conchopata: An Andean Middle Horizon Site. In *Social Perspectives on Ancient Lives from Paleoethnobotanical Data*, first ed. ed.; Springer Cham: 2017; pp pp. 121-144.

99. Itabashi, T.; Matsuishi, N.; Hosoe, T., et al., *Chem. Pharm. Bull.* **2006,** *54* (12), 1639-1641.

100. Qian, S. Y.; Shao, M. Y.; Li, Y. Z., et al., *West Indian Med. J.* **2018,** *67* (2).

101. El-Elimat, T.; Raja, H. A.; Figueroa, M., et al., *J. Nat. Prod.* **2021,** *84* (3), 898-916.

102. Bills, G. F.; Gloer, J. B., *Microbiol. Spectr.* **2016,** *4* (6).

103. Romero, A.; Carrion, G.; Rico-Gray, V., *Fungal Divers.* **2001,** *7*, 81-87.

104. Cantrell, S.; Hanlin, R.; Emiliano, A., *Mycologia* **2007,** *99*, 482-487.

105. Chuaseeharonnachai, C.; Somrithipol, S.; Boonyuen, N., *Mycotaxon* **2016,** *131* (3), 491-502.

106. Morrison-Gardiner, S., *Fungal Divers.* **2002,** *9*, 105-121.

107. Cail, L.; M, C.; Zhangl, K., et al., *Fungal Divers.* **2002,** *9*, 57-70.

108. Azhari, A.; Supratman, U., *Sci. Pharm.* **2021,** *89* (3), 34.

109. Liu, J.-M.; Zhang, D.-W.; Du, W.-Y., et al., *J. Asian Nat. Prod. Res.* **2021**, 1-6.

110. Wu, Y.-H.; Xiao, G.-K.; Chen, G.-D., et al., *Nat. Prod. Commun.* **2015,** *10* (12).

111. Zhang, D.; Ge, H.; Xie, D., et al., *Org. Lett.* **2013,** *15* (7), 1674-1677.

112. Zhang, D.; Ge, H.; Zou, J.-H., et al., *Org. Lett.* **2014,** *16* (5), 1410-1413.

113. Wu, Y.-H.; Chen, G.-D.; He, R.-R., et al., *Science* **2015,** *5* (1), 17082.

114. Knapp, D. G.; Németh, J. B.; Barry, K., et al., *Science* **2018,** *8* (1), 6321.

115. Neumann, C. S.; Fujimori, D. G.; Walsh, C. T., *Chem. Biol.* **2008,** *15* (2), 99-109.

116. Butler, A.; Sandy, M., *Nature* **2009,** *460* (7257), 848-54.

117. Harper, D. B.; O'Hagan, D., *Nat. Prod. Rep.* **1994,** *11* (0), 123-133.

118. Stine, C. M. A., *Ind. Eng. Chem. Res.* **1929,** *21* (5), 434-442.

119. Giles, D.; Turner, W. B., *J. Chem. Soc. C* **1969,** (16), 2187-2189.

120. Inose, K.; Tanaka, K.; Koshino, H., et al., *Tetrahedron* **2019,** *75* (35), 130470.

121. Henderson, G. B.; Hill, R. A., *J. Chem. Soc., Perkin Trans. 1* **1982,** 3037-3039.

122. Holker, J. S. E.; Young, K., *J. Chem. Soc., Chem.* **1975,** (13), 525-526.

123. Höller, U.; König, G. M.; Wright, A. D., *J. Nat. Prod.* **1999,** *62* (1), 114-118.

124. Höller, U.; Wright, A. D.; Matthee, G. F., et al., *Mycol. Res.* **2000,** *104* (11), 1354-1365.

125. Hill, R. A.; Macaulay, G. S.; MacLachlan, W. S., *J. Chem. Soc., Perkin Trans. 1* **1987**, 2209-2215.

126. McMullin, D. R.; Green, B. D.; Prince, N. C., et al., *J. Nat. Prod.* **2017,** *80* (5), 1475-1483.

127. Elsebai, M. F.; Ghabbour, H. A.; Legrave, N., et al., *Med. Chem. Res.* **2018,** *27* (8), 1885-1892.

128. El-Elimat, T.; Raja, H. A.; Day, C. S., et al., *J. Nat. Prod.* **2014,** *77* (9), 2088-2098.

129. El-Elimat, T.; Raja, H. A.; Figueroa, M., et al., *Phytochemistry* **2014,** *104*, 114-120.

130. El-Elimat, T.; Raja, H. A.; Day, C. S., et al., *Bioorg. Med. Chem.* **2017,** *25* (2), 795-804.

131. Hoye, T. R.; Jeffrey, C. S.; Shao, F., *Nat. Protoc.* **2007,** *2* (10), 2451-2458.

132. Barone, G.; Duca, D.; Silvestri, A., et al., *Eur. J. Chem.* **2002,** *8* (14), 3240-3245.

133. Barone, G.; Gomez-Paloma, L.; Duca, D., et al., *Chemistry (Weinheim an der Bergstrasse, Germany)* **2002,** *8* (14), 3233-9.

134. Seco, J. M.; Quiñoá, E.; Riguera, R., *Chem. Rev.* **2004,** *104* (1), 17-118.

135. Smith, S. G.; Goodman, J. M., *J. Org. Chem.* **2009,** *74* (12), 4597-4607.

136. Willoughby, P. H.; Jansma, M. J.; Hoye, T. R., *Nat. Protoc.* **2014,** *9* (3), 643-660.

137. Willoughby, P. H.; Jansma, M. J.; Hoye, T. R., *Nat. Protoc.* **2020,** *15* (7), 2277.

138. Knowles, S. L.; Roberts, C. D.; Augustinović, M., et al., *J. Nat. Prod.* **2021,** *84* (4), 1254-1260.

139. Neuhaus, G. F.; Adpressa, D. A.; Bruhn, T., et al., *J. Nat. Prod.* **2019,** *82* (10), 2780-2789.

140. Smith, S. G.; Goodman, J. M., *J. Am. Chem. Soc.* **2010,** *132* (37), 12946-12959.

141. Grimblat, N.; Gavín, J. A.; Hernández Daranas, A., et al., *Org. Lett.* **2019,** *21* (11), 4003-4007.

142. Zhang, S.; Wang, W.; Tan, J., et al., *Planta Medica* **2021,** *87* (06), 489-497.

143. Fowler, M.; Carter, R. F., *Br. Med J.* **1965,** *2* (5464), 740-742.

144. Figueroa, M.; Jarmusch, A. K.; Raja, H. A., et al., *J. Nat. Prod.* **2014,** *77* (6), 1351-1358.

145. Raja, H. A.; Miller, A. N.; Pearce, C. J., et al., *J. Nat. Prod.* **2017,** *80* (3), 756-770.

146. Gardes, M.; Bruns, T. D., *Mol. Ecol.* **1993,** *2* (2), 113-8.

147. White, T. J.; Bruns, T.; Lee, S., et al., Amplification and direct sequencing of fungal ribosomal RNA genesis for phylogenetics. In *PCR Protocols*, Innis, M. A., et al., Eds. Academic Press: San Diego, 1990; pp 315-322.

148. Markovskaja, S.; Kačergius, A., *Mycol. Prog.* **2014,** *13* (2), 291-302.

149. Tanaka, K.; Hirayama, K.; Yonezawa, H., et al., *Stud. Mycol.* **2015,** *82*, 75-136.

150. Hyde, K. D.; Norphanphoun, C.; Abreu, V. P., et al., *Fungal Divers.* **2017,** *87* (1), 1-235.

151. Dayarathne, M.; Maharachchikumbura, S.; Hyde, K., et al., *Mycosphere* **2020**, 11 (1), 1-188.

152. Dong, W.; Wang, B.; Hyde, K. D., et al., *Fungal Divers.* **2020,** *105* (1), 319-575.

153. Crous, P. W.; Luangsa-Ard, J. J.; Wingfield, M. J., et al., *Persoonia* **2018,** *41*, 238-417.

154. Edgar, R. C., *Nucleic Acids Res.* **2004,** *32* (5), 1792-1797.

155. Gouy, M.; Guindon, S.; Gascuel, O., *Mol. Biol. Evol.* **2010,** *27* (2), 221-224.

156. Talavera, G.; Castresana, J., *Syst. Biol.* **2007,** *56* (4), 564-577.

157. Kalyaanamoorthy, S.; Minh, B. Q.; Wong, T. K. F., et al., *Nat. Methods* **2017,** *14* (6), 587-589.

158. Zhang, D.; Gao, F.; Jakovlić, I., et al., *Mol. Ecol. Resour.* **2020,** *20* (1), 348-355.

159. Nguyen, L.-T.; Schmidt, H. A.; von Haeseler, A., et al., *Mol. Biol. Evol.* **2015,** *32* (1), 268-274.

160. Pang, K.-L.; Jones, E. B. G.; Vrijmoed, L. L. P., et al., *Bot. J. Linn.* **2004,** *146* (2), 223-229.

161. Kohlmeyer, J., *Can. J. Bot.* **1969,** *47* (9), 1469-1487.

162. Al Subeh, Z. Y.; Raja, H. A.; Maldonado, A., et al., *J. Antibiot. (Tokyo)* **2021,** *74* (5), 300-306.

163. Rice, C. A.; Colon, B. L.; Alp, M., et al., *Antimicrob. Agents Chemother.* **2015,** *59* (4), 2037-44.

164. Colon, B. L.; Rice, C. A.; Guy, R. K., et al., *J. Infect. Dis.* **2018,** *219* (7), 1095-1103.

165. Rice, C. A.; Colon, B. L.; Chen, E., et al., *PLoS Negl. Trop. Dis.* **2020,** *14* (9), e0008353.

166. Rice, C. A.; Troth, E. V.; Russell, A. C., et al., *Pathogens* **2020,** *9* (6).

167. Todd, D. A.; Zich, D. B.; Ettefagh, K. A., et al., *J. Microbiol. Methods* **2016,** *127*, 89-94.

168. Grimblat, N.; Zanardi, M. M.; Sarotti, A. M., *J. Org. Chem.* **2015,** *80* (24), 12526-12534.

169. Stephens, P. J.; McCann, D. M.; Devlin, F. J., et al., *J. Nat. Prod.* **2006,** *69* (7), 1055-1064.

170. Srebro, M.; Govind, N.; de Jong, W. A., et al., *J. Phys. Chem. A* **2011,** *115* (40), 10930-10949.

171. Bruhn, T.; Schaumlöffel, A.; Hemberger, Y., et al., *Chirality* **2013,** *25* (4), 243-249.

172. Kulhanek, K.; Steinhauer, N.; Rennich, K., et al., *J. Apic. Res.* **2017,** *56* (4), 328-340.

173. Dolezal, A. G.; Toth, A. L., *Curr. Opin. Insect* **2018,** *26*, 114-119.

174. Dolezal, A. G.; Carrillo-Tripp, J.; Judd, T. M., et al., *R. Soc. Open Sci.* **2019,** *6* (2), 181803-181803.

175. DeGrandi-Hoffman, G.; Chen, Y., *Curr. Opin. Insect* **2015,** *10*, 170-176.

176. Di Pasquale, G.; Alaux, C.; Le Conte, Y., et al., *PLOS ONE* **2016,** *11* (9), e0162818.

177. Brodschneider, R.; Crailsheim, K., *Apidologie* **2010,** *41* (3), 278-294.

178. Crailsheim, K., *Apidologie* **1990,** *21* (5), 417-429.

179. Huang, Z., *Terr. Arthropod Rev.* **2012,** *5* (2), 175-189.

180. Alaux, C.; Dantec, C.; Parrinello, H., et al., *BMC Genom.* **2011,** *12*, 496.

181. Roulston, T. a. H.; Cane, J. H.; Buchmann, S. L., *Ecol.* **2000,** *70* (4), 617-643.

182. Roulston, T. H.; Cane, J. H., *Plant Syst. Evol* **2000,** *222* (1), 187-209.

183. Donkersley, P.; Rhodes, G.; Pickup, R. W., et al., *Ecol. Evol.* **2014,** *4* (21), 4195-206.

184. Sponsler, D. B.; Johnson, R. M., *Peer J* **2015,** *3*, e838.

185. Dolezal, A. G.; Carrillo-Tripp, J.; Miller, W. A., et al., *PLOS ONE* **2016,** *11* (4), e0153531.

186. Vanbergen, A. J.; Initiative, t. I. P., *Front. Ecol. Environ.* **2013,** *11* (5), 251-259.

187. Bartomeus, I.; Ascher, J. S.; Wagner, D., et al., *Proc. Natl. Acad. Sci. U.S.A.* **2011,** *108* (51), 20645-20649.

188. Settele, J.; Bishop, J.; Potts, S. G., *Nat. Plants* **2016,** *2* (7), 16092.

189. Ricigliano V.A., W. S., Oliver R. , *BMC Vet. Res.* **2022,** (in press).

190. Noordyke, E. R.; Ellis, J. D., *Front. Sustain. Food Syst.* **2021,** *5*.

191. Ricigliano, V. A.; Williams, S. T.; Oliver, R., *BMC Vet. Res.* **2022,** *18* (1), 52.

192. Avni, D.; Hendriksma, H. P.; Dag, A., et al., *J. Insect Physiol.* **2014,** *69*, 65-73.

193. Arien, Y.; Dag, A.; Zarchin, S., et al., *Proc. Natl. Acad. Sci. U.S.A.* **2015,** *112* (51), 15761.

194. Wegener, J.; Jakop, U.; Schiller, J., et al., *Insectes. Soc.* **2018,** *65* (3), 381-391.

195. Liao, L.-H.; Pearlstein, D. J.; Wu, W.-Y., et al., *PLOS ONE* **2020,** *15* (12), e0243364.

196. Aylanc, V.; Falcão, S. I.; Ertosun, S., et al., *Trends Food Sci. Technol* **2021,** *109*, 464-481.

197. Madeira, M. S.; Cardoso, C.; Lopes, P. A., et al., *Livest. Sci.* **2017,** *205*, 111-121.

198. Ricigliano, V. A., *Arch. Insect Biochem. Physiol.* **2020,** *104* (1), e21658.

199. Jehlík, T.; Kodrík, D.; Krištůfek, V., et al., *Apidologie* **2019,** *50* (4), 564-577.

200. Ricigliano, V. A.; Simone-Finstrom, M., *Apidologie* **2020,** *51* (5), 898-910.

201. Dettmer, K.; Aronov, P. A.; Hammock, B. D., *Mass Spectrom. Rev.* **2007,** *26* (1), 51-78.

202. Hu, C.; Xu, G., *Trends Analyt. Chem.* **2013,** *52*, 36-46.

203. Chakrabarti, P.; Morré, J. T.; Lucas, H. M., et al., *Metabolomics* **2019,** *15* (10), 127.

204. Pluskal, T.; Castillo, S.; Villar-Briones, A., et al., *BMC Bioinform.* **2010,** *11*, 395.

205. Caesar, L. K.; Kvalheim, O. M.; Cech, N. B., *Anal. Chim. Acta* **2018,** *1021*, 69-77.

206. Goedhart, J.; Luijsterburg, M. S., *Science* **2020,** *10* (1), 20560.

207. Ricigliano, V. A.; Dong, C.; Richardson, L. T., et al., *Food Sci. Technol.* **2021,** *1* (1), 17-26.

208. Ricigliano, V. A.; Ihle, K. E.; Williams, S. T., *Apidologie* **2021,** *52* (4), 873-886.

209. DeGrandi-Hoffman, G.; Chen, Y.; Huang, E., et al., *J. Insect Physiol.* **2010,** *56* (9), 1184-91.

210. Hendriksma, H. P.; Pachow, C. D.; Nieh, J. C., *J. Insect Physiol.* **2019,** *117*, 103906.

211. Corby-Harris, V.; Snyder, L.; Meador, C., et al., *PLOS ONE* **2018,** *13* (1), e0191050.

212. Bridgett, R. J.; Kirk, W. D. J.; Drijfhout, F. P., *Apidologie* **2015,** *46* (3), 315-325.

213. Nowacka-Woszuk, J., *J. Appl. Genet.* **2020,** *61* (1), 93-103.

214. Corby-Harris, V.; Jones, B. M.; Walton, A., et al., *BMC genom.* **2014,** *15*, 134.

215. Ricigliano, V. A.; Mott, B. M.; Maes, P. W., et al., *Sci* **2019,** *9* (1), 4894.

216. Corona, M.; Hughes, K. A.; Weaver, D. B., et al., *Mech. Ageing Dev.* **2005,** *126* (11), 1230-8.

217. Li, C.; Xu, B.; Wang, Y., et al., *Entomol. Exp. Appl.* **2014,** *151* (1), 19-26.

218. Moura, C. S.; Lollo, P. C. B.; Morato, P. N., et al., *Nutrients* **2018,** *10* (6), 683.

219. Tsan, M. F.; Gao, B., *Cell. Mol. Immunol.* **2004,** *1* (4), 274-279.

220. Kešnerová, L.; Mars, R. A. T.; Ellegaard, K. M., et al., *PLOS Biology* **2017,** *15* (12), e2003467.

221. Vinaixa, M.; Schymanski, E. L.; Neumann, S., et al., *Trends Analyt. Chem.* **2016,** *78*, 23-35.

222. Luzzatto-Knaan, T.; Garg, N.; Wang, M., et al., *eLife* **2017,** *6*, e24214.

223. In *Dictionary of Natural Products* London: Taylor & Francis Group: 2021.

224. DeGrandi-Hoffman, G.; Gage, S. L.; Corby-Harris, V., et al., *J. Insect Physiol.* **2018,** *109*, 114-124.

225. Berry, J. P.; Gantar, M.; Perez, M. H., et al., *Mar. Drugs.* **2008,** *6* (2), 117-146.

226. Grosshagauer, S.; Kraemer, K.; Somoza, V., *J. Agric. Food Chem.* **2020,** *68* (14), 4109-4115.

227. Roussel, M.; Villay, A.; Delbac, F., et al., *Carbohydr. Polym.* **2015,** *133*, 213-220.

228. Teimouri, M.; Yeganeh, S.; Mianji, G. R., et al., *Fish. Physiol. Biochem.* **2019,** *45* (3), 977-986.

229. Sumner, L. W.; Amberg, A.; Barrett, D., et al., *Metabolomics* **2007,** *3* (3), 211-221.

230. Guedes, A. C.; Amaro, H. M.; Malcata, F. X., *Mar. Drugs.* **2011,** *9* (4), 625-644.

231. Hassaan, M. S.; Mohammady, E. Y.; Soaudy, M. R., et al., *Fish Shellfish Immunol.* **2021,** *108*, 63-72.

232. Chung, H.; Carroll, S. B., *BioEssays* **2015,** *37* (7), 822-830.

233. Ingleby, F. C., *Insects* **2015,** *6* (3), 732-742.

234. Vernier, C. L.; Krupp, J. J.; Marcus, K., et al., *eLife* **2019,** *8*, e41855.

235. World Health, O., *World malaria report 2017*. World Health Organization: Geneva, 2017.

236. Wells, T. N. C.; van Huijsduijnen, R. H.; Van Voorhis, W. C., *Nat. Rev. Drug Discov.* **2015,** *14* (6), 424-442.

237. Mojab, F., *Avicenna J. Phytomed.* **2012,** *2* (2), 52-62.

238. Chernin, E., *Med. Hist.* **1988,** *32* (2), 119-141.

239. Su, X.-Z.; Miller, L. H., *Sci. China Life Sci.* **2015,** *58* (11), 1175-1179.

240. Newman, D. J.; Cragg, G. M., *J. Nat. Prod.* **2007,** *70* (3), 461-77.

241. L. Hawksworth, D., *Mycol. Res.* **2001,** *105* (12), 1422-1432.

242. Blackwell, M., *Am J. Bot.* **2011,** *98* (3), 426-38.

243. Berdy, J., *J Antibiot (Tokyo)* **2012,** *65* (8), 385-95.

244. Nett, M.; Ikeda, H.; Moore, B. S., *Nat. Prod. Rep.* **2009,** *26* (11), 1362-1384.

245. Bills, G. F.; Gloer, J. B., *Microbiology spectrum* **2016,** *4* (6).

246. Yang, B.; Huang, J.; Zhou, X., et al., *Curr. Med. Chem.* **2018,** *25* (31), 3796-3825.

247. Cank, K. B.; Shepherd, R. A.; Knowles, S. L., et al., *Phytochemistry* **2022**, 113200.

248. Zain, M. E., *J. Saudi Chem. Soc.* **2011,** *15* (2), 129-144.

249. Pitt, J. I., *Br. Med. Bull.* **2000,** *56* (1), 184-192.

250. Díaz Nieto, C. H.; Granero, A. M.; Zon, M. A., et al., *Food Chem. Toxicol.* **2018,** *118*, 460-470.

251. Darkin-Rattray, S. J.; Gurnett, A. M.; Myers, R. W., et al., *Proc. Natl. Acad. Sci. U.S.A.* **1996,** *93* (23), 13143-13147.

252. Shang, Z.; Salim, A. A.; Khalil, Z., et al., *J. Org. Chem.* **2015,** *80* (24), 12501-12508.

253. Chooi, Y.-H.; Cacho, R.; Tang, Y., *Chem. Biol.* **2010,** *17* (5), 483-494.

254. Hutchison, R. D.; Steyn, P. S.; Van Rensburg, S. J., *Toxicol. Appl. Pharmacol.* **1973,** *24* (3), 507-509.

255. Raju, M.; Wu, G.-S.; Gard, A., et al., *J. Nat. Prod.* **1982,** *45* (3), 321-327.

256. Bendele, A. M.; Carlton, W. W.; Nelson, G. E. N., et al., *Toxicol. Lett.* **1984,** *22* (3), 287-291.

257. Bunnag, D.; Karbwang, J.; Na-Bangchang, K., et al., *Southeast Asian J. Trop. Med. Public Health* **1996,** *27*, 15-18.

258. Pradines, B.; Spiegel, A.; Rogier, C., et al., *Am. J. Trop. Med.* **2000,** *62* (1), 82-85.

259. Schwartz, E.; Regev-Yochay, G., *Arch. Clin. Infect. Dis.* **1999,** *29* (6), 1502-1506.

260. Chopra, I.; Roberts, M., *Microbiol. Mol. Biol. Rev.* **2001,** *65* (2), 232-260.

261. Arai, T.; MIKAMI, Y.; FUKUSHIMA, K., et al., *J. Antibiot.* **1973,** *26* (3), 157-161.

262. Brand, M.; Wang, L.; Agnello, S., et al., *Angew. Chem., Int. Ed.* **2021,** *60* (28), 15613-15621.

263. Isogai, A.; Nakayama, J.; Takayama, S., et al., *Biosci.* **1992,** *56* (7), 1079-1085.

264. Martinez, A. F. C.; Moraes, L. A. B., *J. Antibiot.* **2015,** *68* (3), 178-184.

265. Otoguro, K.; Ui, H.; Ishiyama, A., et al., *J. Antibiot.* **2003,** *56* (3), 322-324.

266. Rivera-Chávez, J.; Raja, H. A.; Graf, T. N., et al., *RSC Adv.* **2017,** *7* (72), 45733-45751.

267. Maienfisch, P.; Hall, R. G., *Chimia* **2004,** *58* (3), 93-99.

268. Ojima, I., *Fluorine in medicinal chemistry and chemical biology*. John Wiley & Sons: 2009.

269. Muller, K.; Faeh, C.; Diederich, F., *Science* **2007,** *317* (5846), 1881-1886.

270. Amrine, C. S. M.; Long, J. L.; Raja, H. A., et al., *J. Nat. Prod.* **2019,** *82* (11), 3104-3110.

271. Rivera-Chávez, J.; Raja, H. A.; Graf, T. N., et al., *J. Nat. Prod.* **2017,** *80* (6), 1883-1892.

272. Canfield, C. J.; Pudney, M.; Gutteridge, W. E., *Exp. Parasitol.* **1995,** *80* (3), 373-381.

273. Trager, W.; Jensen, J. B., *Science* **1976,** *193* (4254), 673-675.

274. Lambros, C.; Vanderberg, J. P., *J. Parasitol.* **1979,** *65* (3), 418-420.

275. Roth, A.; Maher, S. P.; Conway, A. J., et al., *Nat. Commun.* **2018,** *9* (1), 1837.

276. Maher, S. P.; Vantaux, A.; Cooper, C. A., et al., *Bio-protocol* **2021,** *11* (23), e4253.

277. Duffy, S.; Avery, V. M., *Am. J. Trop. Med.* **2012,** *86* (1), 84-92.

278. Zhang, J.-H.; Chung, T. D. Y.; Oldenburg, K. R., *J. Biomol. Screen.* **1999,** *4* (2), 67-73.

279. Levenberg, K., *Q. Appl. Math.* **1944,** *2* (2), 164-168.

280. Marquardt, D. W., *J. Soc. Ind. Appl. Math.* **1963,** *11* (2), 431-441.

281. Kil, Y.-S.; Risinger, A. L.; Petersen, C. L., et al., *J. Nat. Prod.* **2020,** *83* (6), 2010-2024.